Jordan Journal of Mechanical and Industrial Engineering (JJMIE)

JJMIE is a high-quality scientific journal devoted to fields of Mechanical and Industrial Engineering. It is published by The Jordanian Ministry of Higher Education and Scientific Research in corporation with the Hashemite University.

SUBMISSION ADDRESS:

Prof. **Mousa S. Mohsen**, Editor-in-Chief
Jordan Journal of Mechanical & Industrial Engineering,
Hashemite University, PO Box 330127, Zarqa, 13133 , Jordan
E-mail: jjmie@hu.edu.jo

Hashemite Kingdom of Jordan

Hashemite University

Jordan Journal of Mechanical and Industrial Engineering

JJMIE

An International Peer-Reviewed Scientific Journal

http://jjmie.hu.edu.jo/

ISSN 1995-6665

Jordan Journal of Mechanical and Industrial Engineering (JJMIE)

JJMIE is a high-quality scientific journal devoted to fields of Mechanical and Industrial Engineering. It is published by The Jordanian Ministry of Higher Education and Scientific Research in corporation with the Hashemite University.

Introduction: The Editorial Board is very committed to build the Journal as one of the leading international journals in mechanical and industrial engineering sciences in the next few years. With the support of the Ministry of Higher Education and Scientific Research and Jordanian Universities, it is expected that a heavy resource to be channeled into the Journal to establish its international reputation. The Journal's reputation will be enhanced from arrangements with several organizers of international conferences in publishing selected best papers of the conference proceedings.

Aims and Scope: Jordan Journal of Mechanical and Industrial Engineering (JJMIE) is a refereed international journal to be of interest and use to all those concerned with research in various fields of, or closely related to, mechanical and industrial engineering disciplines. Jordan Journal of Mechanical and Industrial Engineering aims to provide a highly readable and valuable addition to the literature which will serve as an indispensable reference tool for years to come. The coverage of the journal includes all new theoretical and experimental findings in the fields of mechanical and industrial engineering or any closely related fields. The journal also encourages the submission of critical review articles covering advances in recent research of such fields as well as technical notes.

Guide for Authors

Manuscript Submission

High-quality submissions to this new journal are welcome now and manuscripts may be either submitted online or mail.

Online: For online submission upload one copy of the full paper including graphics and all figures at the online submission site, accessed via E-mail: jjmie@hu.edu.jo. The manuscript must be written in MS Word Format. All correspondence, including notification of the Editor's decision and requests for revision, takes place by e-mail and via the Author's homepage, removing the need for a hard-copy paper trail.

By Mail: Manuscripts (1 original and 3 copies) accompanied by a covering letter may be sent to the Editor-in-Chief. However, a copy of the original manuscript, including original figures, and the electronic files should be sent to the Editor-in-Chief. Authors should also submit electronic files on disk (one disk for text material and a separate disk for graphics), retaining a backup copy for reference and safety.

Note that contributions may be either submitted online or sent by mail. Please do NOT submit via both routes. This will cause confusion and may lead to delay in article publication. Online submission is preferred.

Submission address and contact:

Prof. **Mousa S. Mohsen**, Editor-in-Chief
Jordan Journal of Mechanical & Industrial Engineering,
Hashemite University,
PO Box 330127, Zarqa, 13133 , Jordan
E-mail: jjmie@hu.edu.jo

Types of contributions: Original research papers

Corresponding author: Clearly indicate who is responsible for correspondence at all stages of refereeing and publication, including post-publication. Ensure that telephone and fax numbers (with country and area code) are provided in addition to the e-mail address and the complete postal address. Full postal addresses must be given for all co-authors.

Original material: Submission of an article implies that the work described has not been published previously (except in the form of an abstract or as part of a published lecture or academic thesis), that it is not under consideration for publication elsewhere, that its publication is approved by all authors and that, if accepted, it will not be published elsewhere in the same form, in English or in any other language, without the written consent of the Publisher. Authors found to be deliberately contravening the submission guidelines on originality and exclusivity shall not be considered for future publication in this journal.

Supplying Final Accepted Text on Disk: If online submission is not possible: Once the paper has been accepted by the editor, an electronic version of the text should be submitted together with the final hardcopy of the manuscript. The electronic version must match the hardcopy exactly. We accept MS Word format only. Always keep a backup copy of the electronic file for reference and safety. Label the disk with your name. Electronic files can be stored on CD.

Notification: Authors will be notified of the acceptance of their paper by the editor. The Publisher will also send a notification of receipt of the paper in production.

Copyright: All authors must sign the Transfer of Copyright agreement before the article can be published. This transfer agreement enables Jordan Journal of Mechanical and Industrial Engineering to protect the copyrighted material for the authors, but does not relinquish the authors' proprietary rights. The copyright transfer covers the exclusive rights to reproduce and distribute the article, including reprints, photographic reproductions, microfilm or any other reproductions of similar nature and translations.

<u>PDF Proofs:</u> One set of page proofs in PDF format will be sent by e-mail to the corresponding author, to be checked for typesetting/editing. The corrections should be returned within 48 hours. No changes in, or additions to, the accepted (and subsequently edited) manuscript will be allowed at this stage. Proofreading is solely the author's responsibility. Any queries should be answered in full. Please correct factual errors only, or errors introduced by typesetting. Please note that once your paper has been proofed we publish the identical paper online as in print.

Author Benefits

Page charge: Publication in this journal is free of charge.

Free off-prints: Three journal issues of which the article appears in along with twenty-five off-prints will be supplied free of charge to the corresponding author. Corresponding authors will be given the choice to buy extra off-prints before printing of the article.

Manuscript Preparation:

<u>General:</u> Editors reserve the right to adjust style to certain standards of uniformity. Original manuscripts are discarded after publication unless the Publisher is asked to return original material after use. If online submission is not possible, an electronic copy of the manuscript on disk should accompany the final accepted hardcopy version. Please use MS Word for the text of your manuscript.

<u>Structure:</u> Follow this order when typing manuscripts: Title, Authors, Affiliations, Abstract, Keywords, Introduction, Main text, Conclusions, Acknowledgements, Appendix, References, Figure Captions, Figures and then Tables. For submission in hardcopy, do not import figures into the text - see Illustrations. For online submission, please supply figures imported into the text AND also separately as original graphics files. Collate acknowledgements in a separate section at the end of the article and do not include them on the title page, as a footnote to the title or otherwise.

<u>Text Layout:</u> Use double spacing and wide (3 cm) margins. Ensure that each new paragraph is clearly indicated. Present tables and figure legends on separate pages at the end of the manuscript. If possible, consult a recent issue of the journal to become familiar with layout and conventions. All footnotes (except for table and corresponding author footnotes) should be identified with superscript Arabic numbers. To conserve space, authors are requested to mark the less important parts of the paper (such as records of experimental results) for printing in smaller type. For long papers (more that 4000 words) sections which could be deleted without destroying either the sense or the continuity of the paper should be indicated as a guide for the editor. Nomenclature should conform to that most frequently used in the scientific field concerned. Number all pages consecutively; use 12 or 10 pt font size and standard fonts. If submitting in hardcopy, print the entire manuscript on one side of the paper only.

<u>Corresponding author:</u> Clearly indicate who is responsible for correspondence at all stages of refereeing and publication, including post-publication. The corresponding author should be identified with an asterisk and footnote. Ensure that telephone and fax numbers (with country and area code) are provided in addition to the e-mail address and the complete postal address. Full postal addresses must be given for all co-authors. Please consult a recent journal paper for style if possible.

<u>Abstract:</u> A self-contained abstract outlining in a single paragraph the aims, scope and conclusions of the paper must be supplied.

<u>Keywords:</u> Immediately after the abstract, provide a maximum of six keywords (avoid, for example, 'and', 'of'). Be sparing with abbreviations: only abbreviations firmly established in the field may be eligible.

<u>Symbols:</u> All Greek letters and unusual symbols should be identified by name in the margin, the first time they are used.

<u>Units:</u> Follow internationally accepted rules and conventions: use the international system of units (SI). If other quantities are mentioned, give their equivalent in SI.

<u>Maths:</u> Number consecutively any equations that have to be displayed separately from the text (if referred to explicitly in the text).

<u>References:</u> All publications cited in the text should be presented in a list of references following the text of the manuscript.

Text: Indicate references by number(s) in square brackets in line with the text. The actual authors can be referred to, but the reference number(s) must always be given.

List: Number the references (numbers in square brackets) in the list in the order in which they appear in the text.

<u>Examples:</u>

Reference to a journal publication:

[1] M.S. Mohsen, B.A. Akash, "Evaluation of domestic solar water heating system in Jordan using analytic hierarchy process". Energy Conversion & Management, Vol. 38, No. 9, 1997, 1815-1822.

Reference to a book:

[2] Strunk Jr W, White EB. The elements of style. 3rd ed. New York: Macmillan; 1979.

Reference to a conference proceeding:

[3] B. Akash, S. Odeh, S. Nijmeh, "Modeling of solar-assisted double-tube evaporator heat pump system under local climate conditions". 5th Jordanian International Mechanical Engineering Conference, Amman, Jordan, 2004.

Reference to a chapter in an edited book:

[4] Mettam GR, Adams LB. How to prepare an electronic version of your article. In: Jones BS, Smith RZ, editors. Introduction to the electronic age, New York: E-Publishing Inc; 1999, p. 281-304

<u>Free Online Color:</u> If, together with your accepted article, you submit usable color and black/white figures then the journal will ensure that these figures will appear in color on the journal website electronic version.

<u>Tables:</u> Tables should be numbered consecutively and given suitable captions and each table should begin on a new page. No vertical rules should be used. Tables should not unnecessarily duplicate results presented elsewhere in the manuscript (for example, in graphs). Footnotes to tables should be typed below the table and should be referred to by superscript lowercase letters.

JJMIE

Volume 4, Number 2, March. 2010
ISSN 1995-6665
Pages 234- 245

Jordan Journal of Mechanical and Industrial Engineering

Elaboration of Supervision Process Applied to The Pressurized Nuclear Reactor Using Graphical Approach

Badoud Abd Essalam *, Khemliche Mabrouk and Latrèche Samia

Automatic laboratory, Electrical Engineering Department, University of Setif 19000 Algeria

Abstract

The fault detection and isolation method based on bond graph for nuclear reactor with pressurized water is introduced in this paper. Using a knowledge representation of bond graph modeling, which includes system structural, functional and behavioral information and there relation. The main objective developed in this paper is to find a graphic technique for supervision of the industrial systems. The importance of this method is much apparent when it is about a complex system such as the nuclear reactor with pressurized water. In this case the analytical approach is heavy and does not give a fast idea on the evolution of the system. The simulation demonstrates that the bond graph fault diagnosis method is effective, corrective and flexible.

Keywords: Bond Graph; Directed Graph; Supervision; Pressurized Reactor.

Nomeculre:

PWR : Pressurized water reactor
CEA : Commission of Atomic Energy
SG : Steam Generator
HP : Turbine high pressure
LP : Low pressure turbine
RRAs : Analytical Redundancy Relations
FDI : Fault detection and insulation
f : flow variable
e : effort variable
De : effort detector
Df : flow detector
x_i, y_i : binary variables

1. Introduction

Modeling and simulation of engineering dynamical systems is an essential analysis and synthesis tool. 'Pencil-and-paper' approaches to find the equations of the system and analyzing the implications behind them is tedious for large complex systems. Numerical simulation on digital computer aids in understanding the dynamical behaviour of such systems [1].

Many software packages on multiple platforms are available which perform simulation of complex physical systems that are represented in mathematical form. This has led to enhanced comprehension on the behaviour of the systems. Before embarking on the simulation process, the mathematical representation of the system is an important issue to be considered and overcome. One needs to get a sufficiently accurate model (mathematical representation) of the given system. There are various approaches for modeling systems. Graphical approach consists of the following methods: block diagram, signal flow graph, bond graph from which one gets the mathematical model of the system. Block diagram and signal flow graph provide a picture of the equations. They portray operators acting on the signals. Hence block diagram and signal flow graph do not give much insight into the topology of the system [2].

This paper focuses on the use of bond graph method for modeling, simulating engineering systems and supervision. It seamlessly integrates modelling of multidisciplinary systems like electrical, mechanical, magnetic, thermal, etc. It is a well-established graphical method for modeling dynamical systems.

The causality property of bond graph gives cause effect relationship between the system energy variables. Bond graph with assigned causality displays the structure of state space equations. One can write state equations from the bond graph just by inspection. Further, it provides an algorithmic way of extraction of state equations for computer simulation.

Industrial statistics show that 70% of the industrial accidents are caused by human errors. These abnormal events had the impacts of an economic nature, but especially of the impacts on safety and the environment, like nuclear accident of Three Island Mile in United States 1979 [3]. This accident is classified on 5 level, the most level being 7 in the international scale nuclear events and extremely serious accident of level 7 on the scale INNATE in the nuclear thermal power station of Chernobyl in

* Corresponding author. badoudabde@yahoo.fr.

Ukraine 1986, poses the development problem of supervision techniques [1]. Moreover, industrial statistics show that small accidents are very frequent every day, causing important economic losses.

2. Process Description

In the pressurized water reactor (PWR), the water which passes over the reactor core to act as moderator and coolant does not flow to the turbine, but is contained in a pressurized primary loop. The primary loop water produces steam in the secondary loop which drives the turbine. The obvious advantage to this is that a fuel leak in the core would not pass any radioactive contaminants to the turbine and condenser (see figure 1).

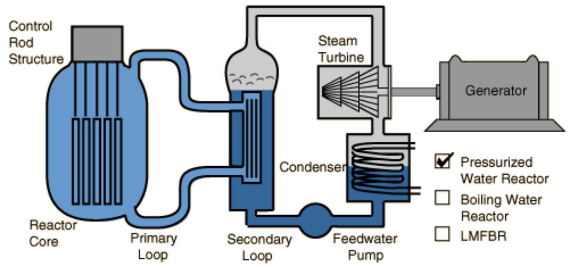

Figure 1. Pressurized Water Reactor.

Another advantage is that the PWR can operate at higher pressure and temperature, about 160 atmospheres and about 315 C. This provides a higher car not efficiency than the BWR, but the reactor is more complicated and more costly to construct. Most of the U.S. reactors are pressurized water reactors [4], [5].

3. Fault Detection and Isolation (FDI)

Immediately after the abstract, provide a maximum of six keywords (avoid, for example, 'and', 'of'). Be sparing with abbreviations: only abbreviations firmly established in the field may be eligible.

A number of methods have been developed for fault detection and isolation [7]. All methods of fault detection work by designing residual functions. The residual represents the difference between an estimated value and a measured one, which should be zero during normal operation, but large in the presence of faults [8].

In practice, there is a distinction between the detection of fast-acting, possibly safety-critical faults, and faults which are non-safety-critical and slower to develop, for example due to wear. The former are most likely to be detected by state-estimation and instantaneous comparison of prediction with measurement, while the latter are detected using parameter estimation techniques which require a certain time window and excitation of the system. Probability analysis can be used to judge, from the residual values, when a fault or change has taken place [7]. This paper is concerned primarily with detection of fast-acting faults, detected via state estimation. Isolation, in the literature, means diagnosis of the faulty component. If faults are allowed to occur simultaneously, then for a diagnosis, at least as many independent residual functions as faults considered are required. In practice, it is usually assumed that only one fault occurs at a time, which facilitates more robust fault diagnosis [8].

4. Bond Graph Modeling of PWR

Bond Graphs were originated by Henry M. Paynter with the specific purpose of handling variety within multi domain dynamic systems, based on energy and information exchange [6]. The physical model developed using Bond Graphs is detailed down to the topological level of the system being studied through a simple set of idealized elements. It is comprehensive as well and captures inter domain dynamic interaction through a uniform notation drawn on the concept of analogies among physical systems residing in different energy domains [7], [8]. The Bond Graph model of a PWR is presented by figure 2.

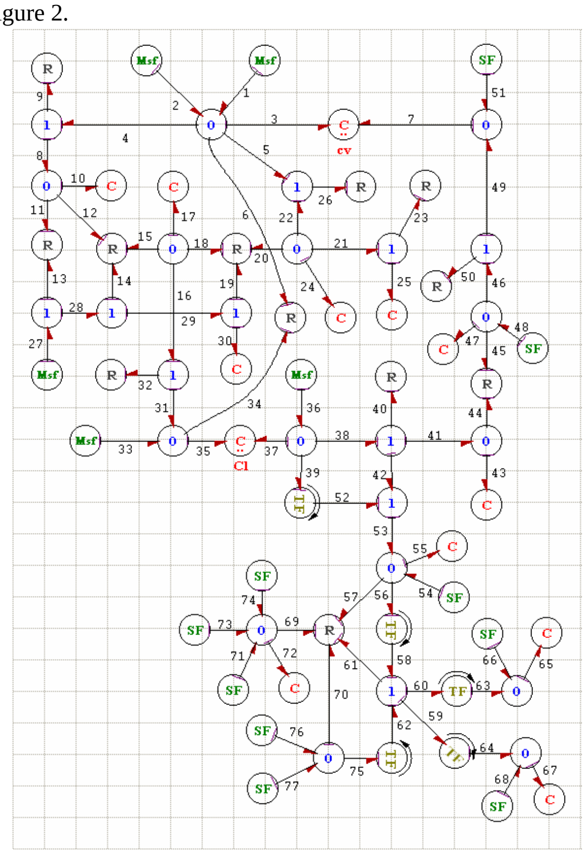

Figure 2. Bond Graph Model detailed of a pressurized water reactor.

5. Operational Characteristics

Table 1 shows the typical operational characteristics of a PWR.

6. Simulation Results

The actual control and FDI properties of the process may differ from that obtained through structural analysis when parameter values, process uncertainties, and sensor noises are taken into consideration. Thus, validations through nonlinear control analysis and simulation are necessary before finalizing the process instrumentation. Simulation requires a behavioral model derived from causal linking of components at the equation level.

Residual sensitivity to faults can be tested by using offline data or a simulation model. This requires linking ARR equations with the behavioral model by using a hybrid simulation tool and solving them together with the introduction of various faults.

7. Representation by A Structural Model

The monitoring of the processes is often based on the analytical redundancy, less expensive than the physical redundancy. The graph theory was largely used in this field like method with models. In this work, we approached the monitoring by the approach structural under the angle of the graphs bipartis [9].

Table 1. shows the typical operational characteristics of a PWR.

characteristic	Value
Thermal power output	3.800 MWth
System pressure	2.250 psia
Fuel enrichment	1.9/2.4/2.9
Coolant flow	1.5910^{3} Ibs/hr
Inlet temperature	565°F
Outlet temperature	622.4 °F
Maximum fuel temperature	3.420 °F
Average linear heat rate	5.34 KW/ft
Maximum linear heat rate	12.51 KW/ft
Average heat flux	206.000 BTU/(hr.fr^{2})
Maximum heat flux	550.000 BTU/(hr.fr^{2})
Minimum Departure from nucleate boiling	1.3
Ratio (DNBR)	
Active height	150 inches
Equivalent active diameter	142.9 inches
Height of diameter ratio	1.05
Active core volume	1413 ft^{3}
Average core power density	2.690 KW/ft^{3}
Fuel weight	103.000 kgs
Specific power	36.9 kW/kg U
Burnup	33.000 Mwdays/MTU
Conversion ratio	0.5
Number of fuel assemblies	241
Fuel element array	16x16
Assembly dimensions	8 in x 8 in
Number of fuel rods per assembly	236
Total number of fuel rods	56.876
Fuel element pitch	0.504 in
Fuel element outer diameter	0.382 in
Pitch diameter ratio	1.33
Cladding thickness	0.025 in
Fuel pellet diameter	0.325 in
Pellet to clad gap size	0.0035 in

8. Constraints

The constraints C can be seen as any relations which connect the variables and the parameters of the system. They are represented by the structural constraints, of behavior, measurement, the control device and the controlled sources [9].

8.1. Structural equations ϕ_s :

They represent the whole of the conservation laws (mass, energy…) and/or equilibrium equations. They are deduced from the equations to the junctions. The number of equations is equal to the number of equations in junctions 0 add of junctions 1 add of the two ports elements (transformer TF, and gyrator GY) [10].

$$\begin{aligned}\phi_s = &\{\phi_{j1_1}\} \cup \phi\{_{j1_2}\} \cup \{\phi_{j1_3}\} \cup \{\phi_{j1_4}\} \cup \{\phi_{j1_5}\} \cup \\ &\{\phi_{j1_6}\} \cup \{\phi_{j1_7}\} \cup \{\phi_{j1_8}\} \cup \{\phi_{j1_9}\} \cup \{\phi_{j1_{10}}\} \cup \{\phi_{j1_{11}}\} \\ &\cup \{\phi_{j0_1}\} \cup \{\phi_{j0_2}\} \cup \{\phi_{j0_3}\} \cup \{\phi_{j0_4}\} \cup \{\phi_{j0_5}\} \cup \{\phi_{j0_6}\} \\ &\cup \{\phi_{j0_7}\} \cup \{\phi_{j0_8}\} \cup \{\phi_{j0_9}\} \cup \{\phi_{j0_{10}}\} \cup \{\phi_{j0_{11}}\} \cup \\ &\{\phi_{j0_{12}}\} \cup \{\phi_{j0_{13}}\} \cup \{\phi_{j0_{14}}\} \cup \{\phi_{jTF_1}\} \cup \{\phi_{jTF_2}\} \cup \{\phi_{jTF_3}\} \\ &\cup \{\phi_{jTF_4}\} \cup \{\phi_{jTF_5}\}\end{aligned} \quad (1)$$

$\phi_C \in \Re^{nj+2n_{2p}}$ n_j : is the number of junctions 0 and 1, and n_{2p} is the number of two ports elements (TF and GY).

8.2. Behavior equations ϕ_b :

The physical laws expressing the way in which energy is converted, represent the model of behavior. The model of behavior of each component expresses the constraints which this component imposes on the variables which are dependent for him. We can thus associate each component a whole of relations whose expression depends on the type of knowledge available on the activity of the component to model. The models of behavior of the components of the system can have varied representations. These models can be linear, nonlinear, static, dynamic, qualitative, containing rules of evolution or numerical tables (for example for models Bond Graphs). The need for a formalism unified to determine the common elements of the various models of the components, justifies the structural approach. This one makes it possible to establish the constraints which exist between the various variables and system relations. This fact we can treat models of components very varied from a complex system being able to cohabit in the same system which does not require the complete definition of the model describing its behavior. In the Bond Graph model, they describe the physical phenomena on the level Bond Graph elements (R, C, and I), and are called "constitutive laws" [11].

$$\phi_b = \{\phi_{C_1}\} \cup \{\phi_{C_2}\} \cup \{\phi_{C_3}\} \cup \{\phi_{C_4}\} \cup \{\phi_{C_5}\} \cup \{\phi_{C_6}\} \cup \{\phi_{C_7}\} \cup \{\phi_{C_8}\} \cup \{\phi_{C_9}\} \cup \{\phi_{R_1}\} \cup \{\phi_{R_2}\} \cup \{\phi_{R_3}\} \cup \{\phi_{R_4}\} \cup \{\phi_{R_5}\} \cup \{\phi_{R_6}\} \quad (2)$$

$\phi_b \in \Re^{n_e}$, n_e : is the total number of the power bonds in the Bond Graph elements, R, C and I.

9. The Measurements Model

It describes available measurements on the Bond Graph model. This model expresses the way in which the sensors transform the state variables of the process into output signals which can be used in the laws development of order and in the failures detection and insulation. In Bond Graph model the sensors are represented by effort and flow detectors (De and Df).

$$\phi_m = \{\phi_{De_1}\} \cup \{\phi_{De_2}\} \cup \{\phi_{De_3}\} \cup \{\phi_{De_4}\} \cup \{\phi_{De_5}\} \cup \{\phi_{De_6}\} \cup \{\phi_{De_7}\} \cup \{\phi_{De_8}\} \cup \{\phi_{De_9}\} \cup \{\phi_{Df_1}\} \cup \{\phi_{Df_2}\} \cup \{\phi_{Df_3}\} \cup \{\phi_{Df_4}\} \cup \{\phi_{Df_5}\} \cup \{\phi_{Df_6}\} \quad (3)$$

n_s : is the number of detectors (or sensors).

9.1. Model of the command algorithms ϕ_C :

It describes the command algorithms in which the entries of the regulators are the values of the instructions and sensors measurement. The regulators output operate the actuators represented by modulated sources of effort or flow. Contrary to the structural and behavior equation which uses the variables of power effort flow like variables of output input, the command and measurement laws use the information signals.

$$\phi_C = \{u\_ref, y_m, \theta_{reg}\} \quad (4)$$

9.2. Model of the controlled sources ϕ_A :

These models describe the controlled or modulated energy sources by the control signals (controlled pump, control tension ...).The input signals U are provided by the regulators and the output signals are the controlled variables MSe and MSf.

$$\phi_{A1}(MSf, u) = 0, \phi_{A2}(MSe, u) = 0 \quad (5)$$

The constraints whole ϕ apply to the variables whole Z: known (K) and unknown factors (X).

$$Z = X \cup K \quad (6)$$

The unknown variables X are the variables of power (flow and effort) supported by the power bonds of the Bond Graph model. Vector X container all the power variables is:

$$X = \{e_1(t), f_1(t)\} \cup ... \cup \{e_{nc}(t), f_{nc}(t)\} \quad (7)$$

The unknown variables of our example are the effort and flow variables of the power bonds in Bond Graph model.

$$X = \{e_{10}(t), f_{10}(t)\} \cup \{e_{17}(t), f_{17}(t)\} \cup \{e_{24}(t), f_{24}(t)\} \cup \{e_{43}(t), f_{43}(t)\} \cup \{e_{47}(t), f_{47}(t)\} \cup \{e_{55}(t), f_{55}(t)\} \cup \{e_{72}(t), f_{72}(t)\} \cup \{e_{65}(t), f_{65}(t)\} \cup \{e_{67}(t), f_{67}(t)\} \cup \{e_9(t), f_9(t)\} \cup \{e_{26}(t), f_{26}(t)\} \cup \{e_{23}(t), f_{23}(t)\} \cup \{e_{32}(t), f_{32}(t)\} \cup \{e_{40}(t), f_{40}(t)\} \cup \{e_{50}(t), f_{50}(t)\} \quad (8)$$

The subset K of the known variables contains the sources values, the regulators output and the measured variables by the sensors.

$$K = MSe \cup MSf \cup Se \cup Sf \cup \phi_m \quad (9)$$

For the Bond Graph model of our application:

$$K = \{Sf_{48}\} \cup \{Sf_{54}\} \cup \{Sf_{71}\} \cup \{Sf_{73}\} \cup \{Sf_{74}\} \cup \{Sf_{66}\} \cup \{Sf_{68}\} \cup \{De_1\} \cup \{De_2\} \cup \{De_3\} \cup \{De_4\} \cup \{De_5\} \cup \{De_6\} \cup \{De_7\} \cup \{De_8\} \cup \{De_9\} \cup \{Df_1\} \cup \{Df_2\} \cup \{Df_3\} \cup \{Df_4\} \cup \{Df_5\} \cup \{Df_6\} \quad (10)$$

$\theta \in \Re^p$: is the parameters vector.

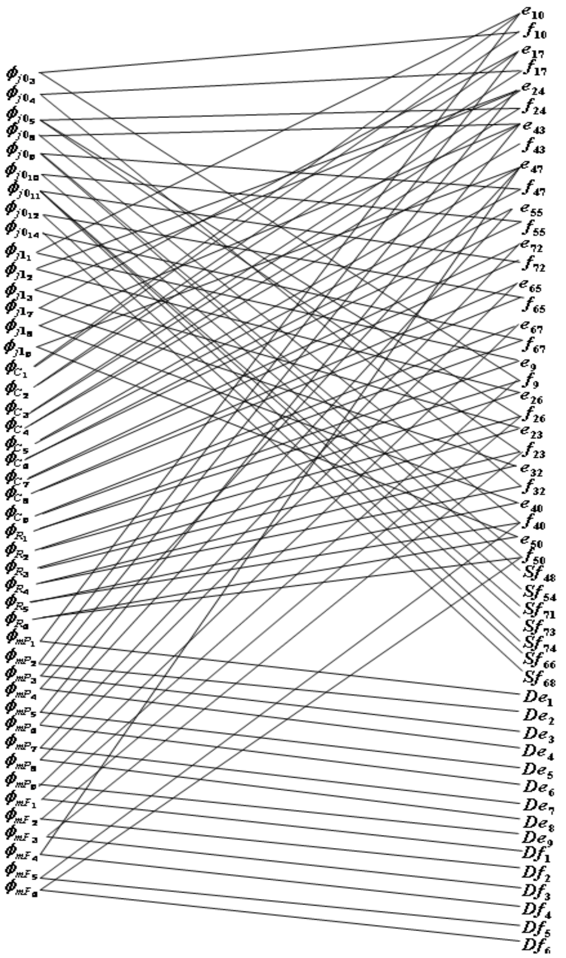

Figure 3. Analyze of Bond Graph model.

10. Adjustment in Steam Generator

The temperature in the boiler varies exponentially according to time because the phenomenon of energy storage with t=1.53s. The temperature becomes stable what carries out the system in a state of permanent balance then the temperature is equal to 300°C (see figure 4).

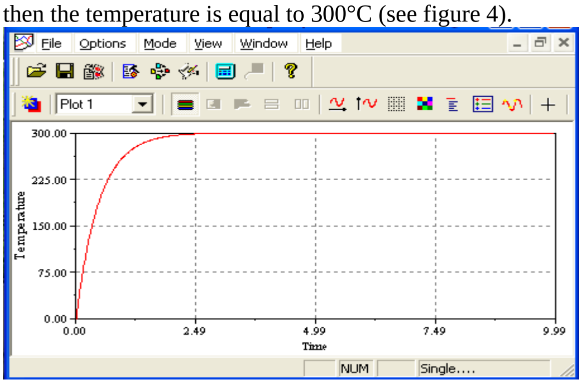

Figure 4. Variation in the temperature according to time in Steam Generator.

Heat is transferred from the nuclear boiler (primary circuit) towards the secondary circuit comprising the turbine via several steam generators and this in the enclosure of the reactor. The steam produced at output of the generators has the temperature is equal to 270°C. The regulator is a PID type (Proportional Integral and Derived). Its adjustments are variable according to the water alimentation temperature. For adapting the regulator to the process characteristics, variables are loaded (figure 5).

The measurement of the steam flow is added on the outlet side of the regulator to constitute the instruction of food water flow. That makes it possible to pre-empt the regulator response at the time of the flow steam transient. Finally, the regulation comprises a control of water flow.

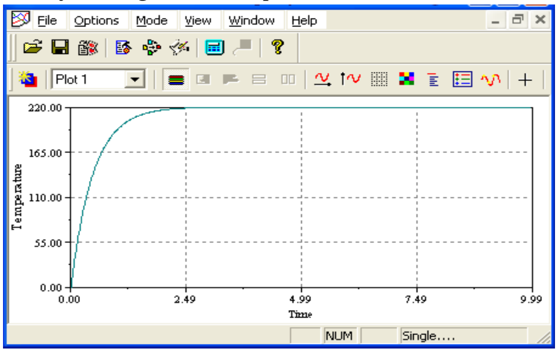

Figure 5. Temperature variation according to time at output of steam generator.

11. Adjustment of mass throughput:

The enthalpy grows exponentially according to time because the influence of the thermal power which provided calorific energy to the boiler and at the moment t=7.5s the mass throughput becomes stable and is equal to 60000 m3/h and according to the temperature stability (figure 6).

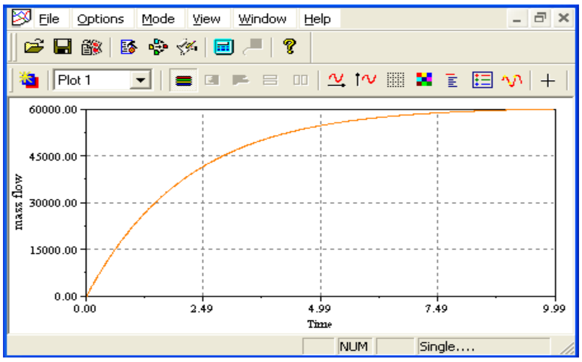

Figure 6. Variation of mass throughput according to time in steam generator.

The total mass in the boiler varies with time exponentially and evolves without stop, which is in conformity with the operation of such a process when it is not controlled.

This phenomenon is explained by the fact why the mass accumulates in the tank and thus increases as much as the alimentation is provided. The adjustment of the temperature in the reactor heart is that the coolant temperature varies exponentially with time up to the end value 320°C at the moment t=5s and remains invariant (permanent mode).

The variation in the temperature i.e. the adjustments are variable in order bars, to adapt the temperature value to the process characteristics which varies in function of the load (see figure 7).

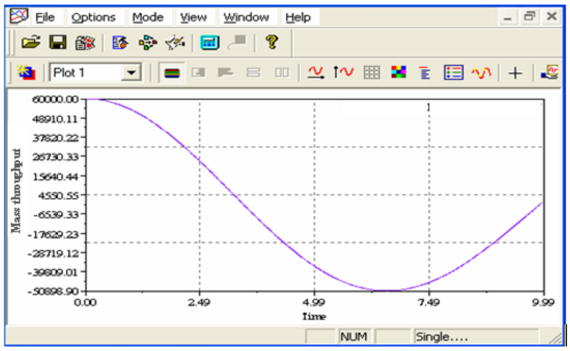

Figure 7. Mass throughput variation according to time at steam generator output

The temperature measurement is made using sensor placement on the level of the reactor heart and its role is to check the temperature value at every moment thus it plays a fundamental role on the control rods movement, otherwise the input and output speed is dregs with the temperature and pressure values (see figure 8).

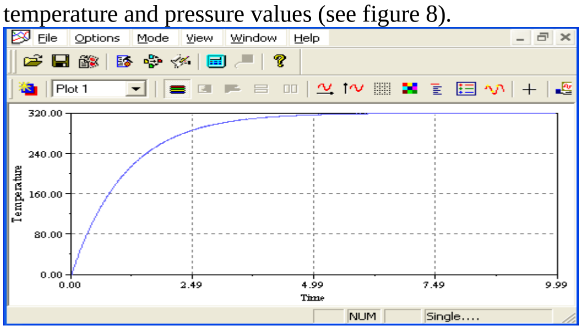

Figure 8. Temperature variation in the reactor heart

12. Adjustment of The Pressure in The Reactor Heart

The pressure varies in the heart of almost linear reactor according to time to 75 bars at the moment 10s (see figure 9). The pressure adjustment of heart consists generally with the introduction of the bars which influences directly on the pressure and the temperature values. The variation of the function of pressure binds to the variation in the temperature i.e. when the temperature also increases the pressure increases.

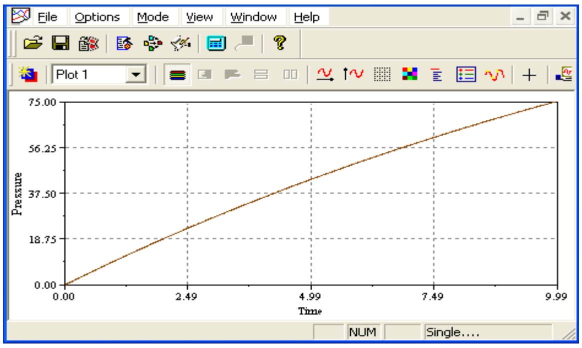

Figure 9. Pressure variation in the reactor heart

13. Power Instantaneous

The instantaneous adjustment of the power consists generally with the introduction of the rigging bars. These rigging bars have as common property which is made of a material strongly absorbing for the neutrons like Bore, Cadmium, Argent or Indium. The physical form can be different; we know for example, needles and plates. According to the aim, we also make the distinction between scram rods, control rods and bars of fine adjustments.

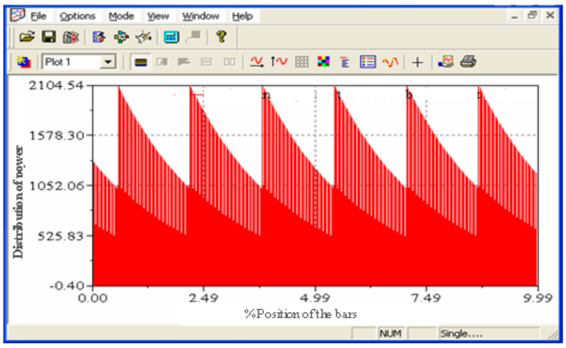

(a)

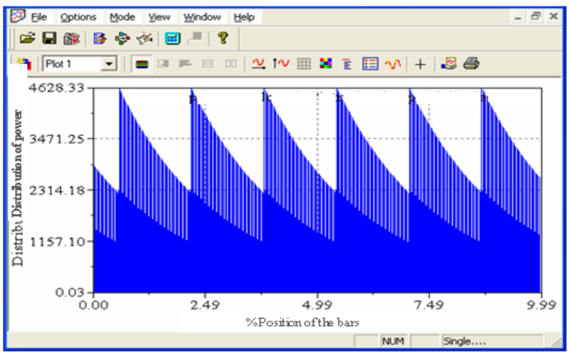

(b)

Figure 10 (a, b). Disturbance of the inflow distribution by the rigging bars

The scram rods are left the engine, in normal operating time and will not be released in the event of urgency to decrease the reactivity and to reduce the power. The control rods are used in normal operating time to obtain transients which are necessary to the starting to the stop and to the stabilization at the desired level.

Moreover, the bars of fine adjustments can be used to maintain the power stable at the level wished without having to use the control rods. The introduction of the control rods involves a deformation of flow owing to the fact that locally more neutrons are absorbed. Figure 10 shows how the distribution of inflow is disturbed by the introduction of an absorbing rigging bar.

14. Reactivity

Figure 11 illustrates the flow radial distribution up to what point is disturbed by the rigging bars introduction. The reactivity change introduced by the fact of inserting or of withdrawing an absorbing bar is depend on the position of the rigging bar.

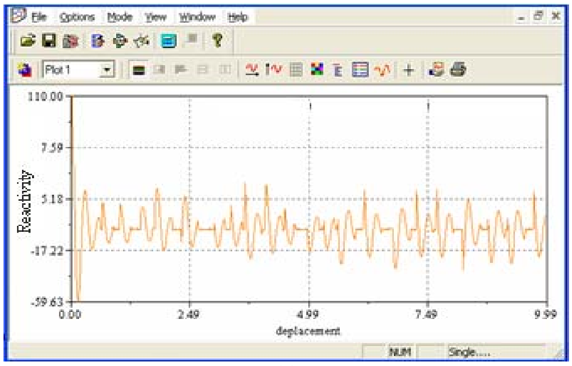

(a)

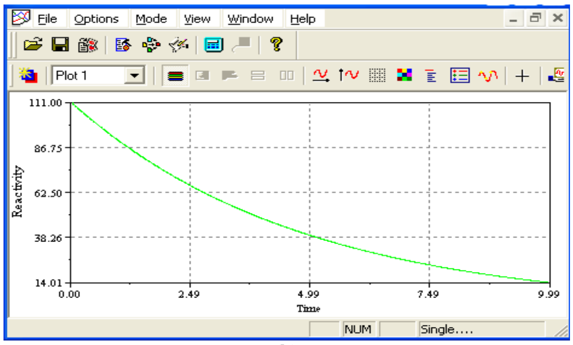

(b)

Figure 11(a, b). Disturbance of the flow radial distribution by absorbing bar

When the rigging bar is located at the core periphery of the reactor. The impact is weaker than when the bar is in the centre of the heart. The relative impact of the rigging bars according to the position is highlighted with the differential effectiveness illustrated in Figure 12.

When we trace the total negative reactivity introduced by the absorbing bars according to the position of the rigging bars, we obtain the integral effectiveness as shown with the following Figure (see figure 13).

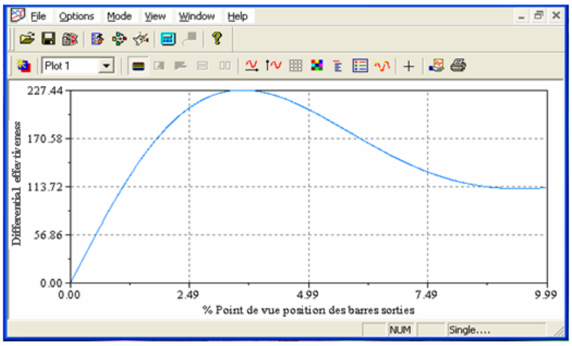

Figure 12. Differential effectiveness of a rigging bar.

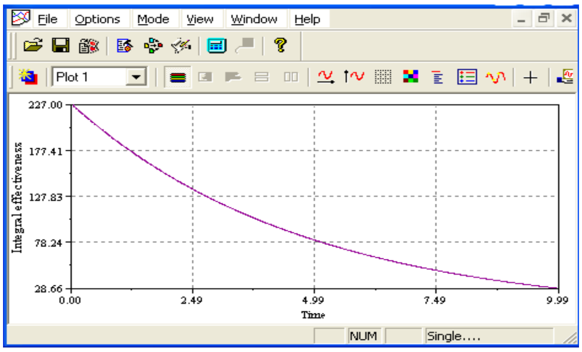

Figure 13. Integral effectiveness of a rigging bar.

15. Adjustment of The Pressure

The pressure is regulated in the pressurisor using valves of sprinkling, connected to the cold branches of the primary circuit, foot-warmers with action proportional and foot-warmers to action all or nothing. The measured pressure is compared with a fixed set point. This variation enters a regulator which orders, with various programs, the valves of sprinkling, the foot-warmers with action proportional and action all or nothing. In the event of excessive increase in the pressure, three spill valves intervene. The openings of those, spread out, are ordered directly, without forwarding by the closed loop.

The curve representing the pressure follows an exponential law according to time checks the empirical equation, this variation is due to accumulate matter in the steam generator which makes increased the pressure up to value 155 bars i.e. 155.105 Pa (see figure 14).

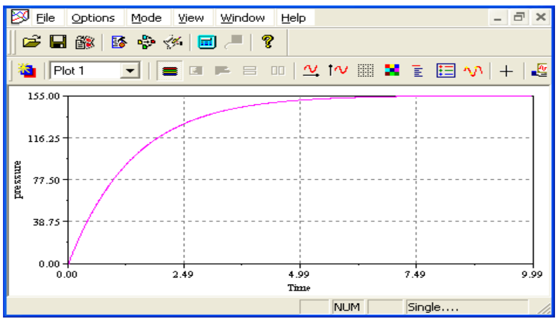

Figure 14. Variation of the pressure according to time.

The temperature of the output steam of steam generator decreases from 155 bars which is the steam pressure produced by the steam generator until-133.68 bars at the moment t=5.92s then augment according to time up to 55 bars at the moment t=10s and as from this moment the value of pressure remains invariant (figure 15).

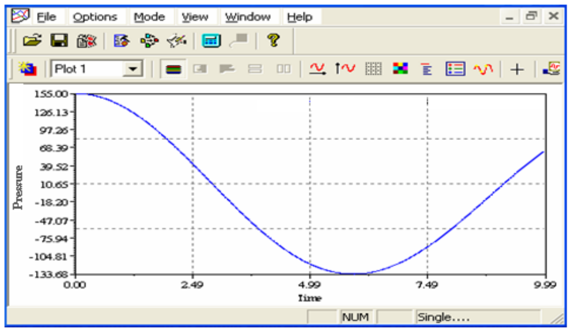

Figure 15. Variation of the pressure according to time at steam generator output.

16. Monitoring of Nuclear

We suppose that sensors and sources are not affected by faults [12]. For our application, the equations in junctions are given by:

For 0i junction we have

$$\begin{cases} e_4 - e_8 - e_9 = 0 \\ f_9 = f_8,\ f_9 = f_4 \\ e_{R1} = e_9 = \phi_{R1}\left[(1-y_1)f_9 + y_1 Df_1\right] \\ f_{R1} = f_9 = (1-y_1)\phi_{R1}^{-1}(e_9) + y_1 Df_1 \end{cases} \tag{11}$$

For 1j junction we have

$$\begin{cases} e_{10} = e_8,\ e_{10} = e_{11},\ e_{10} = e_{12} \\ f_8 - f_{10} - f_{11} - f_{12} = 0 \\ e_{C1} = e_{10} = \dfrac{1}{s}(1-x_1)\phi_{C1}^{-1}(f_{10}) + x_1 De_1 \\ f_{C1} = f_{10} = \phi_{C1}\left[s\{(1-x_1)e_{10} + x_1 De_1\}\right] \end{cases} \tag{12}$$

For TF_k junction we have

$$\begin{cases} e_{52} = \dfrac{1}{m} e_{39} \\ f_{39} = \dfrac{1}{m} f_{52} \end{cases} \tag{13}$$

17. Analytical Redundancy Relations

Analytical redundancy relations (ARR) are symbolic equations representing constraints between different known process variables (parameters, measurements and sources).

ARR are obtained from the behavioral model of the system through different procedures of elimination of unknown variables [13]. Numeric evaluation of each ARR is called a residual, which is used in model based fault detection and isolation (FDI) algorithms [14].

From equations of junctions we obtain the following system:

$$r_1: msf_1 + msf_2 - \overset{*}{Df}_1 - (1-y_1)\phi_{R1}^{-1}(e_9) - (1-y_2)\phi_{R2}^{-1}(e_{26}) + y_2Df_2 - \overset{*}{Df}_2 + y_1Df_1 = 0$$

$$r_2: \phi_{R1}\left[(1-y_1)f_9 + y_1Df_1\right] - \phi_{R1}[(1-y_1)f_9 + y_1Df_1] - \frac{1}{s}(1-x_1)\phi_{C1}^{-1}(f_{10}) + \phi_{C4}[s\{(1-x_4)e_{47} + x_4De_4\}] + x_1De_1 = 0$$

$$r_3: sf_{51} + (1-y_6)\phi_{R6}^{-1}(e_{50}) + y_6Df_6 - \overset{*}{Df}_3 = 0$$

$$r_4: \phi_{R2}\left[(1-y_2)f_{26} + y_2Df_2\right] + msf_1 + \frac{1}{s}(1-x_3)\phi_{C3}^{-1}(f_{24}) + x_3De_3 = 0$$

$$r_5: -\phi_{C1}\left[s\{(1-x_1)e_{10} + x_1De_1\}\right] - (1-y_1)\phi_{R1}^{-1}(e_9) + y_1Df_1 - \overset{*}{Df}_4 - \overset{*}{Df}_5 = 0$$

$$r_6: -\phi_{R3}\left[(1-y_3)f_{23} + y_3Df_3\right] + \frac{1}{s}(1-x_3)\phi_{C3}^{-1}(f_{24}) + x_3De_3 - \overset{*}{De}_1 = 0$$

$$r_7: -\phi_{C2}\left[s\{(1-x_2)e_{17} + x_2De_2\}\right] - (1-y_4)\phi_{R4}^{-1}(e_{32}) - \overset{*}{Df}_6 - \overset{*}{Df}_7 + y_4Df_4 = 0$$

$$r_8: msf_{27} - \overset{*}{Df}_8 - \overset{*}{De}_2 = 0$$

$$r_9: -\phi_{C3}\left[s\{(1-x_3)e_{24} + x_3De_3\}\right] - (1-y_3)\phi_{R3}^{-1}(e_{23}) - (1-y_2)\phi_{R2}^{-1}(e_{26}) + y_2Df_2 - \overset{*}{Df}_9 + y_3Df_3 = 0$$

$$r_{10}: \overset{*}{De}_2 - \overset{*}{De}_3 - \overset{*}{De}_4 = 0$$

$$r_{11}: -\overset{*}{Df}_{10} + (1-y_4)\phi_{R4}^{-1}(e_{32}) + y_4Df_4 + msf_{33} - \overset{*}{Df}_{11} = 0$$

$$r_{12}: \overset{*}{De}_4 - \overset{*}{Df}_{12} - \overset{*}{De}_5 = 0$$

$$r_{13}: -\overset{*}{Df}_{13} + msf_{36} - (1-y_5)\phi_{R5}^{-1}(e_{40}) + y_5Df_5 - \frac{1}{m}((1-y_5)\phi_{R5}^{-1}(e_{40}) + y_5Df_5) = 0 \qquad (13)$$

$$r_{14}: -\phi_{R4}\left[(1-y_4)f_{32} + y_4Df_4\right] + x_2De_2 - msf_{33} + \frac{1}{s}(1-x_2)\phi_{C2}^{-1}(f_{17}) = 0$$

$$r_{15}: -\phi_{C5}\left[s\{(1-x_5)e_{43} + x_5De_5\}\right] + (1-y_5)\phi_{R5}^{-1}(e_{40}) - \overset{*}{Df}_{14} + y_5Df_5 = 0$$

$$r_{16}: -\phi_{R5}\left[(1-y_5)f_{40} + y_5Df_5\right] + msf_{36} + x_5De_5 - \frac{1}{m}msf_{36} + x_6De_6 - \frac{1}{s}(1-x_5)\phi_{C5}^{-1}(f_{43}) - \frac{1}{s}(1-x_6)$$
$$\phi_{C6}^{-1}(f_{55}) = 0$$

$$r_{17}: -\phi_{C5}\left[s\{(1-x_5)e_{43} + x_5De_5\}\right] - \overset{*}{Df}_{15} + sf_{48} + y_6Df_6 - (1-y_6)\phi_{R6}^{-1}(e_{50}) = 0$$

$$r_{18}: -\phi_{R6}\left[(1-y_6)f_{50} + y_6Df_6\right] - sf_{51} + x_4De_4 + \frac{1}{s}(1-x_4)\phi_{C4}^{-1}(f_{47}) = 0$$

$$r_{19}: -\phi_{C6}\left[s\{(1-x_6)e_{55} + x_6De_6\}\right] + sf_{54} + y_5Df_5 - \overset{*}{Df}_{15} - \frac{1}{m}\overset{*}{Df}_{16} + (1-y_5)\phi_{R5}^{-1}(e_{40}) = 0$$

$$r_{20}: \phi_{R5}\left[(1-y_5)f_{40} + y_5Df_5\right] + \frac{1}{m}msf_{39} + x_6De_6 - \frac{1}{s}(1-x_6)\phi_{C6}^{-1}(f_{55}) = 0$$

$$r_{21}: -\phi_{C7}\left[s\{(1-x_7)e_{72} + x_7De_7\}\right] - \overset{*}{Df}_{17} + sf_{71} + sf_{73} + sf_{74} = 0$$

$$r_{22}: -\frac{1}{r}\left(\frac{1}{s}(1-x_6)\phi_{C6}^{-1}(f_{55}) + x_6De_6\right)l(\frac{1}{s}(1-x_9)\phi_{C9}^{-1}(f_{67}) + k(\frac{1}{s}(1-x_8)\phi_{C1}^{-1}(f_{65}) + x_8De_8) - \overset{*}{Df}_{16} + \frac{1}{h}sf_{76}$$
$$+ x_9De_9) - = 0$$

$$r_{23}: k\,\overset{*}{Df}_{16} - \phi_{C8}\left[s\{(1-x_8)e_{65} + x_8De_8\}\right] + sf_{66} = 0$$

$$r_{24} : -\overset{*}{Df}_{18} - \frac{1}{h}\overset{*}{Df}_{16} + sf_{76} + sf_{77} = 0$$

$$r_{25} : k\,\overset{*}{Df}_{16} - \phi_{C9}\left[s\{(1-x_9)e_{67} + x_9 De_9\}\right] + sf_{68} = 0$$

From the binary variables x_i (i=1, 14) and y_j (j=1, 11) we can determine the final structure of the monitorable system. 25-sensor placement combinations provide the monitorability of the all components. The question arises whether we are able to supervise this system by only (15) sensors? And what are the combinations which provide this result?

$For\ [x_1 y_1 x_2 y_2 x_3 y_3 x_4 y_4 x_5 y_5 x_6 y_6 x_7 y_7 x_8 y_8 x_9 y_9\ x_{10} y_{10} x_{11} y_{11} x_{12} x_{13} x_{14}] = [1111111111\quad 111111111\ 111111\quad]$

Table 2: Fault signature table

The fault signatures (table 3) are different from each other and not equal to zero, then the components C_1, C_2, C_3, C_4, C_5, C_6, C_7, C_8, C_9, R_1, R_2, R_3, R_4, R_5 and R_6 are monitorable.

Table 2. Fault signature table.

	C_1	C_2	C_3	C_4	C_5	C_6	C_7	C_8	C_9	R_1	R_2	R_3	R_4	R_5	R_6
r_2	0	0	0	1	0	0	0	0	0	1	0	0	0	0	0
r_4	0	0	0	0	0	0	0	0	0	0	1	0	0	0	0
r_5	1	0	0	0	0	0	0	0	0	0	0	0	0	0	0
r_6	0	0	0	0	0	0	0	0	0	0	0	1	0	0	0
r_7	0	1	0	0	0	0	0	0	0	0	0	0	0	0	0
r_9	0	0	1	0	0	0	0	0	0	0	0	0	0	0	0
r_{14}	0	0	0	0	0	0	0	0	0	0	0	0	1	0	0
r_{15}	0	0	0	0	1	0	0	0	0	0	0	0	0	0	0
r_{16}	0	0	0	0	0	0	0	0	0	0	0	0	0	1	0
r_{17}	0	0	0	0	1	0	0	0	0	0	0	0	0	0	0
r_{18}	0	0	0	0	0	0	0	0	0	0	0	0	0	0	1
r_{19}	0	0	0	0	0	1	0	0	0	0	0	0	0	0	0
r_{20}	0	0	0	0	0	0	0	0	0	0	0	0	0	1	0
r_{21}	0	0	0	0	0	0	1	0	0	0	0	0	0	0	0
r_{23}	0	0	0	0	0	0	0	1	0	0	0	0	0	0	0
r_{25}	0	0	0	0	0	0	0	0	1	0	0	0	0	0	0

$For[x_1 y_1 x_2 y_2 x_3 y_3 x_4 y_4 x_5 y_5 x_6 y_6 x_7 y_7 x_8 y_8 x_9 y_9\ x_{10} y_{10} x_{11} y_{11} x_{12} x_{13} x_{14}] = [0111011010\,0001111\ 11110101]$

It is noticed that the structures of the residuals are different but fault signatures are not different [(C_4 and R_2), (C1 and R_1)] and not equal to zero.

Thus the components C_1, C_4, R_1 and R_2 are not monitorable. And the components C_2, C_3, C_5, C_6, C_7, C_8, C_9, R_3, R_4, R_5 are monitorable (table 3).

Table 3. Fault signature table

	C_1	C_2	C_3	C_4	C_5	C_6	C_7	C_8	C_9	R_1	R_2	R_3	R_4	R_5	R_6
r_1	1	0	0	0	0	0	0	0	0	1	0	0	0	0	0
r_2	0	0	0	0	0	0	0	0	0	0	0	0	0	0	1
r_3	0	0	0	0	0	0	0	0	0	0	0	0	0	0	1
r_4	0	0	1	0	0	0	0	0	0	0	0	1	0	0	0
r_5	0	1	0	0	0	0	0	0	0	0	0	0	1	0	0
r_6	0	0	1	0	0	0	0	0	0	0	0	0	0	0	0
r_7	0	0	0	0	0	0	0	0	0	0	0	0	1	0	0
r_8	0	0	0	0	1	0	0	0	0	0	0	0	0	1	0
r_9	0	0	1	0	0	1	0	0	0	0	0	0	0	1	0
r_{10}	0	0	0	0	1	0	0	0	0	0	0	0	0	0	0
r_{11}	0	0	0	0	0	0	0	0	0	0	0	0	0	0	1
r_{12}	0	0	0	0	0	1	0	0	0	0	0	0	0	1	0
r_{13}	0	0	0	0	0	1	0	0	0	0	0	0	0	1	0
r_{14}	0	0	0	0	0	0	1	0	0	0	0	0	0	0	0
r_{15}	0	0	0	0	0	0	0	1	0	0	0	0	0	0	0
r_{16}	0	0	0	0	0	0	0	0	1	0	0	0	0	0	0

For $[x_1 y_1 x_2 y_2 x_3 y_3 x_4 y_4 x_5 y_5 x_6 y_6 x_7 y_7 x_8 y_8 x_9 y_9 x_{10} y_{10} x_{11} y_{11} x_{12} x_{13} x_{14}] = [1100110010 \quad 1011101 \quad 11010101 \quad]$

The fault signatures (table 4) are different from each other and not equal to zero, then the components C_1, C_2, C_3, C_4, C_5, C_6, C_7, C_8, C_9, R_1, R_2, R_3, R_4, R_5 and R_6 are monitorable.

Table 4. Fault signature table.

	C_1	C_2	C_3	C_4	C_5	C_6	C_7	C_8	C_9	R_1	R_2	R_3	R_4	R_5	R_6
r_1	1	0	0	0	0	0	0	0	0	1	0	0	0	0	0
r_2	0	0	0	0	0	0	0	0	0	0	0	0	0	0	1
r_3	0	0	0	0	0	0	0	0	0	0	0	0	0	0	1
r_4	0	0	1	0	0	0	0	0	0	0	0	1	0	0	0
r_5	0	1	0	0	0	0	0	0	0	0	0	0	1	0	0
r_6	0	0	1	0	0	0	0	0	0	0	0	0	0	0	0
r_7	0	0	0	0	0	0	0	0	0	0	0	0	1	0	0
r_8	0	0	0	0	1	0	0	0	0	0	0	0	0	1	0
r_9	0	0	0	0	0	1	0	0	0	0	0	0	0	1	0
r_{10}	0	0	0	0	1	0	0	0	0	0	0	0	0	0	0
r_{11}	0	0	0	0	0	0	0	0	0	0	0	0	0	0	1
r_{12}	0	0	0	0	0	1	0	0	0	0	0	0	0	1	0
r_{13}	0	0	0	0	0	1	0	0	0	0	0	0	0	1	0
r_{14}	0	0	0	0	0	0	1	0	0	0	0	0	0	0	0
r_{15}	0	0	0	0	0	0	0	1	0	0	0	0	0	0	0
r_{16}	0	0	0	0	0	0	0	0	1	0	0	0	0	0	0

18. Simulation and Interpretation

From SYMBOLS software, we have implanted the uncoupled Bond Graph model. For the faults detection of the nuclear reactor (PWR) we use the precedent analytical redundancy relations (ARRs). We create the faults on monitoring components with this software fault here is considered in the total absence or the deviation of the nominal value given out by the component to monitor [9].The numeric values of components are not considered, only their presence or absences in the relation are taken in account with evaluation term the operators (+, -). It is the qualitative approach for Bond Graph monitoring [10].

19. Sensitivity of detector De_2:

In the first time, we create a fault between the instant t_1=2s and t_2=4s (figure 16).

These accidents, due to a loss of primary cooling agent via a breach located outside the enclosure, located on a circuit connected to the primary circuit and not isolated from this one, would show two particular characteristics:

- The loss of cooling agent taking place outside the enclosure, the recirculation of the system of injection of safety could prove to be impossible;
- In the event of core fusion, the fission products would be slackened directly outside the containment if the breach could not be insulated.

The rupture of the thermal barrier of the primary pumps can lead, for example, with situations of this type. Under ideal operation, the residuals must be constantly null. The following figures present the evolution of residuals ARR_8, ARR_9, ARR_{10}, and ARR_{11} over duration of 4s corresponding to the equations of redundancy.

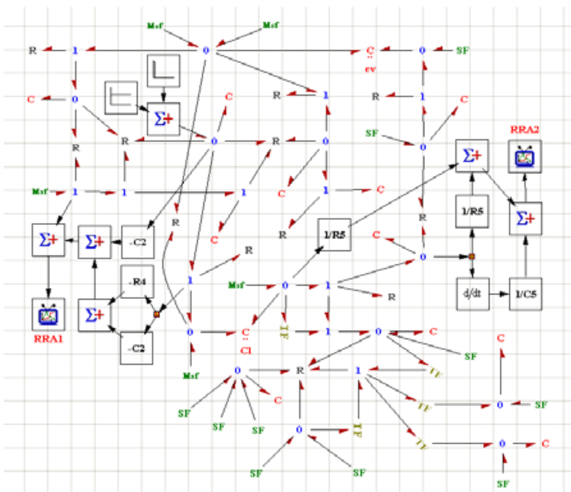

Figure 16. Generated ARR_1 and ARR_2 .

Figure (17) shows the response of the residuals. It is noted that residual ARR_8 presents a short change compared to its initial state between the moments t_1=1.4s and t_2=4s and other residuals ARR_1, ARR_2, ARR_3, ARR_4, ARR_5, ARR_6, ARR_7, ARR_9, ARR_{10}, ARR_{11}, $ARR1_2$, ARR_{13}, ARR_{14} and ARR_{15} remain invariant. If we refer to the signature of the C_2 component given to table 4 we note that this result is in conformity with what is envisaged; i.e. that in the event of failure of the C_2 component only the residual ARR_8 will be sensitive.

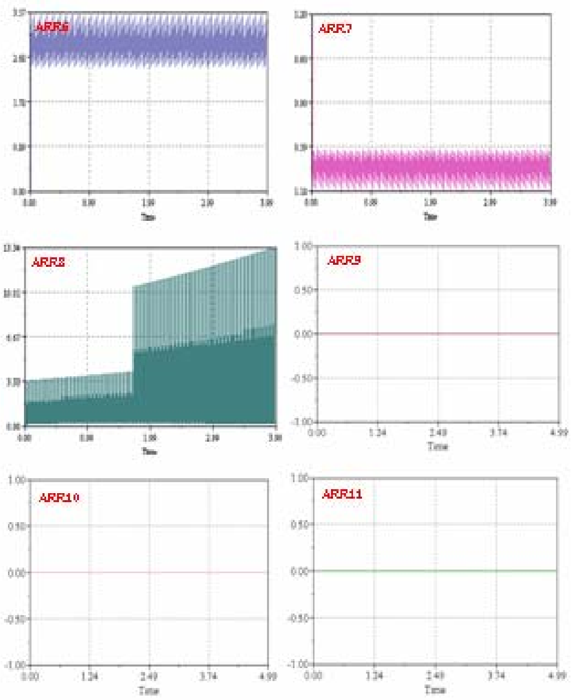

Figure 17. Sensitivity of detector De_2

20. Sensitivity of detector Df_2:

The generated ARRs reaction is very fast see Figure 18.

The deviation of the relations ARR_2,ARR_3, ARR_4, ARR_6, ARR_7, ARR_8, ARR_9, ARR_{10}, ARR_{11}, ARR_{12}, ARR_{13}, ARR_{14} and ARR_{15} in this time are normal (i.e. with constant value). We see that residuals ARR_1 and ARR_5 are sensitive to the failure due to the presence of Df_2 in these relations (see figure 19).

21. Conclusion

The modeling of pressurized nuclear reactor was realized and validated by Software SYMBOLS that is very adapted to the simulation of our problem. Bond graph is very powerful tool of research and recommended for the use of the great industrial systems. The supervision is assured by sensors placement algorithm which has permitted us to generate ARR and fault signature tables for detection and isolation analysis of optimal case.

The method used illustrates the process principle working. We have using the structural junction equations for generating the analytical redundancy relations like failures indicators. The Bond Graph tool is the unified modeling method and it facilitates the functional and structural analysis of the complex systems. The found results proved to be interesting because the found curves reveal a similarity between the found results and the results expected (real) in the specifications.

A method has been demonstrated for detecting faults in complex control systems, by dividing the complete system into simpler subsystems.

Weak coupling between subsystems may be allowed if the resulting errors are small.

The different residuals should be designed to facilitate simple fault diagnosis logic, each using as few measured signals as possible.

The number of possible diagnoses is limited by the number of independent residuals designed, which in turn depends on the number of available measurements.

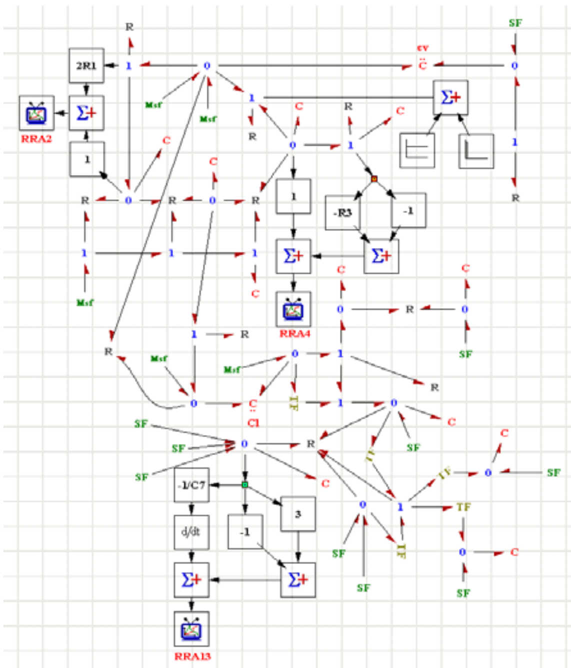

Figure 18. Generated ARR_2, ARR_4 and ARR_{11} .

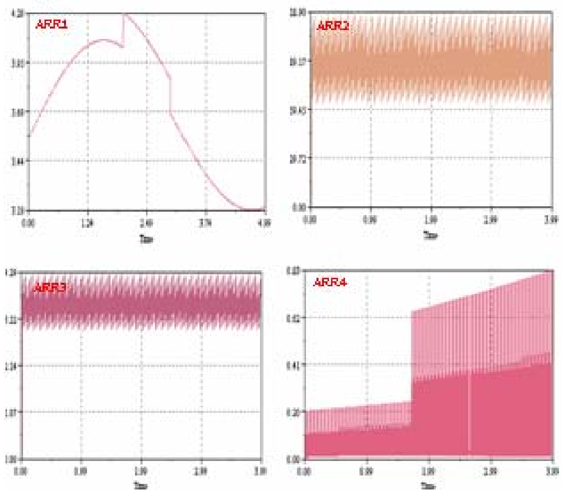

Figure 19. Sensitivity of the detector Df_2.

Acknowledgment

The authors would like to thank Mr HATTI Mustapha professor in the Birine nuclear research center for useful discussions. Research reported in this manuscript was conducted at the automation Laboratory of Setif - 19000 Algeria.

References

[1] G. Slama, « Steam generator maintenance and replacement», 11ème congrès international des centrales électriques Liège, 20-24 Novembre 1993.

[2] N. Suda, T. Hatanaka, «Structural properties of systems represented by bond graphs, in C. & D. Systems». Analysis, Simulation & Control, Congrès IMACS, 1986, 73-80.

[3] P. Ballé, D. Fussel, O. Hetecker, « Detection and isolation of sensor faults on nonlinear processes based on local linear models". In: American Control Conference ACC. Albuquerque, USA, 1997. 468–472.

[4] J.J. Duderstadt et L. Hamilton, Nuclear Reactor Analysis, New York, John Wiley & Sons, Inc. 1976.

[5] J.D. Ladonchamps, J.J. Verdeau, « Réacteurs nucléaires a eau pressurisée : théorie, technologie et applications a la propulsion navale». Masson Cie éditeurs, 1972

[6] M. Vergé, D. Jaume, "Modélisation structurée des systèmes avec les Bond Graphs". Editions TECHNIP 2004.

[7] A. Rahmani, C. Sueur, G. Dauphin-Tanguy, «A new transfer matrix formal determination from bond graph models », 14th IMACS World Congress, School of Mathematics, Georgia Institute of Technology, Atlanta, Juillet 1994.

[8] J. Thoma, B. O. Bouamama, "Modélisation et simulation des processus thermiques et chimiques". Application des bond Graphs en génie des procédé. Juillet 1998.

[9] A. C. Bell, H. R. Martens, "A comparison of linear graphs and bond graphs in the modeling process". Automatic Control Conference, 1974.

[10] C. Olivier, R. Claudine, "Théorie des graphes, problèmes, théorèmes, algorithms". Ed. Vuibert, 2004.

[11] Diestel R. Graph Theory. Third Edition, Springer-Verlag; 2005.

[12] M. Khemliche, B. Ould Bouamama, H. Haffaf, "Sensors and actuators". Journal sensors placement for diagnosability on Bond Graph model, Vol. 4, 2006, 92-98.

[13] A.K. Samantaray, K. Medjaher, B. Ould Bouamama, M. Staroswiecki, G. Dauphin-Tanguy, "Diagnostic bond graphs for online fault detection and isolation". Simulation Modelling Practice and Theory Journal, July 2005, 237–262.

[14] R. M. Alaoui, " Maître IEEA, Conception d'un module de diagnostic a base des suites de bandes temporelles en vue de la super vision des procèdes énérgitique". Application en ligne à un générateur de vapeur', Thèse de doctorat, Université des sciences et technologie de Lille, France, Novembre 2004.

JJMIE

Volume 4, Number 2, March. 2010
ISSN 1995-6665
Pages 246 - 255

Jordan Journal of Mechanical and Industrial Engineering

Abrasive Wear of Continuous Fibre Reinforced Al And Al-Alloy Metal Matrix Composites

Ramadan J. Mustafa *

Faculty of Engineering, Mu'tah University,Karak, Jordan.

Abstract

The abrasive wear testing of continuous ceramic fibre reinforced Al and Al-alloy matrix composites is proven difficult due to inherent complexity of the many wear processes, compounded by the possible interplay with microstructural variables in Metal matrix composites. This paper reports the results of abrasive wear tests on specimens of continuous Silicon Carbide (SiC) and high strength Carbon (H.S.C) fibres reinforced Al(1100) and Al(6061) matrix materials, with 50-60% fibre volume fraction, and made by matrix fibre coating and hot-consolidation fabrication process. The test results for fibres parallel to the sliding direction of Al2O3 (alumina) abrasive papers with abrasive grit sizes 85 μm to 250 μm, at sliding speeds of 76, 110, 160 and 180 mm/s, and applied load ranging from 5 to 15 kg for a time (t), show that the test can be applied to continuous fibre reinforced metal matrix composites, and their addition has resulted in a large reduction of abrasion rate by a factor of more than ten for such composite materials. Optical and Scan Electron Microscope (SEM) investigation of abraded surfaces and just below surfaces show that the wear resistance of 55% v/o SiC-Al(6061) were higher than that of 55% v/o SiC-Al(1100) composite materials, indicating that matrix ductility and fibre-matrix interfacial strength affect the abrasive wear behaviour of such composites. The important variables of this test were discussed and its usefulness in comparing wear resistant materials is demonstrated.

Keywords: Metal-Matrix Composites; Fibre-Reinforced; Abrasive Wear; Alumina; Scanning Electron Microscope.

1. Introduction

In recent years, commercially pure aluminum and Al-alloy based metal matrix composites (MMC) are gaining wide spread acceptance in several interesting applications such as pistons, connecting rods, microwave filters, vibrator components, contactors, impellers and space structures. These composites possess excellent wear resistance in addition to other superior mechanical properties such as strength, modulus and hardness when compared with conventional alloys, [1-8]. Of all the aluminum alloys, 6061 is quite a popular choice as a matrix material to prepare MMCs owing to its better formability characteristics. MMCs offer considerable potential for enhanced wear resistance, because the hard ceramic reinforcements impede the removal of material from abrading surfaces. Their effect is closely dependent on type and shape of reinforcement, [2, 4, 9-13]. Reinforcement of the Al matrix with discontinuous SiC and H.S.C fibres is more effective than Al2O3 fibres for the improvement of wear resistance due to the high hardness of SiC reinforcement, [2, 10, 11]. However, understanding of their wear characteristics is still far from complete. This is due in part to the inherent complexity of many wear processes, the problem is compounded by a possible interplay with microstructural variables in MMC's, such as fibre content, size, orientation, fibre matrix interfacial strength, etc., which greatly influence wear behaviour when sliding surfaces occur. This brings asperities into repeated contact and possibly tearing some of them away from parent body forming fragments of wear debris, [11, 12]. The rate at which material is removed from the body being considered is described by the basic relationship, [1, 10, 13],

$$V = \frac{KW}{H} S \tag{1}$$

Where V is the volume removed, W is the applied load, S is the sliding distance, H is the hardness of the body, and K is a constant called the dimensionless wear resistance. From this simple relationship MMC's are expected to resist wear better than the corresponding unreinforced matrix, because hard fibre reinforcement normally increases strength and hardness. Recent studies pertinent to wear of MMC's with hard reinforcement [2, 3, 11-14] have reported improved wear resistance for Aluminium in both lubricated and dry conditions, after reinforcement with Al2O3 (Silicon Carbide or Alumina) whiskers or particles. These workers found that the 20% v/o SiCp-Al(2014) composite gave a wear rate lower than that of

* Corresponding Ramadan@mutah.edu.jo

unreinforced matrix, corresponding to a decrease in, K, from 10^{-3} to 10^{-4}. Furthermore, they found that the size and the fibre matrix interfacial strength had a strong effect. Some workers, [4], reported a decrease in wear rate accompanied by an increase in coefficient of friction in their comparison of MMC's with that of unreiforced matrices. The limited published data available, [1-15], indicate that fibres offer little or no improvement in wear resistance than do particles of the same material and size. The literature also indicates that the focus has been centered on processing of MMCs and characterization of mechanical properties of MMCs, and little or no information is available pertinent to the abrasive wear behaviour of continuous fibre reinforced aluminium matrix materials.

In this paper, tests on the abrasive wear behaviour of Al (1100) and Al (6061) matrix materials reinforced with 55-60% v/o of continuous Silicon Carbide (SiC) and high strength Carbon (H.S.C) fibres were carried out, by using results of a collaborative program of study on the abrasive wear behaviour of such composites. The abrasive wear testing was carried out using an abrasive wear tester apparatus Al2O3 (alumina) grit papers. Optical and Scan Electron Microscope (SEM) investigation of worn surfaces were also carried out to understand the mechanism of wear in continuous fibre reinforced composites, a discussion of the variables which may control the usefulness of the test is included.

2. Experimental

The MMC's utilized in this work were manufactured by a process called hot-consolidation of matrix coated fibre for producing continuous fibre reinforced MMC's. The process involves coating continuous fibres, (SiC, and H.S.C, table 1, [16-18]), with sufficient material by drawing a preheated continuous fibre strands through the molten metal of commercially pure aluminium (Al (1100) or Al (6061) alloy, tables 2 and 3, [15]), and using a device that controls the thickness and smoothness of the coating, such that during hot-consolidation of the laid up coated fibres into a composite preform, the coatings deformed and bonded together to form the matrix composite(s). The coating thicknesses, therefore, determine the volume fractions of fibre in the finished MMC, fibre volume fraction (v/o) of 40% to 60% of unidirectional specimens were obtained from this process. Detailed information of the processing conditions can be found in [16]. The type and geometry of the test specimens were dictated by the size and quantity of the fabricated materials plates produced. Using a diamond saw, specimens with dimensions 20 x 10 x 3 mm were then cut from unidirectional material plates.

from at least eight measurements determined on each face that was tested in the wear apparatus. Summary of the hardness values of the composite materials studied are listed in table 4. The mechanical properties of the composites are also shown in table 4, refs. [15-18].

Table 1. Properties of the selected continuous fibre reinforcement, [16-18].

Properties	High strength carbon fibre(H.S.C)	Silicon Carbide fibre (SiC)
Fibre Diameter, µm	7-30	12-20
Density, Mg/ m^3	1.75-1.9	2.5
Young's Modulus, GPa	230-270	190-200
Poisson's Ratio (ν)	0.2	0.25
Tensile Strength, GPa	3-4.8	2.5
Failure Strain, %	1.1	-
Thermal Expansivity, $10^{-6}K^{-1}$	(-0.4)-(-1.2)	4.5
Thermal Conductivity, $Wm^{-1}K^{-1}$	24	-

Table 2. Chemical composition of Al (1100) and Al (6061) matrix materials by weight percentage, [15].

Alloy	Si	Mg	Cu	Ti	Fe	Mn	V	Cr	Zn	Be	Other elements
Al(1100)	0.25	0.05	0.05	---	0.04	0.05	0.05	---	---	---	0.03
Al(6061)	0.76	0.92	0.22	0.1	0.28	0.04	0.01	0.07	0.06	0.003	0.45

Table 3. Mechanical properties of Al (1100) and Al (6061) matrix materials, [15].

Material	E (GPa)	σtensile (MPa)	σyield (MPa)	Strain to failure (%)	Poisson ratio (ν)
Al(1100)	69	90	34	50-70	0.33
Al(6061)	72	310	275	12	0.33

Table 4. The mechanical properties of composites, [15-18].

Material	Tensile Modulus (GPa EII)	Strain To failure (%)	Tensile Strength (σ_{II})(MPa)	Hardness (HV)
unreinforced Al(1100)	35	35	90	54
55% v/o SiC-Al(1100)	126	0.7-0.95	897-1026	92
55 % v/o H.S.C-Al(1100)	165	0.55-0.76	780-856	77
unreinforced Al(6061)	275(at P.S of 0.2%)	12	310	130
55 % v/o SiC-Al(6061)	119-214	0.23	1270-1500	284
55% v/o H.S.C-Al(6061)	102-156	0.2	629-1123	225

Abrasive wear behaviour of the composites was examined by using an abrasive wear tester, schematically shown in Figure 1. The tests were carried out in normal atmospheric conditions (25 ºC, and 40-60% humidity) by applying a load (P) ranging from 5 to 15 kg for a time (t). Abrasive tests were carried out against Al2O3 (alumina) abrasive papers with abrasive grit sizes 85 μm to 250 μm , for a total distance of 33 m at sliding speeds of 76, 110, 160 and 180 mm/s. During the abrasive wear tests, it was ensured that the samples always encountered fresh abrasive particles by allowing the abrasive papers to move perpendicular to the sliding direction. Wear loss of the sample was determined at an interval of 5.5 m, by measuring the weight loss of the composites using an electronic balancing device giving readings up to ±0.1mg. The volumetric wear loss of composites was determined using weight loss divided by density. The volumetric wear rate of composites was obtained using volumetric wear loss divided by sliding distance. Four specimens for every composite material were tested and the average volumetric wear was obtained. After performing the wear tests, worn surfaces and subsurfaces of the composites were examined by JEOL JSM T330 Scan Electron Microscope (SEM) and optical microscope.

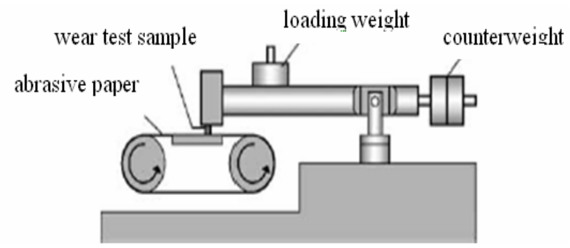

Figure 1. Schematic diagram of abrasive wear testing apparatus.

3. Results and Discussion

The results generated are of enormous amount and only typical results were represented to illustrate the effectiveness of this form of abrasive wear testing. Results of abrasive wear tests conducted on SiC and H.S.C continuous fibre reinforced and unreinforced Al(1100) and Al(6061) matrix materials are shown in Figures (2-8). Figure 2 shows the effect of time on wear volume of a given composite material. The values recorded in this figure with the values of the test conditions load, sliding

speed, and materials hardness were used to calculate the dimensionless wear coefficient (K). Figures 3 to 5 clearly indicate that the wear volumes in the abrasion tests were directly proportional to the time of the test, load applied and speed of sliding. It is evident from these results of the abrasive wear tests that, among the investigated composite materials, minimum wear rate was obtained for SiC and H.S.C continuous fibre reinforced Al(6061) alloy matrix composite. When compared to Al(1100) matrix composites, the wear rate of SiC-Al(6061) alloy matrix composite was about twelve times lower against the alumina abrasive grit size 85 μm and six times lower against 250 μm abrasive. The abrasive wear rate of the reinforced and unreinforced matrix materials also increased with increasing the abrasive Al2O3 particle size (Figure 5). This is in agreement to the observations of previous works [12, 20, 25]. For coarser Al2O3 abrasive particles, the test load is carried by fewer particles in a certain area, which causes a higher contact stress on the tip of coarse abrasive particles than that of fine abrasive particles for the same applied load, (Figure 4.). Accordingly, the increase of wear rate with increased size of abrasive Al2O3 particles is possibly due to the increased depth of penetration causing much damage to intact fibres leading to an increase in the amount of material removal during abrasion tests, [3, 11, 14, 22, 28].

Figure 6 shows that the wear rates are inversely proportional to the hardness of the composite material, and the values of wear coefficient are independent of the hardness of the MMC's under abrasive or abrading particles, as shown in Figure 7. These results indicate that the improvement in wear rates of such composites is accompanied by an increase in fibre matrix interfacial strength and hardness of the composite material, which can be attributed to the fibres remaining intact when struck by asperities or abrading particles. Under such conditions the material would have been ploughed out in the unreiforced material. For reasons of comparison, previous work by, [2, 20-26], on the abrasion rates of two Al-alloy composites reported that the presence of dispersed hard ceramic discontinuous reinforcement has resulted in a decrease of the abrasion rate of these alloys by a factor of five. These results were in close agreement with the results obtained in this research work. The results of abrasion rate presented in Figure 8, show that the presence of continuous ceramic fibre reinforced Al and Al-alloy has also resulted in a large reduction of abrasion rate by a factor of six for SiC-Al(1100) and by a factor of more than ten for SiC-Al(6061) composite materials.

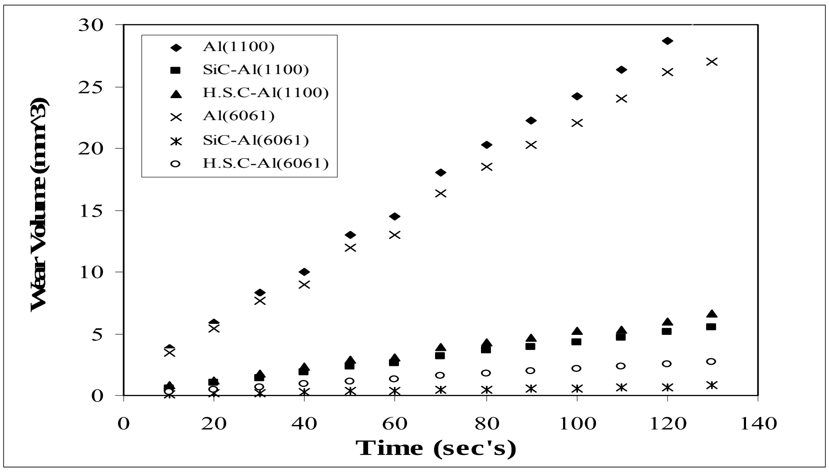

Figure 2. Typical plots of wear volumes versus time to determine wear rates for continuous fibres reinforced and unreinforced Al-matrix composites, with sliding speed 180 mm/s

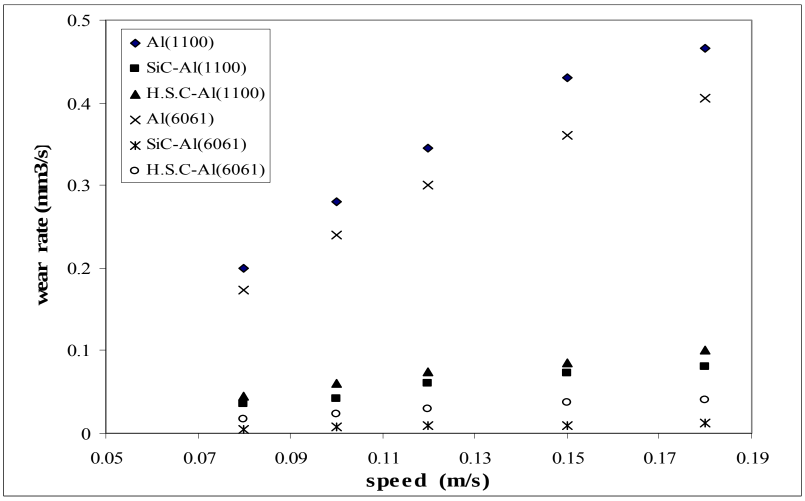

Figure 3. Plots of wear rates versus sliding speed for both continuous fibres Al and Al-alloy matrix composites. With test parameters of; Al2O3 abrasive grit size (250), load 12 kg.

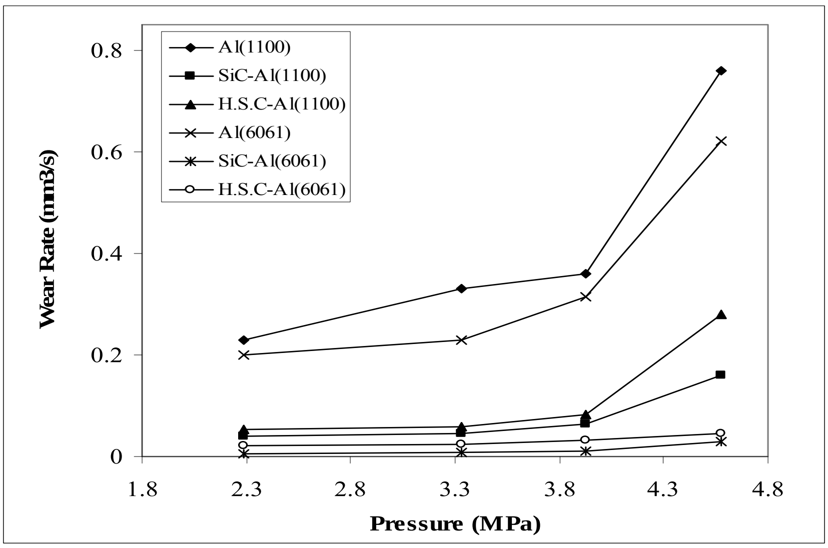

Figure 4. Typical plots of wear rates versus pressure on specimen for both continuous fibres Al and Al-alloy matrix composites. With test parameters of; Al2O3 abrasive grit size (250 μm), sliding speed 180 mm/s.

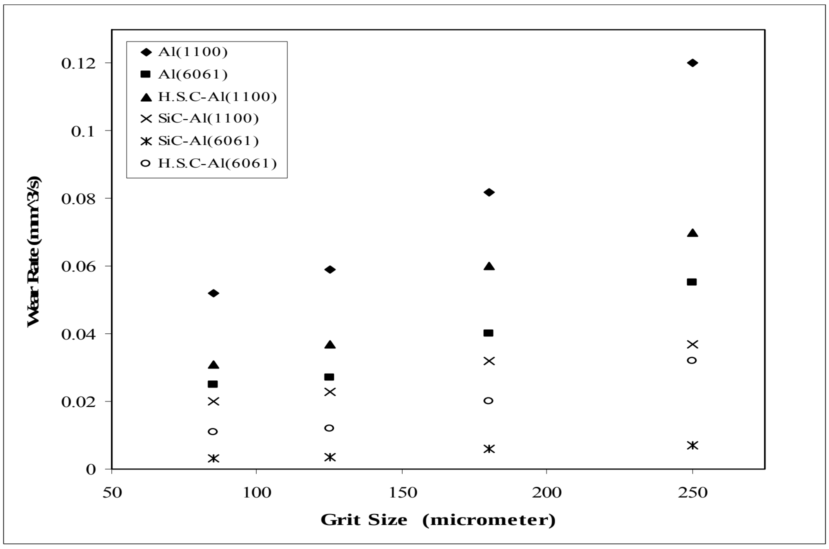

Figure 5. Typical plots of the effect of grit size on wear rates for both continuous fibres Al and Al-alloy matrix composite with test parameters of; load 10 kg, sliding speed 160 mm/s.

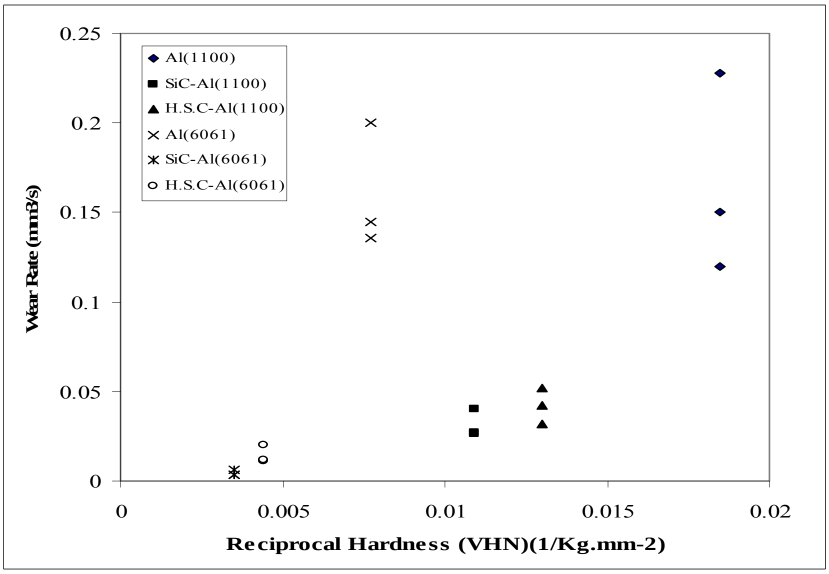

Figure 6. Plots of wear rates versus reciprocal hardness for both Al and Al-alloy matrix composites. With test parameters of; Al2O3 abrasive grit size (250, 180 and 85 μm), load 10 kg, and sliding speed 180 mm/s.

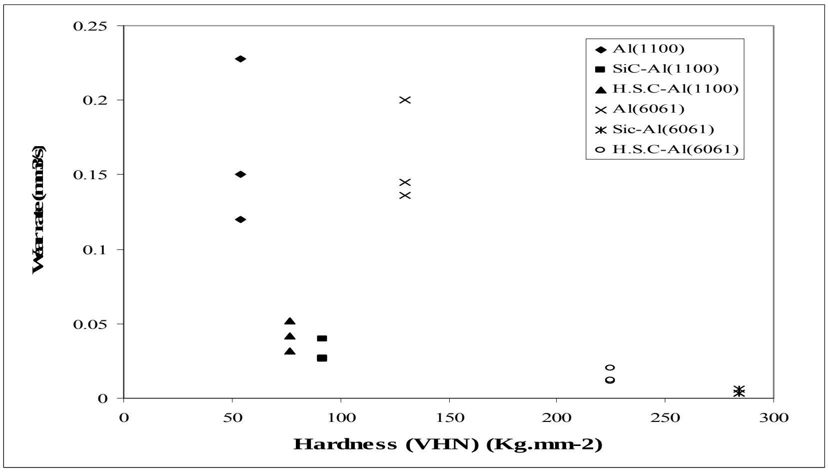

Figure 7. Plots of wear coefficient versus hardness for both Al and Al-alloy matrix composites. With test parameters of; Al2O3 abrasive grit size (250, 180 and 85 μm), load 10 kg, and sliding speed 180 mm/s.

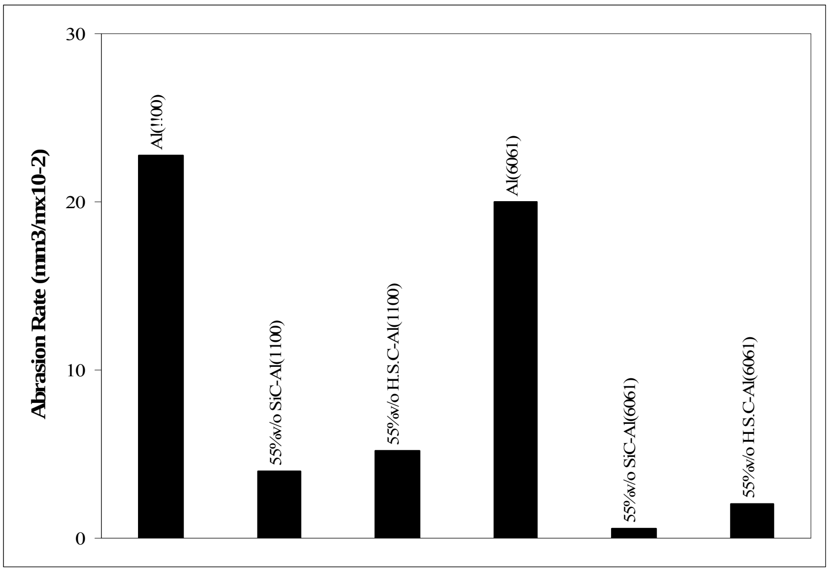

Figure 8. An overall view of, the low stress abrasive wear rates of both continuous fibres Al and Al-alloy matrix composites.

Furthermore, the evidence presented in these Figures (2-8) suggest that under the conditions of these abrasive tests, the simple archard's hypothesis may be used in estimating or predicting the wear rates of composite materials undergoing abrasive wear during service, [25-28]. However, since wear mechanisms in industrial environments are rarely simple, it is possible to assess a group of materials under the same conditions of abrasive wear so that a judgment can be made on the possible relative behaviour of those materials under service conditions, [27-33]. Figure (7) shows the validity of the archard's equation because of its independence of the material type and depends only on the wear operating mechanism and the size of the abrasive particles used. As might be expected, the value shown in Figure 7, for SiC-Al(6061) composite material is K=1.2×10^{-4} using abrasive grit size of 125 μm ; whereas the two extremes of the grit size 250 μm and 85 μm give values of K equal to 6×10^{-4} and about $1.\times10^{-4}$, respectively, which may suggest that another coefficient could be inserted into the wear coefficients to give a relationship that includes the size of the abrading particle in the archard's equation.

The limited published data available, [4, 17, 20, 22, 24], suggest that fibres do not dramatically offer greater improvement in wear resistance than do particles of the same material and diameter [6, 33]. To the contrary, in this work, improvements in wear resistance were evident when high interfacial bond strength exists, as in SiC-Al (6061) composite material. Therefore, it can be said that wear performance is a consequence of enhanced resistance to fibre fracture and excavation which is quite evident in Figure 9 (a, b and c), for SiC-Al (6061) composite showing intact fibres after being struck by the abrading particles. It is also apparent that the diameter and volume of fibre reinforcement, relative to the size of the abrading particles, is of considerable importance, [9-13, 20]. Improvements in wear resistance were observed for fine abrading particles (85 μm grit size), but less obvious when they were larger. This behaviour can be seen from the SEM micrographs of abraded surfaces in Figure 10 (a, and b).

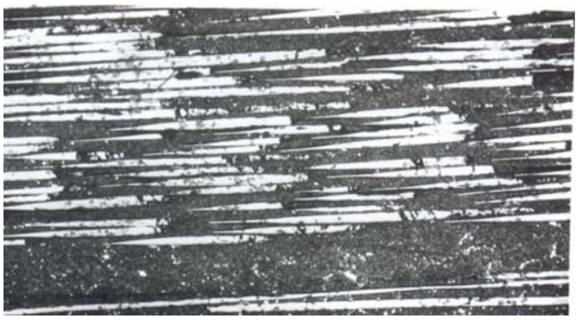

(a)

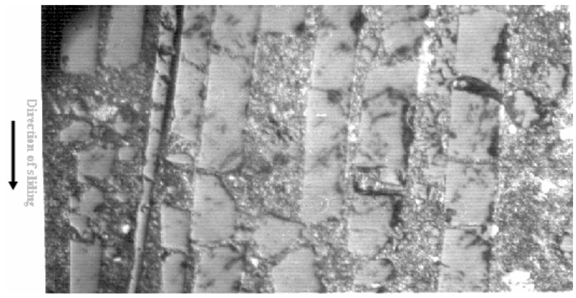

(b)

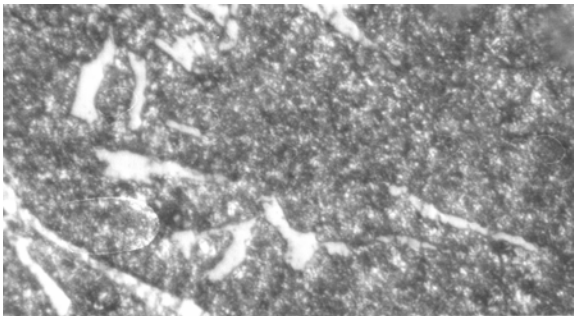

(c)

Figure 9. (a). Mag (252X), (b). Mag (500X), (c). Mag(252X) Optical and SEM micrographs of worn surfaces for SiC-Al(6061), H.S.C-Al(6061) composite materials and Al(6061) matrix material, respectively, with test parameters of; Al2O3 abrasive grit size 250 μm, load 12 kg, time of abrasion 20 seconds.

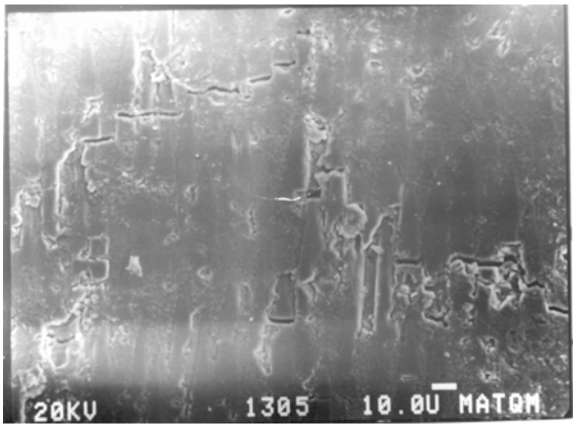

(a)

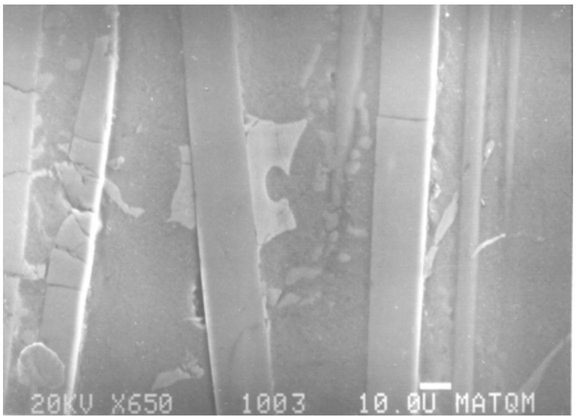

(b)

Figure 10 (a, b). SEM micrographs of abraded surfaces for Sic-Al(1100) and Sic-Al(6061) composite materials, respectively, showing fractured but intact fibres, with test parameters of; Al_2O_3 abrasive grit size 85 μm, load 7 kg, time of abrasion 10 seconds, at high magnification.

with regular furrows probably caused by the ploughing of the weaker interfacial bond strength composite such as SiC-Al(1100) composite material, as in Figure 11(a and b). However, this ploughing has been significantly reduced by the presence of broken but intact fibres just below the surface of the abraded composites, as shown in Figure 12

This figure shows the unreinforced matrix after abrasion with finer particles, and b), hence, protecting the aluminium alloy matrix from further abrasion providing that the fibre-interface is strong enough. It is also evident that the role of the Al-alloy matrix should not be underestimated because it provides support to hard fibre phase and imparts ductility to the composites, [24]. This may explain the reason for the high resistance to abrasion of the SiC-Al (6061) compared with that of SiC-Al (1100) composite materials. With larger abrading particles, however, both matrix and fibres became slightly ploughed, as in Figures 9(b), 11(b), and 12(b), were fibres became cracked and in some cases fractured under the higher load to which they are subjected particularly with larger abrading particles, hence becoming excavated along with a physically deformed matrix.

4. Conclusions

The experimental results on the abrasive wear behaviour of Al (1100) and Al (6061) matrix materials reinforced with 55% v/o of continuous SiC and H.S.C

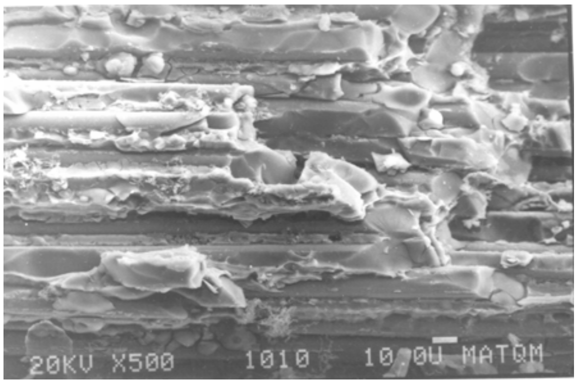

(a)

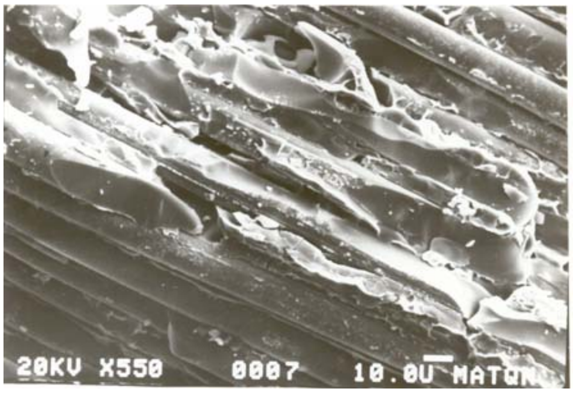

(b)

Figure 11. (a and b) SEM micrographs of abraded subsurfaces for Sic-Al(1100) and C-Al(1100) composite materials, respectively, showing fractured fibre surfaces (due to contact with abrading particles), bare and intact fibre(s) surfaces just below abraded surface, with test parameters of; Al_2O_3 abrasive grit size 85 μm, load 12 kg, time of abrasion 130 seconds, at high magnifications.

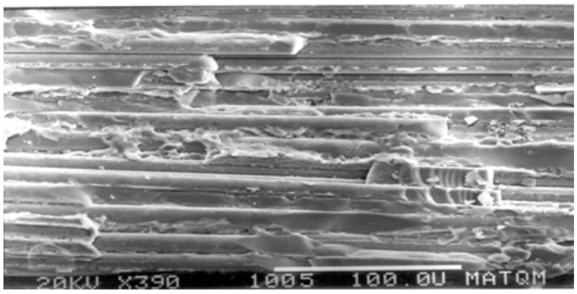

(a)

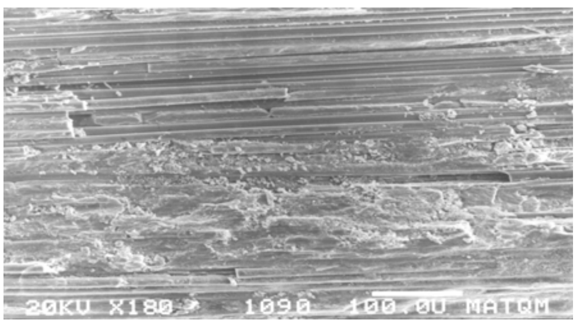

(b)

Figure 12. (a, b) SEM micrographs of abraded subsurfaces for Sic-Al(6061) and C-Al(6061) composite materials, respectively, again showing fractured and intact fibre surfaces, adhered matrix to fibre(s) surfaces just below abraded surface, with test

parameters of; Al_2O_3 abrasive grit size 85 μm, load 12 kg, time of abrasion 120 seconds, at high magnifications.

fibres, show that the wear volumes in the abrasion tests were directly proportional to the time of the test, load applied and speed of sliding. These results and SEM investigations of abraded surfaces clearly show that the presence of continuous ceramic fibres have resulted in a large reduction of abrasion rate in both reinforced metal matrix materials, and this improvement in wear rates of such composites is accompanied by an increase in fibre matrix interfacial strength and hardness of the composite materials, which can be attributed to the fibres remaining intact when struck by asperities or abrading particles.

The obtained values for the wear coefficient (K) of both continuous fibre reinforced Al matrix materials, seem to depend on the exact wear mechanism in operation, fibre-matrix interfacial strength, and matrix ductility used in the abrasive wear tests. From the results obtained, it is possible to use the abrasive wear test apparatus to relate the abrasive wear of continuous fibre reinforced metal matrix composite materials, with test conditions of load, time, speed and hardness. The simple relationship (Archard's hypothesis) can also be used, because it appears to be independent of the material type and depends only on the wear operating mechanism.

References

[1] F.M.Hosking, F.Folgar-Portillo, R.Wunderlin, And R.Mehrabian, in "Composite of Aluminium alloys; Fabrication and Wear Behaviour", J. Mat. Sci., Vol. 17, 1982, 477-98.

[2] K.J.Bhansali and R.Mehrabian, in "Abrasive Wear of Aluminium Matrix Composites", J. Metals, Vol. 32, 1982, 30-40.

[3] Y.M.Pan, M.E.Fine and H.S.Cheng, in "Wear Mechanism of Al-Based Metal Matrix Composites under Rolling and Sliding Contact", in Tribology of Composite Materials, P.K.Rohatgi, B.G.Blau and C.S. Yust (eds) ASM, 1990, 93-101.

[4] I.M.Hutchings in "Abrasive and Erosive wear of MMC's, in Proc. 2nd European Conf. on Adv. Mat., Euromat '91, Cambridge, U.K, T.W.Clyne and P.J.Withers (eds), Inst. Of Metals, 1991, 56-64

[5] J. J. Ahan, and S. Ochiai, "The Effect of Wear Environment Temperature on The Wear Behaviour and Friction Coefficient of SiCw-Al Composite", J. Compos. Mater., Vol 37, 2003, 1083.

[6] K.Akutagawa, H.Ohtsuki, J.Hasegawa and M.Miyazaki in "Reduction of Friction Coefficient of MMC under Dry Conditions" SAE Tech. report 870441, 1987.

[7] S.V. Prasad and P.K. Rohatgi, J. Metals., Nov, 1987, 22.

[8] A. Shashishankar, M. Krishna and C.S. Chandrasekhara Murthy, A study on sliding behaviour of flyash reinforced aluminium 7075 alloy composites. In: E.S. Dwarakadas and C.G. Krishnadas Nair, Editors, Proceedings of the Third International Conference on Advances in Composites. Bangalore, 2002, 583–589.

[9] X.Y. Li and K.N. Tandon, Microstructural characterization of mechanically mixed layer and wear debris in sliding wear of an Al alloy and an Al based composite, Vol. 245, 2000, 148–161.

[10] A. Wang and H.J. Rack, Transition wear behavior of SiC particulate and SiC whisker reinforced 7091 Al metal matrix composite. Mater. Sci. Eng. Vol. 147, 1991, 211–224.

[11] A. Wang and I.M. Hutchings, Wear of alumina fiber: aluminum metal matrix composite by two body abrasion. Mater. Sci. Vol. 5, 1989, 71–76

[12] Lee GY, Dharan CK, Ritchi RO. A physically-based abrasive wear model for composite materials., wear, Vol. 252, 2002, 322-331.

[13] Mondal DP, Das S, Jha AK, Yegnesswaran AH. Abrasive wear of Al alloy-Al O particle reinforced composite: a study on the combined effect of load and size of abrasive. Wear ,Vol. 223, 1998, 131-138.

[14] Sheu S.Y, Lin S.J. Particle size effect on the abrasion wear of 20 vol% SiCp/7075 Al composites. Scripta Mater, 1996; 11: 71-76.

[15] American Society for Metals, "Properties and Selection: Nonferrous alloy and pure metals", Metals Handbook, 9th edition, Vol.2, 1979, 63 and 161.

[16] Ramadan J. Mustafa and Yassin L. Nimir, "A New Process for Manufacturing Continuously Reinforced Aluminium Alloy MMC." Mu'tah Lil-Buhuth wad-Dirasat (Mu'tah Journal for Research and Studies, Vol. 21, No. 2, 2006, 183-205.

[17] M. Wang and W. Bonfield, "Effect of heat treatment on the mechanical properties and failure modes of carbon fibre-aluminium alloy composites", Metal Matrix Composites, 2nd Conference, the Royal Society, U.K., 1989.

[18] Ming Yang, V.D. Scott and R.L.Trumper, "The role of interface on the mechanical behaviour of carbon fibre reinforced aluminium alloy composites". Metal Matrix Composites, 2nd Conference, the Royal Society, U.K, 1989.

[19] J.A. Hawk, R.D. Wilson, J.H. Tylczak and O.N. Dogan, Laboratory abrasive wear tests: investigation of test methods and alloy correlation. Wear 225–229, 1999, 1031–1042.

[20] T. Miyajima and Y. Iwai, Effects of reinforcements on sliding wear behaviour of aluminium matrix composites, Wear, Vol. 225, 2003, 606–616.

[21] J. Zhang and T. Alpas, Transition between mild and severe wear in aluminium alloys. Acta Mater. 45, 1997, 513–528

[22] J.A. Hawk, and D.E. Alman,. Abrasive wear of intermetallic-based alloys and composites. Mater. Sci. and Eng. A 239-240, 1997, 899–906.

[23] A.T. Alpas and J.D. Emburey, Sliding and abrasive wear behavior of an Al 2014–SiC particle reinforced composite. Scripta Metall. , Vol. 24, 1990, 931–935.

[24] Z. Liu, J. Sun and W. Shen, Study of plowing and friction at the surfaces of plastic deformed metals. Tribol. , Vol. 35, 2002, 511–522.

[25] L.J. Yang, Determination of transient wear distance in the adhesive wear of A6061 aluminium alloy reinforced with alumina, in: Proceedings of the Second Asiatrib International Conference, Jeju Island, Korea, October, 2002, 217–218.

[26] Zhang ZF, Zhang LC, Mai YW. Particle effects on friction and wear of aluminium matrix composites, J. Mater Sci.,Vol. 30, 5999-6004.

[27] Bindumahavan PN, Wah HK, Prabhakar O,. Dual particle size (DPS) composites: effect on wear and mechanical properties of particulate metal matrix composites. Wear, Vol.248, 2001, 112-120.

[28] Sahin Y, Ozdin K. The effect of abrasive particle size in the wear of metal matrix composites. In: Numiform 2004 conference, The Ohio State University, Department of Mechanical Engineering, 650 Ackerman Road, Columbus, OH 43202, USA.

[29] Dues RL, Subramanian C, Yellup JM. Abrasive wear of Al alloy composites: a review. Wear, Vol. 201, 1996, 132-144.

[30] Sahin Y. Wear behaviour of aluminium alloy and its composites reinforced by SiC particles using statistical analysis. Mater Des, Vol. 24, 2003, 95-103.

[31] Colaco R, Vilar R. A model for the abrasive wear of metallic matrix particle reinforced materials. Wear, Vol. 254, 2003, 625-634.

[32] Sahin Y. Tribological behaviour of composites and its alloy, Mater Des, Vol. 28, 2007, 1348-1352.

[33] Esteban Fennandez J, Rocio Fennandez M, Vijande Diaz R, Tucho Navarro R. Abrasive wear analysis using factorial experiment design. Wear, Vol. 255, 2003, 38-43.

JJMIE

Volume 4, Number 2, March. 2010
ISSN 1995-6665
Pages 256 - 269

Jordan Journal of Mechanical and Industrial Engineering

Analysis of a Modular Housing Production System Using Simulation

Souma Alhaj Ali[a], Ayman Abu Hammad[b], Mark Hastak[c], and Matt Syal[d]

[a] Industrial Engineering Department, The Hashemite University, Zarqa, Jordan.

[b] Department of Civil Engineering, College of Engineering, Applied Science University, Amman, Jordan.

[c] School of Civil Engineering, Purdue University, 550 Stadium Mall Drive, West Lafayette, IN 47907-2051, U.S.A

[d] Construction Management Program, Michigan State University, U.S.A

Abstract

This paper presents the development of a simulation model for an existing modular housing factory. The activities of the system under study were mapped out, and the process time and total cycle time data of approximately 20 cycles were collected for all activities at the assembly and subassembly stations. Modeling assumptions were determined based on the real system constraints that were observed during the data collection process. The observed constraints included types and sizes of housing units produced and the ways these various types were processed through the system. The model was verified by observing the animation of the entities at a low speed run after each development committed on the model to check that entities are directed through the correct logic. The model was validated by comparing the production output of the model performance measures with the real system outputs. The run results showed a bottleneck free system with average queue time at stations one to station three of 60, 5, and 3.6 minutes respectively over a one week of operation, which is considered to be insignificant. The simulation model provides an efficient tool for production managers to evaluate and analyze the MH production system i) decide the appropriate product mix batch sizes and ii) locate potential bottlenecks hindering the productivity.

Keywords: Modular Housing; Simulation; Productivity; Construction Operations; Factory Layout; Production Line.

1. Introduction

Modular Housing (MH) is a major type of Factory-Built Housing that is fully constructed in a factory. MH units are produced in the form of a single section or multiple sections (usually two sections). Recently, the manufactured housing industry has started to construct two story housing units. MH is emerging to satisfy new trends of customer demand. The housing units can be assembled on rented or owned lots, within MH communities or private land lots, respectively. Since the implementation of the Housing and Community Development Act in 1976, the manufactured homes (termed mobile homes before the issuance of the 1976 HCDA) had become the first form of permanent housing built to meet the national standard of construction and safety.

MH dominates a respectable market share in the United States; and has started to appear as a valid competitor against the on-site constructed house. Their lower initial cost (approximately 1/2 of the site built house cost) makes them economically attractive to low income households, young families, elderly and retired persons [1]. The increasing demand for modular houses has urged production managers to (i) improve the productivity of the modular housing construction processes by reducing production cycle time and (ii) enhance the quality of both materials and workmanship.

Cost and Quality play an important role in favor of modular housing compared to other conventional types of housing; Table 1 shows cost and size comparison of modular housing or manufactured homes to site built homes. Maintaining these criteria would qualify MH to be a major provider of housing units to satisfy the increasing housing demand in the United States.

* Corresponding author. siva_appisetty1@yahoo.co.in

Table 1. Cost and size comparisons for new modular homes and new single-family site-built homes (2001-2007) [2].

Year	**2001**	**2002**	**2003**	**2004**	**2005**	**2006**	**2007**
New Manufactured Homes (Including typical installation cost)							
(All Homes)							
Average Sales Price	$48,900	$51,300	$54,900	$58,200	$62,600	$64,300	$65,100
Average Square Footage	1,545	1,590	1,620	1,625	1,595	1,605	1,595
Cost Per Square Foot	$31.65	$32.26	$33.89	$35.82	$39.25	$40.06	$40.82
Single-Section							
Average Sales Price	$30,400	$30,900	$31,900	$32,900	$34,100	$36,100	$37,200
Average Square Footage	1,115	1,125	1,100	1,090	1,085	1,105	1,095
Cost Per Square Foot	$27.26	$27.47	$29.00	$30.18	$31.43	$32.67	$33.97
Multisection							
Average Sales Price	$55,200	$56,100	$59,700	$63,400	$68,700	$71,300	$74,100
Average Square Footage	1,695	1,710	1,735	1,745	1,720	1,745	1,775
Cost Per Square Foot	$32.57	$32.81	$34.41	$36,33	$39.94	$40.86	$41.75
New Single Family Site-Built Homes sold (house and the land sold as a package)							
Average Sales Price	$213,200	$228,700	$246,300	$274,500	$297,000	$305,900	$313,600
Less Land Price	-49,056	-54,560	-62,929	-73,082	-78,219	-79,973	-84,268
Price of Structure	$164,144	$174,140	$183,371	$201,418	$218,781	$225,927	$229,332
Average Square Footage	**2,282**	**2,301**	**2,315**	**2,366**	**2,414**	**2,456**	**2,479**
Cost Per Square Foot	**$71.93**	**$75.68**	**$79.21**	**$85.13**	**$90.63**	**$91.99**	**$92.51**
Manufactured Home Shipments							
Year	2001	2002	2003	2004	2005	2006	2007
Total	193,120	168,489	130,815	130,748	146,881	117,373	95,769
Single	48,924	37,156	26,202	33,995	52,027	33,033	30,729
Multi	144,196	131,333	104,613	96,783	94,854	84,340	65,040
Estimated Retail Sales (billions)	$9.5	$8.6	$7.2	$7.7	$9.2	$7.5	$6.2

In 2000, 22 million Americans (about 8.0 percent of the U.S. population) lived full-time in 10.0 million modular homes. In the same year multi section homes represented 70.1 percent of all industry shipments. In 2001, the average cost of modular home was $48,800. Although, in 2000, 1/6th of new single-family housing starts were modular homes, when the industry shipped 250,550 homes from 280 manufacturing facilities [2].

The increased demand on multisection units and on MH units in general suggests that production managers should improve the productivity of their factories in order to fill the existing gap between supply and demand.

2. Research Background

MH production problems stem from the fact that a typical modular housing plant is unable to meet the high production demand due to the lack of a streamlined assembly process [3-8]. Moreover, the MH industry has not been able to emerge as a technologically advanced industry due to the adoption of labor driven processes, coupled with the lack of applied technology and computerization [9]. A streamlined assembly line for MH can be achieved through balancing the assembly line activities and their respective workloads. MH production lines are constrained by the mixed model manufacturing that involves the production of different housing unit sizes at the same production line. In order to streamline the production, it is important to equalize the workload variations in the mixed-model manufacturing systems [10]. Modularization and mass production of MH facilities are undermined by the unique nature of the house product. Therefore, production managers should apply new innovative techniques to identify system bottlenecks and to maintain a balance between efficiency and the implications of product design variations. Two strategies had been suggested for productivity improvement in MH; namely: extensive automation and lean production: extensive automation was concluded as a risky strategy that is subject to wild market swings while lean production may provide many of the same benefits [11-12].

This paper covers the development process of a simulation model for analyzing the production process of an existing MH facility in Indiana/ United States. The factory name is not revealed for confidentiality reasons. Simulation models offer a flexible tool for conducting a what-if-scenario analysis that targets the overall system improvement. Furthermore, simulation models can be extremely useful in (i) predicting the performance of virtual system designs, (ii) understanding how the real system functions, and (iii) evaluating the real system performance accurately. The overall goal of the research is to improve the productivity of the MH production systems, by identifying and removing process bottlenecks. Improved productivity would consequently improve the affordability of MH in order to serve the crucial demand of the middle and low-income households in the United States.

3. Simulation Model

The sequential steps that were adopted for developing the simulation model are depicted in Figure 1: i) Understand how the existing system operates; by observing the system components then capturing the logic of the product flow through the system, ii) Define the system constraints that result in specific assumptions which are applied to the simulation model development, iii) Collect cycle time data for the stations and for the sub activities running within the stations, iv) Define the probability distributions of the cycle time data for each station using the Input Analyzer tool provided by the simulation software, v) Develop the simulation model according to the existing system assumptions and constraints, vi) Verify the model during the development phase by checking the animation display in order to insure compatibility with the modeling assumptions, and vii) Validate the model by comparing the model results with the real system outputs.

The model assumptions are determined by the real system operating conditions, the station sequencing (i.e., organization of the factory layout), and the product sequencing (i.e., the flow logic of the housing sections through the system.

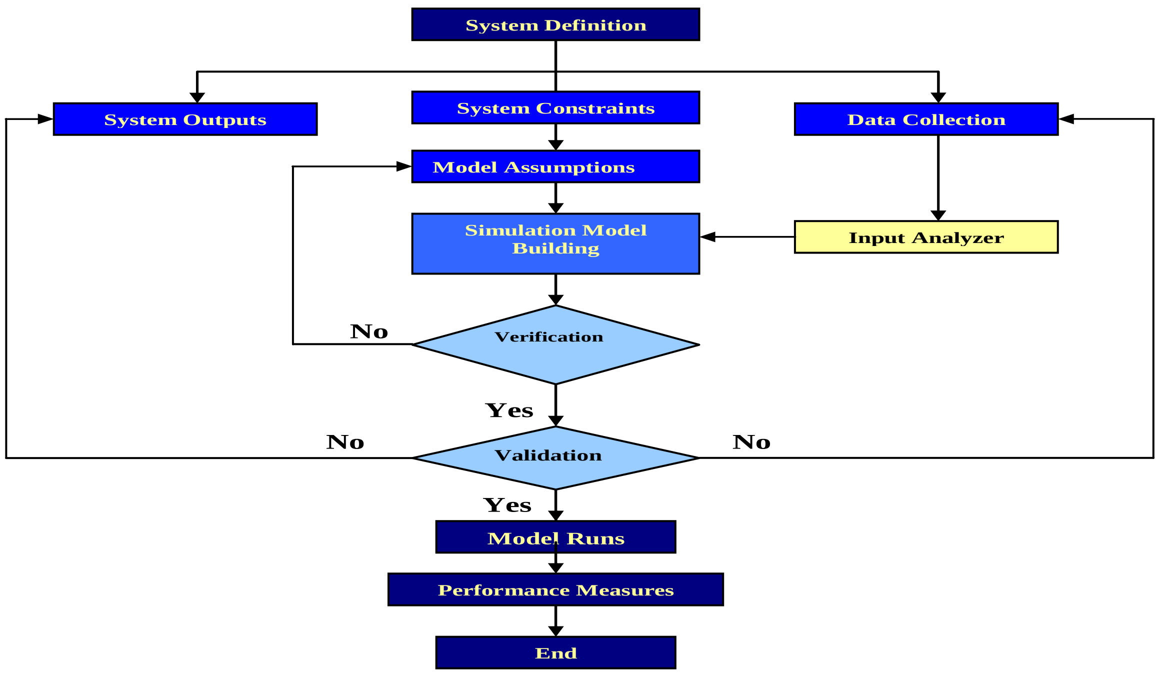

Figure 1. Methodology of developing the simulation model.

3.1. Production Process Description

The list of assembly and subassembly stations of the production line are depicted in Table 2. The U-Shape flow pattern was observed as a dominant physical shape of MH assembly lines. Additionally, the facility employs *double section processing*, which enables the processing of one full house (two sections) simultaneously at some stations. The floor subassembly (i.e., floor jig) provides assembled floor sections to the floor decking assembly station shown in Figure 2. The ready floor components are placed in a *hopper* or overhead storage that enables continuous processing of the next component while the ready component is attached to the chassis at the floor Decking station. Roofing activities were observed to be independent from the activities of the exterior and interior finishes, where the three operations occupy three successively independent stations.

Table 2. Description of stations activities and sub activities.

No.	Station Name	Description of Stations Sub activities
I-Main assembly stations		
1	Chassis Entries	Chassis on wheel and axle pulled into the factory, main wood frame is fixed.
2	Floor Decking	Place assembled floor frame with insulation, ductwork and wiring over the chassis, fastening, floor decking.
3	Interior Walls	Placement of Vinyl tile.
		Placement of interior walls (one sided studs panels).
		Placement of cabinets, toilet compartment, bathtub, and kitchen sink.
4	Exterior Wall Station	Placement of exterior walls.
5	Electromechanical Equipment	Rough electrical and mechanical, and final exterior walls installation. Installation of all electrical and mechanical equipment.
6	Roofing	Roof installation.
		Installation of shingles on the roof and cut outs for doors and windows.
7	Exterior Finish	Exterior wall finishes and installation of siding. Trim and installation of Exterior door and windows.
8	Interior Finish	Begin interior finishes, install carpet foam, complete interior drywall finish. Install carpet, final electrical and plumbing finishes, install marriage walls.
9	Cleanup and testing	Interior Finishing and cleanup, placement of material to be installed at site.
II-Feeder Stations or Sub-assembly stations		
10	Heat duct and Networks	Fabrication and storage of ductwork and plumbing, and placement of tires.
11	Floor Building feeder	Assemble floor frame, place water insulation, place heat insulation (rockwool), place floor joist, place wire and duct work, stapling.
12	Interior wall feeder	Sub-assembly of interior walls.
13	Assembly of cabinets, kitchen, and toilet sinks.	
14	Sub-assembly station for roofing main activity stations.	
15	Fabrication of roof truss, installation of ceiling board, painting, and drying.	
16	Installation of loose and rigid insulation.	
III-Storages		
17	Storage of ductwork and plumbing pipes.	
18	Storage of cabinets.	
19	Storage of drywall panels.	
20	Storage of drywall, doors and windows, and sheathing.	
21	Storage of roof shingles.	
22	Storage of foam and carpet and drywall (marriage).	
23	Storage of wall boards and tools.	
24	Storage of mirror and appliances.	
25	Storage of drapes and appliances.	
26	Storage of toilets and materials to be shipped to the site for onsite installation.	
27	Storage of drywall panels and wooden members for roof frame fabrication.	

The material handling system (the mobility system for the housing sections) permits the movement of the sections in the lateral direction of the layout by using bearing-wheeled U-sections attached beneath the wheels of the housing sections.

Although the product types and sizes are similar to other case study factories with approximately similar labor force size, the production of this factory was observed to have higher productivity output of 10 sections/ day, instead of 7 sections/ day observed at other comparable factories [7].

Figure 2 shows the stations located at the beginning and end of the assembly line. These stations consist of floor decking, interior and exterior wall, roof insulation and roof set. The factory layout, the exact distribution of operations, their respective activities throughout the different assembly, and subassembly stations are depicted in Figure 3.

The building blocks of the existing factory layout are shown in Figure 4. The building blocks are the basic stations of the assembly line associated with defined work component and time durations (i.e., station processing time) that have direct impact on the total product (i.e., housing unit) cycle time. Additionally, the building units diagram shows the exact sequence of stations and dependencies between the different operations running within the factory shop floor. The station processing times were collected from the real system; and will be discussed in the following section. The simulation model simulates the building units as processors and utilizes specified real time data for every processor of the system.

Figure 2. Different stations of the production line.

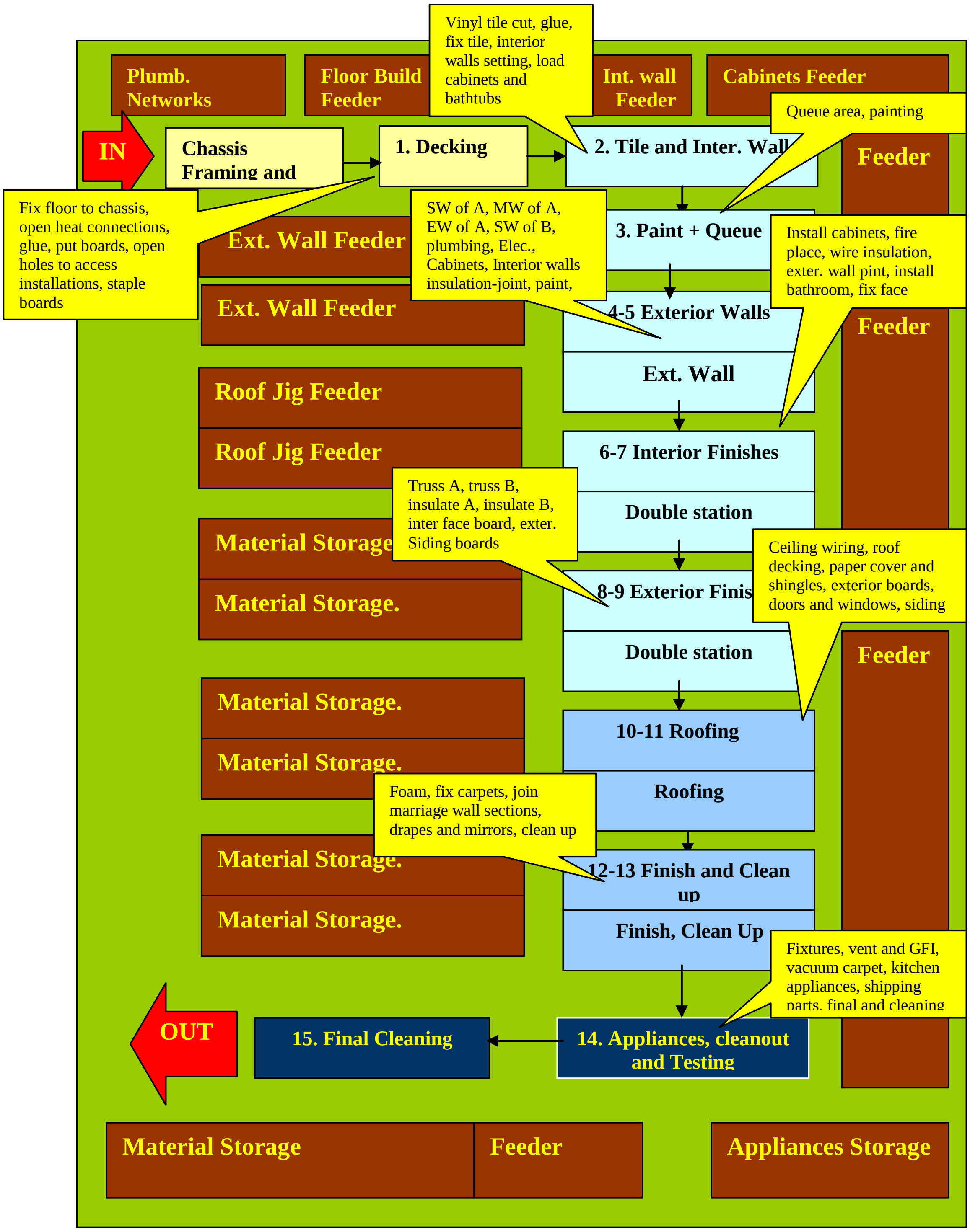

Figure 3. Factory layout, material flow pattern, and activity breakdown.

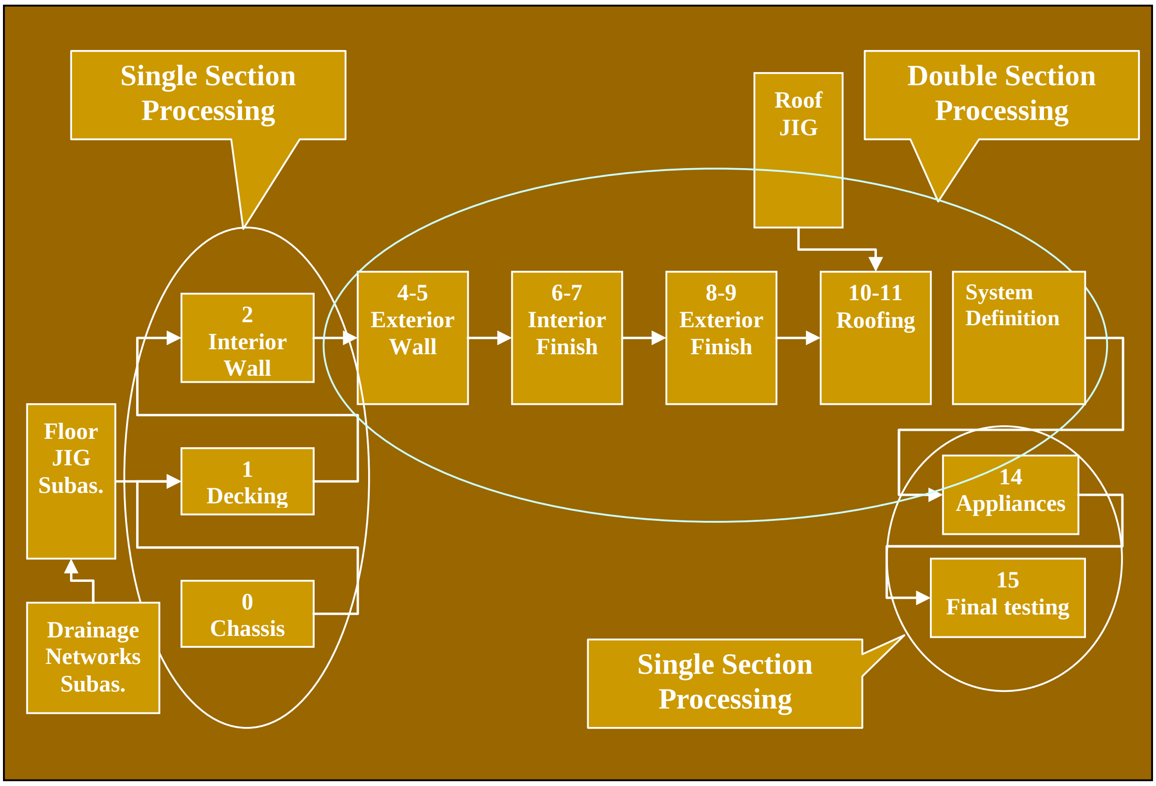

Figure 4. The building units of the real system.

3.2. Data Collection

The production process was mapped out at all assembly and subassembly stations. Table 2 shows the activity distribution on the assembly and subassembly stations of the factory. Furthermore, the factory production line, the actual flow of materials, and products through the system were observed as shown in Figure 3, in order to understand the system behavior and to determine the system constraints, which are used in developing the simulation model.

Two types of process time data were collected from the factory: i) the total station cycle time, and ii) the process time of all activities running in the station. 30 cycle data were collected for the total cycle time for each station and for every activity running at each station. The total cycle time for each housing floor (one section) is approximately two days. Data were collected over several field trips by a data collection team. The factory maps were prepared at the first visit and were used to prepare data collection sheets on Excel. The data collection tables were filled with time data relevant to each floor number copied from the tag on each chassis. During each visit, 10 data sets relevant to 10 sections were collected in the data collection sheet. As depicted by the steps described in Figure 1, the real time data (i.e., station cycle times) were transformed into stochastic time distributions using the Input Data Analyzer tool accompanying the simulation software (Arena), the distributions are described in Table 3.

Table 3. Data distributions obtained via the Input Analyzer tool in the simulation software.

No. of Server	Distribution	Expression	Square Error	Average	Standard Deviation
Server 1	Normal	NORM(38.1, 10.8)	0.035242	38.1	10.9
Server 2	Triangular	TRIA(19.5, 42.3, 54.5)	0.039624	38.8	8.28
Server 3	Normal	NORM(34.8, 7.29)	0.029086	34.8	7.41
Servers 4-5	Weibull	80.5 + 71 * BETA(0.722, 1.55)	0.052994	103	18.3
Servers 6-7	Weibull	80.5 + WEIB(28, 1.24)	0.049658	107	20.1
Servers 8-9	Beta	33.5 + 31 * BETA(0.692, 0.794)	0.050311	47.9	9.8
Servers 10-11	Normal	NORM(99.5, 12.6)	0.048788	99.5	13
Servers 12-13	Normal	NORM(192, 26.8)	0.055613	192	27.5
Server 14	Poisson	POIS(77.9)	0.181286	77.9	8.38
Server 15	Beta	39.5 + 21 * BETA(0.94, 1.16)	0.062861	48.5	6.12
Time between arrivals: 15.5 + 66 * BETA(0.967, 1.44), Square error= 0.058028.					

3.3. Model Assumptions

The model was built based on the following assumptions to match the nature of the real manufacturing system and reflect the logic i.e., sequence, and constraints i.e., space, layout shape, and distances among stations which are captured via the time data of travel and transport of material from station to station:

1. Section (b) always follows section (a) at all stations.
2. When section (a) is processed at a station, section (b) is simultaneously being processed at the previous station;
3. Section (a) should enter station 4. But section (b) should not. It rather wait in queue behind (a) then follow it to station 5;
4. The two housing sections for double-bay units are matched at the exterior wall and roofing stations and are processed simultaneously. The two sections are then split before passing through the finishing stations.
5. Housing unit of 80 ft length, for example, spends a certain processing time at each station that is different from the 55 ft length. Therefore, processing times for each section size was modeled via a statistics data distribution that includes all processing times.

3.4. Model Verification

Verification is the process to check that the model is running according to the modeling assumptions [13]. Model verification involves testing whether the model incorporates all the real system operations, such as: i) station sequencing (*i.e.,* organization of the factory shop-floor layout); ii) floor sequencing (*i.e.,* the flow logic of the floor units between the stations); and iii) inspection and rework that are included in the simulation model as approximate data; and were estimated by the production manager of the factory [16-17].

The model was verified by observing the animation of the entities at a low speed run after each development committed on the model to check that entities are directed through the correct logic as stated in the above assumptions. The batch size, processing times, and inter arrival time were controlled to observe different effects on the model outputs. The simulation model was developed, checked, modified to match SIMAN code, the model assumptions, and the actual plant conditions and specific sequence and nature of the activities.

Arena simulation software was used because it is specific to industrial and manufacturing applications. Furthermore, Arena has an efficient interface capability (animation display) that enables the modeler to follow the model logic and to verify it. Arena simulation package includes two statistical interfaces: the Input Data Analyzer and the Output Data Analyzer. The two statistical tools were used to convert the real time data into stochastic distributions and to obtain the 95% confidence intervals of the model performance measures respectively [13]. The model provides a run report that includes statistical data for many performance measures of interest such as: i) the mean product cycle time, and ii) the mean queue time at every station of the assembly line. The performance measures provide a clear idea about how the system operates and the system-specific characteristics. A stochastic simulation model has one or more random variables as inputs. The output can only be treated as a statistical estimate (confidence interval estimate) of the true characteristics of the real system [13-15]. Moreover, the model outputs identify the problems (i.e., process bottlenecks) of the simulated system.

3.5. Model Validation

Validation is the process to ensure that the behavior of the model matches the behavior of the real system [13]. Major limitation of the model is the work incentive nature of the operations. Whenever a group finishes 6-7 sections, they stop work and leave. The other lagging groups stay longer time to finish their quota before they leave. This limitation hinders the two conditions we need to satisfy in order to validate the model:

1. The cycle time of the housing section is approximately two days.
2. The production for one working day is approximately equal to 10 sections.

The model validation process involves a comparison of the real system outputs and the simulation model outputs for the 95% confidence interval on the mean production rate value, which was obtained and found to be conforming to the above two validation items [15].

3.6. The Simulation Model Components

MH processes include inter-activity relationships, interactions, and mutual impacts, which can be modeled by Arena. For the purpose of developing the simulation model, the manufacturing plant was divided into different modules. Every module represents a conceptual abstraction of activities which can be functionally classified together as a group. Different modules of the simulation model are depicted in Figure 5, based on the actual sequence of stations observed in Figure 3.

The Arrive Module is the first module of the system in which all housing section sizes (45ft, 55ft, 65ft, 75ft, 85ft) are generated.

The entities are generated according to an assigned accumulative probability [DISC(.2,1,.4,2,.6,3,.8,4,1,5)]. The time between the entity arrivals is a Beta distribution [15.5 + 66 * BETA (0.967, 1.44)] with a computed Square error = 0.058028], with a maximum batch size of 50 entities.

The two sections, (a) and (b), of the double bay house move together through the system. Therefore, the two entities are joined together at the Choose Module. Thus, the Choose Module is included in the model logic to accumulate two similar entities together, based on their assigned attribute. The if-statement of the Choose Module joins the two entities together according to similar assigned attribute numbers 1-5. The attribute numbers refer to different entity sizes. When two similar entities are accumulated in the Choose Module, they are directed immediately to the Pick Queue Module. The Pick Queue Module keeps the two entities in a storage state until they are sent directly to the Match Module. The function of the Match Module is to match the two entities together, so that they move together through the rest of the system's modules.

All house entities exit the five match modules corresponding to each house size, and enter the first Server Module (station 1: the floor decking assembly station). Then it is sent to stations 2 and 3: the interior wall assembly station and the queue paint station, respectively.

The entities are processed inside each server according to an assigned process time that is referenced in the Sequences Module. The function of the Sequences Module is to specify, in a list format, the time distribution associated with every entity size at every Server Module.

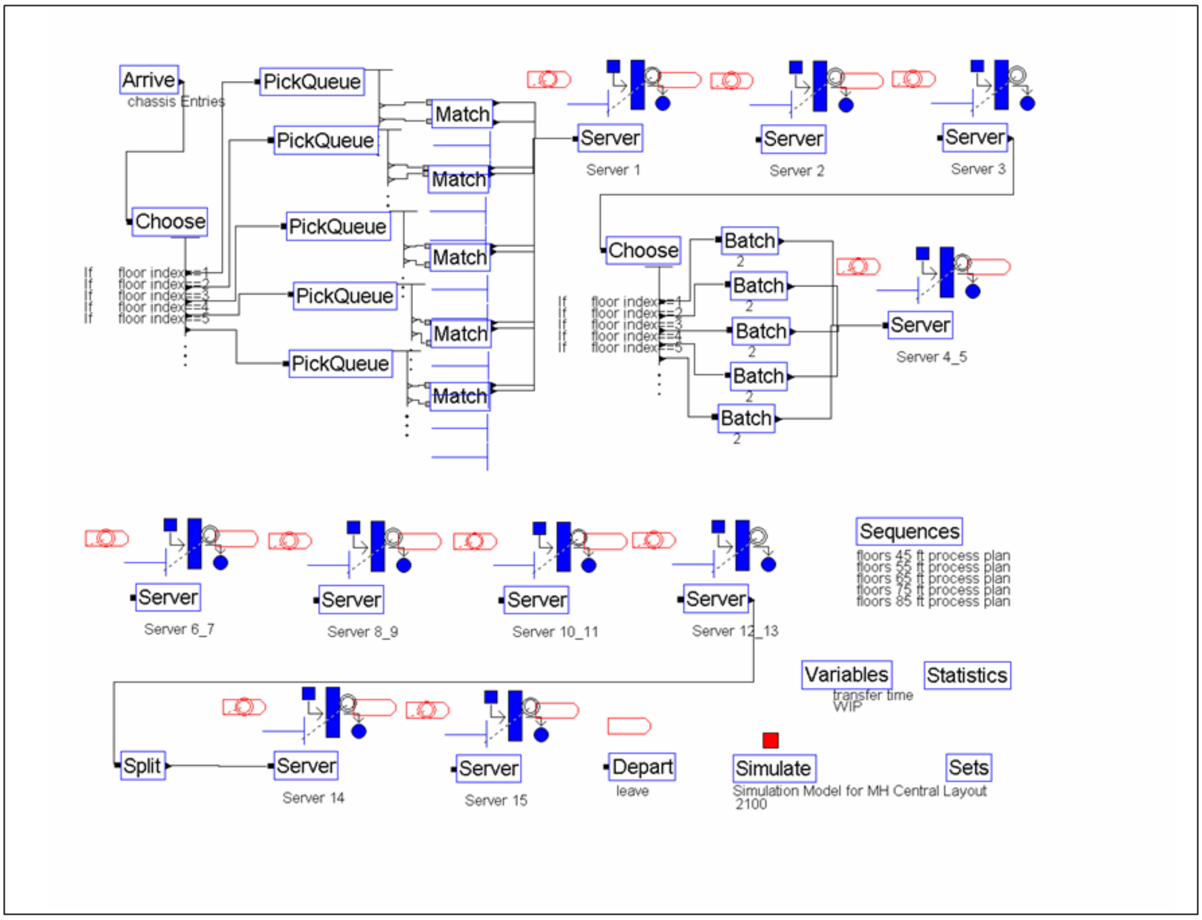

Figure 5. Simulation model layout.

As shown in Figure 3, all the stations after station 3 are observed to be *double section* processing stations. The double section processing describes the station that processes one full house (i.e., two sections) simultaneously. Therefore, in the simulation model, a cluster of different modules is used (i.e., Choose Module and Batch Module) to capture the logic of the double section concept. The two entities leave the Batch Module as one entity. After stations 12-13, the two entities are split, using a Split Module, into two independent entities and then processed independently at the last two stations 14 and 15, the appliances and final cleaning stations, respectively.

All entities leave the last station and enter into the Leave Module. The function of the Leave Module is to collect different statistics for the specified performance measures listed in the Module's menu and in the Sets Module menu.

The Simulate Module is added to the model as an independent component. The function of the Simulate Module is to specify the number and length of replications needed to make the model run over a specific period of time. The model collects the performance measures of interest in the form of a report at the end of the run as depicted in Figure 6.

4. Results and Discussion

The run results for 100 replications are included in Figures 6-11. Figure 6 shows the output values of the production counter relative to each product size. The total production rate is equal to 48 sections per week. One week's production is equivalent to 7 hours per day, five days per week. Additionally, the average cycle time for relative product size appears in the output part of Figure 6. The average cycle time of the biggest size units i.e., 85 ft. is 297.98 minutes compared to the smallest size units of 45 ft. with average cycle time of 281.32 minutes. The 55 ft and 75 ft floors are observed from Table 6 to have the maximum average cycle time. This might be attributed to the creation of small numbers of these two sizes (4 and 8 respectively) at the arrive module, compared to other sizes of 10 -14 sections count each. Although the average floor cycle times lie between 300-400 minutes approximately; it is imperative to equalize the average time among the different sizes. Consequently, decreasing the time span of the interval in order to make the production operation leaner and smoother. Therefore, it is suggested to analyze closely the applied technology, and to propose changes to sequence, tooling, and other manufacturing factors to achieve this goal.

COUNTERS

Identifier	Count	Limit
floors 65 ft productio	14	Infinite
floors 75 ft productio	4	Infinite
floors 85 ft productio	12	Infinite
floors 45 ft productio	10	Infinite
floors 55 ft productio	8	Infinite

OUTPUTS

Identifier	Value
TAVG(FLOORS 65 FT CYCL	297.39
TAVG(FLOORS 55 FT CYCL	392.74
TAVG(FLOORS 85 FT CYCL	297.98
TAVG(FLOORS 45 FT CYCL	281.32
TAVG(FLOORS 75 FT CYCL	386.82

Figure 6. Production measures of the simulation model.

The confidence intervals (CI) of the number of housing units waiting in the server queue relative to each product size are displayed in Figure 7. The production rates vary for each product size according to the percentages assigned at the Arrive Module (the assigned model mix).

The CI for the truncated production values over the 100 runs are depicted in Figure 8. The production measure of the model matches the actual production of the factory. The actual production rate at the factory was observed to be 9-10 sections per day. Therefore, the model is considered to be a good representation of the real system; thus, could be used in system improvement scenarios.

Figure 9 shows the run result statistics of the average product cycle time. The average product cycle time ranges from 281.32 minutes to 392.74 minutes. However, Figure 10 displays the 95% CI of the average station cycle time.

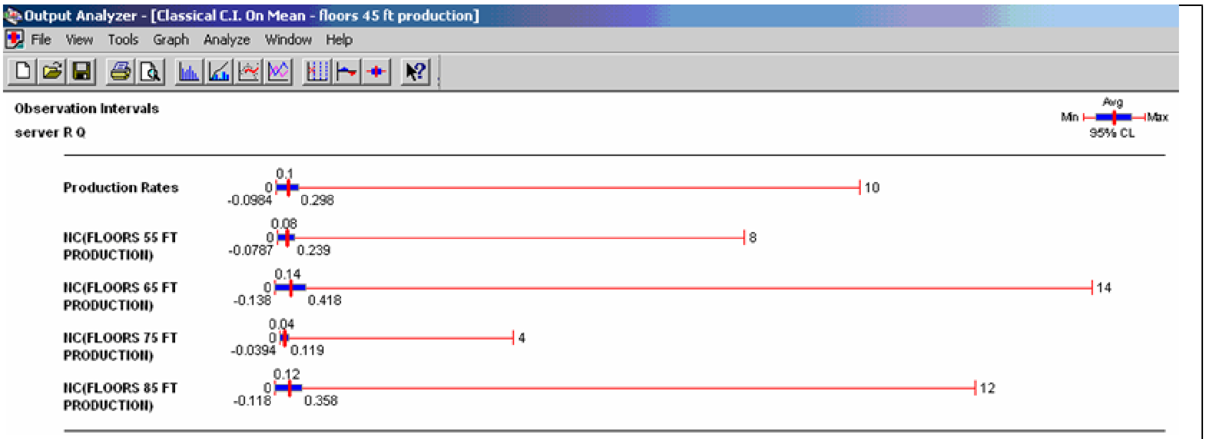

Classical C.I. Intervals Summary

server R Q

IDENTIFIER	AVERAGE	STANDARD DEVIATION	0.950 C.I. HALF-WIDTH	MINIMUM VALUE	MAXIMUM VALUE	NUMBER OF OBS.
Production Rates	0.1	1	0.198	0	10	100
NC(FLOORS 55 FT PRODUCTION)	0.08	0.8	0.159	0	8	100
NC(FLOORS 65 FT PRODUCTION)	0.14	1.4	0.278	0	14	100
NC(FLOORS 75 FT PRODUCTION)	0.04	0.4	0.0794	0	4	100
NC(FLOORS 85 FT PRODUCTION)	0.12	1.2	0.238	0	12	100

Figure 7. The 95% Confidence Intervals of the number of units waiting in Server Queue.

The results compare the cycle time of the different product sizes. It is concluded from the figure that the CI of the different products should be similar in order to obtain a bottleneck-free system.

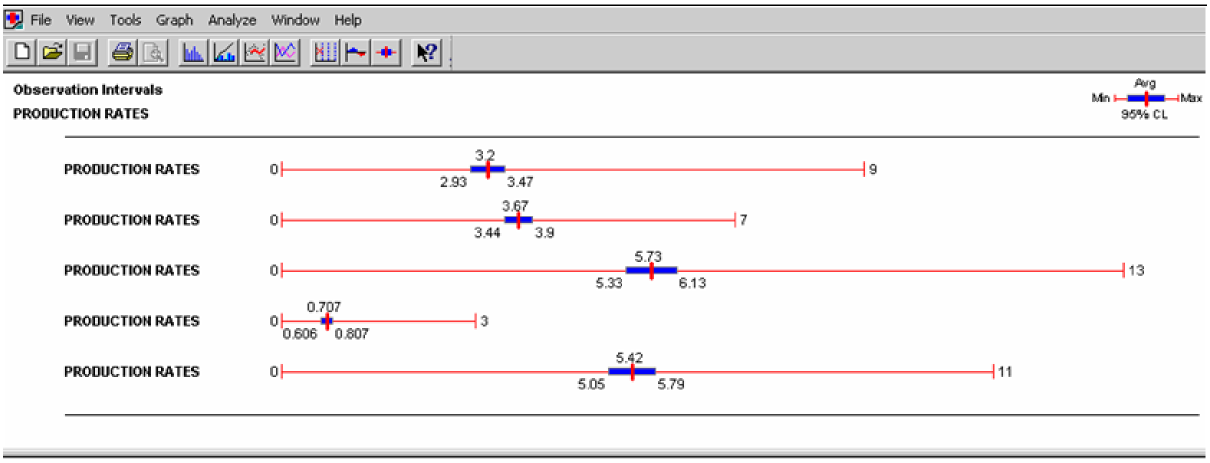

Classical C.I. Intervals Summary
PRODUCTION RATES

IDENTIFIER	AVERAGE	STANDARD DEVIATION	0.950 C.I. HALF-WIDTH	MINIMUM VALUE	MAXIMUM VALUE	NUMBER OF OBS.
PRODUCTION RATES	3.2	2.53	0.27	0	9	339
PRODUCTION RATES	3.67	2.31	0.228	0	7	397
PRODUCTION RATES	5.73	4.12	0.4	0	13	409
PRODUCTION RATES	0.707	0.977	0.1	0	3	366
PRODUCTION RATES	5.42	3.65	0.367	0	11	382

Figure 8. The 95% CI Statistics for Truncated (Interpolated) productivity values.

The average queue time statistics, shown in Figure 11, indicate station 1 as the only bottleneck station having a relatively high average queue time. The average queue time of station 1 is approximately equal to one hour per week of operation, which can be considered as an acceptable delay value over five operating days. This observation doesn't pose a problem to the actual production because it is controllable by the workers at station 1. New floor sections are only provided to station 1 when required by the station.

ARENA Simulation Results

Output Summary for 100 Replications

Project: Simulation Model
Analyst: Souma Alhaj Ali

Run execution date : 12/20/2008
Model revision date: 11/23/2008

OUTPUTS

Identifier	Average	Half-width	Minimum	Maximum	# Replications
TAVG(FLOORS 65 FT CYCL	297.39	1.2757E-13	297.39	297.39	100
TAVG(FLOORS 55 FT CYCL	392.74	6.9584E-14	392.74	392.74	100
TAVG(FLOORS 85 FT CYCL	297.98	9.2779E-14	297.98	297.98	100
TAVG(FLOORS 45 FT CYCL	281.32	1.2757E-13	281.32	281.32	100
TAVG(FLOORS 75 FT CYCL	386.82	1.1597E-14	386.82	386.82	100

Simulation run time: 0.03 minutes.
Simulation run complete.

Figure 9. Run results for 100 replications of the simulation model.

The long queue time at station 1 is related to the waiting state for two entities to accumulate in the Batch Module, in order to be sent as one full house to station 1. Additionally, another cause of the long waiting time at station 1 is the long time duration between arrivals [Beta distribution [15.5 + 66 * BETA (0.967, 1.44)], coupled with a low batch size of one entity at a time. Therefore, station 1 does not have a bottleneck. The run report shows that most of the other system servers (stations) have an average queue time of zero. Additionally, the same is observed for the number in queue statistics at all the servers of the system.

4.1. Sensitivity Analysis

The simulation model is sensitive to changes committed to station cycle times, which was done by

  - Volume 4, Number 2 (ISSN 1995-6665)

entering the new time in the processor menu directly, because the model processes the entity according to the new value and not per the time distributions stored in the sequences module. Therefore, if the cycle time of a particular station is changed, a corresponding change to all the model performance measures will occur *i.e.*, the number of entities in queue, the average queue time for predecessor and successor stations, station utilization, and product cycle time.

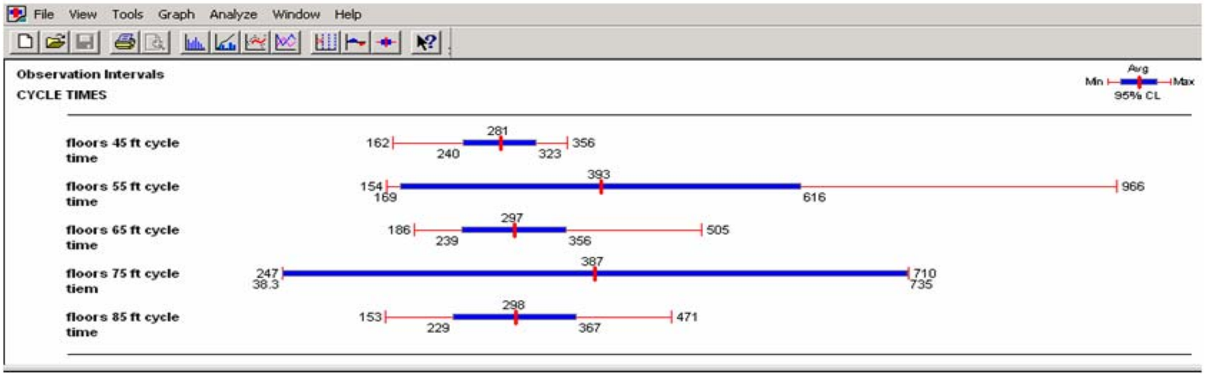

Classical C.I. Intervals Summary CYCLE TIMES

IDENTIFIER	AVERAGE	STANDARD DEVIATION	0.950 C.I. HALF-WIDTH	MINIMUM VALUE	MAXIMUM VALUE	NUMBER OF OBS.
floors 45 ft cycle time	281	57.8	41.4	162	356	10
floors 55 ft cycle time	393	267	223	154	966	8
floors 65 ft cycle time	297	101	58.4	186	505	14
floors 75 ft cycle time	387	219	348	247	710	4
floors 85 ft cycle time	298	108	68.9	153	471	12

Figure 10. The 95% Confidence Intervals of the mean product cycle times.

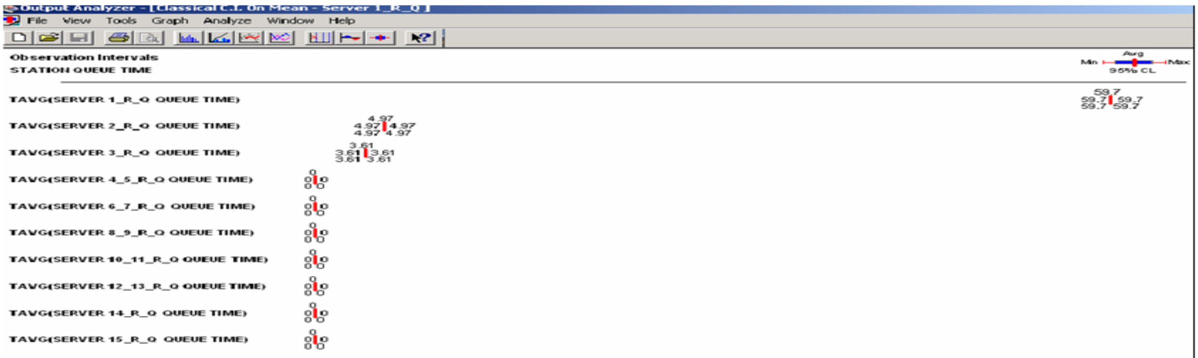

Classical C.I. Intervals Summary
STATION QUEUE TIME

IDENTIFIER	AVERAGE	STANDARD DEVIATION	0.950 C.I. HALF-WIDTH	MINIMUM VALUE	MAXIMUM VALUE	NUMBER OF OBS.
TAVG(SERVER 1_R_Q QUEUE TIME)	59.7	3.07e-006	6.09e-007	59.7	59.7	100
TAVG(SERVER 2_R_Q QUEUE TIME)	4.97	2.54e-007	5.03e-008	4.97	4.97	100
TAVG(SERVER 3_R_Q QUEUE TIME)	3.61	0	0	3.61	3.61	100
TAVG(SERVER 4_5_R_QUEUE TIME)	0	0	0	0	0	100
TAVG(SERVER 6_7_R_QUEUE TIME) QUEUE TIME)	0	0	0	0	0	100
TAVG(SERVER 8_9_R_QUEUE TIME)	0	0	0	0	0	100
TAVG(SERVER 10_11_QUEUE TIME)	0	0	0	0	0	100
TAVG(SERVER 12_13_QUEUE TIME)	0	0	0	0	0	100
TAVG(SERVER 14_R_QUEUE TIME)	0	0	0	0	0	100
TAVG(SERVER 15_R_QUEUE TIME)	0	0	0	0	0	100

Figure 11. The 95% Confidence Intervals of the mean station Queue Time.

However, it was observed that the production rate remains unchanged after modifying the processing time of a particular station. This is justified since the product cycle time is very long compared to the difference in station cycle time. Thus, it will not be substantial to cause any change to the production rate. Finally, committing any changes to the flow of logic or model constraints will consequently impact all the output performance measures including production rate.

5. Conclusions

A real time simulation model was developed for a MH production system. The model was validated by comparing the statistical measures of the simulation model with the factory output measures. The actual weekly production rates range was 45-52 sections per week. The production output measure of the simulation model was 48 sections per week, which falls within the actual production range. Therefore, the model can be used virtually in conducting what-if scenarios targeting system productivity improvement prior to implementation in a cost effective manner. The run results indicated that the system is free from bottlenecks. However, changes in the model mix would impact productivity and can be tracked down via the model. In addition, another proposition for improvement should seek alterations committed to the system layout, and to check improvements realized via the model. Scenarios targeting productivity improvement via the model are left for future work.

References

[1] A. Lee, J. Englin, “Using a Model and Empirical Data to Analyze Manufactured Home Conservation Retrofit”. Energy and Buildings, Vol. 13, 1989, 73-83.

[2] MHI Manufactured Housing Institute, “Trends and Information about the Manufactured Housing Industry: Quick Facts 2009”. 2009, http://www.manufacturedhousing.org/media_center/quick_facts/default.htm.

[3] Bernhardt A D. Building tomorrow: the mobile/manufactured housing industry. Cambridge, MA: MIT Press; 1980.

[4] Senghore O. Production and Material Flow Process for Manufactured Housing. Michigan: Michigan State University; 2001.

[5] Mehrotra N. Manufactured Housing Production Plant Layout-Design Process. Michigan: Michigan State University; 2002

[6] A. Abu Hammad, M. Hastak, M. Syal, “Simulation Model for Manufactured Housing Processes”. ASCE Civil Engineering Conference and Exposition, Washington, DC, 2002.

[7] A. Abu Hammad, M. Hastak, M. Syal, “Comparative Study of Manufactured Housing Production Systems”. ASCE Journal of Architectural Engineering, Vol. 10, No. 4, 2004, 136-142.

[8] G. F. Allen, “Upscale Manufactured Home Communities”. Journal of Property Management, 1999, 46-48.

[9] Partnership for the Advancement of Technology in Housing (PATH), “The Third Road mapping on the Whole House and Process Redesign”. 2002, www.pathnet.org.

[10] Scholl A. Balancing and Sequencing of Assembly Lines. 2nd Edition, New York: Physica-Verlag Heidelberg; 1999.

[11] M. Mullens, “Innovation in the U.S. Industrialized Housing Industry: A Tale of Two Strategies”. International Journal for Housing Science and Its Applications. Vol. 32, No. 3, 2008, 163-178.

[12] I. Nahmens, M. Mullens, “The Impact of Product Choice on Lean Homebuilding”. Construction Innovation: Information, Process and Management, Vol. 9, No. 1, 2009, 84-100.

[13] Kelton D, Sadowski R, Sadowski D. Simulation with Arena. USA: McGraw-Hill Companies, Inc.; 1998.

[14] Aho AV, Hopcrofl J, Ullman J. The Design and Analysis of Computer Algorithms. Massachusetts: Addison-Wesley, Reading; 1974.

[15] Markowitz, HM. Simscript: Past, present, and some thoughts about the future, in Current Issues in Computer Simulation Computer Simulation. New York: Academic Press; 1979.

[16] R.E. Nance, “The Time and State Relationships in Simulation Modeling”. Communications of the ACM, Vol. 24, No. 4, 1981, 173-179.

[17] Poole TG, Szymankiewicz JZ. Using Simulation to Solve Problems. Maidenhead, England: McGraw-Hill (U.K.) Limited; 1977.

JJMIE

Volume 4, Number 2, March. 2010
ISSN 1995-6665
Pages 270- 279

Jordan Journal of Mechanical and Industrial Engineering

Structural Reliability of Thin Plates with Random Geometrical Imperfections Subjected to Uniform Axial Compression

AV. Raviprakash [*], A. Adhithya Plato Sidharth, B. Prabu, N. Alagumurthi

Department of Mechanical Engineering, Pondicherry Engineering College, Pondicherry - 605014, India

Abstract

It is generally known that the load carrying capacity of thin plate structures under axial compression are partially dependent on the initial geometric imperfections. Since these initial geometric imperfections are random in nature, the strength distribution will also be random. Hence a probabilistic approach is required for a reliable design of these thin plate structures. In this paper, by keeping the variance of imperfections of all the models at assumed manufacturing tolerance of 1.71 mm and maintaining the maximum amplitude of imperfections within ±8 mm, 1024 random geometrical imperfect plate models are generated by the linear combination of first 10 eigen affine mode shapes using 2^k factorial design. These imperfection models are analyzed using ANSYS non-linear FE buckling analysis including both geometrical and material nonlinearities. From these FE analysis results, the strength distribution of the plate is obtained and using Mean Value First Order Second Moment (MVFOSM) method, reliability analysis is carried out.

Keywords: Buckling Strength; Thin Plates; Geometrical Imperfections; Random Modeling; Reliability Based Design.

Nomenclature

E	Young's modulus in N/m^2
$f_G(g)$	Distribution of failure function
G	Failure function
i	Number of nodes
j	Number of eigen affine mode shapes.
l	Length of the plate in m
L	Load distribution
m	Number of transverse half lobes
M	Modal imperfection magnitude vector
n	Number of longitudinal half lobes
P_f	Probability of failure
R	Reliability of structure
ROTZ	Rotationabout z-direction
S	Strength distribution
t	Thickness of the plate in mm
Ux	Displacement along x-direction
Uy	Displacement along y-direction
Uz	Displacement along z-direction
w	Width of the plate in m

Greek Letters

γ	Poisson's ratio
σ_y	Yield strength in MPa
ρ	Density in kg/m^3
Δ	Nodal imperfection amplitude vectors in m
σ^2_Δ	Variance of Nodal imperfection amplitude vectors
σ^2_M	Variance of Modal imperfection amplitude vectors
σ^2_{tol}	Variance of tolerance
μ_Δ	Mean of Nodal imperfection amplitude vectors
μ_M	Mean of Modal imperfection amplitude vectors
Φ	Eigen vector matrix
Φ^*	Pseudo inverse of Φ matrix
Φ^T	Transpose of Φ matrix
μ_S	Mean of strength distribution
μ_L	Mean of load distribution
σ_S	Standard deviation of strength distribution
σ_L	Standard deviation of load distribution
φ	Cumulative normal distribution function
β	Safety index

Abbreviations

BSR	Buckling Strength Ratio
MVFOSM	Mean Value First Order Second Moment Method
RSM	Response Surface Methodology

[*] Corresponding author. avrp@sify.com.

1. Introduction

Thin plate structures are widely used for applications like mechanical, marine, aerospace and in civil engineering structures. The manufacturing process involved in making perfect thin plate is difficult because there will be some geometrical imperfections like local indentations, swelling, non-uniform thickness etc., and material imperfections like heterogeneities, cracks, vacancies, impurities etc., and also other imperfections like residual stresses and strains induced during manufacturing. These imperfections generally affect the buckling behavior of plates such that studying about this effect requires complete information about their nature. Among these imperfections, geometrical imperfections are more dominant in determining the load carrying capacity of thin shell structures. Reliable prediction of buckling strength of these structures is important because buckling failure is catastrophic in nature. The geometrical imperfections present in these structures are highly random in nature which requires probabilistic approach to determine the safe load for these structures.

The Joint Committee on Structural Safety classified the structural reliability design analysis and the safety checking into three groups namely level 1, level 2, and level 3 methods [1]. In level 1 method, appropriate levels of structural reliability are provided on a structural element basis by specifying a number of partial safety factors, related to some predefined characteristic values of the basic variables. In level 2 method, safety checks are done only at selected points on the boundary as defined by appropriate limit stage equations in the space of the basic variables using the mean and variance of these variables. In level 3 method, safety checking is done based on exact probabilistic analysis for whole structure systems or elements using a full distribution approach based on failure probabilities, possibly derived from optimization studies or assessed by other approaches.

Level 2 methods are more practical oriented and quite suitable for design, and they are also used for calibration of codes for the evaluation of partial safety factors in a rational manner. Hence in this paper, the level 2 Mean Value First Order Second Moment (MVFOSM) Method is adopted to determine the safe critical load of the plate.

2. Literature Review

The modeling of imperfections can be classified into deterministic and random geometrical imperfection modeling. In case of the deterministic approach, imperfections are either obtained from actual measurement (for example, Athiannan and Palaninathan [2], Elishakoff and Arbocz [3], Arbocz and Hol [4], Scheneider [5], Singer [6]) or from assumed imperfection pattern. The assumed imperfection pattern may be axisymmetric (for example, Pircher et al [7] and Khamlichi et al. [8]) or first eigen mode shape pattern (for example Teng and Song [9], Kim and Kim [10], Khelil [11], Featherston [12]), or a combination of axisymmetric and asymmetric (for example, Arbocz and Babcock [13] & Arbocz and Sechler [14]) mode shape pattern.

There are two ways by which random modeling of imperfections can be achieved. The first is by varying the nodal locations of the structural model randomly, and the second is the stochastic FE approach.

Each manufacturing process has its own characteristic shapes that can be represented by double Fourier series. In the earlier studies, these Fourier coefficients were made as random variables to get different random geometrical imperfection models (for example Athiannan and Palaninathan [2], Scheneider [5]).

Amazigo and Budiansky [15] studied buckling strength of cylindrical shells with random axisymmetric type geometrical imperfections pattern and derived asymptotic formula for maximum load carrying capacity of the cylindrical shell. Elishakoff [16] gave a reliability method based on Monte Carlo simulation technique, and applied that to the problem of buckling of finite column with initial geometrical imperfections, which is assumed as Gaussian random fields.

In the work of Elishakoff and Arbocz [3], the random geometrical imperfections were represented by the buckling modes of its perfect structure in Fourier form. By varying the Fourier coefficients at random, large numbers of imperfect cylindrical shell models were created and their buckling strengths were determined. Elishakoff et al. [17] explained about the MVFOSM method to predict the reliability of cylindrical shell possessing axisymmetric and asymmetric random geometrical imperfections. For this, they used the second order statistical properties obtained from measured initial geometric imperfections. Results of reliability calculations were verified with results from Monte Carlo simulation.

Chryssanthopoulos et al. [18] presented Response Surface Methodology (RSM) to determine the reliability of stiffened cylindrical and plate shells subjected to axial compression, considering the manufacturing variabilities such as initial geometrical imperfections and welding residual stresses.

In the work by Arbocz and Hol [4], using MVFOSM method, the reliability of the isotropic, orthotropic and anisotropic circular cylindrical shells under axial compression were evaluated, assuming Fourier coefficients obtained from measurement of geometrical imperfections as random. Chryssanthopoulos and Poggi [19] generated random geometrical imperfections by varied Fourier coefficients multimode combinations of characteristic wave forms obtained from measured random geometrical imperfections. A suggestion was given that in the absence of detailed statistical analysis and characteristics shapes, it is reasonable to estimate the knockdown factor of the cylindrical shells by setting the maximum amplitude of an imperfection mode (which is affine to buckling mode or as a combination of two modes) equal to average maximum imperfection measured on the specimen.

Warren [20] generated random geometrical imperfections by linear combinations of eigen buckling affine mode shapes using 2^k factorial design of Design of Experiments (DoE), and the variance of the models were maintained within the tolerance of manufacturing and adopted RSM to determine reliability of framed structures. Náprstek [21] explained about stochastic finite element methodology taking large displacement as source of nonlinearities and studied about the response of the structures with random imperfection of Gaussian type.

Bielewicz et al. [22] developed a simulation method to generate random geometrical imperfections using non-homogeneous two dimensional random fields on regular nets. Schenk and Schueller [23] in their work, using imperfection databank at Delft University of Technology, generated geometrical imperfection models utilizing Karhunen-Loéve expansion method. From the deterministic analysis of random models, buckling strength distribution was obtained from which the reliability of the structure is determined using Monte Carlo Technique.

Papadopoulos and Papadrakakis [24] developed a nonlinear triangular composite element to carry out stochastic structural stability analysis of thin shell structures with random geometrical initial imperfections, which can be described as a two-dimensional univaried homogeneous stochastic field. Craig and Roux [25] also used the Karhunen–Lo`eve expansion as a method to incorporate random geometrical imperfections into the FE buckling analysis and verified the numerical results with other numerical and experimental results.

In the present work, random geometrical imperfections are generated using first 10 eigen affine mode shapes of perfect plate taken for study as suggested by Arbocz and Hol [4], Chryssanthopoulos and Poggi [19] and combine linearly, following 2^k factorial design of Design of Experiments (DoE) and the variance of the models were maintained within the tolerance of manufacturing as suggested by Warren [20]. From the deterministic FE analysis, strength distribution is obtained from which the reliability of structure is determined using MVFOSM method..

3. Finite Element Modelling

An eight noded quadrilateral shell element, SHELL93 of ANSYS is used for modeling the thin plates. This element can handle membrane, bending and transverse shear effect, and also able to form curvilinear surface satisfactorily. This element also has plasticity, stress stiffening, large deflection and large strain capabilities.

3.1. Thin Plate Shell Model

The thin structural steel plate model taken for study is [26]:

Length (l) = 1m
Width (w) = 1m
Thickness (t) = 8 mm
Poisson's ratio (γ) = 0.3
Young's modulus (E) = 205.8 GPa
Yield stress (σ_y) = 313.6 Mpa
Density (ρ) = 7800 kg/m^3
Zero strain hardening effect is assumed.

3.2. Boundary Conditions

Simply supported boundary conditions as shown in Figure 1, are applied on all the edges of the thin plate and uniform displacement loading is applied on one side of the plate model and corresponding opposite side is restrained from moving along load direction [26].

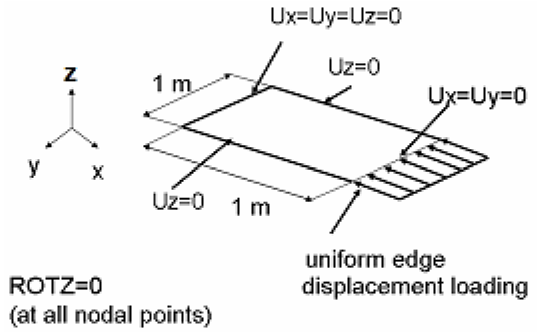

Figure 1. Geometry, boundary, and loading conditions used in buckling analysis of a thin plate (not to scale)

3.3. Model Validation and Determination of Eigen Affine Mode Shapes

3.3.1. Eigen Buckling Analysis

The mesh convergence study is done to choose the optimum number of elements for the analysis, and it is found that 40 elements along both directions give accurate solution, and hence same number of elements is used for all analysis. The analytical solution [27] of the perfect thin plate is compared with the FE eigen buckling analysis result and is shown in Table 1 such that FE model validation is ensured. In the table, m and n represent the number of transverse and longitudinal lobes respectively.

Table 1. Comparison of analytical solution with FE eigen buckling analysis result.

Mode.No	m	n	Analytical Solution(N)	FE Solution(N)	% Error
1	1	1	380936	378115.3	0.7404
2	2	1	595213	591989.6	0.5415
3	3	1	1058160	1053573.8	0.4334
4	2	2	1523750	1510774.2	0.8515
5	4	1	1720170	1712254.2	0.4601
6	3	2	1788280	1773286.6	0.8384
7	4	2	2385590	2361591.1	1.0059
8	1	2	2385590	2367998.9	0.7373
9	5	1	2580260	2560567.4	0.7632
10	5	2	3210060	3176441.5	1.0472

3.3.2. Non linear FE analysis

Validation of the developed FE model is done with the published result of Suneel Kumar et al. [28]. For this purpose, an unstiffened plate of dimensions 500x500x3.2 mm is taken for the study with the following material properties: Yield strength = 264.6 MPa, Young's modulus = 205.8 GPa and Poisson's ratio = 0.3. For a mesh size of 20x20 elements, the ultimate strength of the plate obtained from nonlinear FE analysis is 394.96 kN. The ultimate strength of the same plate, given by Suneel Kumar et al., is 392.93 kN [28] which is very much in agreement with the result obtained from nonlinear FE analysis.

3.4. Modeling of Imperfect Plates

To ensure the amplitude of imperfections at any nodal point of FE model (except the nodes at boundary edges) to be random, the first ten eigen affine mode shapes of linear buckling of thin plate are combined linearly using 2^k factorial design of Design of Experiments (DoE).

The modeling of the initial random geometrical imperfections is accomplished using the following assumptions/ conditions.

- Δ - imperfection amplitudes at all nodes except the nodes at the boundary edges should follow independent normal distribution.
- Mean value of imperfection amplitude of a node from all random models should be made equal to zero.
- Equal importance should be given for the all eigen affine mode shapes considered for random modeling.
- The random imperfection shapes generated should be linear combinations of the eigen affine mode shapes considered.

Based on the above assumptions, the nodal amplitude of imperfection vector for the entire structure (except the edge nodes, where the displacements are constrained) is given by

$$\Delta_{i\times 1} = \phi_{i\times j} \times M_{j\times 1} \quad (1)$$

where, Δ- Nodal imperfection amplitude vector

ϕ- The matrix of eigen vectors containing the modal imperfection amplitudes at all nodal points of selected eigen affine mode shapes with equal maximum amplitude of imperfections

M- Modal imperfection magnitude vector

i- number of nodes

j- number of eigen affine mode shapes

If the nodal amplitudes of imperfections are known, the modal imperfection magnitudes can be obtained using the relation

$$M_{j\times 1} = \phi^*_{j\times i} \times \Delta_{i\times 1} \quad (2)$$

where the matrix ϕ^* is the pseudo-inverse of the matrix ϕ. The pseudo-inverse is calculated using the following equation based on method of least squares

$$\phi^* = \left(\phi^T \phi\right)^{-1} \phi^T \quad (3)$$

If the nodal imperfections Δ_i are independent and normally distributed random variables then the mean value and variance of each modal magnitude is given by

$$\mu_{M\,j} = \sum_1^j \phi^*_{ji}\, \mu_{\Delta i} \quad (4)$$

$$\sigma^2_{M\,j} = \sum_1^j \left(\phi^*_{ji}\right)^2 \sigma^2_{\Delta i} \quad (5)$$

where, $\mu_{\Delta i}$ and σ^2_Δ - mean and variance of the nodal imperfection amplitude.

μ_M ,σ^2_M - mean and variance of the modal imperfection magnitude.

Similarly, mean and variance of each nodal amplitude is given by

$$\mu_{\Delta i} = \sum_1^j \phi_{ij}\, \mu_{M\,j} \quad (6)$$

$$\sigma^2_{\Delta i} = \sum_1^j \left(\phi_{ij}\right)^2 \sigma^2_{M\,j} \quad (7)$$

Since it is required to have nodal amplitude Δ_i of any node i of the structure to follow normal distribution with μ_Δ=0 and as per Eq. 4, μ_M also becomes zero. Hence, to get amplitude of imperfections of all nodes for each model, the modal magnitude of each model has to be obtained by using Eq. 5. Using the modal magnitudes obtained from previous step, the nodal amplitudes of imperfections can be obtained by using the Eq. 1. Thus by varying the modal magnitudes of imperfections randomly using 2^k factorial design matrix of Design of Experiments, random geometrical imperfection models can be generated.

3.5. Steps Followed in Random Geometrical Imperfections Modeling

Step –I

Initially, substitute variance of modal imperfection magnitude vector as

$$\sigma^2_M = \begin{bmatrix} 1 \\ 1 \\ 1 \\ 1 \\ 1 \\ 1 \end{bmatrix} \quad (8)$$

STEP-II

Using Eq.(7) the variance of nodal imperfection amplitude vector σ^2_Δ is determined.

Step –III

Each element of the resulting σ^2_Δ vector from Step-II is normalized with the maximum value of element in that vector. Each value of normalized σ^2_Δ is multiplied by σ^2_{tol} so as to limit the maximum amplitude of imperfections.

Step –IV

Using the σ^2_Δ vector obtained from the Step-III, new σ^2_M vector is found using Eq.5.

Step –V

Since, $\mu_\Delta = 0$, $\mu_M = 0$, using σ^2_M new vector determines the modal imperfection magnitude vector M such that $M = \pm\sigma_M$.

Step –VI

Using 2^k factorial design, design matrix is generated, and each column of design matrix is selected and is multiplied by corresponding element in the M vector obtained from previous step. This new design matrix is used to generate 2^k (for k=10, 2^{10} = 1024) random geometrical imperfection models.

$\Delta = \phi$ x new design matrix (9)

With the value of modal imperfection magnitude vector M, Δ nodal imperfection vector is determined using the Eq.1. But the ± value of the modal imperfection magnitude is decided by +1 or -1 of the design matrix obtained from DoE. The Δ matrix, thus formed has 1024 rows, and each row corresponds to nodal displacements of all nodes of one random imperfect plate model. By adopting the procedure explained above, 512 pairs of mirror image random imperfect plate models can be generated.

Here, in this work, 1024 random geometrical imperfect plate models are generated keeping RMS value of imperfections = 1.711 mm, and the maximum amplitude of imperfection is maintained within ±8mm. The maximum amplitude of imperfections in all 1024 models is shown in Figure 2. From this Figure it can be noted that maximum amplitude of imperfections from model number 1 to 512 are exactly mirrored between model numbers 1024 to 513.

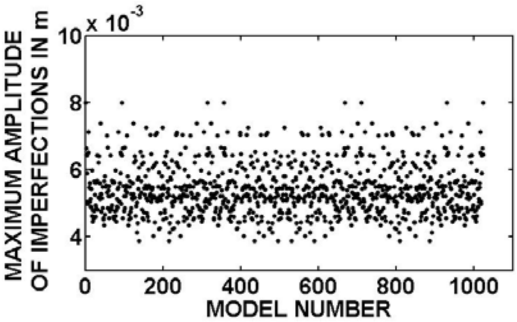

Figure 2. Scatter of maximum amplitude of imperfections from 1024 models

A sample of a pair of thin plate models with mirror image random imperfections are shown in Figure 3.

To verify the assumptions made that imperfection amplitude of a node except boundary nodes are randomly distributed**,** the distribution of out of plane displacements of a particular node from all 1024 random plate models is plotted as shown in Figure 4 (a) and (b).

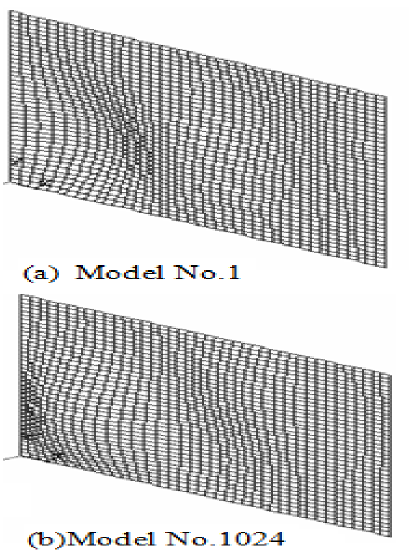

Figure 3. A pair of mirror image random imperfections plate models (amplitude enlarged by 50 times)

From Figure 4, it can be seen that the out of plane displacement of nodal point distribution follows normal distribution with mean (μ_Δ) = 0.

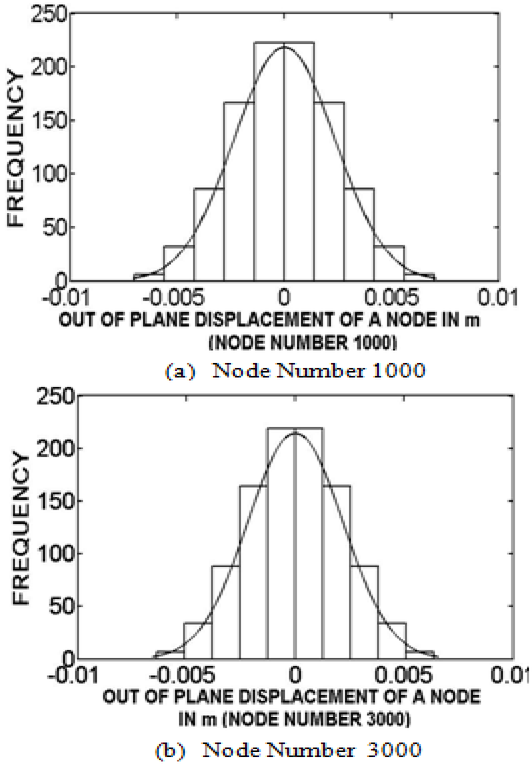

Figure 4. Normal distribution of out of plane displacements of a particular node from all 1024 random plate models

4. Reliability Analysis

For any structure, the strength and load are highly probabilistic, assuming that the strength (S) and load (L) are normally distributed as shown in Figure 5.

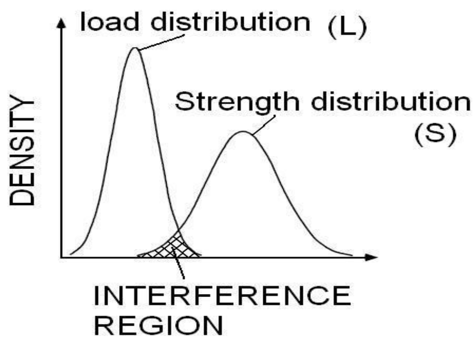

Figure 5. Load and strength distributions.

Let us define the failure function as,

$G = S - L$ (10)

Then, the distribution of failure function f_G (g) is shown in Figure 6. The probability of failure of the structure is given by

$Pf = P (G < 0)$ (11)

The reliability of the structure is given as,

$R = 1 - Pf$ (12)

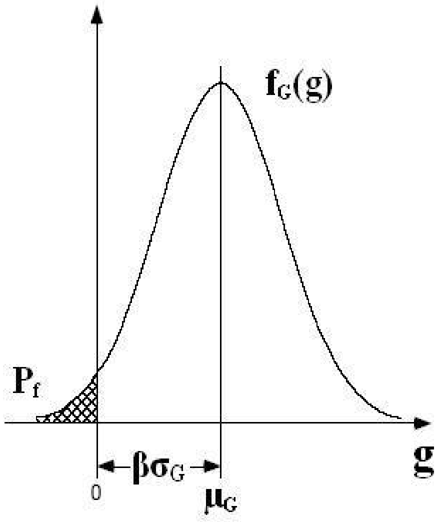

Figure 6. Normal distribution of failure function

In the MVFOSM method of determining the reliability of the structure, the mean and variance of the random variables (in this case, the strength and load) are considered.

The first order approximation of failure function f_G (g) is used for finding the mean and variance of the failure function. Thus, the mean and variance of the strength and load variables are required in order to carry out the reliability analysis.

5. Results and Discussion

Using nonlinear FE analysis, buckling strength of first 512 models is determined including both material and geometrical nonlinearities. Determining the buckling strength of the next 512 models is nothing but inverting the first 512 models and obtaining the buckling strength. For reliability calculation buckling strength of 1024 models or first 512 models can be considered because it will not affect the reliability calculations. By considering 1024 models, only the frequency of buckling strength values occurrence will be doubled. But here for reliability calculation, buckling strength ratio (BSR) values of first 512 models are considered, where BSR can be defined as ratio between buckling strength of imperfect plate to that of the first eigen buckling strength of perfect plate. Since thin plates are having positive post buckling behavior, its BSR values are greater than 1 [12]. Figure 7 shows the BSR values of first 512 random models.

Figure 8 shows the stiffness curve obtained for model number 1. From this Figure, it can be seen that at limit load condition, the plate structure fails as the slope of the stiffness curve becomes zero. Figure 9 shows the von Mises stress contour obtained for model 1 at limit load condition.

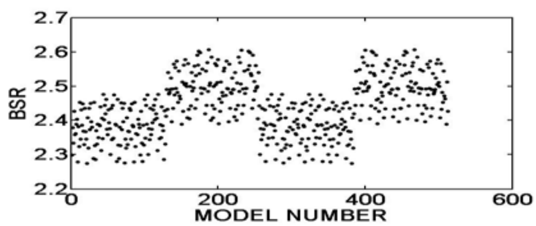

Figure 7. Model Number Vs BSR

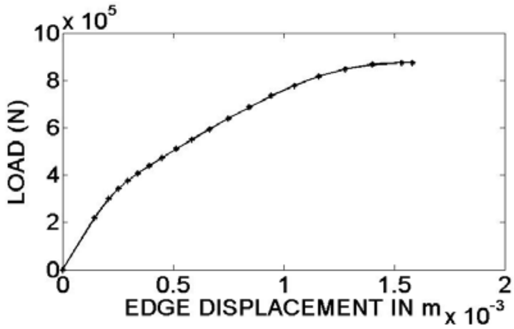

Figure 8. Stiffness curves random imperfection of model 1

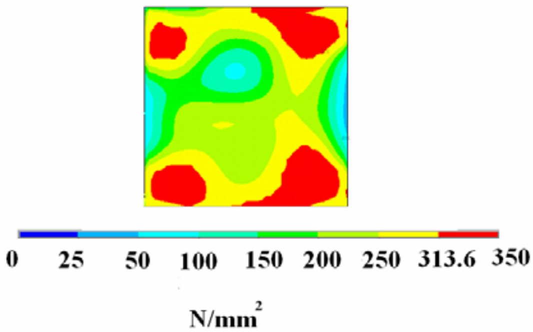

Figure 9. The von Mises stress contour of random imperfection of model 1 at its limit load condition.

To obtain the strength distribution for reliability analysis, the BSR values of 512 random models are considered and are shown in Figure.10. From the figure, it can be seen that, the distribution does not follow normal distribution exactly but it is a skewed normal distribution.

Since the normal distribution shape is the simplest, best developed, most known and expedient [29], the skewed strength distribution is converted into an equivalent normal distribution using Central limit theorem.

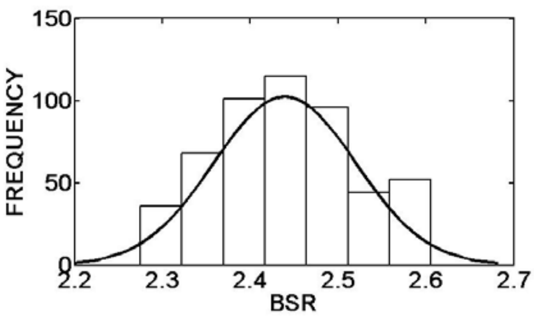

Mean of distribution = 2.4393
Mode of distribution = 2.4285
Standard deviation = 0.0808
Figure 10. Actual Strength distribution obtained using BSR values

According to Central limit theorem if a random sample of n observation is selected from any population, then, when the sample size is sufficiently large (n>=30) the sampling distribution of the mean tends to approximate the normal distribution. The larger the sample size is, the better the normal approximation to the sampling distribution of the mean will be.

Hence, 100 samples were taken with each set containing 200 observations drawn randomly from BSR of 512 models. The mean of 200 observations, taken randomly in each sample, was calculated, and the means of all 100 samples are plotted in Figure 11. The equivalent normal strength obtained from means of 100 samples is found to satisfy the normal distribution with 5% level of significance as shown in Figure 12.

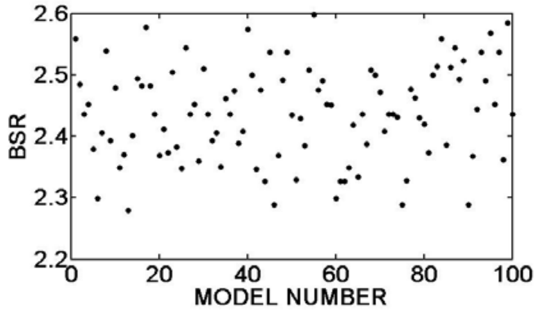

Figure 11. Sample set number and their corresponding mean

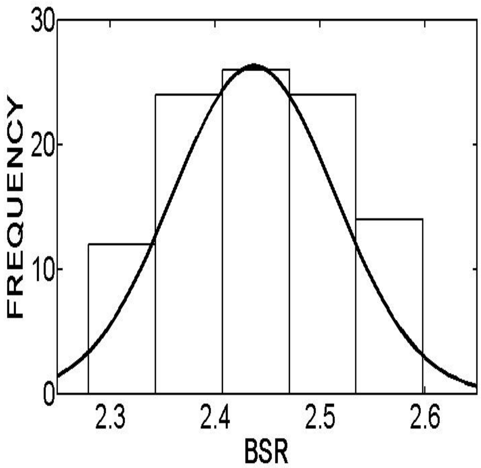

Mean of distribution = 2.4369

Mode of distribution = 2.5373

Standard deviation = 0.0775

Figure 12. Equivalent strength distribution obtained by Central Limit Theorem for reliability calculations

The mean of the distribution obtained from Central Limit Theorem and the mean of the actual distribution differ by only - 0.098 %. Moreover, the skewness of the distribution is approximately = 0 (i.e., - 0.05), which also confirms that the distribution is Gaussian.

According to the Mean Value First Order Second Moment (MVFOSM) method, the reliability index is defined as

$$\beta = \frac{\mu_S - \mu_L}{\sqrt{\sigma^2_S + \sigma^2_L}} \qquad (13)$$

μ_S = Mean of strength distribution

μ_L = Mean of load distribution

σ_S = Standard deviation of strength Distribution

σ_L = Standard deviation of load distribution

β = Safety index

The probability of failure is given by,

$$P_f = \varphi(-\beta) \qquad (14)$$

where φ is cumulative normal distribution function

Then, reliability of the structure is given as,

$$R = 1 - P_f \qquad (15)$$

In this case, the load applied is assumed as a deterministic single value. Hence, $\sigma_L = 0$ and now β is defined as,

$$\beta = \frac{\mu_S - \text{Load applied (BSR)}}{\sigma_S} \qquad (16)$$

By varying the load applied, the reliability of the structure at each load is obtained. The failure probability at different loads is shown in Figure 13.

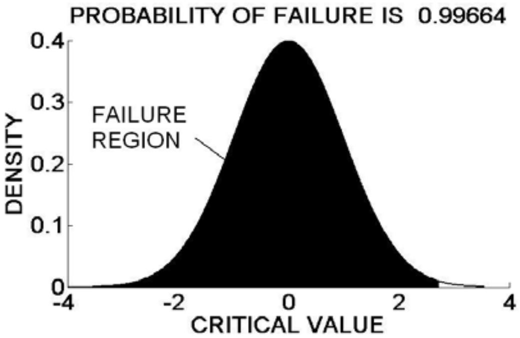

(a) Load applied is 2.602 times more than the first eigen mode buckling strength

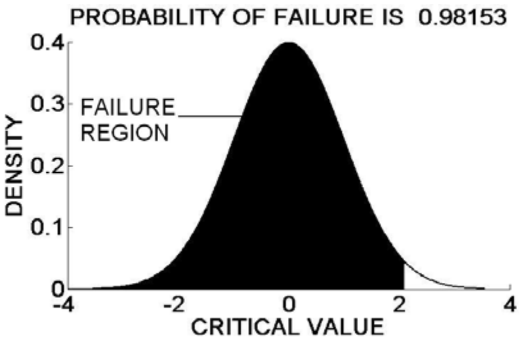

(b) Load applied is 2.532 times more than the first eigen mode buckling strength

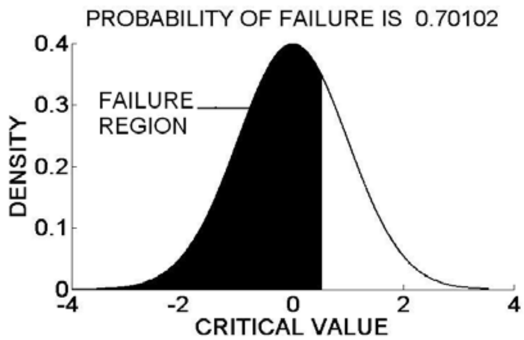

(c) Load applied is 2.412 times more than the first eigen mode buckling strength

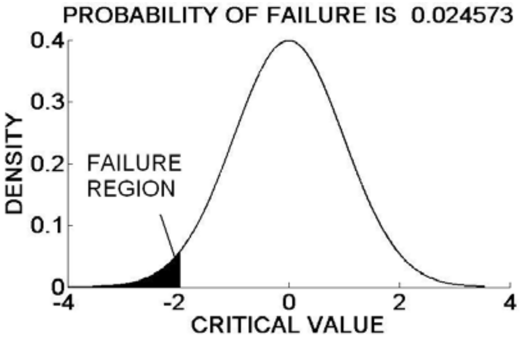

(d) Load applied is 2.25 times more than the first eigen mode buckling strength

Figure 13. Failure probability at different loads.

The variation of reliability with respect to the BSR is shown in Figure 14. From the reliability curve, it can be noted that for the plate taken for study, if BSR is upto 2.1 times of that of the perfect plate, the reliability is100%, and when the load applied is more than 2.65 times the strength of perfect plate, the reliability is zero.

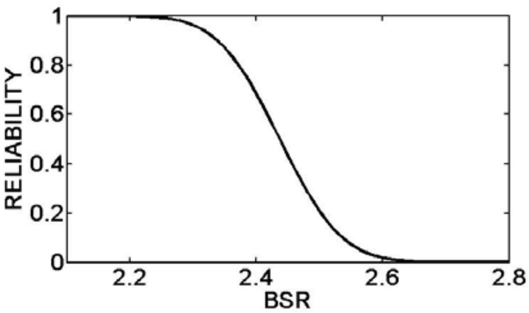

Figure 14. Reliability Vs BSR

6. Conclusions

The following conclusions are derived from the analysis carried out for the thin plate structure taken for study.

- The slope of stiffness curve decreases gradually as the load applied increases and becomes zero at limit load condition and thereby imperfect thin plates collapse.
- To increase reliable prediction of safe load of the structure further, more number of eigen affine mode shapes can be considered.
- Buckling strength of imperfect thin plate is more than two times that of perfect thin plate.
- Using the adopted MVFOSM method of reliability, it is found that the reliability of thin plate taken for study under axial compression is 100% up to 2.25 times of the strength of perfect plate. And the reliability becomes zero when the load applied is more than 2.65 times of the strength of perfect plate.

Acknowledgements

The authors would like to thank the management of Bharathiyar College of Engineering and Technology, Karaikal, India for providing the necessary computing facilities.

References

[1] Ranganathan R. Structural reliability analysis & design, New Delhi: Jaico Publishing House; 2000.

[2] K. Athiannan, R. Palaninathan, "Experimental investigations of buckling of cylindrical shells under axial compression and transverse shear". Sadhana, Vol. 29, 2004, 93-115.

[3] Elishakoff, J. Arbocz, "Reliability of axially compressed cylindrical shells with random axisymmetric imperfections". Int. J. Solids and Structures, Vol. 18, No. 7, 1982, 563-585.

[4] J. Arbocz, J.M.A.M. Hol, "Collapse of axially compressed cylindrical shells with random imperfections". AIAA J., Vol. 29, No. 12, 1991, 2247-2256.

[5] M.H. Schneider Jr., "Investigation of stability of imperfect cylinders using structural models". Engineering Structures, Vol. 18, No. 10, 1996, 792-800.

[6] J. Singer, "On the importance of shell buckling experiments". Journal of Applied Mechanics Rev., Vol. 52, No. 6, 1999, 17-25.

[7] M. Pircher, P.A. Berry, X. Ding, R.Q. Bridge, "The shape of circumferential weld-induced imperfections in thin-walled steel silos and tanks". Thin-Walled Structures, Vol. 39, No. 12, 2001, 999-1014.

[8] Khamlichi, M. Bezzazi, A. Limam, "Buckling of elastic cylindrical shells considering the effect of localized axisymmetric imperfections". Thin Walled Structures, Vol. 42, 2004, 1035-1047.

[9] J.G. Teng, C.Y. Song, "Numerical models for nonlinear analysis of elastic shells with eigen mode-affine imperfections". Int. J. Solids and Structures, Vol. 38, 2001, 3263-3280.

[10] Kim Seung-Eock, Kim Chang-Sung, "Buckling strength of the cylindrical shell and tank subjected to axially compressive loads". Thin Walled Structures, Vol. 40, 2002, 329-353.

[11] Khelil, "Buckling of steel shells subjected to non-uniform axial and pressure loadings". Thin Walled Structures, Vol. 40, 2002, 955-970.

[12] C.A. Featherston, "Imperfection sensitivity of curved panels under combined compression and shear". Int. J. of Non-Linear Mechanics, Vol. 38, 2003, 225-238.

[13] J. Arbocz, D. Babcock Charles Jr., "The effect of general imperfection on the buckling of cylindrical shells". Journal of Applied Mechanics-Transactions of ASME, Vol. 36, 1969, 28-38.

[14] J. Arbocz, E.E. Sechler, "On the buckling of stiffened imperfect cylindrical shells under axial compression". AIAA J., Vol. 9, 1976, 1611-1617.

[15] J.C. Amazigo, B. Budiansky "Asymptotic formulas for the buckling stresses of axially compressed cylinders with localized or random axisymmetric imperfections". Journal of Applied Mechanics-Transactions of ASME, Vol. 39, 1972, 179-184.

[16] Elishakoff, "Buckling of a stochastically imperfect finite column on a nonlinear elastic foundation - A reliability study". J. Applied Mechanics, Vol. 46, 1976, 411-416.

[17] I. Elishakoff, S. Van Manen, P.G. Vermeulen, J. Arbocz, "First Order Second Moment analysis of the buckling of shells with random imperfections". AIAA J., Vol. 25, No. 8, 1987, 1113-1117.

[18] M.K. Chryssanthopoulos, M.J. Baker, P.J. Dowling, "Imperfection modeling for buckling analysis of stiffened cylinders". J. Structural Engineering Division, Vol. 117, No. 7, 1991, 1998-2017.

[19] M.K. Chryssanthopoulos, C. Poggi, "Probabilistic imperfection sensitivity analysis of axially compressed composite cylinders". Engineering Structures, Vol.17, No. 6, 1995, 398-406.

[20] J.E. Warren Jr., "Nonlinear stability analysis of frame-type structures with random geometric imperfections using a total-lagrangian finite element formulation", Ph.D. Thesis, Virginia Polytechnic Institute and State University, 1997.

[21] J. Náprstek, "Strongly non-linear stochastic response of a system with random initial imperfections". Probabilistic Engineering Mechanics, Vol. 14 (1-2), 1999, 141-148.

[22] E. Bielewicz, J. Gorski, "Shells with random geometric imperfections simulation - based approach". Int. J. of Non-Linear Mechanics, Vol.37, 2002, 777-784.

[23] C.A. Schenk, G.I. Schueller, "Buckling analysis of cylindrical shells with random geometric imperfections". Int. J. Non-Linear Mech. Vol. 38, 2003, 1119-1132.

[24] V. Papadopoulos, M. Papadrakakis, "Finite element analysis of cylindrical panels with random initial imperfections". Journal of Engineering Mechanics, ASCE, Vol. 130, No. 8, 2004, 867-876.

[25] K.J. Craig, W.J. Roux, "On the investigation of shell buckling due to random geometrical imperfections implemented using Karhunen-Loève expansions". Int. J. for Numerical Methods in Engineering, Vol. 73, No. 12, 2007, 1715-1726.

[26] Minoru Harada, Masahiko Fujikubo, "Estimation of buckling and ultimate strength of rectangular plate with cutout". 12^{th} International Offshore and Polar Engineering Conference, Kitakyushu, Japan, 2002.

[27] Timoshenko SP, Gere JM. Theory of elastic stability. 2nd ed. McGraw-Hill; 1965.

[28] M. Suneel Kumar, P. Alagusundaramoorthy, R. Sundaravadivelu, "Ultimate strength of square plate with rectangular opening under axial compression". Journal of Naval Architecture and Marine Engineering, Vol. 4, 2007, 15-26.

[29] V. Verderaime, "Illustrated structural application of universal first order reliability method". NASA technical paper 3501, 1994.

JJMIE

Volume 4, Number 2, March. 2010
ISSN 1995-6665
Pages 280 - 285

Jordan Journal of Mechanical and Industrial Engineering

In-Production Product Value: A New Method for Part Type Prioritization

Safwan A. Altarazi [a,*], Nabeel Mandahawai [b], Khaled Gharaibah [c]

[a]Industrial Engineering and Management Systems Department, German-Jordanian University, Amman 11180, Jordan

[b]Industrial Engineering Department, The Hashemite University, Zarqa, Jordan

[c] Government Tenders Directorate, Amman, Jordan

Abstract

Typically, the value of a product is addressed in the fields of marketing, neoclassical economics, or classical economics. Product value in these fields is associated with the final shape of a product. This paper presents a new different perspective for defining product value. It introduces a formula for evaluating product value while it is in production. Contributors of the proposed formula include the product revenue, the percentage of the product's finished-cycle time, the product criticality, and the due date of the product. Based on the "in-production product value" formula, an algorithm for "part type priority" and scheduling is presented. The algorithm was applied to a hypothetical manufacturing example and the simulation results proved the validity and applicability of the proposed algorithm.

Keywords: Part type priority, scheduling, product value, simulation.

Nomenclature

$CPV_{product}$	is the constraint product value for a product ($)
$CS_{product}$	is the constraint's occupation time for one
$\left(\frac{ATP}{CS}\right)_{constraint}$	is the average throughput per constraint time for all products on the constraint ($/sec)
$MC_{product}$	is the material cost of the product ($/unit)
$ATP_{constraint}$	is the average throughput for the constraint ($/unit)
K	is the number of products produced by the analyzed constraint
MC_i	is the material cost of the product ($/unit)
ASP_i	is the average selling price for product i ($/unit)
D_i	is the sold demand of product i (units)
CT_C	is the amount of completed product's cycle time
CT_p	is the product's total cycle time
%VAP	is the percentage of value added processes in CT_C
R_P	is a linear normalization factor of the considered product with respect to all produced products
CT_{min}	is the minimum cycle time among all produced products
CT_{max}	is the maximum cycle time among all produced products

* Corresponding author. Safwan.altarazi@gju.edu.jo

1. Introduction

The value of a product can be viewed from various perspectives; accordingly, it can be defined differently. For example, in marketing, the value of a product is the consumer's expectations of product quality in relation to the actual amount paid for it. It is often expressed by the ratio of received quality to price or customer expectations. On the other hand, in neoclassical economics, the value of an object or service is often seen as nothing but the price it would bring in an open and competitive market [1]. This is determined primarily by the demand for the object relative to supply. In classical economics, price and value are not equal. According to Keen [2], value refers to "the innate worth of a commodity, which determines the normal ratio at which two commodities exchange." Ludwig von Mises [3] asserted that value is always a subjective quality.\ There is no value implicit in objects or things, and value is derived entirely from the psychology of market participants. Neap and Celik [4] emphasized that value reflects the owner/buyer desire to retain or obtain a product which introduces subjective aspects to the value of a product.

The above product's value definitions are associated with the final shape of a product in which the external customer is the one who perceives the product and evaluates it. The current research views the product's value from a different perspective, that is, it tires to evaluate the product's value during production phase. According to these two perspectives, the factors that affect the value of a product are different. For example, the final customer perception of product value is the combined result of the product price, delivery time, and product quality-considering the eight dimensions of quality (performance, features, reliability, conformance, durability, serviceability, aesthetics, and perceived quality [5]). In contrast, the factors that contribute to the product value while the product is still in production include the product's production time, due date, and demand.

In literature, factors contributing to the "in-production product value" are linked to the parameters used for determining the machining sequence for a group of parts. For example, for determining part types priorities before machining Bilkay et al. [6] considered the bath size, due date, total processing time, and tool slots needed. Similar parameters were used in other studies, especially those focusing on throughput maximization and work in process (WIP) minimization [7-9]. These part-priorities algorithms are static in nature. They rank products based on pre-machining information and do not have the capability to accommodate changes of these information while the product is moving through the production line.

In this study, an attempt is made to define the value of products while it is still in production. Four factors, which contribute to this value, are considered: the product's revenue, percentage of completed-cycle time, due date, and criticality. An "in-production product value" formula is proposed and utilized to determine part type priorities. The formula can be used either at the starting of production or for products that have been partially machined and their priorities need to be reevaluated. Based on the resulted part type priority, a scheduling algorithm is presented and simulation is used to validate the applicability of the algorithm.

The present paper is organized in five sections. The next section introduces the "in-production product value" formula. Section three presents the proposed "part priority type" algorithm and its scheduling output. The algorithm applicability is demonstrated in the fourth section and the paper ends with concluding remarks in section five.

2. The "In-Production Product Value" Formula

The proposed "in-production product value" formula algorithm considered four inputs: product's revenue, product's percentage of completed cycle time, product's due date, and product's criticality. The factors are described below.

2.1. Product's Revenue (R)

The net profit generated by a product is essential in making the production decision for this product. The profit is a function of the total production cost of a product and its selling price. Traditionally, a product's revenue is represented either by subtracting the total cost from the selling price or by using the selling price/total cost ratio. Another way to analyze revenue is by using the thought process of Theory of Constraints (TOC) [10]. The TOC proposes that total throughput of a system is only affected by the throughput produced by the system's constraint. Because the production time of the constraint is limited, job scheduling for the constraint should be carefully performed in order to generate maximum throughput per the constraint's unit time. In addition, products which consume a large portion of constraint time should be assigned a higher value than products which use less constraint time.

Constraint Product Value (CPV) is a way to compare products based on their revenue contribution generated by a factory constraint. It combines the product's material cost and the product's throughput rate (revenue/unit time) on the constraint [11]. CPV for a given product can be defined as:

$$CPV_{product} = \left(CS_{product} * \left(\frac{ATP}{CS} \right)_{constraint} \right) + MC_{product} \tag{1}$$

To find the time required for one yielded product on the constraint ($CS_{product}$), the production rate of the product in the constraint, typically given in units per hour, is needed. For a product that visits the constraint one time, $CS_{product}$ in seconds per unit is given by:

$$CS_{product} = \frac{3600}{\text{Production rate (in units per hr)}} \tag{2}$$

For the calculation of the average throughput per constraint time for the constraint being analyzed, i.e., $\left(\frac{ATP}{CS} \right)_{constraint}$, the $ATP_{constraint}$ and the $CS_{constraint}$ are calculated as follows:

$$ATP_{constraint} = \sum_{i}^{k} (ASP_i - MC_i) \times D_i \tag{3}$$

Also, $CS_{constraint}$ can be found as:

$$CS_{constraint} = \sum_{i}^{k} CS_{product(i)} \times D_i \tag{4}$$

Once the $ATP_{constraint}$ and the $CS_{constraint}$ are calculated separately, the $\left(\frac{ATP}{CS} \right)_{constraint}$ can be found as:

$$\left(\frac{ATP}{CS} \right)_{constraint} = \frac{ATP_{constraint}}{CS_{constraint}} \tag{5}$$

Finally, for a group of products, the normalized contribution function of the revenue (PV_R) for product i, toward the in-production product value, is defined as the ratio of the difference of the CPV of product i and minimum CPV, to the difference of the maximum and minimum CPV.

$$PV_R = \frac{CPV_p - CPV_{min}}{CPV_{max} - CPV_{min}} \tag{6}$$

2.2. Product's Percentage of Completed Cycle Time (%CT)

The cycle time of a given product, also called flow time, refers to the average time a product spends as WIP, or the average time from the release of a job at the beginning of a product's route until it reaches the point of finished product inventory [12]. Considering the percentage of finished cycle time toward defining a product's value is very reasonable. For example, for the same product, a unit with a 90% finished cycle time is more valuable than a unit with a 10% finished cycle time. However, for two different products, 10%-finshed cycle time of product A can be more valuable than a 90%-finished cycle time of product B. Therefore, in a situation where multiple products are considered for production, both the percentage of finished cycle time and the product's total cycle time should be considered.

Although all processing times are counted in the cycle time, many of these times do not add any extra value to the product. In lean manufacturing terminology, these non added-value processes, such as WIP inventory, are labeled as waste. In contrast, processes which add to the value of a product are called value-added processes. Hence, only value-added processes should be considered to contribute toward the product's value.

Therefore, PV_{CT} is used to represent the contribution function of the percentage of completed cycle time, the total cycle time, and the value-added processes, toward the in-production product value.

$$\mathrm{PV}_{\mathrm{CT}} = \left(\frac{CT_C}{CT_p} \times \%VAP \times R_p \right) \tag{7}$$

where R_P can be calculated from:

$$\mathrm{R}_{\mathrm{p}} = \frac{CT_p - CT_{\min}}{CT_{\max} - CT_{\min}} \tag{8}$$

2.3. Product's Due Date (DD)

Due date should be strictly met in order to eliminate delay penalties. Hence, due date is an important factor for the generation of comprehensive definition of the in-production product value. It is assumed that the value of product i increases as its due date is earlier, that is, as the time remaining to deliver is shorter. For a single product, the due date effect toward its in-production value (DD_{effect}) is defined as the ratio of the time remaining to finalize production to the time remaining to deliver.

$$\mathrm{DD}_{\mathrm{effect}} = \frac{\text{Time to finalize production}}{\text{Time to deliver}} \tag{9}$$

Moreover, for a group of products the normalized contribution function of due date (PV_{DD}) for product i, toward the in-production product value, is defined as the ratio of difference of the DD_{effect} of product i and minimum DD_{effect} , to the difference of the maximum and minimum DD_{effect}.

$$\mathrm{PV}_{\mathrm{DD}} = \frac{DD_{effect\,(p)} - DD_{effect\,(\min)}}{DD_{effect\,(\max)} - DD_{effect\,(\min)}} \tag{10}$$

Product's Criticality (PC)

Product criticality is related to the classifications of product characteristics. A characteristics classification is applied usually during the first stages of product and process design. Yet, because of manufacturability, quality or handling considerations, the classifications may be upgraded by suppliers, the internal process, installation, or quality planners. A typical product characteristics classification is [13]:

- Critical: when a small deviation will produce or lead to a substantial safety hazard or a complete performance loss.
- Major: when a small deviation will produce or lead to some safety hazard, significant performance or reliability reduction or complete loss of further manufacturability.
- Minor: when a small deviation may produce or lead to minimal safety hazard, some performance or reliability reduction, or substantial manufacturability problems.
- Incidental: when a small deviation cannot produce or lead to any safety hazard, performance, or reliability reduction but may cause minimal manufacturability problems.

These classifications are often distinguished by reference to measures of process capability ratio (PCR), such as C_p or C_{pk}. A typical approach might have the critical characteristic classes assigned to a higher than 1.33 PCR processes, major characteristics assigned to 1.33 PCR processes, minor characteristics assigned to 1 to 1.33 PCR processes, and incident characteristics products assigned to a 1.00 PCR processes. In the current research, it is assumed that the criticality classifications of the analyzed products are known. Furthermore, the associated PCR ratios of these products are used as the criticality contribution to their in-production value, notated by PV_{PC}. Then, the normalized contribution function of product criticality (PV_{PC}) for product i, toward the in-production product value, is defined as the ratio of the difference of the PCR of product i and minimum PCR, to the difference of the maximum and minimum PCR.

$$\mathrm{PV}_{\mathrm{PC}} = \frac{PCR_p - PCR_{\min}}{PCR_{\max} - PCR_{\min}} \tag{11}$$

2.4. The Proposed PV Formula

Based on the previous discussion, a formula for the in-production product value which summarizes the effects of the revenue, percentage of completed cycle time, due date, and product's criticality is given by:

$$\text{Product Value } (\mathrm{PV}_{\mathrm{NET}}) = \left[w_1\ w_2\ w_3\ w_4 \right] . \begin{bmatrix} \mathrm{PV}_{\mathrm{R}} \\ \mathrm{PV}_{\mathrm{CT}} \\ \mathrm{PV}_{\mathrm{DD}} \\ \mathrm{PV}_{\mathrm{PC}} \end{bmatrix} \tag{12}$$

where w_1, w_2, w_3, and w_4 are weights of the four factors. For determining these weights, expert's knowledge can be consulted.

It is worth mentioning here that the suggested PV_{NET} formula would return a dimensionless number between zero and one. Hence, this normalized number can be used as a selection criterion between products in applications where products priorities are needed. The next section shows the application of this formula in scheduling.

3. The Proposed "Part Priority Type" Algorithm and Scheduling

The proposed "part priority type" algorithm can be described by the following steps:

- Step 0-algorithm inputs: the available machines, the products to be produced, the process plan for each product associated with the cycle time at each operation (machine), the system's constraint (the bottleneck machine), product's raw-material costs, product's selling prices and demand, and product's delivery due dates.
- Step 1: at time equals zero (starting of the production), evaluate all products using the PV_{NET} formula. Then, generate products-machines assignments accordingly. That is, the product with the highest PV_{NET} will be firstly assigned the required machine. After that, the product with the next PV_{NET} will be assigned the required machine (if it was not assigned to the first part), and assignments will continue. Products with low PV_{NET} may wait if the machines they need are assigned to products with higher PV_{NET} values.
- Step 2: start the production of the products with the available assigned machines.
- Step 3: at any state when the processing time of any product on any machine is finished, reevaluate all products using the PV_{NET} formula. Then, generate a new scheduling plan for the products, run the production.
- Step 4: rerun step 3 until all products are finished. If any of the products has finished its process plan exclude it from the PV_{NET} calculations.

Step 5: output the scheduling plan of all products.

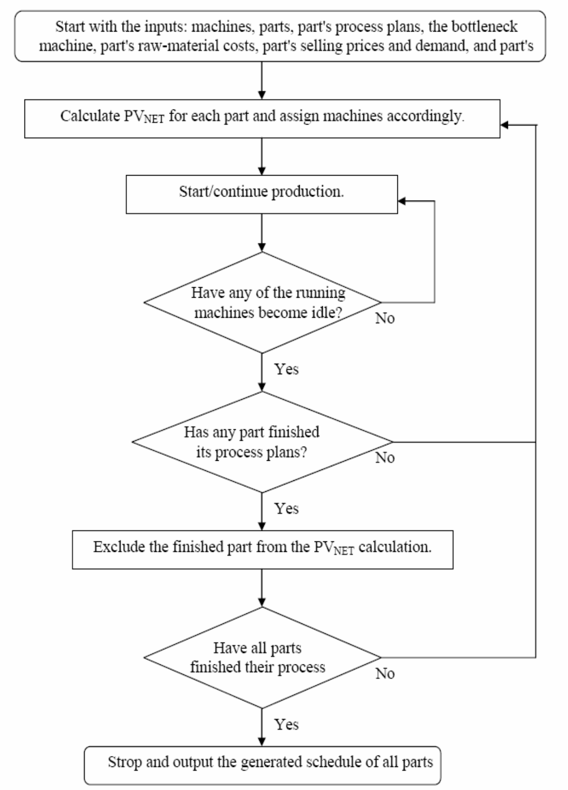

Figure 1. flowchart of the proposed scheduling algorithm.

Figure 1 presents the flowchart of the algorithm. A simulation model using Matlab 6.5 was generated to run the model. The next section presents a demonstration example for the algorithm application and the simulation results.

4. Demonstration Example

The validity of the proposed algorithm is tested by applying it to a hypothetical example that is described in the next subsection while subsection 4.2 introduces the scheduling plan resulted from the Matlab simulation.

4.1. Example Definition

This demonstration example considers a manufacturing facility with four machines and five products. Each product has different process plan to follow. Yet, all products need to go through the second machine which is assumed to be the system's constraint. Table 1 lists the process plans of each product associated with the processing times on each machine, hence, the production rate of each product on each machine can be calculated-especially for the system's constraint. In addition, table 1 includes the following information for each product: $MC_{Product}$, ASP_i, D_i, CT_P, the "time to deliver", and the product's characteristics. Note that CT_C is not tabulated as it equals zero for all products at the beginning of the production. However, CT_C would be updated as can be seen in step 3 of the proposed algorithm.

4.2. The simulation output

Figure 2 shows the scheduling plan resulted from running the simulation model for the current example. Several comments can be observed from the figure:

- At the beginning of the production, products 1, 4, and 5 had the highest PV_{NET} scores; hence, they were processed first. Products 2 and 3 were delayed since they required starting with machines that have been assigned to products with higher priorities, that is, higher PV_{NET} scores.
- PV_{NET} scores are reevaluated at any each situation when the processing time of any product on any machine is finished, and the assignments of machines will be based on these reevaluations.
- The on-line reevaluation of the in-production products value assures that no simultaneous machine assignments occur. That is, only one product will be assigned to a machine at particular time period.
- As the second machine was designed to be the system constraint, it has the highest utilization among the available five machines.
- The five products will finish production as the following: part 4, part 1, part 3, part 2, and finally part 5. Moreover, the makespan of the whole five products production is 42 min.

5. Conclusions

A new part type priority algorithm for products scheduling was presented in this paper. The algorithm is based on a new approach for defining the in-production products value. The proposed approach integrated the contribution of four parameters to product value. The parameters are the part's revenue, percentage of completed cycle time, due date, and criticality. Simulation results approved the effectiveness of the proposed algorithm.

The proposed algorithm can be improved and utilized in many ways. For example, the four considered parameters can be evaluated as linguistic variables; and

Table 1. Input information of the demonstration example

Part No.	Process plan (machines sequence)	Processing time/ machine (min)	Production rate on 2nd machine, (unit/hr)	$MC_{Product}$, ($)	ASP_i, ($)	D_i, (units)	CT_P (min)	Time to deliver (min)	Part characteristics
1	1-2-3	10-8-4	10	50	400	30	22	10	Critical (PCR = 1.66)
2	2-1-4-3	8-3-5-6	5	30	350	50	22	15	Critical (PCR = 2.00)
3	1-2-4	4-7-3	8	60	800	10	14	7	Minor (PCR = 1.16)
4	2-3-4	10-2-3	12	35	700	75	15	4	Major (PCR = 1.33)
5	3-4-2-1	5-6-5-4	15	35	100	20	20	35	Incidental (PCR=1.00)

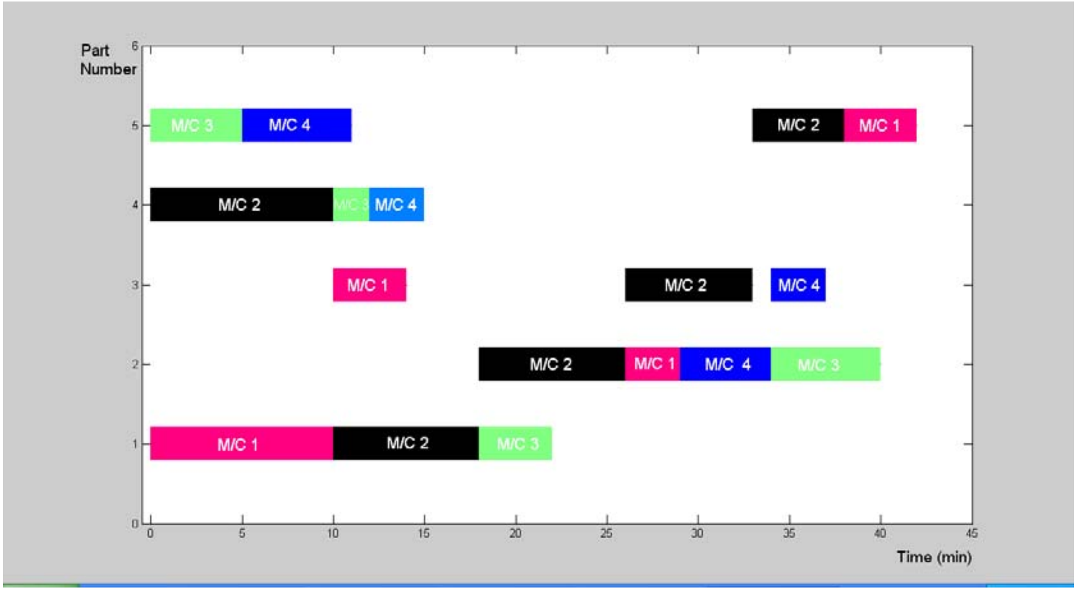

Figure 2. The scheduling plan resulted from the simulation model

then processed by using fuzzy logic. Furthermore, the suggested PV_{NET} formula can be integrated with process planning models to help in assigning high capable machines for high-value products.

References

[1] H. Stretton H. Economics: A new introduction. Sydney: UNSW Press; 1999.

[2] S. Keen. Debunking Economics: The naked emperor of the social sciences. London: Zed Books; 2001.

[3] Ludwig von Mises. A treatise on economics. Connecticut: Yale University Press; 1949.

[4] H.S. Neap, T.I. Celik, "Value of a product: A definition". International Journal of Value-Based Management, Vol. 12, 1999, 181-191.

[5] D.A. Garvin, "What does product quality really mean?". Sloan Management Review, Vol. 3, 1984, 25-40.

[6] O. Bilkay, O. Analgan, S.E. Kilic, "Job scheduling using fuzzy logic". International Journal of Advanced Manufacturing Technology, Vol. 23, 2004, 606-619.

[7] V. Kannan, S. Ghosh, "An evaluation of the interaction between dispatching rules and truncation procedures in job shop scheduling". International Journal of Production Research, Vol. 31, 1993, 1637-1654.

[8] F. Chan, H. Chan, "Dynamic scheduling for a flexible manufacturing system: The pre-emptive approach". International Journal of Advanced Manufacturing Technology, Vol. 17, 2001, 760-768.

[9] S. Barman, "Simple priority rule combinations: An approach to improve both flow time and tardiness". International Journal of Production Research, Vol. 35, 1997, 2857-2870.

[10] Goldratt, E.M. Theory of constraints, New York: North River Press Inc.; 1990.

[11] D. Witte, M. Ashline, "Determining product value based on consumption of factory constraints". IEEE/SEMI Advanced Semiconductor Manufacturing Conference, 1997.

[12] Hopp, W.J., Spearman, M.L. Factory physics: Foundations of manufacturing management. 2nd ed. New York: McGraw-Hill; 1999.

[13] Gaplan, F. The quality system. 2nd ed. Pennsylvania: Chilton Book Company; 1990.

JJMIE

Volume 4, Number 2, March. 2010
ISSN 1995-6665
Pages 286 - 291

Jordan Journal of Mechanical and Industrial Engineering

Computational Modelling for Solid-State Variable-Frequency Induction Motor Drive - II

Saleh A. Al-Jufout [a,*], Kamal A. Khandakji [b]

[a] Tafila Technical University, Faculty of Engineering, Department of Electrical Engineering,
[b] Yanbu Industrial College, Department of Electrical and Electronics Technology

Abstract

This contribution describes a computational model of the solid-state variable-frequency induction motor drive. The model of the induction motor has been represented as a system of differential equations for flux linkages and angular velocity. These equations have been represented in Cartesian coordinate system, the use of which decreased their number to 7 instead of 10 equations and restricted the use of the model only for symmetrical conditions of operation. The output voltages applied to the terminals of the motor have been given according to voltage-versus-frequency patterns of constant V/f^{2} and constant $V/f^{(1/2)}$. This model has been developed for both transient and steady-state conditions analyses. The waveforms of the current and electromagnetic torque of the motor during sudden acceleration and deceleration have been illustrated and analyzed.

Keywords: Induction Motor; Mathematical Modelling; Solid-State; Variable-Frequency.

1. Introduction

Industrial electronic control, in its wide sense, includes all methods used to control the performance of an engineering system; and has gained a wide acceptance in power technology. When applied to machinery, it involves the starting, acceleration, reversal, deceleration and stopping of a motor and the attached load.

Loads attached to the induction motor may vary greatly. Some of them, like fans, require very little torque at starting or running at low speeds; and have torques which increase as the square of speed.

Other loads might be harder to start, requiring more than rated full-load torque of the motor to get the load moving, such as in hoisting mechanism. Until the advent of modern solid-state drives, induction motors (IM) in general were not the suitable machines for applications requiring considerable speed control.

The method of choice, today, for induction motor speed control, is the solid-state variable-frequency induction motor drive (VFD).

Recently, many papers are devoted to the variable-frequency drives. In Ref. [1], field tests at five sites showed that the pump performance at the reduced speed using VFD could reasonably match the throttled conditions at a reduced horsepower demand. Ref. [2] introduces the application principles, describes the optimal methods of stack sizing, and presents an example which showed that multi-stack and VFD techniques can reduce both the make-up airflow rate and fan energy in the constant speed fan exhaust system. In Ref. [3], a comparison was conducted between on/off and VFD systems to control greenhouse ventilation fans where the results show that the VFD system has a greater potential to reduce the range of amplitude variations in the air temperature and humidity ratio within the greenhouse.

The solid-state variable-frequency induction motor drive provides a variety of voltage-versus-frequency patterns that can be selected to match the torque from the induction motor to the torque required by its load.

At 14th European Simulation Multiconference (ESM'2000) held in May, 2000 in Belgium, the first author of this paper presented a paper entitled: "Computational Modelling for Solid-State Variable-Frequency Induction Motor Drive" [4], in which the output voltages applied to the terminals of the motor had been given according to the general-purpose standard voltage-versus-frequency pattern (*V/f=constant)*. Where the output voltage linearly changes with changes in the output frequency for speeds below the base speed and holds the output voltage constant for speeds above the base speed.

To complete the work done in Ref. [4], in this paper, the output voltages applied to the terminals of the induction motor are given according to the voltage-versus-frequency patterns of $V/f^{2}=constant$ and $V/f^{(1/2)}=constant$. Thus this paper is entitled the same as Ref. [4], but with index (II): "Computational Modelling for Solid-State Variable-Frequency Induction Motor Drive - II".

* Corresponding author. drjufout@ttu.edu.jo.

2. Mathematical Modelling

The three-phase, deep-bar cage induction motor can be mathematically modeled by representing it as a system of differential equations for flux linkages and angular velocity. To take in account the skin effect, the rotor is represented as two parallel-connected resistive-inductive circuits.

To decrease the number of differential equations, the model of the motor is represented in Cartesian coordinate system instead of the phase coordinates, thus the system of differential equations comprises 7 equations instead of 10. This approach decreases the time of computations, but restricts the use of the model only for symmetrical modes of operation [5]. The differential equations can be expressed in orthogonal axes (α, β) as follows [6]:

$$\frac{d\lambda_{S\alpha}}{dt}=v_{S\alpha}-\frac{R_S}{L_{\sigma S}}(\lambda_{S\alpha}-\lambda_{\mu\alpha}) \quad (1)$$

$$\frac{d\lambda_{S\beta}}{dt}=v_{S\beta}-\frac{R_S}{L_{\sigma S}}(\lambda_{S\beta}-\lambda_{\mu\beta}) \quad (2)$$

$$\frac{d\lambda_{R\alpha}^{(1)}}{dt}=-\frac{R_R^{(1)}}{L_{\sigma R}^{(1)}}(\lambda_{R\alpha}^{(1)}-\lambda_{\mu\alpha})-\omega\,\lambda_{R\beta}^{(1)} \quad (3)$$

$$\frac{d\lambda_{R\beta}^{(1)}}{dt}=-\frac{R_R^{(1)}}{L_{\sigma R}^{(1)}}(\lambda_{R\beta}^{(1)}-\lambda_{\mu\beta})+\omega\,\lambda_{R\alpha}^{(1)} \quad (4)$$

$$\frac{d\lambda_{R\alpha}^{(2)}}{dt}=-\frac{R_R^{(2)}}{L_{\sigma R}^{(2)}}(\lambda_{R\alpha}^{(2)}-\lambda_{\mu\alpha})-\omega\,\lambda_{R\beta}^{(2)} \quad (5)$$

$$\frac{d\lambda_{R\beta}^{(2)}}{dt}=-\frac{R_R^{(2)}}{L_{\sigma R}^{(1)}}(\lambda_{R\beta}^{(2)}-\lambda_{\mu\beta})+\omega\,\lambda_{R\alpha}^{(2)} \quad (6)$$

$$\frac{d\omega}{dt}=\frac{1}{J}(\tau_e-\tau_m) \quad (7)$$

where

$\lambda_{S\alpha}, \lambda_{R\alpha}^{(1)}, \lambda_{R\alpha}^{(2)}, \lambda_{S\beta}, \lambda_{R\beta}^{(1)}, \lambda_{R\beta}^{(2)}$ - The flux linkages of the stator and the rotor circuits in α, β coordinates respectively;

$R_S, R_R^{(1)}, R_R^{(2)}$ - The resistances of the stator and the rotor circuits respectively;

$L_{\sigma S}, L_{\sigma R}^{(1)}, L_{\sigma R}^{(2)}$ - The leakage inductances of the stator and the rotor circuits respectively;

$v_{S\alpha}, v_{S\beta}$ - The applied voltages in α, β coordinates respectively;

$\lambda_{\mu\alpha}, \lambda_{\mu\beta}$ - The flux linkages of the magnetization branch in α, β coordinates respectively;

ω - The angular velocity of the motor;

J - The combined rotor and mechanical load inertia;

τ_e, τ_m - The electromagnetic and the mechanical torque respectively.

The electromagnetic torque and the flux linkages of the magnetization branch can be calculated as follows:

$$\tau_e=\frac{1}{L_{\sigma S}}\left[\lambda_{S\beta}\sum_{i=1}^{2}k_R^{(i)}\lambda_{R\alpha}^{(i)}-\lambda_{S\alpha}\sum_{i=1}^{2}k_R^{(i)}\lambda_{R\beta}^{(i)}\right] \quad (8)$$

$$\lambda_{\mu\alpha}=k_S\lambda_{S\alpha}+\sum_{i=1}^{2}k_R^{(i)}\lambda_{R\alpha}^{(i)} \quad (9)$$

$$\lambda_{\mu\beta}=k_S\lambda_{S\beta}+\sum_{i=1}^{2}k_R^{(i)}\lambda_{R\beta}^{(i)} \quad (10)$$

Where the contribution coefficients can be calculated as follows:

$$k_S=\frac{1}{L_{\sigma S}}\left[\frac{1}{L_{\sigma S}}+\frac{1}{L_\mu}+\sum_{i=1}^{2}\frac{1}{L_{\sigma R}^{(i)}}\right]^{-1} \quad (11)$$

$$k_R^{(1)}=\frac{1}{L_{\sigma R}^{(1)}}\left[\frac{1}{L_{\sigma S}}+\frac{1}{L_\mu}+\sum_{i=1}^{2}\frac{1}{L_{\sigma R}^{(i)}}\right]^{-1} \quad (12)$$

$$k_R^{(2)}=\frac{1}{L_{\sigma R}^{(2)}}\left[\frac{1}{L_{\sigma S}}+\frac{1}{L_\mu}+\sum_{i=1}^{2}\frac{1}{L_{\sigma R}^{(i)}}\right]^{-1} \quad (13)$$

where

L_μ - The inductance of the magnetization branch.

The stator currents can be calculated as follows:

$$i_{S\alpha}=\frac{\lambda_{S\alpha}-\lambda_{\mu\alpha}}{L_{\sigma S}} \quad (14)$$

$$i_{S\beta}=\frac{\lambda_{S\beta}-\lambda_{\mu\beta}}{L_{\sigma S}} \quad (15)$$

The above mentioned differential equations can be solved by fourth-order Runge-Kutta method [7]. The equivalent circuit parameters (resistances and inductances) can be defined in per unit (p.u.) by engineering methods [8, 9]. And the mechanical load can be either a constant or as a function of the angular velocity. To simulate the solid-state variable-frequency drive, it is suggested that the applied voltages to be given according to the voltage-versus-frequency pattern of V/f^2=*constant* as follows:

$$v_a=k_dV_{\max}\sin(\sqrt{k_d}\,\omega t) \quad (15)$$

$$v_b=k_dV_{\max}\sin(\sqrt{k_d}\,\omega t-120^o) \quad (16)$$

$$v_c=k_dV_{\max}\sin(\sqrt{k_d}\,\omega t-240^o) \quad (17)$$

where

k_d - the scaling coefficient:

$0 < k_d \le 1$

The phase voltages can be represented in Cartesian coordinate system as follows:

$$v_\alpha = v_a \tag{18}$$

$$v_\beta = \frac{v_b - v_c}{\sqrt{3}} \tag{19}$$

The mechanical torque is given as a function of the angular velocity:

$$\tau_m = f(\omega) \tag{20}$$

To simulate the drive according to the voltage-versus-frequency pattern of $V/f^{(1/2)}$=*constant*, it is suggested that (15), (16) and (17) to be replaced by the following equations:

$$v_a = k_d V_{\max} \sin(k_d^{\,2}\,\omega t) \tag{21}$$

$$v_b = k_d V_{\max} \sin(k_d^{\,2}\,\omega t - 120^o) \tag{22}$$

$$v_c = k_d V_{\max} \sin(k_d^{\,2}\,\omega t - 240^o) \tag{23}$$

3. Case Study

In this section, starting with low frequency followed by sudden acceleration and starting with rated frequency followed by sudden deceleration are simulated.

This case study is modeled and simulated for both voltage-versus-frequency patterns ($V/f^{\,2}$=*constant* and $V/f^{(1/2)}$=*constant*).

Fig. 1, and Fig. 2, show, respectively, the phase currents and electromagnetic torque of the motor during starting with 50-Hz frequency followed by a sudden deceleration to the half of the rated speed according to the pattern of $V/f^{\,2}$=*constant*. As shown from Fig. 1, the inrush current during direct on-line starting is about 8.42 p.u. and the starting duration is about 0.76 s. Then suddenly the applied voltages are changed to 25% of the rated with a frequency of 25 Hz that simulates a sudden deceleration from the rated speed to half of the rated. The inrush current associated with this sudden deceleration is about 6.53 p.u. Fig. 2 shows the electromagnetic torque of the motor from which it is obvious that the inrush starting torque is about 2.41 p.u. and is about 4.12 p.u. at the sudden deceleration. Here the negative torque indicates that the motor operates in the second quadrant (generation mode) until it loses the extra kinetic energy stored in its rotor. The motor should be protected from these large values of currents and electromagnetic torque, thus this process is performed through independently adjustable acceleration and deceleration ramps mainly controlled by time. Fig. 3 and Fig. 4 show the same values shown in Fig. 1 and Fig. 2, but during starting by applying 25% of the rated voltage with 25-Hz frequency followed by a sudden acceleration to the rated speed. By comparing the starting processes, it is obvious that, in the later case, it is softer and longer.

The sudden acceleration is also associated with large inrush values of current (7.46 p.u.) and electromagnetic torque (2.88 p.u.), while the motor operates in the first quadrant during all the process time.

It is noticed also from these figures that the developed model can be used for both transient and steady-state conditions. The steady-state values of the phase currents and electromagnetic torque are different after both sudden acceleration and deceleration because the mechanical torque is given as a function of the angular velocity.

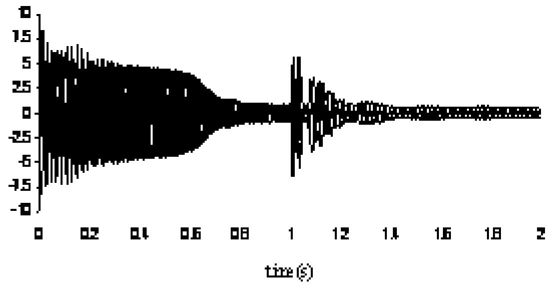

Figure 1. Phase currents of IM in p.u. during starting with 50-Hz frequency followed by a sudden deceleration to the half of the rated speed where the voltage is applied according to the pattern of $V/f^{\,2}$=*constant*.

Fig. 5 and Fig. 6 show, respectively, the phase currents and electromagnetic torque of the motor during starting by applying 50-Hz rated voltages followed by a sudden deceleration to the half of the rated speed according to the pattern of $V/f^{(1/2)}$=*constant*.

As shown from Fig. 5, the inrush current at the sudden deceleration is about 10.68 p.u., while the inrush electromagnetic torque is about 8.79 p.u. (Fig. 6).

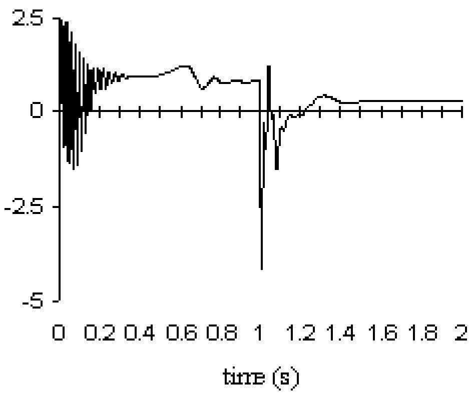

Figure 2. Electromagnetic torque of IM in p.u. during starting with 50-Hz frequency followed by a sudden deceleration to the half of the rated speed where the voltage is applied according to the pattern of $V/f^{\,2}$= *constant*

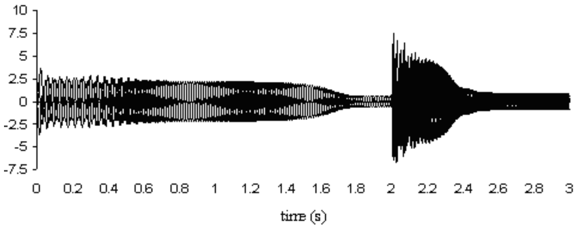

Figure 3. Phase currents of IM in p.u. during starting with 25-Hz frequency followed by a sudden acceleration to the rated speed where the voltage is applied according to the pattern of *V/f* ^{2}*=constant.*

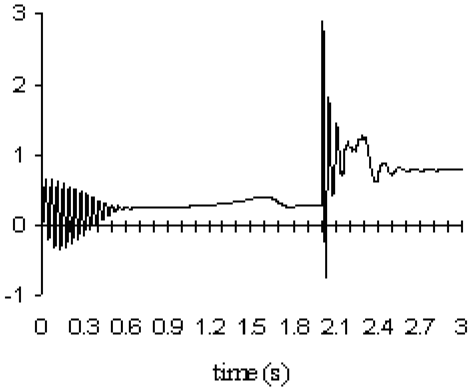

Figure 4. Electromagnetic torque of IM in p.u. during starting with 25-Hz frequency followed by a sudden acceleration to the rated speed where the voltage is applied according to the pattern of *V/f* ^{2}*=constant.*

Fig. 7 and Fig. 8 show the same values shown in Fig. 5 and Fig. 6, but the applied voltages, during starting, are 70.7% of the rated with 25-Hz frequency. When Comparing Fig. 3 with Fig. 7, it is obvious that the starting duration, in the later, is shorter because the applied voltages are 70.7% of the rated.

It is noticed also that this starting duration is shorter than in the case of full-voltage starting of Fig. 1 and Fig 5,because of the dependence of the mechanical load on the angular velocity.

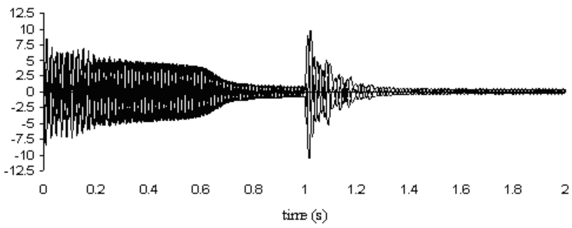

Figure 5. Phase currents of IM in p.u. during starting with 50-Hz frequency followed by a sudden deceleration to the half of the rated speed where the voltage is applied according to the pattern of *V/f* $^{(1/2)}$*=constant.*

Practically, when the desired speed of the motor is changed, the solid-state variable-frequency controlling it will also change the voltage and frequency to bring the motor to the new operating speed. If the change is sudden, the drive does not try to make the motor instantaneously jump to the new desired speed. Instead, the rate of the induction motor acceleration or deceleration is limited to safe rates by special circuits built into the electronics of the solid-state drive. These rates can be adjusted independently for accelerations and decelerations.

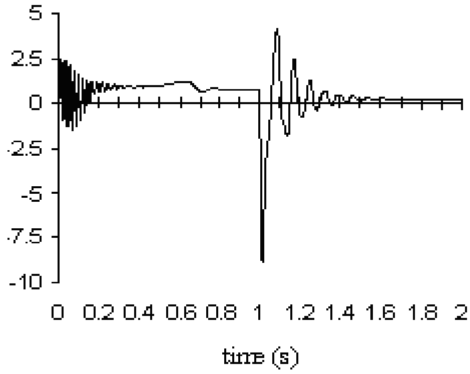

Figure 6. Electromagnetic torque of IM in p.u. during starting with 50-Hz frequency followed by a sudden deceleration to the half of the rated speed where the voltage is applied according to the pattern of *V/f* $^{(1/2)}$*= constant.*

The results of the assumed case study and their analysis can be used for condition analysis, determining the independent rates of accelerations and decelerations for a certain drive with a certain mechanism and load characteristic, and for engineering education.

Here also the importance of computational modelling and simulation can be obviously noticed since the assumed case study cannot be performed experimentally due to the dangerous consequences of sudden acceleration and deceleration.

Finally, the obtained results confirm that the processes of sudden acceleration and deceleration are associated with undesirable large values of inrush currents and electromagnetic torques.

Avoiding these large values is performed by limiting the rate of acceleration or deceleration to a safe level that can be adjusted independently by the use of the developed model.

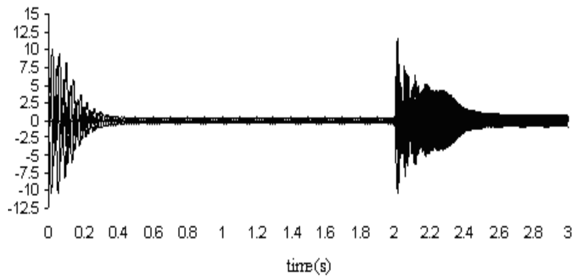

Figure 7. Phase currents of IM in p.u. during starting with 25-Hz frequency followed by a sudden acceleration to the rated speed where the voltage is applied according to the pattern of *V/f* $^{(1/2)}$*=constant*

4. Conclusion

The computational model of the solid-state variable-frequency induction motor drive is developed. The model of the induction motor is represented as a system of differential equations for flux linkages and angular velocity. These equations are represented in Cartesian coordinate system, the use of which decreases their number to 7 instead of 10 equations and restricts the use of the model only for symmetrical conditions of operation.

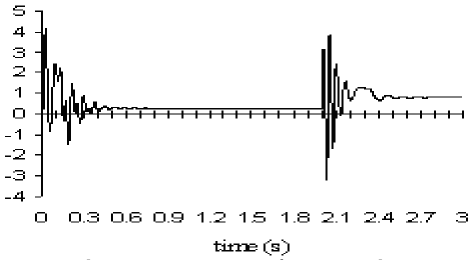

Figure 8. Electromagnetic torque of IM in p.u. during starting with 25-Hz frequency followed by a sudden acceleration to the rated speed where the voltage is applied according to the pattern of $V/f^{(1/2)}=constant$.

The starting process followed by sudden acceleration or deceleration according to two different voltage-versus-frequency patterns ($V/f^{2}=constant$ and $V/f^{(1/2)}=constant$) are simulated and the corresponding waveforms of the phase currents and electromagnetic torque are illustrated and analyzed. The obtained results confirm that the processes of sudden acceleration and deceleration are associated with undesirable large values of inrush currents and electromagnetic torques. Avoiding these large values is performed by limiting the rate of acceleration or deceleration to a safe level by special circuits built into the electronics of the solid-state drive. The developed model is recommended for optimum determination of these rates.

References

[1] B. Hanson, C. Weigand, S. Orloff, "Performance of electric irrigation pumping plants using variable frequency drives". Journal of Irrigation and Drainage Engineering. Vol. 122, No. 3, 1996, 179-182.

[2] G. Wang, M. Liu, Y. Cui, D. Yuill, "Retrofit constant speed fan laboratory exhaust systems using multi-stack and variable frequency drive techniques". Journal of Solar Energy Engineering. Vol. 126, No. 1, 2004, 610-613.

[3] M. Teitel, Y. Zhao, M. Barak, E. Bar-lev, D. Shmuel, "Effect on energy use and greenhouse microclimate through fan motor control by variable frequency drives". Energy Conversion and Management. Vol. 45, No. 1, 2004, 209-223.

[4] S. Al-Jufout, "Computational modelling for solid-state variable-frequency induction motor drive". 14th European Simulation Multiconference, Ghent, Belgium, 2000.

[5] S. Al-Jufout, "Fault simulation by hypothetical stub moving along medium-length transmission line". 13th IEEE Mediterranean Electrotechnical Conference, Benalmadena, Spain, 2006.

[6] S. Al-Jufout, "Modelling of the cage induction motor for symmetrical and asymmetrical modes of operation". Computers and Electrical Engineering. Vol. 29, No. 11, 2003, 851-860.

[7]Richard L, Douglas J. Numerical analysis. 7th ed. Brooks/Cole Publishing Company, Kentucky: Florence; 2002.

[8] Sivokobylenko V. Transients in multi-machine power supply systems of power stations. DonNTU, Ukraine: Donetsk; 1984.

[9]Sivokobylenko V, Kostenko V. Electrical motors mathematical modelling of the power station auxiliaries. DonNTU, Ukraine: Donetsk; 1979.

JJMIE
Volume 4, Number 2, March. 2010
ISSN 1995-6665
Pages 292 - 299
Jordan Journal of Mechanical and Industrial Engineering

A Development of Technology for Making Porous Metal Foams Castings

A. K. Shaik dawood [a,*], S. S. Mohamed Nazirudeen [b]

[a]Institute of Technology, Coimbatore, India, [b]Department of Metallurgy, P.S.G. College of Technology, Coimbatore, India

Abstract

Metal foams are revolutionary materials that exhibit different attractive characteristics when compared to their solid material counterparts. Cellular structure of these materials provides the tool for the realization of optimal combination of properties. In the past, when a large dense metal contained any kind of pores, it was considered “defect” and therefore unsuitable for engineering purposes. In recent years, a great importance has been attached to a new class of engineering material, known as “Porous metals or metal foams” as a result to their unique mechanical and physical properties. This paper deals with the method of producing porous gray cast iron castings. Experimentation is done and involves the development of a porous gray iron casting, using casting techniques, Box-Behnken Design is applied and density, percentage porosity is found out also radiography, microstructure, SEM analysis, compression and hardness testing is done.

Keywords: Metal foams; Porosity; DOE; Hardness; SEM; Radiography.

1. Introduction

Metal foams are a subgroup of cellular metals, usually having polyhedral cells, but shapes may vary in cases where directional solidification creates different morphologies. Metal foams are either open cell, closed cell, or a combination of the two. Owing to their pores, metal foams are classified into open cell, closed cell metal foams. Open cell foam forms a network of interconnected solid struts. Open cell foam allows fluid media to pass through it. Closed cell foam is made up of a network of adjacent sealed pores, all sharing walls with each other. The difference between the closed and open cell configuration is clearly seen in pores. Open cell allows the passage of fluids and gasses for different applications ranging from filtering to heat exchange and gives the foam its increased surface area while the closed cell configuration is optimal for energy absorption and structural applications like in car bumpers, bridges and buildings. A fluid media can not pass through closed cell foam. Closed cell foams are being used in light-weight constructions due to their high stiffness and low density. The development of metal foams improves the properties when compared to non-metal foams and solid metals. Compared to non-metal foams, metal foams offer higher stiffness, better strength to weight ratios, increased impact energy absorption, a greater tolerance to high temperatures, and adverse environmental conditions. In comparison to solid metals, metal foams offer higher specific stiffness (stiffness to weight ratio) and by altering the size, shape, and volume fraction of cells, mechanical properties can be engineered to meet the demands of a wide range of applications. In this paper, Design of Experiments (DoE) is implemented as it is widely used in research and development, where a large proportion of the resources go towards solving optimization problems. The key to minimizing optimization costs is to conduct as few experiments as possible. DoE requires only a small set of experiments, and thus helps to reduce costs.

2. Literature Survey

The first metal foam was invented in 1943, by Benjamin Sosnick of San Francisco California. A pore is the open volume within the metal matrix or network with uniform distribution and length of passages. By manipulation of the process parameters, the pore structure can assume continuous or discontinuous geometries, a range of pore sizes, pore fractions, and a controllable shape of the final product. The continuous pores are connected together and to the surfaces of the component to allow fluid flow from one side to the other. Banhart has summarized the potential applications of metallic foams as a function of their porosity. High porosity metallic and nonmetallic media are engineered materials designed for special properties which can be used in many industrial applications including transportation. Metallic foams possess unique combinations of properties such as unusual

* Corresponding author. siva_appisetty1@yahoo.co.in

acoustic properties, altitudinous damping energy capacity, and in automotive industry, the most important driving forces are cost reductions. The development of new porous structures can be a relevant challenge for materials scientists.

The ways by which cellular metallic materials can be produced are Liquid Metallurgy Route & Powder Metallurgy. Liquid Metallurgy Route method involves foaming of metallic melt either by using reactant and foaming agent, or by inert gas injection in the melt. The foaming agent and the reactant are mixed after pretreatment into the melt through mechanical stirrer; and is allowed to dissociate the foaming agent to release gases so that the metallic foam is formed. Powder Metallurgy powder route involves metal and foaming agent which are mixed and compacted. Then the compacted mass is heated just above the solidus temperature under pressure. The powder compaction of metal and foaming agent can be subsequently hot rolled to obtain sheet of porous metallic foam.

2.1. Foams Made from Metallurgy Route Using Filler Materials

A first group of foam making processes starts from the molten metal that is processed to a porous material by either foaming it directly, by using an indirect method as by casting the liquid metal around solid filler materials which reserve space for the pores or which remain in the foam. Light-weight porous metals can be produced by casting around inorganic granules or hollow spheres of low density or by infiltrating such materials with a liquid melting. The granules are then introduced into the melt, or the melt is poured over the bulk of filler material. The heat capacity and conductivity of the granules is very low and therefore does not disturb the flow of the metal too much. A wide range of metals can be processed this way including aluminum, magnesium, iron, zinc, lead, tin etc. Parts of a predefined shape can be fabricated by designing a mould of the appropriate geometry. In this paper, sand balls are introduced in molten gray cast iron for the production of porous castings.

2.2. Gray Cast Iron

Gray iron is one of the most easily cast of all metals in the foundry. It has the lowest pouring temperature of the ferrous metals, which is reflected in its high fluidity and its ability to be cast into intricate shapes. The graphite flakes which are rosettes in three dimensions, have a low density, and hence compensate for the freezing contraction, thus giving good castings. The flakes of graphite have good damping characteristics and good machinability because the graphite acts as a chip-breaker and lubricates the cutting tools. In applications involving wear, the graphite is beneficial because it helps to retain lubricants.

In this paper, Design of Experiments is applied, and it is one of the Quality tool. Taguchi has developed a system of tabulated designs (arrays) that allow for the maximum number of main effects to be estimated in an unbiased (orthogonal) manner, with a minimum number of runs in the experiment. Here Box-Behnken design is a response surface methodology design. It is used to further study the effect of factors after identifying the significant factors using screening factorial experiments.

3. Experimentation

3.1. Casting Metal around Granules

It is a manufacturing process by which a liquid material is usually poured into a mold which contains a hollow cavity of the desired shape, and then allowed to solidify. The solidified part is also known as a casting, which is ejected or broken out of the mold to complete the process. The casting of metals and alloys around a filler material has recently attracted a lot of interest. In this process, the following three steps are done as Preparation of space-holder filler, by using either inorganic or organic granules Infiltration of the filler with a metal, Removal of filler granules.

3.2. Preparation of Sand Balls

Sand balls were prepared manually, using core box with the mixture consisting of Silica sand, Bentonite, Dextrin and Sodium silicate as filler materials, Fig. 1 showing the picture sand balls.

Figure 1. Showing the picture of sand balls.

3.3. Melting & pouring of gray cast iron

A wooden pattern 180mm X 170mm X 65mm was used to produce a mould, using green sand mold with 5% clay and 3.5% moisture. The sand balls were filled in to the mould cavity. Sand casting done with molding box of 640mm X 480mm X 150mm made of cast iron was used. Gray cast iron was melted in an induction furnace with the following proportions as listed in table 1 and inoculated with 0.2% Barium based inoculant added at the ladle was poured into the mould cavity at various temperatures as 1380 °C. (2516° F), 1385 °C. (2525° F) and 1390° C. (2534° F)composition shown in table 1,table 2& table 3 The poured mould was knocked off, separated from the gating system and shot blasted for all three different pouring temperatures.

Table 1. Proportion of gray cast iron at 1380 C. (2516 F)

Element	C	Si	Mn	S	P
Wt %	3.34	2.18	0.56	0.14	0.25

Table 2. Proportion of gray cast iron at 1385 C. (2525 F)

Element	C	Si	Mn	S	P
Wt %	3.38	2.20	0.60	0.16	0.28

Table 3. Proportion of gray cast iron at 1390 C. (2534 F)

Element	C	Si	Mn	S	P
Wt %	3.36	2.20	0.58	0.15	0.27

4. Testing of Porous Gray Cast Iron

4.1. Density and Development of porosity

The foams are characterized in terms of their density since the mechanical properties of metallic foams depend largely on the density. Density is a physical characteristic; and is a measure of mass per unit of volume of a material or substance.

Density = weight of the porous casting / volume of the casting produced.

Percentage Porosity is a rough measure of the open volume equal to 100% minus the part density. The total open volumes of interconnected and isolated porosity are normally found out. Here, experiment was done with a non porous model initially to find the density and with porous models from run 1 to trail 15 using Box-Behnken design analysis.

$$\% \text{ Porosity} = \frac{(\text{Bulk casting density} - \text{Produced casting density})}{\text{Bulk casting density}} \times 100$$

Table 4. Showing Pattern size, weight, density and % Porosity of nonporous sample

Type of Casting	Sand balls size, mm	Pattern size(l x b xw), mm	Weight, kg	Density,10–6 kgfmm–3	% porosity
Non porous	Nil	180 X 170 X 65	14.32	7.2	Nil

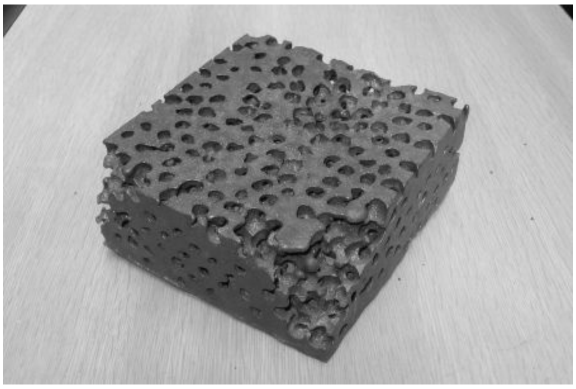

Figure 2.Minimum % porosity 43.61.

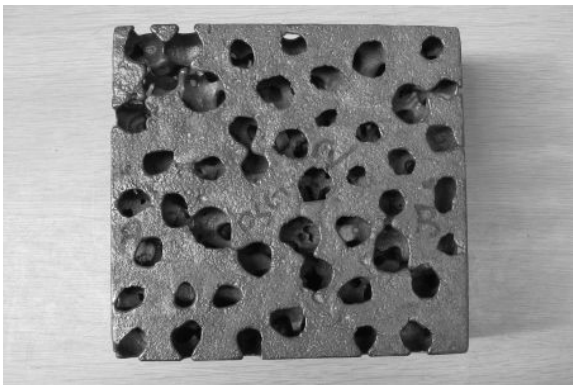

Figure 3.Maximum % porosity 72.08.

4.2. Factors Which Influence The Castings

a). Pouring temperature, (b). Composition, (c). Casting Prcessing techniques in foundry, (d). % Bentonite in sand mixture, (e). Size of sand balls, (f).Solidification & Cooling rates, (g). Inoculation, (h). Mould material.

In this research paper, factors like which influence the porous gray iron casting are temperature, % Bentonite in sand ball mixture and size of sand balls and the response factors are weight, density and percentage porosity.

The percentage porosity is being considered as a main property for structural applications as designed parts have their dimensions, defined according to the known material strength. The changes are seen in percentage porosity levels when weight and density decrease and the understanding the relationship with the processing variables may be accomplished by applying statistical techniques as design of experiments (DOE).

Design of experiments is an advanced statistical tool to efficiently study the effect of a large number of variables with a minimum effort in data collection. The inputs and outputs are described as factors, and responses and the experimental settings of the factors are designed with orthogonal arrays. Statistical means are available for analysis of the response data. This method can give maximum amount of information with a given amount of experimental data, in other words more information can be obtained through a minimum number of experiments. Box-Behnken designs are experimental designs for response surface methodology, devised by George E. P. Box and Donald Behnken in 1960,Table 5 showing the response factors. Table 6 shows BOX-Behnken design matrix. By using Box-Behnken design, Table 7 is formed and weignt,density & % porosity is shown. Using Box-Behnken design response, the results are shown in ANOVA table 8 as Analysis of variance

Table 5. Showing the response factors.

Process parameter	-1	0	1
Temperature °C	1380	1390	1398
% of Bentonite in sand balls mixture	6	8	10
Sand ball size (mm)	15	30	45

Table 6. Box-Behnken design matrix.

RUN	X1	X2	X3
1	-1	-1	0
2	-1	1	0
3	1	-1	0
4	1	1	0
5	-1	0	-1
6	-1	0	1
7	1	0	-1
8	1	0	1
9	0	-1	-1
10	0	-1	1
11	0	1	-1
12	0	1	1
13	0	0	0
14	0	0	0
15	0	0	0

Excel's Solver is a good tool for solving simple problems (continuous and discrete). The model can be incorporated into existing spreadsheets. Objective functions and constraints can reference and be referenced by other aspects of the worksheet, because spreadsheets are excellent tools for viewing data and for building models. Moreover, spreadsheets provide utilities such as graphing capabilities that facilitate analysis. And finally they offer links to other utilities that greatly expand the domain of an application.

Table 7. Box-Behnken design matrix showing weight, density & % porosity.

Run	X1	X2	X3	Weight	Density	% porosity
1	1380	6	30	5.3	2.66	63.05
2	1380	10	30	4.9	2.46	65.83
3	1398	6	30	5.4	2.71	62.36
4	1398	10	30	5.0	2.51	65.13
5	1380	8	15	7.2	3.61	49.86
6	1380	8	45	4.2	2.11	70.69
7	1398	8	15	7.0	3.51	51.25
8	1398	8	45	4.3	2.16	70.00
9	1390	6	15	7.3	3.67	49.02
10	1390	6	45	4.1	2.06	43.61
11	1390	10	15	6.8	3.41	52.63
12	1390	10	45	4.0	2.01	72.08
13	1390	8	30	5.2	2.61	63.75
14	1390	8	30	5.1	2.56	64.44
15	1390	8	30	5.0	2.51	65.13

Table 8.ANOVA table showing analysis of variances.

Factors	WEIGHT		DENSITY		% POROSITY	
Source	Regress-ion	Residual	Regression	Residual	Regression	Resid-ual
Sum of squares	18.33	0.047	4.602	0.012	942.152	171..015
Df	9	5	9	5	9	5
Mean squares	2.037	0.009	0.511	0.002	104.684	34.23
F-ratio	214.38		212.59		3.061	
P-value	0		0		0.175	
R	0.999		0.999		0.920	

ANOVA table evaluated results using SYSTAT-15 software, Multiple value "R" for weight gives 0.999 then Multiple value "R" for Density denotes 0.999 and Multiple value "R" denotes for % porosity as 0.920,hence all are in good agreement at acceptable levels. Using solver it is solved and optimized

DY-Linear model equation for **DENSITY** analysis

DY=2.560+0.006*A-0.089*B-0.732*C+0.043*A^2-0.017*B^2+0.245*C^2+0.038*A*C+0.052*B*C

Ans= 2.0077

Table 9. the coded and uncoded values for optimising temperature

Factors	Coded values	Uncoded values
Temperature	-0.5116	1384.7

Using lagrangian method of interpolation, temperature final values are optimized

Table 10 Showing the levels for optimising temperature .

x	-1	0	1
y	1380	1385	1390

X=0. -0.5116(coded value) from table 9

Y=(x-0)(x-0)/(-1-0)(-1-1)*(1380)+(x+1)(x-1)/(0+1)(0-1)*(1385)+(x+1)(x-0)/(1+1)(1-0)*(1395)

Y=1384.7

Linear model equation for WEIGHT analysis

WT=5.100+0.012*A-0.175*B-1.463*C+0.088*A^2-0.037*B^2+0.487*C^2+0.075*C*A+0.100*B*C

Ans = 3.990

Table 11. the coded and uncoded values for optimizing % of Bentonite in sand ball mixture

Factors	Coded values	Uncoded values
% of Bentonite in sand ball mixture	1	10

Using lagrangian method interpolation, % of Bentonite in sand ball mixture final values are optimized

Table 12 the levels for optimising % of Bentonite in sand ball mixture

x	-1	0	1
y	6	8	10

X=1(coded value) from table 11

Y=(x-0)(x-0)/(-1-0)(-1-1)*(6)+(x+1)(x-1)/(0+1)(0-1)*(8)+(x+1)(x-0)/(1+1)(1-0)*(10)

Y=10

Linear model equation for % POROSITY analysis

PY=64.440-0.086*A+4.704*B+6.702*C+2.884*A^2-3.231*B^2-6.874*C^2-0.003*A*B-0.520*A*C+6.215*B*C

Ans=74.297

Table 13. Showing the coded and uncoded values for optimizing size of sand balls

Factors	Coded values	Uncoded values
Size of sand balls	0.90173	43.5

Using lagrangian method interpolation, size of sand ball, final values are optimized

Table 14 Showing the levels for optimizing size of sand balls

x	-1	0	1
y	15	30	45

X=0.90173 (coded value) from table 13

Y=(x-0)(x-0)/(-1-0)(-1-1)*(15)+(x+1)(x-1)/(0+1)(0-1)*(30)+(x+1)(x-0)/(1+1)(1-0)*(45)

Y=43.5

Results after optimization

Predicted values and obtained values using model equations were in very good agreement with the experimental values.

5. Testing of Porous Gray Cast Iron

5.1. Radiography Test

Radiography is an effective method of nondestructively detecting internal flaws in materials and structures. The radiation source emits energy that travels in straight lines and penetrates the test piece. The major objective of radiographic testing of castings is the disclosure of defects that adversely affect the strength of the product. The castings used to produce the standard radiographs have been destructively analyzed to confirm the size and type of discontinuities present. Castings are a product form that often receive radiographic inspection since many of the defects produced by the casting process are volumetric in nature; and are thus relatively easy to detect with this method. The porous gray iron samples were subjected to radiographic inspection for analyzing the pores formed in the metal. The dark region of the film represents the more penetrable part of the object than the light regions which were more opaque. Fig 4 shows the radiography image of % porosity of minimum porosity of 43.61 and Fig 5 shows the radiography image of % porosity of maximum porosity of 72.03.

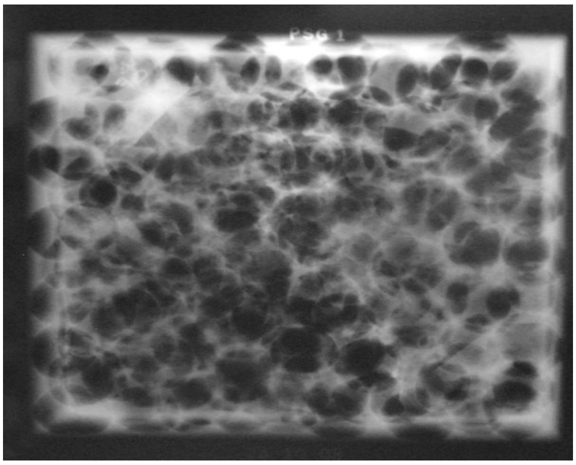

Figure4. Radiography view, % porosity 43.61.

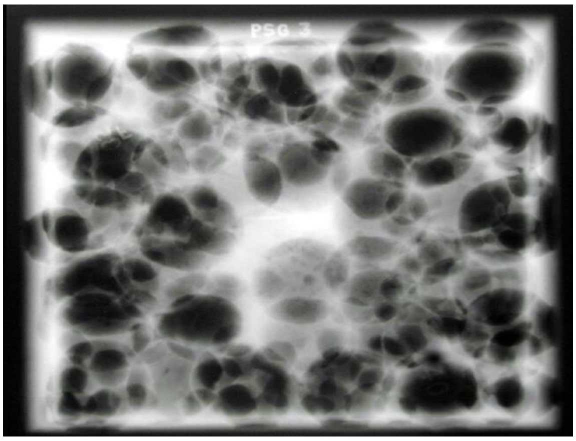

Figure 5. Radiography view, % porosity 72.03

5.2. Hardness Testing -Brinell Hardness Test

The Metals Handbook defines hardness as "Resistance of metal to plastic deformation, usually by indentation. The greater the hardness of the metal is, the greater resistance it has to deformation. Brinell hardness is used as an indication of machinability, resistance to wear, and tensile strength. For light sections, such as piston rings and other light castings have a small graphite size. The Brinell hardness test is a specialized compression test and measures the combined effect of matrix hardness, graphite configuration, and volume of graphite. The full load is normally applied for 10 to 15 seconds in the case of iron and steel and for at least 30 seconds in the case of other metals. Table 9 shows Brinell hardness test for non porous and porous gray cast iron. The diameter of the indentation left in the test material was measured with a low powered microscope. The Brinell harness number is calculated by dividing the load applied by the surface area of the indentation.

HB = 2F/ (3.14D*(D-(D² - d²)½))

$$HB = 2F / (3.14D*(D-(D^2 - d^2)^{1/2}))$$

F- applied load kgf, **D** – indenter diameter mm , d – indentation diameter, mm.

Table 9 showing Brinell hardness test for non porous and porous gray cast iron

Test surfaces	Material	Diameter of indenter “D”(mm)	Load “F”(kgf)	Diameter of indentation “d”(mm)	BHN
Non porous surface	Non Porous gray cast iron	10	3000	3.9	242
Porous sample 1	Porous gray cast iron	10	3000	4	230
Porous sample 2	Porous gray cast iron	10	3000	4.1	218
Porous sample 3	Porous gray cast iron	10	3000	4.2	208

5.3. Compression Test

The compression test of metallic foams is considered as one of the most applicable tests for the characterizations of their mechanical stability. It is the method for determining behavior of materials under crushing loads. Porous Sample was compressed and deformation was recorded.

Table 10. Compression load on non porous and porous samples.

Specimen	Breakable Load, KN	Size(l x b x w) mm
Non-Porous Sample	1400 & above	90x85x65
Porous Sample 1	325	90x85x65
Porous Sample 2	375	90x85x65
Porous sample 3	400	90x85x65

It was seen that during compressive loading of such material are much smoother than those of previously-available melt route materials. Table 10 shows the compression load test which indicates breakable-load capacity for non porous and porous samples.

6. Metallographic Characterisation

The preparation of the samples for the metallographic examination is to preserve the foamed structure, and then the samples containing the pores were sawed carefully to avoid of cast iron specimens usually consists of five stages sampling, cold or hot mounting, grinding, polishing, and etching with a suitable etchant to reveal the microstructure.

Figure 6. Microstructure at unetched condition.

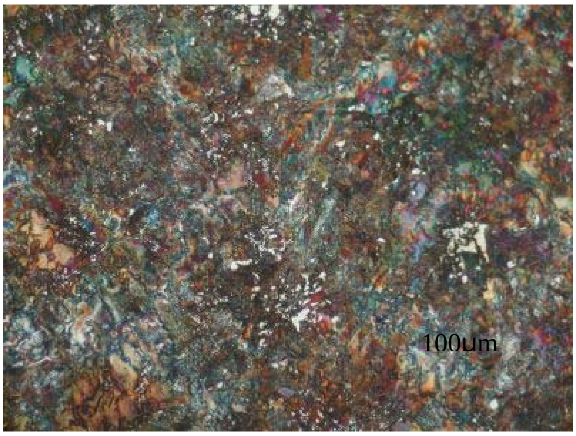

Figure 7. nital etch condition.

Microstructure of gray cast iron etched with 2% nitric acid in ethanol (nital) in fig.7 with 200X nital etched and in Fig.6 with 100X unetched condition.The study of microstructure reveals type A & D graphite with 60-70% pearlite and rest ferrite.

6.1. Scanning Electron Microscope

Scanning electron microscopy is used for inspecting topographies of specimens at very high magnifications, using a piece of equipment called the scanning electron microscope. SEM inspection is often used in the analysis of cracks and fracture surfaces, bond failures, and physical defects on surface. For this research JOEL JSM 6360 was used with an acceleration voltage of 25 kV in order to provide details of the cell wall failure as shown if Fig 8. SEM of porous sample, 500X and Fig 9.SEM of porous sample, 1000X

It is an important tool for materials and failure analysis can provide high magnification, high resolution images of samples at magnifications up to 50,000X.

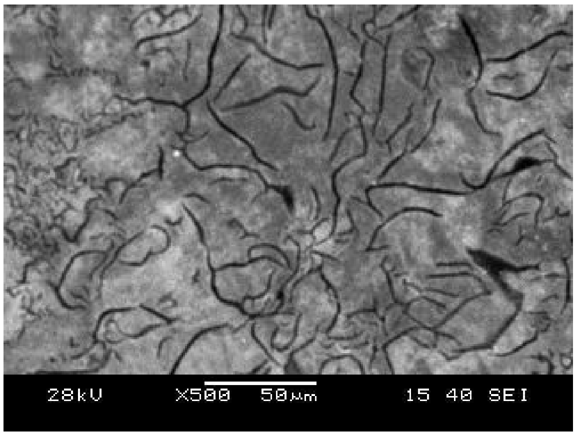

Figure 8. SEM of porous sample, 500X.

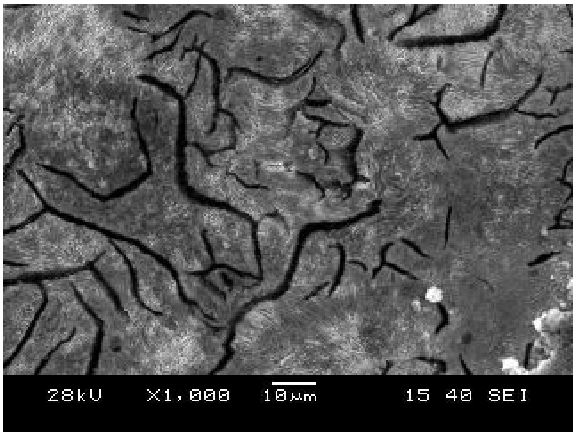

Figure 9.SEM of porous sample, 1000X.

7. Application

- Porous cast iron is used as carrier element for a vechicle body, it relates to a support element, in a cavity is filled with cast iron foam. This metal foam leads to an increase in mechanical strength. Weight saving of over 50% compared to steel.
- Porous cast iron skillet, a Frey pan for faster cooking.
- Porous cast iron bonded diamond grinding wheels used as abrasive grains.
- Porous bearings are very useful in locations with required access when regular lubrication systems are difficult to implement

8. Conclusion

A technique has been developed for preparation of Porous gray cast iron metal foam. The technique is based on casting metal around granules and achieved a maximum percentage porosity in gray cast iron to 72.03%. To determine the dependence of the mechanical properties on varying porosities, the tests are carried out on porous gray cast iron foams of different densities. Design of

Experiment involves designing experiments, in which all relevant factors are varied systematically; the results of these experiments are analyzed using Box-Behnken design. Using these sets of experimental data obtained by mathematical software package (SYSTAT 15), mathematical models were developed to show the effect of each parameter and their interactions. Predicted values and obtained values using model equations were in good agreement with the experimental values. This study proved that Box-Behnken design could efficiently be applied for finding the percentage porosity in porous gray cast iron, they help to identify optimal conditions, the factors that most influence the results. Furthermore, Study of foam cell structures a metallographic examination gives an insight into the pore structure and reveals information on pore size, pore distribution and the interconnections of the open cells. SEM photographs reveal a fractured surface of porous gray cast iron. Radiography test confirms that no mass segregation of the metal at any place in the casting. From Compression test, it is identified that due to porosity, a minimum load of 325 KN was utilized to compress the porous piece whereas maximum load for non-porous model was above 1400 KN and Hardness testing gives 242 BHP to nonporous gray cast iron and 208 to porous gray cast iron.

Acknowledgements

The author thank PSG & Sons Charities Metallurgy & Foundry division, Neelambur, Coimbatore, India for supporting the authour during the study.

References

[1] Ashby, M. F., Evans, A. G., Fleck, N. A., Gibson, L. J., Hutchingson, J. W. and Wadley, “Metal Foams, A Design Guide,” Butterworth- Heinemann, Woburn, MA, Chapter1, 181-188,2000.

[2]. ASM Metals Handbook: Ninth Edition, Volume 15, Casting, ASM, 1988.

[3] Lu Tianjian,‘Ultra light porous metals: from fundamentals to applications ‘ (Department of Engineering, University of Cambridge, Trumpington Street, Cambridge CB2 1PZ, UK), 2002.

[4] J. Banhart, “Manufacture, Characterization And Application Of Cellular Metals And Metal Foams”, Progress In Materials Science, Vol. 46, 2001, 559-632.

[5]. Scheidegger,A.E.,“The Physics of Flows through Porous Media, Thirded” University of Toronto Press, Toronto, 1974.

[6]. The Effects of Porosity on Mechanical Properties of Cast Discontinuous ,Reinforced... Ahmad et al. Journal of Composite Materials, 2005.

[7]. V. Gergely, "Melt Route Processing for Production of Metallic Foams", (Ph.D. thesis, University of Cambridge, pp 64-77,(2000).

[8]. Koji Matsumaru, Atsushi Takata* and Kozo Ishizaki Nagaoka Gijutsu-Kagaku Daiga “Porous cast-iron bonded diamond grinding wheel” Nagaoka University of Technology), Nagaoka, Niigata 940-2188, Japan Nano Tem Co., Ltd., 4-11-5 Hasugata Nagaoka, Niigata 940-2023, Japan, (2002).

[9]. Lennart Elmquist and Attila Diószegi ,‘Influence of Solidification on the Primary Austenite Structure of Grey Cast Iron” Department of Mechanical Engineering/Component Technology – Castings, Jönköping University, P.O. Box 1026, SE- 551 11 Jönköping, Sweden, (2008).

[10]. Angel R. Álvarez Hernández, “Combined flow and heat transfer characterization of Open cell aluminum foams” University of Puerto rico , Mayagüez campus, (2005).

[11]. Ashby, M. F., Evans, A., Fleck, N. A., Gibson, L. J., Hutchinson, J. W., & Wadley, “Metal Foams: A Design Guide’, Butterworth-Heinmann, Massachusetts, (2000).

[12]. Soong –Keun Hyun,Hideo Nakajima,’Fabrication of lotus-structured porous iron by unidirectional solidification under nitrogen gas’,Institute of Scientific & Industrial research Osaka University, (2002).

[13]. Janina M. Radzikowska, ”Metallography and Microstructures of Cast Iron”

The Foundry Research Institute, Krakow, Poland, (2007).

[14]. Babcsán.N1, Banhart.J1, and Leitlmeier.D2, Metal foams – manufacture and physics of foaming, 1Hahn-Meitner Institute, Berlin, Germany, 2ARC Leicht metallkom petenzzentrum Ranshofen GmbH, Austria, (2005).

[15]. Krause.D.E. “ Gray Iron-A Unique Engineering Material”, Executive Director (The Gray Iron Research Institute, Inc.).The Iron Casting Research Institute, (1969).

[16]. Kawaguchi, Kenryo (Yamato, JP), “Process for producing porous cast iron’, United States Patent 4173500, (1997).

[17]. Tsubouchi, Toshiyasu, Ihara, Tomohiko, “Process for producing porous iron metal body”, US Patent 5725750 ,(1998).

[18] Behr, Thomas (Elchingen, DE), Eipper, Konrad (Rottenburg, DE) et al , “Cast carrier element for a vehicle body’, United States Patent 20050035628, (2005).

[19]. John Banhart 1 ,Denis Weaire 2, On the road again: Metal foams find favour,1 Hahn-meltner Institution in Berlin,Germany. 2 Trinity college in Dublin in Ireland, (2002).

JJMIE

Volume 4, Number 2, March. 2010
ISSN 1995-6665
Pages 300 - 303

Jordan Journal of Mechanical and Industrial Engineering

Experimental Study of Oil Shale and Olive Cake Dust Explosion by Burning Mixtures of Coarse and Fine Particles

A. Sakhrieh[*,a], M.A. Hamdan[a], Y.Abdullat[b]

[a]*Department of Mechanical Engineering, Jordan University, Amman 11942, Jordan*

[b]*Department of Industrial Engineering, Jordan University, Amman 11942, Jordan*

Abstract

The inhibition effect of using different mixtures of coarse and fine particles of oil shale and olive cake solid fuels were investigated. Measuring the maximum permissible oxygen concentration that is required to ignite the mixtures of each type of fuel was carried out. In general, it was found that olive cake might be ignited easier, than oil shale fuel over all mixtures range of coarse and fine particles. Further, it was found that the mixture with 30% coarse particles is the most probable to explode among all other particle sizes for both oil shale and olive cake.

Keywords: Oil Shale; Olive Cake; Dust Explosion; Solid Fuel.

1. Introduction

Combustible solid materials, which are commonly used in industry, should be handled with care against explosion, which is a phenomenon of ignition and flame propagation between solid particles suspended in air. Generally a dust explosion occurs only when it is dispersed in air, or can be dispersed by some means whilst the source of ignition is present. Dust explosions have been known for many years. In spite of considerable research world wide, their hazards have not been eliminated. Eckhoff [1] reported good database on the damage caused by mines explosions and fires in many countries.

The ignition of a dust cloud in a heated environment has been investigated by extending the Frank Kamenetskii theory of steady state thermal ignition to a combustible dust cloud [2]. It was shown that the temperature required for ignition of a dust cloud is lower than the ignition temperature of a single particle. Also an expression for the ignition of dust clouds was proposed. The expression shows that the ignition temperature decreases as the dimensions of the dust cloud increase. The minimum ignition temperature, maximum pressure, and maximum rate of pressure rise for three fractions of wheat and grain sorghum at five concentrations [3]. It was found that the accepted minimum explosive concentrations are lower than actual concentrations required for propagation of an explosion.

Oil shale dust explosion experiments showed that the fine particles in the range from 63 to 75 microns are the most probable to explode among all other particle sizes. [4].This was achieved by studying the minimum ignition temperature and minimum explosive concentrations of oil shale.

Coal dust explosion was studied to improve safety in mining and other industries that process or use coal. The tests were conducted in the USBM 20-liter laboratory explosibility chamber. The parameters measured included minimum explosible concentrations, maximum explosion pressure, maximum rates of pressure rise, minimum oxygen concentration and the amount of limestone rock dust required to inert the coals. The dust explosibility data have been compared to those of other hydrocarbons, such as polyethylene dust [5]. It was found that for various coals the higher volatile and finer sized coals and more hazardous. Further the ignitability of coal dust air and methane coal dust air mixtures was studied by conducting an experimental investigation of coal dust explosion in a 26 L spherical chamber [6]. The experiments showed that the ignitability of dust reduces with the presence of methane

The combustible dust hazards pose a serious industrial safety problem in the United States [7]. It was found that hundreds of combustible dust incidents resulting in large losses of lives, numerous injuries and significant business loss. These incidents occur nationwide involving many different industries and materials. Three fatal dust explosions that all occurred in 2003 in the United States were investigated [8]. These explosions caused the deaths of 14 people and injured hundreds more. Two of the facilities were damaged beyond repair, and several

[*] Corresponding author. asakhrieh@ju.edu.jo

hundred employees lost their jobs. The dust explosion state-of-the-art was presented [9]. Illustrative case studies and past accident analyses reflect the high frequency, geographic spread, and damage potential of dust explosions across the world. The sources and triggers of dust explosions and the measures with which different factors associated with dust explosions can be quantified and are reviewed alongside dust explosion mechanism. This promotes research on relevant dust explosion fundamental phenomena and development of the practical means for preventing and mitigating dust explosions in industry [10]

In this work, the effect of adding coarse particles to the fine ones of both oil shale and olive cake fuels on the maximum permissible oxygen concentration will be investigated. This will be carried out by studying the ignition possibility of mixtures with different percentages of coarse particles from certain values of dust concentration.

In the next few years, Jordan will start using oil shale as fuel. Because of the low hydrocarbon content in Jordan's oil shale, direct burning method is one of the most appropriate methods to make use of it. Also olive cake is produced and used in Jordan. This study comes as a preliminary study to reduce the explosion hazards of using these two materials as fuel.

2. Experimental Setup

In this work a well established apparatus, Godbert-Greenwold Furnace Apparatus with slight modifications, is used [11]. The general layout of the furnace apparatus is shown in figure 1.

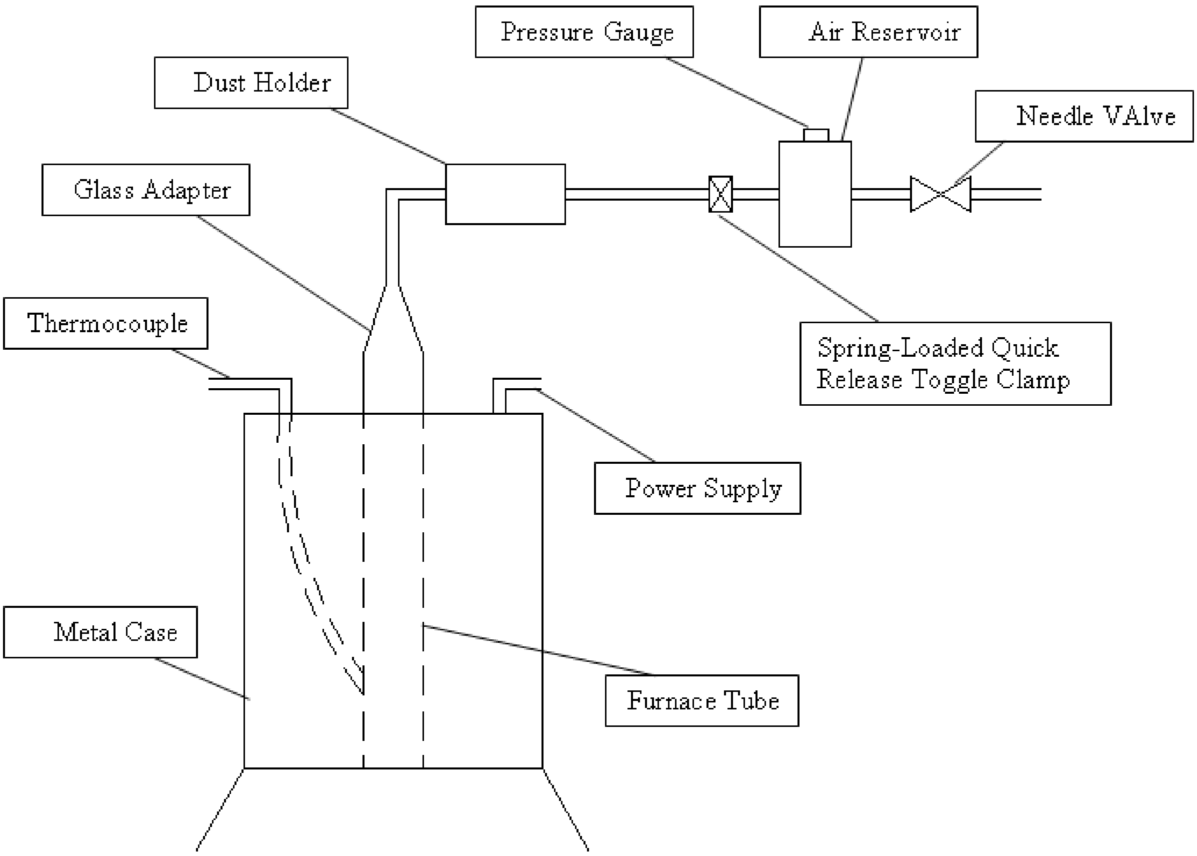

Figure 1.Experimental apparatus.

It consists of a silica furnace tube 21.6 cm long and 3.75 cm inside diameter. The furnace tube is heated externally by an electric winding of 20 SWG, 80/20 nickel/chrome wire with a resistance of 1.3 ohm. A thin layer of heat resisting cement (Alsrax) is used to cover the electric winding. The furnace tube is mounted vertically in a mild steel case lined with asbestos wood and filled up with bulkwool (Triton Kaowool) to act as a thermal insulation. The top of the furnace tube is fitted to Pyrex glass adapter with a right angle bend, which in turn is connected to the dust holder. The dust holder is 10.2 cm long and contains a stainless steel barrel of 0.94 cm inside diameter. The dust holder is connected to the air reservoir of 460 cm^3 capacity. The modifications are that the reservoir is supplied by two inlets, one for air and the other for Nitrogen. The furnace space is filled with air/nitrogen mixture; also the air nitrogen mixture is used to disperse the dust into the furnace. The temperature of the furnace is held constant. By varying the composition of air/nitrogen mixture, the maximum permissible oxygen concentration is obtained.

3. Experimental procedure

The experimental procedure involves measuring of the maximum permissible oxygen concentration of a dust cloud needed to prevent oil shale and olive cake explosion by using air/nitrogen mixture as the dispersing gas. The following steps were followed for each sample.

As a first step in this work oil shale and olive cake were crushed and then sieved using sieves with the appropriate mish to obtain the desired particle size ranges. Then mixtures of coarse particles (250 μm<d<355 μm) and fine particles (d<63 μm) were made up. Each mixture has a certain percentage of coarse particles. These percentage values are: 0.0, 30, 50, 70 and 100%. After preparing the oil shale and olive cake samples, and in order to measure the maximum permissible oxygen concentration of the dust cloud, the furnace tube was electrically heated to a fixed desirable temperature which was recorded by a thermocouple. Then air reservoir was charged up to 70 kN/m^2 with the required air/nitrogen ratio, then the mixture was released to fill the furnace space instead of air, and the bottom open mouth of the furnace was closed, then a known quantity of the dust was placed in the dust holder, and the air reservoir was again charged up to desired dispersion pressure (70 kN/m^2) with the same air/nitrogen ratio. Finally the dust was dispersed through the furnace by an air blast (after opening the bottom open mouth of the furnace).

The occurrence of an explosion was indicated by direct observation of a flame at the bottom of the furnace. If explosion occurs, i.e. observation of a flame at the bottom mouth of the furnace, the nitrogen amount is increased and the same procedure was followed until mixture is reached at no explosion occurs. At this air/nitrogen ratio experiment was repeated three times to make sure that no explosion occurs at this mixture. The lowest nitrogen amount at which no explosion occurs was taken as the maximum permissible oxygen concentration. The concentration of oil shale and olive cake dust samples was varied between 0.3 and 5 g/L, and the furnace tube was cleaned after each test by blowing air through it.

4. Results and Discussion

If a dust is shown to be explosive, further information on the extent of the explosion hazard may be required when considering suitable precautions for the safety and handling of the dust. One of the main parameters to be considered is the maximum permissible oxygen concentration of the atmosphere to prevent ignition in a dust cloud. In this study, the effect of adding coarse particles to the fine ones of both oil shale and olive cake fuels on the maximum permissible oxygen concentration were investigated and the obtained results are presented in curves. It should be noted that each of the obtained curve represents a boundary, below which dust explosion is not possible, while above it explosion is possible.

The variation of maximum permissible oxygen concentration with dust concentration for several mixtures of coarse and fine particles of both oil shale and olive cake is shown in figures 2 and 3, respectively.

Each point on these curves represents the maximum permissible oxygen concentration at which no explosion occurs for the corresponding concentration. The general behavior of these curves is that the maximum permissible oxygen concentration decreases with dust concentration to a minimum value, beyond which it starts to increase.

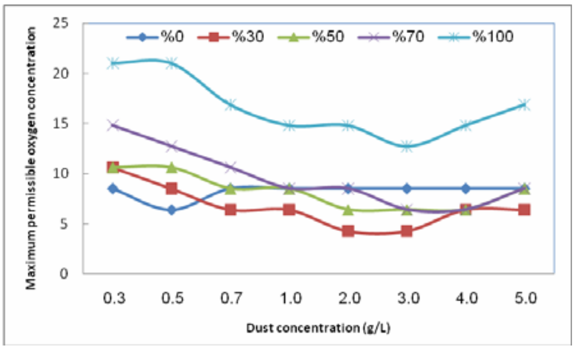

Figure 2. Variation of Maximum permissible oxygen concentration with dust concentration of oil shale for different weight percents of coarse particles in the mixture.

This is due to the fact that any increase in concentration (in the amount of solid fuel) makes the occurrence of the explosion easier, and consequently the maximum permissible oxygen concentration is reduced to prevent the explosion. Further increase in concentration leads to the decrease of the oxidant (air) in the mixture, this makes the occurrence of the explosion harder and consequently the maximum permissible oxygen concentration is increased.

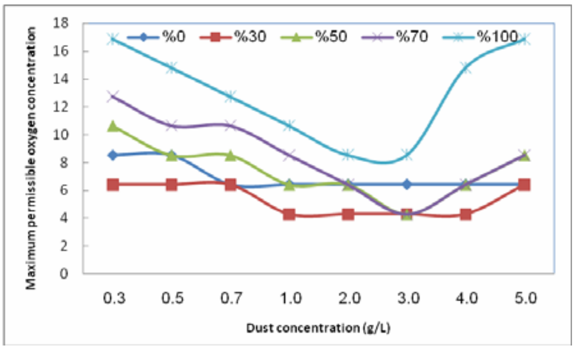

Figure 3. Variation of Maximum permissible oxygen concentration with dust concentration of olive cake for different weight percents of coarse particles in the mixture.

In order to show the effect of the fraction of coarse particles in the mixture on the maximum permissible oxygen concentration, Figures 4 and 5 were plotted for different values of dust concentration.

As it may be seen, and for values of dust concentrations, the general trend of these curves is that, initially the maximum permissible oxygen concentration decreases with the percentage of coarse particles to a minimum values, beyond which it starts to increase with the percentage of coarse particles in the mixture. This is due to the fact that at low percentages of coarse particles the mixture is dominated by fine particle size. Under such conditions the fine particles became more and more cohesive, and then they agglomerate together and behave as if they were effectively of greater size, hence ignition becomes more difficult. However, as the percentage of the coarse

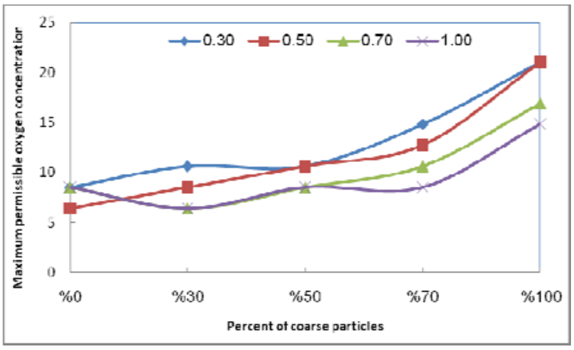

Figure 4. Variation of Maximum permissible oxygen concentration with percent of coarse particles in the mixtures of oil shale for different dust concentration

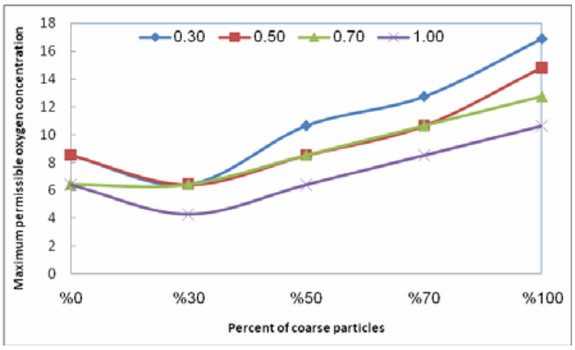

Figure 5. Variation of Maximum permissible oxygen concentration with percent of coarse particles in the mixtures of olive cake for different dust concentration

increases continuously, the average particle size in the mixture increases, ignition becomes easier, until a certain value is reached beyond which the surface area of the particles per unit weight is exposed to the oxidant increases, and consequently the maximum permissible oxygen required for ignition increases.

Figure 6 shows that olive cake is easily ignited compared with oil shale over all the specified mixtures and dust concentration. This is due that the percent by weight of the organic matter of olive cake is higher than that of oil shale.

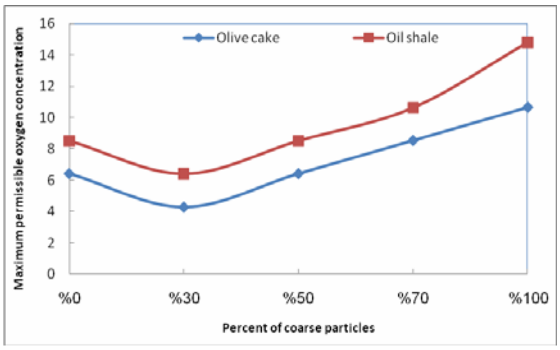

Figure 6. Variation of Maximum permissible oxygen concentration with percent of coarse particles in the mixtures for oil shale and olive cake for dust concentration of (1.0 g/L).

5. Conclusions

This study was carried out to investigate the inhibition of fine particles of oil shale and olive cake by mixing them with coarse particles of same fuels. This was achieved by introducing an explosive mixture of air and each fuel in Godbert-Greenwold Furnace Apparatus, which is electrically heated. Ignition of either fuel may be visually inspected at the bottom end of this apparatus. The study involved the measurement of the maximum permissible oxygen concentration to prevent ignition of both oil shale and olive cake under variable fuel concentration in the dust and under variable values of percentage amount of coarse particles in the combustible mixtures. It was found that, and for all values of coarse particles in the mixture, the maximum permissible oxygen concentration decreases with dust concentration to a minimum value beyond which it starts to increase. Further, the maximum permissible oxygen concentration was also found to initially decrease with coarse particles, and further increase of coarse particles leads to an increase in the maximum permissible oxygen concentration required for ignition. Finally, it was found that olive cake is easily ignited than oil shale all over the range of particle sizes and the fuel concentration in the dust samples.

References

[1] R.K. Eckhoff. Dust explosion in the process industries. 3rd edition, elsevier, 2003.

[2] H. Cassel, and H. Liebman, "Ignition of dust clouds". Combustion and flame, Vol.3, 1959, 467-475.

[3] B. Lesikar, C. Parnell, and A. Garcia, "Determination of grain dust explosibility parameters". American society of Agricultural engineering, Vol. 34 , No. 2, 1987, 571-576.

[4] Al-Qubbaj. Oil shale dust explosion. Master thesis, University of Jordan, Jordan, 1996.

[5] K. Cashdollar, "Coal dust explicability". Journal of Loss. Prev. Proces Ind., Vol. 9, No.1, 1996, 65-76.

[6] P. Amyotte, K. Minez, M.Pegg and Y. Sum, "The ignitability of coal dust-air and methane coal dust in air mixtures". Fuel, Vol. 72, No. 5, 1993, 671-679.

[7] G. Joseph, "Combustible dusts: A serious industrial hazard". Journal of Hazardous Materials, vol. 142, 2006, 589-591.

[8] S. Blair, "Dust explosion incidents and regulations in the United States". Journal of loss prevention in the process industries, Vol. 20, 2007, 523-529.

[9] T. Abbasi and S.A. Abbasi, "Dust explosion-cases, causes, consequences, and control". Journal of Hazardous Materials, Vol. 140, 2007, 7-44.

[10] R.K. Eckhoff, "Current status and expected future trends in dust explosion research". Journal of loss prevention in the process industries, Vol. 18, 2005, 225-237.

[11] Sakhrieh, Inhibition of dust explosion, Master Thesis, University of Jordan, Amman-Jordan, 1997.

JJMIE

Volume 4, Number 2, March. 2010
ISSN 1995-6665
Pages 304 - 313

Jordan Journal of Mechanical and Industrial Engineering

The Implementation of Total Quality Management (TQM) for The Banking Sector in Jordan

Salman D. Al-Shobaki [a], Rami H. Fouad [b], Adnan Al-Bashir [b]

[a] Aramex Corporate University, Aramex International, P.O.Box: 960913, Amman, Jordan

[b] Industrial Engineering Department / Hashemite University, Amman, Jordan

Abstract

After its development and phenomenal success, Total Quality Management (TQM) was applied outside the industrial sectors to service organizations, such as banks. This paper investigates the application of TQM to a service organizations using Jordanian baking sector as a model example. Banking is an important sector in Jordan. The government has introduced several laws and constitutions aimed to further develop this sector, improve its ability to compete within a global market and encourage investment in the country. However, little work has been done to measure and control quality in this sector. The work will show that the use of TQM can be of great benefit to the Jordanian banks, as it will lead to an increase in the organization customer orientation and competitive edge. The paper will also investigate the relation between the application of TQM and the increase in the organization performance and efficiency. The results show that the application of TQM in the Jordanian banking sector lead to increased productivity and ability to compete in the global markets.

Keywords: Total Quality Management (TQM); Services; Banking Sector; Jordan.

1. Introduction

In today's world, organizations are facing the growing challenges from global competition and more sophisticated customers in terms of what they want and their changing needs. Most organizations are starting to apply the Japanese methods of production and philosophies in the hope of achieving the required growth in the markets increasing profit. One of the main ideas that came from the Japanese industry is TQM, which means that all workers within a given organization must participate in improving the product or service quality, an activity that was previously the concern of the quality control department employees. Feigenbaum defines TQM as "An efficient system that aims to achieve total quality through the combined effort of all the employees within the organization in order to produce a product/service that will meet the needs and expectations of the customer with minimum cost" [1].

Due to the large success of TQM in manufacturing companies, service organisations have started to follow in their footsteps and consider the application of TQM. This was mainly due to the nature service industries in terms of its customer orientation. Thus TQM was applied to banks [2], hospitals [3], hotels and education [4] [5] [6] [7] [8]. In order to apply TQM to a service sector it is important to decide on how to evaluate the quality of service. Service can be evaluated according to cost, flexibility, acquirability, totality, and response time [9] [10]. This paper will concentrate on the affect of applying TQM to the service industry and will use banks in Jordan as a model company (or organization).

Most bankers would like to believe that banks are in the finance sector, and not in the service industry. Thus they tend to compete in terms of financial prowess (e.g. Asset base, amount of loans released, cash flow … etc.) rather than service quality. However, banks depend on customer satisfaction to continue business. This classifies them as a service company. When the customer interacts with the front line personnel and requires a certain service, it is this moment of truth that decides whether the customer will come back or shift to the next-door competitor. Thus banks tend to benefit from the TQM customer first motto.

Ramadan [2] considered the nature of services that the banks provide. Setting the quality aspects for these services is an aspect that was discussed by [11]. Dusseav

* Corresponding author. rafouad@hu.edu.jo

[6] considered the effect of applying TQM on the financial capability and return of a given organisation. He concluded that there is a strong correlation between these two issues, however it may take from four to eight years to see such an improvement depending on the organisation nature and business. Eriksson [12] considered the winners of the Swedish quality awards and showed that their financial performance using several indices exceeds their competitors on most of the studied indicators. Yeu-Shiang [13] investigated the application of the TQM philosophy in Taiwanese service and manufacturing organizations, and concluded that the Taiwanese economy survival in the current economic regional decline was due in part to the impact of using quality management techniques in these organizations. Other researchers considered the implications of applying TQM to organizations in different countries and concluded that large gains can be achieved if the momentum of TQM application can be maintained [14-18].

2. Banking in Jordan

In Jordan, and due to the country large economic liberalisation, the banking sector is starting to play an important role in the country movement toward free market trade. This sector is showing staggering prospects for expansion and diversification and accounted 44.6% of total stock market capitalization, and contributed 18.7% to GDP in 2004 [19]. The Jordanian government is placing great emphasis on the banking organisations development and it is hoped they will be able to finance projects and deal with incoming capital investment. At the end of 1999, twenty-two national and five international commercial banks were operating in the country with a structural network of 466 branches. Having to play such a vital role in the revival of the Jordanian economy and country future, the government has introduced several laws and constitutions aimed to further develop financial organisations. This effort is mainly targeted toward improving the quality of offered services, increase the organisations ability to compete within a global market and encourage investment in the country.

The Central Bank of Jordan has liberalized almost all-direct control on interest rates, applying fiscal, monetary and commercial deregulation. This has exposed Jordanian banks to increasing foreign competition. The challenge of providing local competitive banking services is increasing. Computerization and modernization of banking services is under way in most local banks, enabling them to adapt to their new integral role in world economies.

However, little work has been done to measure and control quality in this sector and to see the effect of employing quality assurance techniques on the overall efficiency and productivity of the sector. Maala [20] has attempted to measure quality in the banking sector in Jordan. The research considered the customer point of view as a benchmark to the effect of the implementation of TQM. It concluded that there is a big gap between the level of service expected by the customer to that offered by the bank, and recommended that banks should try to improve their services. However, the research did not consider the management and the what it's doing to improve the quality of service, time frame of implementation of quality improvements schemes, study the obstacles in the implementation of TQM, and the provision of a subjective measure (response time, profit, cost of service) that indicates improvements in the performance when TQM was applied (if any), as the study used customer satisfaction as a measure.

Belbissi [21] considered the application of TQM in the Jordanian banking sector from the banks managers' point of view. The study aimed to identify the relationship between TQM principles and the banks performance. It concluded Jordanian banks adapted TQM concepts and that there is a relationship between the banks accommodation of TQM principles and organizational performance. The study recommended that more research on the banking sector in Jordan should be done where both banks customer and employees viewpoints.

This paper will consider the application of TQM to the service sector from the customer, employee and managers points of view. Due to its importance to the Jordanian economy, banks will be used as a model of a service organisation. In this first stage a survey will be conducted regarding the current state of application of TQM in banks, study the effect of the introduction of TQM to the sector and the factors that prevent the implementation of TQM. In future work, a TQM implementation framework will be developed that is targeted toward the banks.

3. TQM Model

In order to achieve the goals and aims of the study, a model that reflects the relation between the dependent and independent variables was constructed. This model can be seen in Figure 1.

The model shows the interaction between the elements of TQM in order to achieve a continuous improvement in the production and operation of the target organisation, thus achieving customer satisfaction. The model structure is made of three building blocks:

1. Requirements: These are the basic requirements and building blocks for the initial implementation of TQM. These are: Approval of the philosophy, commitment toward the philosophy and availability of critical information needed for the implementation and measurement of performance.
2. Actions: These are the activities needed for the implementation of the philosophy in the organisation. These include: training of employees in the aspects of TQM and the meaning of the philosophy, participation and involvement of the upper management in the implementation phase and structural organisational change needed for implementation in terms of responsibilities, departments and management levels.
3. Results: These are the results from implementing TQM in a financial organisation, which include customer satisfaction and financial development. Two financial development indicators were used here:

- Profitability: It's the degree of organization success in achievement of its predetermined objectives or, it's the degree of organization success in available resources distribution in order to achieve the highest profit from its investment, and it can be measured quantitatively by [2]:

Profitability = Net Income After Tax / Total Assets

- Productivity: Its the quantity of necessary resources required to produce one unit from the total production[1] and its measured quantitatively by:
  Productivity = Total Deposits At The End Of Year / Total Number Of Employees
  Embedded in the model is the continuous improvement concept. This is because banks that intend to apply the model will have to measure their performance and compare it to the competitor's performance. This will allow the banks to get a feed back about the level of required improvement and what must be done to achieve better results.

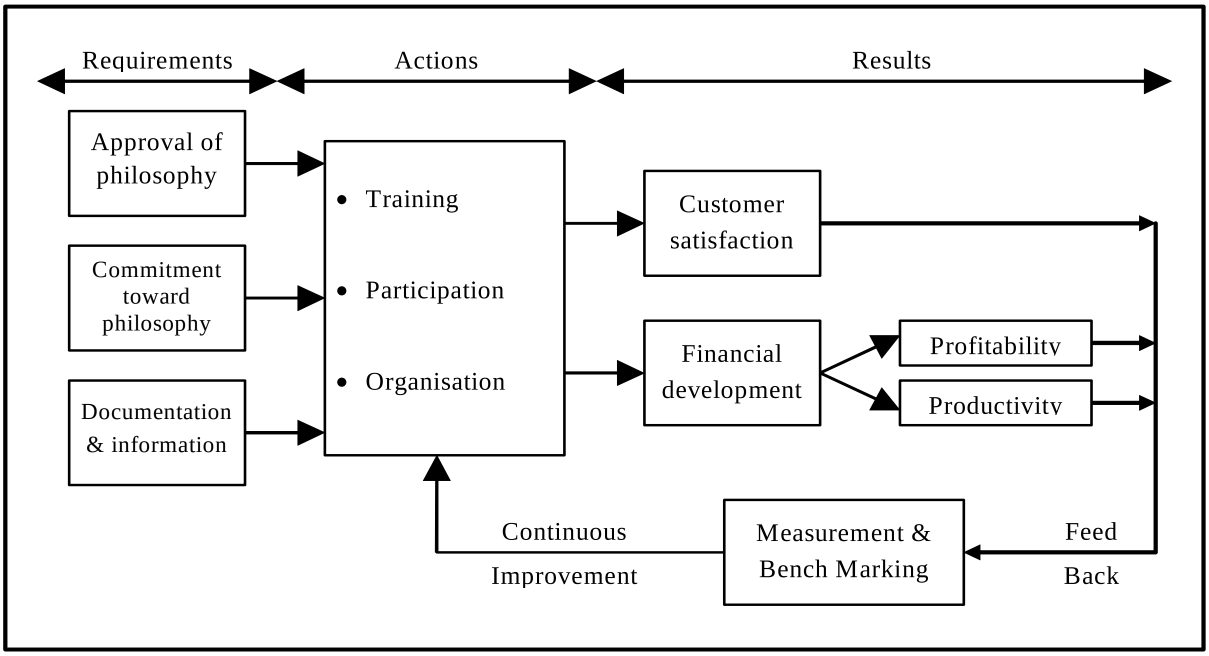

Figure 1. The proposed TQM model for the study

4. Research Methodology

In order to understand the current state of application of TQM in the banking sector in Jordan based on the model shown in Figure 1, a survey was conducted to measure each of the level of readiness and implementation of the three basic building blocks. The results from the implementation of TQM in banks (customer satisfaction and financial development) were measured as follows:

- Customer satisfaction was measured via a questionnaire, which evaluated their level of satisfaction from the services rendered by the bank.
- Financial development (profitability and productivity) was measured from the data provided by the banks annual reports.

The requirements and actions needed for the implementation of the TQM philosophy were measured by a second questionnaire answered by the bank employee and management personnel. This questionnaire investigated the requirements of TQM (approval of philosophy, commitment toward philosophy and documentation and information) and actions should be taken to achieve TQM implementation through questions related to TQM principles.

4.1. Study Sample

The study sample was divided into two groups: bank employees and bank customers.

For the bank employees, (100) Questionnaires were distributed on (5) Jordanian commercial banks that were selected randomly and according to banks management's cooperation with researchers Two of these banks are ISO certified, while the other three are committed to TQM principles according to top management memorandums and strategic plans. The questionnaires were distributed to the employees of these banks in different work levels and different branches all within the capital city Amman. (82) Questionnaires were retrieved. Table 1shows frequency and percentage of the employee's distribution on the banks under study.

For the bank customers group, (400) Questionnaires were distributed on Jordanian banks customers that were selected randomly from the banks under study in different branches inside and outside the capital city Amman. (219) Questionnaires were retrieved. Table 1 shows frequency and percentage of the collected customer questionnaires from the banks under study.

Table 1. The distribution of the employees on the different banks: ISO certification comments were in effect at the time of the study

Bank Name	ISO certified	Employees Questionnaire		Customers Questionnaire	
		Frequ-ency	Percent %	Frequency	Percent %
Jordan Bank	No	25	30.5	80	36.5
Islamic Bank	In process	13	15.9	43	19.6
Housing Bank	ISO 9001	6	7.3	35	16.0
Jordan National Bank	No	33	40.2	32	14.6
Jordan Kuwaiti Bank	No	5	6.1	29	13.2
Total		82	100.0	219	100.0

* At the time of the study

4.2. Study Hypotheses

The study aimed to investigate several hypotheses about the relation between the model elements. As indicated these are divided into two groups:

1. Group 1: Management and employee related hypothesis set that cover the application of TQM concepts in Jordanian commercial banks from management and employees view. This group is also divided into two basic hypothesis that consider:

- Adaption of the Jordanian banks to TQM concept.
- Relationship been the application of TQM principles and bank performance.

Each of the above is also divided into a set of sub hypothesis that relate to focus on customer principles, employee needs, continuous improvement, competition needs, and bank performance. Table 2 shows the hypotheses set for this group.

2. Group 2: Customer related hypothesis set that cover the level of customer satisfaction from financial services quality in the banks after the implementation of TQM from a customer view. These are five hypotheses that focus on the customer evaluation of provided service based on previous experience with the bank (duration and frequency) and/or dealings with other banks. Table 3 shows the hypothesis set for this group.

Table 2. Employee and management questionnaire hypotheses.

No	**H**	Basic Hypothesis	No.	**H**	Sub Hypotheses
1	**H_0**	The Jordanian banks don't adapt the TQM concept.	1.1	**H_0**	The banks don't adapt focus on customer principle.
				H_1	The banks adapt focus on customer principle.
			1.2	**H_0**	The banks don't adapt focus on employee needs principle.
				H_1	The banks adapt focus on employee needs principle.
	H_1	The Jordanian banks adapt TQM concept.	1.3	**H_0**	The banks don't adapt focus on continuous improvement principle.
				H_1	The banks adapt focus on continuous improvement principle.
			1.4	**H_0**	The banks don't adapt focus on management competition needs principle.
				H_1	The banks adapt focus on management competition needs principle.
2	**H_0**	There is no relationship between the application of the TQM principles and the bank performance (measured by profitability and productivity).	2.1	**H_0**	No relationship between the bank commitment to satisfying the customer needs and the bank performance.
				H_1	A relationship exists between the bank commitment to satisfying the customer needs and the bank performance.
			2.2	**H_0**	No relationship between the bank commitment to satisfying the employee's needs and the bank performance.
				H_1	A relationship exists between the bank commitment to satisfying the employee's needs and the bank performance.
	H_1	There is a relationship between the application of the TQM principles and the bank performance (measured by profitability and productivity).	2.3	**H_0**	No relationship between the bank commitment to process continuous improvement and bank performance.
				H_1	A relationship exists between the bank commitment to process continuous improvement and the bank performance.
			2.4	**H_0**	No relationship between the bank commitment to satisfying management competition needs and its performance.
				H_1	There is a relationship between the bank commitment to satisfying management competition needs and its performance.

Table 3. Customer satisfaction questionnaire hypotheses

No.	**H**	Basic Hypothesis
1	**H_0**	The customer's evaluation to the provided services quality level was negative.
	H_1	The customer's evaluation to the provided services quality level was positive.
2	**H_0**	The percentage importance that the customers used to evaluate the provided financial services quality doesn't differ (between them).
	H_1	The percentage importance that the customers used to evaluate the provided financial services quality differs.
3	**H_0**	The evaluation of customers to the actual provided services quality level doesn't differ depending on the number of dealing years with the bank.
	H_1	The evaluation of customers to the actual provided services quality level differs depending on the number of dealing years with the bank.
4	**H_0**	The evaluation of customers to the actual provided services quality level doesn't differ depending on the number of dealing frequency with the bank.
	H_1	The evaluation of customers to the actual provided services quality level differs depending on the number of dealing frequency with the bank.
5	**H_0**	The evaluation of customers to the actual provided services quality level doesn't differ depending on their dealing with other banks.
	H_1	The evaluation of customers to the actual provided services quality level differs depending on their dealing with other banks.

5. Results and Analysis

The 5-Likert scale has been used in the questionnaire with the following values: highly agree (5), agree (4), approximately agree (3), disagree (2), and completely disagree (1). The mean and the standard deviation of the different questions were calculated. It was considered that the customer or the employee agree on a given statement when the mean is (3.5) or more. A mean below this value, indicate a negative response. For the purpose of testing hypotheses, the joint mean for all statements was calculated to be considered as the factor of analysis (reference), while the individual mean of single questions representing for the same hypothesis was calculated to be compared with the reference using One Way Analysis of Variance (ANOVA).

5.1. Employee Questionnaire Analysis And Results

The results of the retrieved questionnaires, its frequencies, and percentages were shown in Table 1. Table 4 shows the employees questionnaire statement and the average mean for each statement. These statements were arranged according to the basic issues relating the introduction of TQM philosophy. Figure 2 shows a plot of the overall average mark for the statements for the five components of TQM. It is noted that employees accept and agree that their banks are focusing on introducing TQM concepts, the customer, employee and competition needs and on continuous improvement. From Table 4, it is noted that the employees:

- Agree on the introduction of TQM concepts by the management. They believe that there is a strong relation between TQM introduction and the success of the bank. They believe that written material such as pamphlets will help the introduction process. However, they criticize the management for not changing the organisation structure and work practices to facilitate the achievement of TQM concepts.
- Believe that the bank management is “customer focused”, as they run surveys to find out what are the customer needs, and they listen and try to provide immediate solution to the problems at hand. However this contradicts with the customer opinion (from customer satisfaction questionnaire) about the bank interest in them, as they do not note these actions and attitudes.
- Agree that the bank management focus on employees needs as they try to improve their performance by holding training programs, encourage creative thinking and teamwork to enhance their professionalism, allow them the chance to express them self’s and giving rewards for excellent performance.
- Believe that the bank management tries to improve the quality continuously by trying to avoid mistakes, minimize the cost of financial services, keeping a good documentation system and continuous modification of work practices
- Believe that the bank management is keen on developing their competitive edge by creating effective communication between them and the customers and follow the customer’s needs. They indicate that the ISO certificate has increased the bank performance level compared to the competitors.

Table 4. Results for the employee questionnaire statements regarding TQM components and their means.

	No	Sentence	Mean	Overall
Employees viewpoint of TQM concepts introduction	1	The bank employees believe in the relationship between the application of the TQM concept and the success of the bank.	4.16	3.8
	2	The management introduces the TQM concept to their employees.	4.13	
	3	The management reengineered and developed the organizational structure to suit the TQM concept	3.98	
	4	The management has a completely and written plan to introduce the TQM concept to their employees	3.94	
	5	The management improved and developed the motivation structure to suit the TQM concept.	3.35	
	6	The management distribute a book about quality on their employees explain the service quality improvement steps.	3.12	
Focus on customer needs	7	The bank management listening to the customer complaints and provide an immediate solutions.	4.32	4.2
	8	The bank management making surveys to know the customer needs and wants.	4.00	
Focus on meeting employees needs	9	The bank has a training department (provided with annual budget and equipment needed for training).	4.55	4.0
	10	Training programs includes employees form all management levels.	4.51	
	11	The training programs aimed to minimize the mistakes and achieving high level of quality	4.29	
	12	The training programs concentrate on the financial service quality importance.	4.21	
	13	The bank management encourages and adapts the new ideas.	3.94	
	14	The senior management encourages their employees for the teamwork.	3.89	
	15	The bank management share its employees in finding the suitable solutions to the problems that face the department they are working in.	3.79	
	16	The employees have the chance to demonstrate their opinions about the jobs they are doing.	3.78	
	17	The bank management follows up the trainer after finishing his training.	3.73	
	18	The bank management forms teams work to improve the bank quality involving employees in all levels.	3.72	

Table 4 continues next page ………………

	19	The bank management grants awards to their employees about their excellent performance.	3.71	
	20	The bank has teams work that meeting continuously to discuss the work problems and make decisions.	3.68	
Focus on continuous improvement	21	The bank management and its employees are making preventive and immediate corrective actions for the mistakes.	4.26	4.0
	22	The management aimed to minimize the cost of different financial processes.	4.11	
	23	The bank has a documentation system that is introduced and applicable from employees in all levels.	4.04	
	24	The bank has methods to analysis the activities required to provide the service.	3.88	
	25	The bank has a program to simplify the steps required to provide the service.	3.88	
	26	The bank has a program to eliminate the unnecessary activities and training work.	3.59	
Focus on management competition needs	27	There is an active communication method between customers and employees.	4.26	4.1
	28	The bank management has general strategic goals for the quality dependent on the wants and needs of depositor, loan, and beneficiary.	4.18	
	29	The bank management studies the situation of the other competitors to improve the service.	4.15	
	30	The bank has a system to study the market and the economic changes.	4.09	
	31	The bank management has methods to follow up changes in customer wants and needs.	4.07	
	32	The senior management has a long term plans for the service quality.	4.04	
	33	The ISO certificate increases the bank performance level compared to other banks that don't have ISO certificate.	4.00	
	34	The bank management revises the statistics used to measure the performance quality to make sure it's valid for the future operations.	3.91	

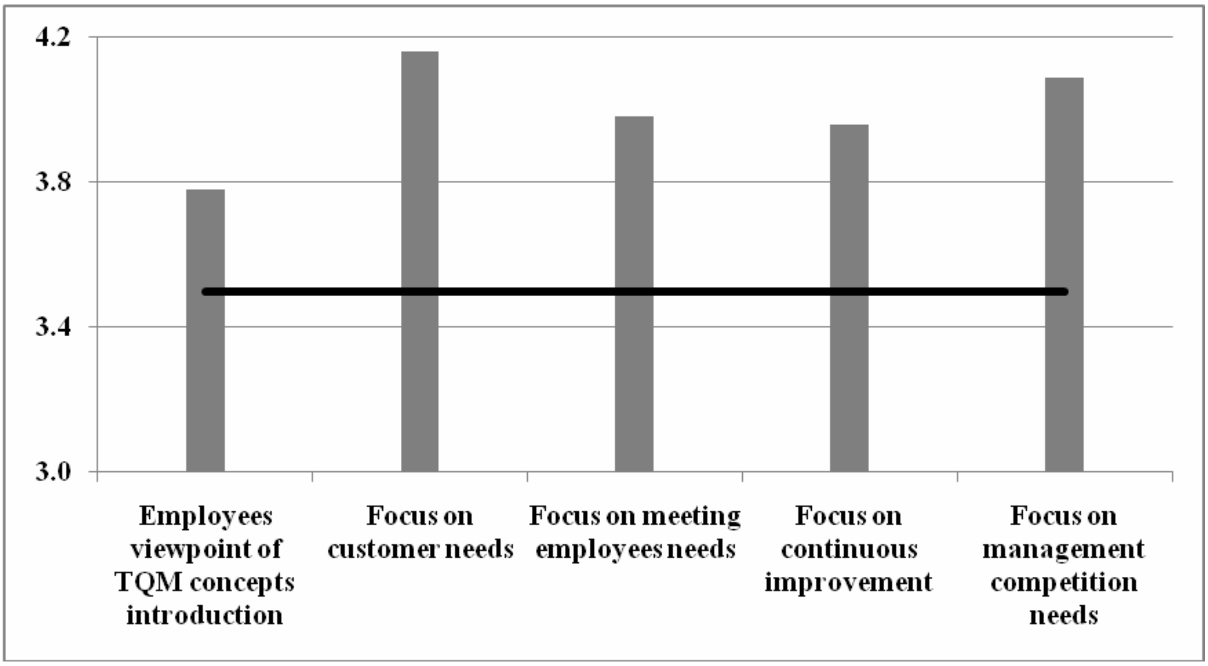

Figure 2. Average results for employee's statements verses the five basic components of TQM. The line represents the pass mark of 3.5 at which the statements is accepted in the analysis.

The hypotheses for the employee questionnaire were analysed statistically using F-test. The results of the analysis for the first hypothesis and its subgroup hypotheses can be seen in

The results of the analysis for the second hypothesis and its subgroup hypotheses can be seen in Table 6. Here

Table 5. The hypotheses were tested using the one-way analysis of variance with a 95% confidence level. Note that the hypotheses are referred to using their respective numbers shown previously in Table 2. The results indicate

the F statistic to the hypothesis was calculated in order to find the if the statement is accepted or not.

that Jordanian banks adapt TQM principles and its main basic elements such as focus on customer and employees needs, focus on continuous improvement and focus on management competition needs.

The results of the analysis for the second hypothesis and its subgroup hypotheses can be seen in Table 6. Here the F statistic to the hypothesis was calculated in order to find the if the statement is accepted or not.

Table 5. First employee questionnaire hypothesis test.

Hypothesis	Test	DF	Calculated F	Sig.	Tabulated F	Result
1	Between Groups	46	4.847	.0001	1.687	Accept H1
	Within Groups	35				
	Total	81				
1.1	Between Groups	46	6.220	.0001	1.687	Accept H1
	Within Groups	35				
	Total	81				
1.2	Between Groups	46	9.354	.0001	1.687	Accept H1
	Within Groups	35				
	Total	81				
1.3	Between Groups	46	5.529	.0001	1.687	Accept H1
	Within Groups	35				
	Total	81				
1.4	Between Groups	46	6.502	.0001	1.687	Accept H1
	Within Groups	35				
	Total	81				

Table 6. Second employee basic hypothesis test.

Hypothesis	Test	Calculated F	Sig	R	R²	Result
2	Profitability	10.835	0.0001	0.8356	0.6982	Accept H1
	Productivity	9.354	0.003	0.9356	0.8753	Accept H1
2.1	Profitability	8.856	0.0023	0.7632	0.5825	Accept H1
	Productivity	9.456	0.0001	0.8962	0.8032	Accept H1
2.2	Profitability	12.987	0.0001	0.8562	0.733	Accept H1
	Productivity	13.562	0.0001	0.9524	0.9071	Accept H1
2.3	Profitability	15.897	0.0001	0.9789	0.9582	Accept H1
	Productivity	13.456	0.0001	0.8563	0.7332	Accept H1
2.4	Profitability	13.897	0.001	0.7564	0.5721	Accept H1
	Productivity	12.456	0.001	0.7956	0.6330	Accept H1

5.2. Customer Questionnaire Analysis And Results

The results of the retrieved questionnaires, its frequencies, and percentages were shown in Table 1. Table 7 shows the customer questionnaire statements and the average mean for each statement. From Table 7 it is noted that the customers:

- Agree that their bank has modern technical equipments that are necessary in developing the level of provided service and plays an important role in the continuity of the bank. Thus they agree that the A.T.M services introduced by their banks are appreciable and that this service helps in save their times and facilitate their deal with the banks.
- Agree that their bank deliver on their promises, although the agreement on this component of quality management was less as compared to many other criteria. The lack of promises delivery may be due to the bureaucracy procedures that exist in some banks and that any new step or procedure must be approved from upper management. It can be seen that the means trend for the customers' answers starts to decrease when the statement are concerned with the bank inside procedures.
- Agree that their bank is reliable and does have good documentation that they can depend on.
- Agree that their bank employees are qualified. Customers also believe that they receive immediate services and that the employees and the bank management care for their needs. This reflects the fact that customers feel that they are the focus of the bank operation, which satisfies an important criterion in the TQM implementation process. On the other hand they agree that the banks do not take into consideration their

suggestions to improve financial services quality and that bank management takes care in trying to solve their problems, although the mean for that statement was low. There is a contradiction between the customer belief about the level of offered service and the customer feeling that he/she is the focus of the operations in the bank.

- Agree that their bank employees are trust worthy. This trust is critical; else the customer will not deal with his bank any more.
- Agree that their bank working hours are suitable for them.
- Marginally agrees that their bank offers financial service with a good quality level and about the continuous effort to improve the provided service. However the mean of these statements was low and on the edge of acceptance.
- Do not agree that the interest rate their bank is giving is lower than other rates offered by other banks. This is true because the interest rate in most cases is limited through the Central Bank of Jordan.

Table 7. Result for the customer questionnaire statements with their respective means.

No	Sentence	Mean
1	The A.T.M services help to save time and facilitate service achievement.	4.61
2	The bank provides the A.T.M services	4.31
3	The bank management has accurate documentations.	4.18
4	The bank has a modern techniques equipments	4.13
5	I can depend on the management of the bank that I deal with.	4.09
6	I trust the bank employees that I deal with.	4.08
7	The general appearance of the bank compatible with the offered services.	4.06
8	When the bank management promises their customers to do anything on a specific time it do it.	3.96
9	The bank management doesn’t give the customer any personal care.	3.88
10	The bank employees don’t know the customer needs	3.84
11	The bank has a continuous improvement in its financial services quality.	3.82
12	The bank has high-qualified employees.	3.76
13	If the customers have any problems, bank management would support them.	3.72
14	The bank employees always don’t have the will to help the customers.	3.68
15	The bank management doesn’t give the customer any individual care.	3.65
16	The bank has economic counsellors with high experience.	3.63
17	The bank introduces the quality importance of the financial services.	3.52
18	The bank management considers the suggestions and comments of the customer on their financial services quality.	3.48
19	The bank management doesn’t put the upper benefit of the customers in their care.	3.4
20	The bank provides financial services with high quality and low cost.	3.40
21	The bank interest loans provided are lower than the other banks.	3.33
22	The customer doesn’t have immediate services form the banks employees	3.32
23	The bank services are better than the other bank services	3.31
24	The working times of the bank don’t suit all the customers.	2.97

The results of the analysis for the customer satisfaction hypothesis can be seen in Table 8. The hypothesis was tested using the one-way analysis of variance with a 95% confidence level. Note that the hypotheses are referred to using their respective numbers shown previously in Table 2 The results indicate that there is good level of implementation of certain TQM concepts in the bank. However other concepts seam to be lacking since the customer does not feel that he/she is the focus of operations in the bank.

Table 8. Customer questionnaire hypotheses test.

Hypothesis	Test	DF	Calculated F	Sig.	Tabulated F	Result
1	Between Groups	36	12.233	.0001	1.418	Accept H_1
	Within Groups	182				
	Total	218				
2	Between Groups	36	7.516	.0001	1.418	Accept H_1
	Within Groups	182				
	Total	218				
3	Between Groups	2	0.587	0.557	3	Accept H_o
	Within Groups	212				
	Total	214				
4	Between Groups	2	7.386	0.001	3	Accept H_1
	Within Groups	216				
	Total	218				
5	Between Groups	4	2.772	.028	2.37	Accept H_1
	Within Groups	214				
	Total	218				

6. Conclusions

The study revealed that there is a general approval of the study sample that the level of TQM implementation is moderate. This indicates that there is a high awareness from the top management to adapt the TQM concept as important guide to the local and national competition. The attitudes of the respondents regarding the principles of the TQM were within a high mean. The results shows that there is nearly equal adaptation from the banks to all principles of TQM. While in reality there is little focus on customer needs and complaints regarding to customers viewpoint.

The study revealed that there is a high rational relationship between all TQM principles and the organization performance in commercial Jordanian banks measured in productivity and profitability. The evaluation of commercial Jordanian banks customers to the provided services quality level was positive although the general feeling of customers was not satisfied. It could also be concluded that there is no relationship between the evaluation of commercial Jordanian banks customers to the actual provided services quality level and the number of dealing years with the bank.

On the customer side, the study showed that customer's evaluations regarding the provided financial services quality differs, and this gives to the management an indication of the need of giving high priority to develop quality approaches. The modern techniques equipments available in the bank have nearly the highest importance in customer evaluation, so the banks should give it most priority in their development process. There is a relationship between the evaluation of commercial Jordanian banks customers to the actual provided services quality level and the number of dealing frequency with the bank. Frequent dealing with the bank make a strong relationship between the customers and the bank employees and this affect the customer's evaluation. The evaluation of commercial Jordanian banks customers to the actual provided services quality level differ dependent on dealing with other banks. This give a true customer evaluation to actual services quality level provided by the evaluated banks compared to other banks they deal with.

Acknowledgment

The authors would like to thank the Hashemite University for funding this research work.

References

[1] Krajweski, L., Ritzman, L.P., "Operations management: Strategy and Analysis", 8th Edition Pearson – Prentice Hall, 2007.

[2] Ramadan, Z., Management of Banking Businesses", 1st ed., Amman, 1995.

[3] Hart, M., **"**Improving the quality of NHS out-patient clinics: the applications and misapplications of TQM", International Journal of Health Care Quality Assurance, 1996, **V**ol. 9, No. 2, 20 – 27.

[4] Chadwick, P., " TQM at South Bank University: issues in teaching and learning", Quality Assurance in Education, 1995, Vol. 3, No. 1, 39 - 44

[5] Kelsey, K.D., Bond, J.A., "A model for measuring customer satisfaction within an academic centre of excellence", Managing Service Quality, 2001, **Vol.** 11, No. 5, 359 – 368.

[6] Dusseav, S.P.,"An analysis of the relationship between financial performance and TQM", University of Missouri, 1997.

[7] Bergquist, T.,"TQM firm performance", University of Oregon, 1997.

[8] Donelan, S., "Good setting and job satisfaction", Boston College, 1997.

[9] Evans J.R., "Applied production and operations management", 4th edition, West Publishing Com., 1993.

[10] Tokan, K., "The ISO-9000 series and its importance in applying Total Quality Management", The Jordanian Engineer, 1995

[11] Kadra, O.M., “Total Quality Management in Banks”, Banks in Jordan, No. 4, 1998.

[12] Eriksson; H., Hansson, J., “The impact of TQM on financial performance”, Measuring Business Excellence, **Vol.** 7, No. 1, 2003, 36 – 50.

[13] Yeu-Shiang, H., Bertrand, M.T.L., “An empirical investigation of total quality management: a Taiwanese case” The TQM Magazine, **V**ol. 14, 2002, No. 3, 172 – 180.

[14] Yong;J., Wilkinson, A., “In search of quality: the quality management experience in Singapore”, Int. J of Quality & Reliability Management, **V**ol. 18, 2001, No. 8, 813 – 835.

[15] Werner, V., Crous, M.J., “Training and education for TQM in the commercial banking industry of South Africa”, Managing Service Quality, **V**ol. 10, 2000, No. 1, 61 – 67.

[16] Sureshchandar, G.S., Chandrasekharan, R., Anantharaman, R.N., Kamalanabhan, T., “Management's perception of total quality service in the banking sector of a developing economy - a critical analysis”, The Int. J of Bank Marketing, 2002, **V**ol. 20, No. 4, 2002, 181 – 196.

[17] Osuagwu, L., “TQM strategies in a developing economy: Empirical evidence from Nigerian companies”, Business Process Management Journal, **Vol.** 8, No. 2, 140 – 160.

[18] Robson, A., Prabhu, V., Mitchell, E., “TQM enablers and business sustainability: An empirical study of the service sector in the North East of England”, International Journal of Quality & Reliability Management, **Vol.** 19, 2002, No. 5, 610 – 632.

[19] Central Bank Report, Jordan, 2004.

[20] Maala, N., ”Measuring the quality of services in Jordanian banks”, Derasat, Vol. 25, No. 2, 1998, Jordan University

[21] Belbissi, B., 2000, Total Quality Management and Performance – An Applied Study on the Commercial Sector in Jordan, M.Sc. thesis, Jordan University, Amman, Jordan.

JJMIE

Volume 4, Number 2, March. 2010
ISSN 1995-6665
Pages 314 - 323

Jordan Journal of Mechanical and Industrial Engineering

An Effective Approach for Solving The Multi-Response Problem in Taguchi Method

Abbas Al-Refaie [a,*], Tai-Hsi Wu [b], Ming-Hsien Li [c]

[a] *Dept. of Industrial Engineering, University of Jordan, Amman, Jordan*

[b] *Dept. of Industrial Engineering and Systems Management, Feng Chia University, Taichung, Taiwan*

[c] *Dept. of Business Administration, National Taipei University, Taipei, Taiwan*

Abstract

This research proposes a simple, yet very effective, approach for solving the multi-response problem in the Taguchi method. Each quality response is transformed into signal-to-noise (S/N) ratio. The average S/N ratio is calculated for each factor level, and then weighted with respect to the level of the largest average S/N ratio for this factor. The average weight of each factor level, or level weight, is obtained from all responses. The factor level with the largest level weight is selected as the optimal level for that factor. Three case studies in manufacturing are employed for illustration of the proposed approach; where in all of which provides it the largest total anticipated improvements. In contrast with other approaches in previous literature, the proposed approach not only reduces the complexity and effort of data analysis and the need for statistical skills, but also does not require estimation of a weight for each response, and thus eliminates human involvement in the decision making process for optimal factor levels. In conclusion, the simplicity and effectiveness of this approach shall make it attractive to practitioners for solving the multi-response problem in a wide range of applications on the Taguchi method.

Keywords: Multi-Response Problem; Taguchi Method; S/N Ratio.

1. Introduction

Robust design in quality engineering, as proposed by Taguchi [1], has significantly improved quality and yield in product and manufacturing process design. Nevertheless, most of the published researches [2 and 3] on the applications of the Taguchi method have focused on optimizing a single quality response.

In today's high-tech processes, however, manufactured products have more than one quality response of main interest. The Taguchi method primarily uses engineering judgment to decide optimal factor levels for multi-responses [4], which increases uncertainty during the decision-making process. Recently, the optimization of multi-response problem has received an increasing attention from many authors. Among them, Shiau [5] assigned a weight to the S/N ratio of each quality response. Then, the combined S/N ratio was employed to determine the optimal factor levels. Tong et al. [6] adopted the sum of the weighted normalized quality losses of all responses, then used multi-response S/N ratio to decide optimal factor levels. In reality, it remains difficult to determine and define a weight for each response. Logothetis and Haigh [7] and Pignatello [8] determined tentative optimal factor levels by using regression techniques which increase the complexity of computational processes. Su and Tong [9] and Antony [10] utilized principal component analysis (PCA) to transform multi-responses into few uncorrelated responses, which were then utilized for solving the multi-response problem. However, PCA has two shortcomings: (1) when multiple principal components of an eigenvalue that is greater than one are chosen, how to trade off to decide the feasible solution is still unknown; and (2) when the selected principal components have less variation than can be explained by total variation, the performance index of multi-responses is not evident enough to replace the original response variables. Liao and Chen [11] utilized data envelopment analysis (DEA) based ranking approach (DEAR) for deciding optimal factor levels for multi-response problem in Taguchi method. Unfortunately, most of the traditional DEA models allow for complete weight

* Corresponding author.abbas.alrefai@ju.edu.jo

flexibility which may result in identifying a decision making unit with an unrealistic weighing scheme [12 and 13]. Jeyapaul et al. [14] utilized genetic algorithm (GA) with the Taguchi method to determine a weight for the S/N ratio of each response. The sum of the weighted S/N ratios was then used to decide optimal factor levels. Genetic algorithm, however, is a search heuristic that provides near-optimal solutions for complex search spaces; such as, production scheduling and transportation problems.

This research proposes a simple yet effective approach for solving the multi-response problem in the Taguchi method. The basic idea is that the average S/N ratio for each factor level from each response is weighted with respect to the largest average S/N ratio for that factor. Then, the average weight from all responses is used as a quality measure to decide optimal factor levels. That is, the factor level corresponding to the largest average weight among all factor levels is calculated to be the optimal level for that factor. The remainder of this research is organized as follows. Section two presents the proposed approach. Section three provides three case studies for illustrational purposes. Section four summarizes research results. Finally, conclusions are made in section four.

2. Proposed Approach

In robust design, the Taguchi method adopts a fractional factorial experimental design called an orthogonal array (OA), which reduces the number of experiments under permissive reliability. In an OA, the columns are pairwise orthogonal. That is, for every pair of columns, all combinations of factor levels occur an equal number of times. The columns of the OA represent factors to be investigated, while the rows denote individual experiments. The quality response can be divided into three main types involving: (1) the smaller-the-better (STB) type response, in which the response is continuous, nonnegative, and its most desired value is zero; (2) the nominal-the-best (NTB) type response, in which the response is continuous, nonnegative, and its target is nonzero and finite; and (3) the larger-the-better (LTB) type response, which can be transformed into the STB type by considering the reciprocal of the response. The Taguchi method employs the S/N ratio as a quality measure. Regardless of the response type, the optimal factor level is the factor level which maximizes the S/N ratio, η. That is, the objective function to be maximized is

for the STB type response:

$$\eta = -10\log_{10}\left(\frac{1}{n}\sum_{i=1}^{n} y_i^2\right) \tag{1}$$

for the NTB type response

$$\eta = 10\log_{10}\frac{\mu^2}{\sigma^2} \tag{2}$$

for the LTB type response

$$\eta = -10\log_{10}\left(\frac{1}{n}\sum_{i=1}^{n}\left(\frac{1}{y_i^2}\right)\right) \tag{3}$$

where n is the number of replicates for y, μ is the response mean and σ is the standard deviation. Based on the above, the proposed approach for solving the multi-response problem in the Taguchi method is outlined in the following steps:

***Step* 1**:

Let r be the number of responses in an OA. Let η_j (j =1, ... , r) be the S/N ratio of response j. Then, calculate η_j for all j values using a proper formula from Eqs. (1-3).

***Step* 2**:

Assume a process factor l is assigned at K levels. Let η_{jlk} be the sum of η_js for the experiments at level k (k = 1, ..., K) of factor l, and let $\bar{\eta}_{jlk}$ be the average of η_{jlk}. Calculate $\bar{\eta}_{jlk}$ of each factor level for all responses.

***Step* 3**:

Let w_{jlk} be the weight of level k for factor l from response j, which is estimated as

$$w_{jlk} = \begin{cases} \dfrac{\max_k \bar{\eta}_{jlk}}{\bar{\eta}_{jlk}} & \text{for the STB type response} \\ \dfrac{\bar{\eta}_{jlk}}{\max_k \bar{\eta}_{jlk}} & \text{for the NTB and LTB type responses} \end{cases} \tag{4}$$

Calculate w_{jlk} values of factor l from each response j. The value of w_{jlk} surely lies between zero and one. Let $\bar{w}_{lk}$ be the average of w_{jlk} over all responses. Estimate the $\bar{w}_{lk}$ values for all levels of factor l. Typically, larger $\bar{w}_{lk}$ indicates better performance. Consequently, identify the factor level corresponding to the maximum of $\bar{w}_{lk}$ (k =1, 2, … , K) as the optimal level of factor l.

Step 4:

Calculate the anticipated improvement in each response due to setting process factors at optimal levels and compare the total anticipated improvements with those obtained in previous studies. The anticipated improvement is calculated as the S/N ratios at optimal factor level minus the S/N ratio at initial factor level

3. Illustrations

The following three previously studied case-studies are employed to illustrate the proposed approach.

3.1. Optimization of a Gear Hobbing Operation

Jeyapaul *et al*. [14] used genetic algorithm to investigate the effect of machining parameters on multiple performance characteristics of a gear hobbing operation. The objective was to determine the levels of machining parameters which optimize the profile and helix errors. Four STB type quality responses were selected, namely: left profile (LP) error, right profile (RP) error, left helix (LH) error, and right helix (RH) error. Six process-controllable factors were investigated, including: direction of hobbing (A, two levels), number of passes (B, two levels), source of hob (C, two levels), feed (D, three levels), speed (E, three levels), and job run out (F, three levels). The initial factor level was $A_1B_2C_2D_2E_1F_3$. The L_{18} array, which contains 18 experiments, was then selected for conducting the experiments. However, the L_{18}

array can accommodate one factor at two levels and seven factors, each at three levels. Thus, the two factors B and C were combined into one factor (BC) of B_1C_1, B_2C_1, and B_2C_2 for level 1, 2, and 3, respectively. The proposed approach is implemented as follows:

Step 1:

Four STB type responses (LP error, RP error, LH error, and RH error) are considered in this case study (r = 4). Let response j (j = 1, ..., 4) denote LP error, RP error, LH error, and RH error, respectively. The S/N ratio, η_j, of response j for each experiment is calculated using Eq. (1) for all j values and shown in Table 1 for all of the 18 experiments in L_{18} array.

Table 1. The S/N ratios for gear hobbing operation.

Exp.	Control factor*								S/N ratio (dB)			
	A	BC	D	E	F	*e*	*e*	*e*	LP error	RP error	LH error	RH error
1	1	1	1	1	1	1	1	1	-37.2117	-37.3816	-33.7785	-33.1746
2	1	1	2	2	2	2	2	2	-37.5854	-37.4182	-30.5984	-32.5739
3	1	1	3	3	3	3	3	3	-37.4127	-37.2801	-34.5825	-34.3794
4	1	2	1	1	2	2	3	3	-37.4870	-37.7535	-35.8931	-35.1224
5	1	2	2	2	3	3	1	1	-37.5440	-37.6162	-38.3929	-35.6160
6	1	2	3	3	1	1	2	2	-37.1266	-37.3865	-31.2694	-32.5408
7	1	3	1	2	1	3	2	3	-37.5136	-37.1455	-34.7481	-35.6156
8	1	3	2	3	2	1	3	1	-37.7367	-37.4789	-35.0478	-33.1795
9	1	3	3	1	3	2	1	2	-37.8079	-37.1797	-35.3629	-35.9544
10	2	1	1	3	3	2	2	1	-37.3458	-37.7101	-32.5646	-33.5220
11	2	1	2	1	1	3	3	2	-37.4196	-37.9687	-34.3192	-31.3069
12	2	1	3	2	2	1	1	3	-37.1512	-37.5440	-32.4770	-29.7669
13	2	2	1	2	3	1	3	2	-37.5158	-37.4474	-30.9765	-31.1584
14	2	2	2	3	1	2	1	3	-37.6769	-37.4492	-32.3626	-31.6810
15	2	2	3	1	2	3	2	1	-37.2493	-37.4868	-32.7771	-32.1360
16	2	3	1	3	2	3	1	2	-37.5777	-37.9395	-33.3351	-31.0950
17	2	3	2	1	3	1	2	3	-37.5474	-37.7383	-32.8354	-31.9022
18	2	3	3	2	1	2	3	1	-37.6057	-37.1483	-34.2558	-33.5637

Step 2:

First, the process factor A is chosen; it is assigned at two levels; A1 and A2. The $\overline{\eta}_{jA_1}$ and $\overline{\eta}_{jA_2}$; the average S/N ratios for A1 and A2, respectively, are estimated from each response j and shown in Table 2. Similarly, the S/N ratio averages for the levels of factors B to F are calculated from each response j and also displayed in Table 2 for all j values.

Table 2. The S/N ratio averages for gear hobbing operation.

Response (dB)	Factor (l) / Level (k)*	A	B	C	D	E	F
LP error	1	-37.4917	**-37.3544**	**-37.3938**	-37.4419	**-37.4538**	**-37.4257**
	2	**-37.4544**	-37.5324	-37.6315	-37.5850	-37.4859	-37.4646
	3				**-37.3922**	-37.4794	-37.5289
RP error	1	**-37.4045**	-37.5504	-37.5368	-37.5629	-37.5848	**-37.4133**
	2	-37.6036	**-37.4808**	**-37.4384**	-37.6116	**-37.3866**	-37.6035
	3				**-37.3376**	-37.5407	-37.4953
LH error	1	-34.4082	**-33.0534**	**-33.3327**	-33.5493	-34.1610	-33.4556
	2	**-32.8781**	-33.9381	-34.2642	-33.9261	-33.5748	**-33.3548**
	3				**-33.4541**	**-33.1937**	-34.1192
RH error	1	-34.2396	**-32.454**	**-32.7482**	-33.2813	-33.2661	-32.9804
	2	**-31.7925**	-33.2971	-33.5517	**-32.7099**	-33.0491	**-32.3123**
	3				-33.0569	**-32.733**	-33.7554

* Optimal factor levels for each response are identified by boldtype.

As mentioned earlier, B_1C_1, B_2C_1, and B_2C_2 are assigned at levels 1, 2, and 3, respectively, for the combined factor BC. The calculated S/N ratio averages for levels 1, 2, and 3 of factor BC from LP error are -37.3544,

-37.4333, and -37.6315 dB, respectively. The average S/N ratio for B_1 is equal to the average S/N ratio for level 1 of factor BC (= -37.3544 dB), while the average S/N ratio for B_2 (= -37.5324 dB) is estimated as the average of the S/N ratios averages for levels 2 and 3 of factor BC. Conversely, the average S/N ratio for C_1 (= -37.3938 dB) is calculated as the average of the S/N ratio averages for levels 2 and 3 of factor BC, while the average S/N ratio for C_2 (= -37.6315 dB) is equal to the average S/N ratio for level 3. In a similar manner, the S/N ratio averages for the two levels of factors B and C are estimated from each of the other three responses. Finally, the S/N ratio averages for the levels of factors D to E are calculated from each response *j* as the sum of the S/N ratios at each factor level divided by six, which is the number of experiments at that level. In Table 2, using the Taguchi method the combination of optimal factor levels for each of the LP error, RP error, LH error, and RH error is $A_2B_1C_1D_3E_1F_1$, $A_1B_2C_2D_3E_2F_1$, $A_2B_1C_1D_3E_3F_2$ and $A_2B_1C_1D_2E_3F_2$, respectively. Obviously, there exists a conflict among these combinations regarding the optimal factor levels for the four responses simultaneously.

Step 3:

The level weights for factors A to F are calculated from each response *j* using Eq. (4) and displayed in Table 3 for all *j* values.

Table 3. The level weights for gear hobbing operation.

Response	Factor (*l*) / Level (*k*)	A	B	C	D	E	F
LP error	1	0.9990	1.0000	1.0000	0.9987	1.0000	1.0000
	2	1.0000	0.9953	0.9937	0.9949	0.9991	0.9990
	3				1.0000	0.9993	0.9972
RP error	1	1.0000	0.9981	0.9974	0.9940	0.9947	1.0000
	2	0.9947	1.0000	1.0000	0.9927	1.0000	0.9949
	3				1.0000	0.9959	0.9978
LH error	1	0.9555	1.0000	1.0000	0.9972	0.9717	0.9970
	2	1.0000	0.9739	0.9728	0.9861	0.9886	1.0000
	3				1.0000	1.0000	0.9776
RH error	1	0.9285	1.0000	1.0000	0.9828	0.9840	0.9797
	2	1.0000	0.9747	0.9761	1.0000	0.9904	1.0000
	3				0.9895	1.0000	0.9572
Level weight*	1	0.9708	**0.9995**	**0.9993**	0.9932	0.9876	0.9942
	2	**0.9987**	0.9860	0.9856	0.9934	0.9946	**0.9985**
	3				**0.9974**	**0.9988**	0.9825

* Optimal factor levels are identified by boldtype.

The level weights for factor A, w_{jA1} and w_{jA2}, from LP error (*j* = 1) are calculated as follows. In Table 2, the $\bar{\eta}_{1A_1}$ and $\bar{\eta}_{1A_2}$ from LP error are calculated to be -37.4917 and -37.4544 dB, respectively. The largest S/N ratio, $\bar{\eta}_{A1}$, for factor A from LP error equals -37.4544 dB. The w_{1A1} is estimated as 0.9990 (= -37.4544/-37.4917), while w_{1A2} is calculated as 1.00 (= -37.4544/-37.4544). The w_{jA1} and w_{jA2} values from each of RP error, LH error, and RH error are estimated similarly. The average level weights for factor A are calculated from all of the four responses. It is obtained that $\bar{w}_{A_1}$ equals 0.9708, while $\bar{w}_{A_2}$ is 0.9987. As a result, the optimal level of factor A is determined to be A_2. Similar calculations are made for factors B to F and their optimal levels are fixed at B_1, C_1, D_3, E_3, and F_2, respectively. However, the combination of optimal factor levels was calculated as $A_1B_2C_2D_1E_1F_3$ by using genetic algorithm [14].

Step 4:

The anticipated improvement in each response, which is calculated from Table 2 as the average S/N ratios at optimal factor levels ($A_2B_1C_1D_3E_3F_2$) minus the average S/N ratios at initial factor levels ($A_1B_2C_2D_1E_1F_3$), is displayed in Table 4 for the four responses. The anticipated improvements from use of the genetic algorithm are also listed in Table 4.

It can be seen in Table 4 that the proposed approach results in a total anticipated improvement of 11.8005 dB, which is about three times that gained using the genetic algorithm (= 4.1499 dB).

3.2. Optimization of a polysilicon deposition process

This case study was considered by Phadke [4] and it aimed at improving the quality of a polysilicon process. Three quality responses were selected including: surface defects (the STB type response), thickness (the NTB type response, target is 3600 Å), and deposition rate (the LTB type response). The surface defects were considered as the key quality problem that causes significant scrap.

Table 4. Anticipated improvements for gear hobbing operation.

Response (dB)	Starting condition (I)	Optimal condition (II)		Anticipated improvement (II) - (I)	
		Genetic algorithm [14]	Proposed approach	Genetic algorithm [14]	Proposed approach
LP error	-37.8581	-37.4917	-37.1735	0.3664	0.6846
RP error	-37.4952	-37.4045	-37.6525	0.0907	-0.1573
LH error	-36.6009	-34.4082	-31.0508	2.1927	5.5501
RH error	-35.7397	-34.2396	-30.0166	1.5001	5.7231
Total anticipated improvement (dB)				4.1499	11.8005

Six process controllable factors were selected at three levels each; the factors were: deposition temperature (A), deposition pressure (B), nitrogen flow (C), silane flow (D), settling time (E), and cleaning method (F). The combination of initial factor levels was selected as $A_2B_2C_1D_3E_1F_1$. The orthogonal array L_{18} was selected for the experiment design. The proposed approach for the polysilicon process was implemented as follows:

Step 1:

Three responses are considered in this case study. The S/N ratios for surface defects (STB type), thickness (NTB type), and deposition rate (LTB type) are estimated for each experiment using Eqs. (1), (2), and (3), respectively, and listed in Table 5 for all of the 18 experiments.

Table 5. The S/N ratios of each response for polysilicon process.

Exp.	Control factor*								S/N ratio (dB)		
	e	A	B	C	D	E	*e*	F	Surface defects	Thickness	Deposition rate
1	1	1	1	1	1	1	1	1	0.51	35.22	23.23
2	1	1	2	2	2	2	2	2	-37.30	35.76	31.27
3	1	1	3	3	3	3	3	3	-45.17	36.02	32.34
4	1	2	1	1	2	2	3	3	-25.76	42.25	31.15
5	1	2	2	2	3	3	1	1	-62.54	21.43	37.27
6	1	2	3	3	1	1	2	2	-62.23	32.91	33.89
7	1	3	1	2	1	3	2	3	-59.88	21.39	37.68
8	1	3	2	3	2	1	3	1	-71.69	22.84	40.46
9	1	3	3	1	3	2	1	2	-68.15	30.60	41.21
10	2	1	1	3	3	2	2	1	-3.47	26.85	27.89
11	2	1	2	1	1	3	3	2	-5.08	38.80	26.02
12	2	1	3	2	2	1	1	3	-54.85	38.06	31.82
13	2	2	1	2	3	1	3	2	-49.38	32.07	34.50
14	2	2	2	3	1	2	1	3	-36.54	43.34	33.20
15	2	2	3	1	2	3	2	1	-64.18	37.44	34.76
16	2	3	1	3	2	3	1	2	-27.31	31.86	37.71
17	2	3	2	1	3	1	2	3	-71.51	22.01	40.45
18	2	3	3	2	1	2	3	1	-72.00	18.42	39.22

* Empty column for error.

Step 2:

Let response *j* where *j* equals 1, 2, and 3 denote surface defects, thickness, and deposition rate, respectively. The average S/N ratios, $\bar{\eta}_{jl_1}$, $\bar{\eta}_{jl_2}$, and $\bar{\eta}_{jl_3}$, for the three levels of each factor are estimated from each response *j* and displayed in Table 6. For illustration, the $\bar{\eta}_{1A_1}$ for A_1 from surface defects response, -24.23 dB, is calculated as the summation of the S/N ratios of experiments 1, 2, 3, 10, 11, and 12, divided by six. In a similar manner, the $\bar{\eta}_{1A_2}$ and $\bar{\eta}_{1A_3}$ values of -50.11 and -61.76, respectively, are calculated from surface defects. Similarly, the $\bar{\eta}_{jA_1}$, $\bar{\eta}_{jA_2}$, and $\bar{\eta}_{jA_3}$ are calculated from response *j* equal to 2 and 3 for thickness and deposition rate, respectively. Finally, the average S/N ratios for the three levels of factors B to F are estimated from each response *j* for all *j* values.

In Table 6, the optimal factor levels for surface defects, thickness, and deposition rate using the Taguchi method are decided as $A_1B_1C_1D_1E_2F_2$, $A_1B_3C_1D_2E_2F_3$, and $A_3B_3C_2D_3E_3F_3$, respectively. Obviously, a conflict exists among the optimal factor levels for the three responses. Thus, Phadke [4] selected the combination of optimal factor levels by engineering judgment as $A_1B_2C_1D_3E_2F_2$.

Step 3:

The w_{jlk} and $\overline{W}_{lk}$ values of each factor level are calculated from each response *j* using Eq. (4) for all *j* values; they are listed in Table 7 for all factor levels. For example, the w_{1A1}, w_{1A2}, and w_{1A3} of the three levels of factor A are calculated from surface defects as 1.00 (= -

Table 6. The S/N ratio averages for polysilicon process.

Response (dB)	Factor (l) / Level (k) *	A	B	C	D	E	F
Surface defects	1	**-24.23**	**-27.55**	**-39.03**	**-39.20**	-51.53	-45.56
	2	-50.11	-47.44	-55.99	-46.85	**-40.54**	**-41.58**
	3	-61.76	-61.10	-41.07	-50.04	-44.03	-48.95
Thickness	1	**35.12**	31.61	**34.39**	31.68	30.52	27.04
	2	34.91	30.70	27.86	**34.70**	**32.87**	33.67
	3	24.52	**32.24**	32.30	28.16	31.16	**33.85**
Deposition rate	1	28.76	32.03	32.80	32.21	34.06	33.81
	2	34.13	34.78	**35.29**	34.53	33.99	34.10
	3	**39.46**	**35.54**	34.25	**35.61**	**34.30**	**34.44**

* Optimal factor levels for each response are identified by boldtype.

24.23/-24.23), 0.4835 (= -24.23/-50.11) and 0.3923 (= -24.23/-61.76), respectively. Similarly, the w_{jA1}, w_{jA2} and w_{jA3} are estimated from each response j for j equals 2 and 3 for thickness and deposition rate, respectively. The $\overline{w}_{A_1}$, $\overline{w}_{A_2}$ and $\overline{w}_{A_3}$ are then calculated from the three responses as 0.9096, 0.7808, and 0.6968, respectively. Since the maximum level weight for factor A corresponds to A_1, the optimal level of factor A is decided at A_1. Similarly, the w_{jlk} and $\overline{w}_{lk}$ values are estimated for factors B to F, where their optimal levels are estimated as B_1, C_1, D_1, E_2, and F_2, respectively.

Table 7. The level weights for polysilicon process.

Response	Factor (l) / Level (k)	A	B	C	D	E	F
Surface defects	1	1.0000	1.0000	1.0000	1.0000	0.7867	0.9126
	2	0.4835	0.5807	0.6971	0.8367	1.0000	1.0000
	3	0.3923	0.4509	0.9503	0.7834	0.9207	0.8494
Thickness	1	1.0000	0.9805	1.0000	0.9130	0.9285	0.7988
	2	0.9940	0.9522	0.8101	1.0000	1.0000	0.9947
	3	0.6982	1.0000	0.9392	0.8115	0.9480	1.0000
Deposition rate	1	0.7288	0.9012	0.9294	0.9045	0.9930	0.9817
	2	0.8649	0.9786	1.0000	0.9697	0.9910	0.9901
	3	1.0000	1.0000	0.9705	1.0000	1.0000	1.0000
Level weight*	1	**0.9096**	**0.9606**	**0.9859**	**0.9392**	0.9027	0.8977
	2	0.7808	0.8372	0.8357	0.9355	**0.9970**	**0.9949**
	3	0.6968	0.8170	0.9534	0.8650	0.9562	0.9498

* Optimal factor levels are identified by boldtype.

Step 4:

The anticipated improvements in surface defects, thickness, and deposition rate are calculated at $A_1B_1C_1D_1E_2F_2$ and listed in Table 8. The sum of the weighted normalized quality loss [6], PCA [9], and DEAR [11] approaches discussed this case study and their anticipated improvements are also summarized and compared in Table 8.

Table 8. Anticipated improvement for polysilicon process.

Response (dB)	Starting condition (I)	Optimal condition (II)					Anticipated improvement (II) - (I)				
		Engineering judgment [4]	Weighted quality loss [6]	PCA [9]	DEAR [11]	Proposed approach	Engineering judgment [4]	Weighted quality loss [6]	PCA [9]	DEAR [11]	Proposed approach
Surface defects	-56.69	-19.84	-24.22	-2.29	1.20	14.68	36.85	32.47	54.40	57.89	71.37
Thickness	29.95	36.79	40.24	41.23	41.32	41.77	6.84	10.29	11.28	11.37	11.82
Deposition rate	34.97	29.60	32.44	27.21	27.21	23.32	-5.37	-2.53	-7.76	-7.76	-11.66
Total anticipated improvement (dB)							38.32	40.23	57.92	61.5	71.53

In Table 8, using the proposed approach, the surface defects are reduced by 71.37 dB and thickness is improved by 11.82 dB; these are the largest among the anticipated improvements for all examined approaches. Deposition rate, however, is decreased by 11.66 dB, which is the worst anticipated improvement because it is correlated to surface defects. Despite that, the proposed approach contributes the largest total anticipated improvement of 71.53 dB.

3.3. Optimization of a Plasma-Enhanced Chemical Vapour Deposition

This case study was conducted by Tong *et al*. [6] to improve the performance of a plasma-enhanced chemical vapour deposition process. Two quality responses were studied, including deposition thickness (DT, the target is 1000 Å) and refractive index (RI, the target value is 2). Eight controllable process factors (A to H) were investigated. Factor A was decided at two levels, while factors B to H were each selected at three levels. The L_{18} array was selected for experimental design. The experiments were performed by the Industrial Technology Research Institute, Taiwan. The proposed approach can be briefly described as follows:

Step 1:

The S/N ratios of each DT and RI, which are NTB type responses, are calculated using Eq. (2) for each experiment; values for all of the 18 experiments are shown in Table 9.

Table 9. Experimental data for plasma-enhanced process.

Exp.	Control factors								Deposition thickness (DT)			Refractive index (RI)		
	A	B	C	D	E	F	G	H	Average	Standard deviation	S/N ratio	Average	Standard deviation	S/N ratio
1	1	1	1	1	1	1	1	1	730.60	62.4884	21.36	2.03	0.0802	28.07
2	1	1	2	2	2	2	2	2	874.20	25.8979	30.57	2.22	0.0412	34.64
3	1	1	3	3	3	3	3	3	967.20	52.1076	25.37	2.61	0.1026	28.11
4	1	2	1	1	2	2	3	3	800.80	34.6222	27.28	2.02	0.0557	31.19
5	1	2	2	2	3	3	1	1	789.20	113.1159	16.87	1.97	0.0751	28.36
6	1	2	3	3	1	1	2	2	796.20	48.6487	24.28	1.88	0.0675	28.89
7	1	3	1	2	1	3	2	3	909.80	194.8017	13.39	1.89	0.0873	26.73
8	1	3	2	3	2	1	3	1	648.80	93.5452	16.82	1.78	0.0351	34.08
9	1	3	3	1	3	2	1	2	646.60	93.5698	16.79	1.70	0.0197	38.69
10	2	1	1	3	3	2	2	1	1013.40	112.0750	19.13	1.97	0.0838	27.44
11	2	1	2	1	1	3	3	2	1493.60	327.3894	13.18	1.83	0.1655	20.86
12	2	1	3	2	2	1	1	3	900.60	59.0788	23.66	1.90	0.0559	30.60
13	2	2	1	2	3	1	3	2	902.40	94.5637	19.59	1.83	0.0551	30.42
14	2	2	2	3	1	2	1	3	824.80	85.2508	19.71	2.04	0.0610	30.50
15	2	2	3	1	2	3	2	1	792.60	104.4811	17.60	2.10	0.0888	27.46
16	2	3	1	3	2	3	1	2	814.60	146.6332	14.89	2.19	0.0632	30.80
17	2	3	2	1	3	1	2	3	818.00	43.9431	25.40	1.91	0.0165	41.29
18	2	3	3	2	1	2	3	1	738.80	36.2036	26.20	2.02	0.0635	30.06

Step 2:

Let *j* of 1 and 2 represent DT and RI, respectively. The $\overline{\eta}_{jA_1}$ and $\overline{\eta}_{jA_2}$ for factor A, and the $\overline{\eta}_{jl_1}$, $\overline{\eta}_{jl_2}$, and $\overline{\eta}_{jl_3}$ for factors B to H are estimated from each response *j* and displayed in Table 10 for all *j* values. In this table, the optimal combinations of factor levels using the Taguchi method are $A_1B_1C_3D_2E_2F_2G_2H_3$ and $A_1B_3C_2D_1E_3F_1G_1H_3$ for DT and RI, respectively. Clearly, there is a conflict among the optimal factor levels for the two responses.

Step 3:

The values of w_{jlk} are estimated for all factor levels from each response *j* using Eq. (4). All w_{jlk} values are shown in Table 11. The $\overline{w}_{A_1}$ and $\overline{w}_{A_2}$ for factor A and $\overline{w}_{l_1}$, $\overline{w}_{l_2}$, and $\overline{w}_{l_3}$ for factors B to H are then estimated from the two responses. It is found that the combination of optimal factor levels is $A_1B_3C_3D_2E_2F_2G_2H_3$. However, the combination of optimal factor levels using the sum of the weighted normalized quality losses [6] was $A_1B_3C_2D_2E_2F_2G_2H_3$.

Step 4:

The anticipated improvements in DT and RI are calculated at $A_1B_3C_3D_2E_2F_2G_2H_3$ and shown with the anticipated improvements by the sum of the weighted normalized quality losses approach are also displayed and compared in Table 11.

In this table, it is obvious that the proposed approach results in better anticipated improvements than the sum of the weighted normalized quality losses approach in both the DT and RI responses.

Table 10. The S/N ratio averages for plasma-enhanced process.

Response (*j*)	Factor (*l*) / Level (*k*) *	A	B	C	D	E	F	G	H
Deposition Thickness (DT)	1	**21.41**	**22.21**	19.27	20.27	19.69	21.85	18.88	19.66
	2	19.93	20.89	20.43	**21.71**	**21.80**	**23.28**	**21.73**	19.88
	3		18.91	**22.32**	20.03	20.53	16.89	21.41	**22.47**
Refractive index (RI)	1	**30.97**	28.29	29.11	**31.26**	27.52	**32.23**	**31.17**	29.24
	2	29.94	29.47	**31.62**	30.13	31.46	32.09	31.07	30.72
	3		**33.61**	30.64	29.97	**32.39**	27.05	29.12	**31.40**

* Optimal factor levels for each response are identified by boldtype.

Table 11. Anticipated improvement for plasma-enhanced process.

Response (dB)	Starting condition (I)	Optimal condition (II)		Anticipated improvement (II) - (I)	
		Weighted quality loss [6]	Proposed approach	Weighted quality loss [6]	Proposed approach
Deposition thickness (DT)	21.62	25.44	28.93	3.77	7.31
Refractive index (RI)	32.09	37.93	38.19	5.84	6.10
Total anticipated improvement (dB)				9.61	13.41

4. Research Results

The proposed approach has been adopted for solving the multi-response problem in the Taguchi method for three case studies. It is found that the proposed approach has the largest anticipated improvement in reducing profile and helix variation for gear hobbing operation, in dramatically improving the performance of polysilicon process, and effectively optimizing the plasma-enhanced chemical vapour deposition. Moreover, several advantages of the proposed approach have been noticed, including: (1) it is not based on rigid assumptions as PCA does, (2) it is simple since it does not require advanced statistical skills or *a priori* information about the response weights or importance, and (3) it requires minimal computational effort. Definitely, these advantages shall attract product/process engineering to adopt it for solving the multi-response problem in the Taguchi method in a wide range of engineering applications.

5. Conclusions

This research proposed a simple, yet very effective, approach for solving the multi-response problem in the Taguchi method. In this approach, the S/N ratio of each response is calculated. Then, the average S/N ratio for each factor level from all responses is estimated and used to decide the optimal levels for all process factors. Three case studies were provided for illustration, and the proposed approach provided the largest total anticipated improvement in multi-responses among all used approaches, including PCA, DEAR, and genetic algorithm. The primary advantage of this approach is that it is characterized by simple and straightforward calculations without the need for statistical skills or *a priori* information about response weights or importance. In conclusion, the simplicity and effectiveness of this approach provides great assistance to practitioners for solving the multi-response problems in a wide range of applications on the Taguchi method.

References

[1] G. Taguchi, "*Taguchi Methods. Research and Development. Vol.* 1," Dearborn, MI, American Suppliers Institute Press, 1991.

[2] K. Bilen, S. Yapici, C.A. Celik, "Taguchi approach for investigation of heat transfer from a surface equipped with rectangular blocks," *Energy Conversion and Management*, Vol. 42 , 2001, 951-961.

[3] A.R. Khoei, I. Masters, D.T. Gethin, "Design optimization of Aluminium recycling processes using Taguchi technique," *Journal of Materials Processing Technology*, Vol.127, 2002, 96-106.

[4] M.S. Phadke, "Quality Engineering Using Robust Design," NJ, Prentice-Hall, Englewood Cliffs, 1989.

[5] G.H. Shiau, "A study of the sintering properties of iron ores using the Taguchi's parameter design," *Journal of the Chinese Statistical Association*, Vol. 28 , 1990, 253-275.

[6] L.I. Tong, C.T. Su, C.H. Wang The optimization of multi-response problems in the Taguchi method. *International Journal of Quality and Reliability Management*, Vol. 14, No.4 , 1997, 367-380.

[7] N. Logothetis, A. Haigh, "Characterizing and solving multi-response processes by the Taguchi method," *Quality and Reliability Engineering International*, Vol. 4, No. 2 , 1988, 159-169.

[8] J.J. Pignatello,"Strategies for robust multiresponse quality engineering," *IIE Transactions*, Vol. 25, 1993, 5-15.

[9] C.T. Su, L.I. Tong, "Multi-response robust design by principal component analysis," *Total Quality Management*, Vol. 8, No. 6 , 1997, 409-416.

[10] J. Antony, "Multi-response optimization in industrial experiments using Taguchi's quality loss function and principal component analysis," *Quality and Reliability Engineering International*, Vol.16 , 2000, 3-8.

[11] H.C. Liao, Y.K. Chen, "Solving multi-response problem in the Taguchi method by DEA based ranking method," *International Journal of Quality & Reliability Management*, Vol. 19, No. 7, 2002, 825-837.

[12] Y.H.W. Wong, J.E. Beasley, "Restricting weight flexibility in DEA," *The Journal of the Operational Research Society*, Vol. 41, 1990, 829-835.

[13] R.C. Baker, S. Talluri (1997). A closer look at the use of data envelopment analysis for technology selection. *Computers and Industrial Engineering*, Vol. 28, 1997, 101-108.

[14] R. Jeyapaul, P. Shahabudeen, K. Krishnaiah, "Simultaneous optimization of multi-response problems in the Taguchi method using genetic algorithm," *International Journal of Advanced Manufacturing Technology*, Vol. 30, 2006, 870-878.

JJMIE

Volume 4, Number 2, March. 2010
ISSN 1995-6665
Pages 324 - 329

Jordan Journal of Mechanical and Industrial Engineering

Confidence Estimates of Operators' Group Activity in Man-Machine Systems

R. T. Al-Kasasbeh[a], F. Ionescou[b], A. Mukattash[c], R. Btoush[d]

[a]Al-Balqa Applied University, Jordan, [b]Konstanz University of Applied Science, Germany, [c]The Hashemite University, Jordan, [d]National Center for Security and Crisis Management, Amman, Jordan

Abstract

Methods for the selection of candidates for operators of man-machine systems operator are analyzed. Vector mean estimates of group intelligence and estimates defining the group's collective decision-making ability to obtain the unified solution to the problem, to retain the correct original solutions, and estimates of solution quality and interoperability in correct decision-making are proposed. The properties of the suggested estimates are studied with a test example of five candidates. Amongst these properties are estimates of the group's psychological traits, such as average estimates of the professional competence of groups, static components of the intelligence vector for tested candidates, components of the trainability vector for tested candidates, average intelligence estimates for tested candidates, average estimates for the basis of groups, average stability estimates of groups, variations in the like-mindedness of operators, and the stability variation in operators' reasoning.

Keywords: Artificial Intelligence; Man-Machine Systems; Vector Estimates; Average Stability Estimates.

1. Introduction

The problem of optimizing a small group's activity currently grows increasingly more difficult, given the complexity of technical control systems processes and the requirement to expand operator activity in man-machine systems (MMS). In complex systems not only the behavior of one person, but that of an interoperable group of people, whose functions are tightly interconnected, the so-called "small group", have to be analyzed. This group might be a transport crew, a group of military specialists, operators of automated control systems, etc. During the establishment of such groups, specialists encounter a wide range of problems that include such problems as the estimate of the group's ability for correct decision-making under uncertainty conditions, the determination of the optimum number of a group, the compatibility of group members taking into account the personal traits of each individual, etc.

Procedures that are commonly used for the estimation of work effectiveness of a single person as an MMS operator are based on that candidate's test and evaluation, according to one or another scale of their reasoning ability, in completing work necessary for the MMS (Sidorenko, 2002).

An approach to intelligence rating is known [1], based on the computation of an artificial intelligence system using the test results of vector estimates, that include static probability components which estimate the ability to solve indistinct application problems, and dynamic probability components, which estimate the system's ability for self-learning. It is evident that such an approach may be used also for the objective estimate of an operator's professional suitability for work in one or another man-machine system (MMS). In this case the comparison and selection of the best candidates from the group of those tested may rely on a numerical estimate of the dynamic test results, when test results are recorded within various time intervals, into which the whole test run is divided.

However, because of specific differences between the group activity of the operators and a single person – the MMS operator – the recommended formulae for calculating the components of the group operator's vector estimate cannot be directly applied to the estimation of the group operator′s professional suitability, on the basis of the candidates' dynamic test results. In particular, as shown in [2-4], there are factors such as group reaction time, the time required for correct or crucial decision-making, and other characteristics of single operators and groups of operators. The article [5] discussed measurements and perception in MMS. That method deals with a possibility to objectively determine (using purely instrumental methods) human sensor system parameters which influence the operator's adaptability to the natural and technological environment. The approach [6] simulated the cognitive process of an operator and the plant behavior as affected by the operator's actions in accidental situations of an NPP (nuclear power plant). The simulation system consists of an operator model and a plant model which are

* Corresponding author. Adnanm63@yahoo.com

coupled dynamically. The operator model simulates an operator's cognitive behavior in accidental situations based on the decision ladder model of Rasmussen, and is implemented using the AI-techniques of the distributed cooperative inference method with the so-called blackboard architecture. Rule-based behavior is simulated using knowledge representation with If-Then rule types.

Modelling and identification play very significant roles in the present-day analysis of complex dynamic systems. Statistical modelling of any system is necessary to understand its dynamic behavior [7-9]. The structure of a mathematical model involves parameters which characterise the system and these parameters are determined using estimation techniques. Mathematical modelling of aeroplanes is very important since many applications require information in the form of aerodynamic derivatives (also called stability and control derivatives). These derivatives appear in the mathematical model (of the dynamics) of an aeroplane. The aerodynamic derivatives are required to explain aerodynamic stability and the control behaviour of the vehicle, thereby describing its static/dynamic behaviour, in mathematical models for the design of flight control systems, and in high fidelity simulators which need accurate mathematical models for aircraft. For the estimation of these derivatives, three main approaches are generally employed: firstly analytical methods [10], secondly wind tunnel testing of scaled models of aircraft, and thirdly flight testing and subsequent data analysis [11]. In this paper, the third approach is pursued and aircraft parameter estimation techniques to determine the aerodynamic derivatives from flight data are investigated. Some new approaches and results are presented. However, the methods discussed will be applied in a future paper to estimates of the group's psychological traits, such as average estimates of the professional competence of groups, static components of the intelligence vector for tested candidates, components of the trainability vector for tested candidates, average intelligence estimates for tested candidates, average estimates for the basis of groups, average stability estimates of groups, variations in the like-mindedness of operators, and the stability variation in operators' reasoning.

2. Mean Estimates of Group Intelligence

There are a considerable number of MMS's, in which decision-making is performed by a group of operators with equal rights. In this case it is simplest to estimate group intelligence by a vector, whose components are mean arithmetic values of the components of the group members. It is usually recommended to have a group with an even number of members, to maintain parity. A majority of two members will take the decision. In this case it's possible to build five groups of tested and estimated candidates. These groups are:

№ 1: (1 2 3 4); № 2: (1 2 3 5); № 3: (1 2 4 5); № 4: (1 3 4 5); № 5: (2 3 4 5)

Static components of the intelligence vector of tested candidates,

, are given in Table 1 and shown in Figure 1. These components are the following estimates:

Table 1. Static components of the intelligence vector for candidates

I	1	2	3	4	5
I_{Oi}	0,376	0,671	0,633	0,697	0,844
I_{Gi}	0,723	0,64	0,633	0,78	0,617
I_{Hi}	0,536	0,311	0,547	0,633	0,507
I_{Li}	0,434	0,151	0,414	0,526	0,467

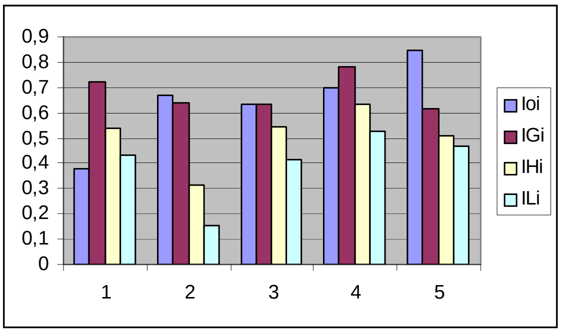

Figure 1. Static components of the intelligence vector for tested candidates

The obtained order differs from the ranking by average estimate of like-mindedness with the exception of the first two places. Therefore, it is appropriate to use an average estimate of the different-mindedness during selection of group members by test results.

The ***basis of a group*** is calculated as follows (Table 2 and Figure 2): $b_i(K) = n_{bi}(K)/n_{ai}(K)$, (21)

where: $n_{bi}(K)$ is the number of coincident correct answers of all members of the i-th group during the solution of all problems by time $K(t - t_0)$.

Table 2. Basis of group.

K	1	2	3	4	5	6	7	8	9	10
b1	0	0,091	0,141	0,088	0,479	0,69	0,442	0,375	0,447	0,485
b2	0	0,062	0,047	0,069	0,463	0,586	0,419	0,432	0,474	0,548
b3	0	0,048	0,033	0,069	0,388	0,567	0,442	0,395	0,486	0,562
b4	0	0,032	0,034	0,135	0,487	0,531	0,6	0,593	0,76	0,75
b5	0,05	0,031	0,048	0,071	0,487	0,548	0,439	0,457	0,514	0,586

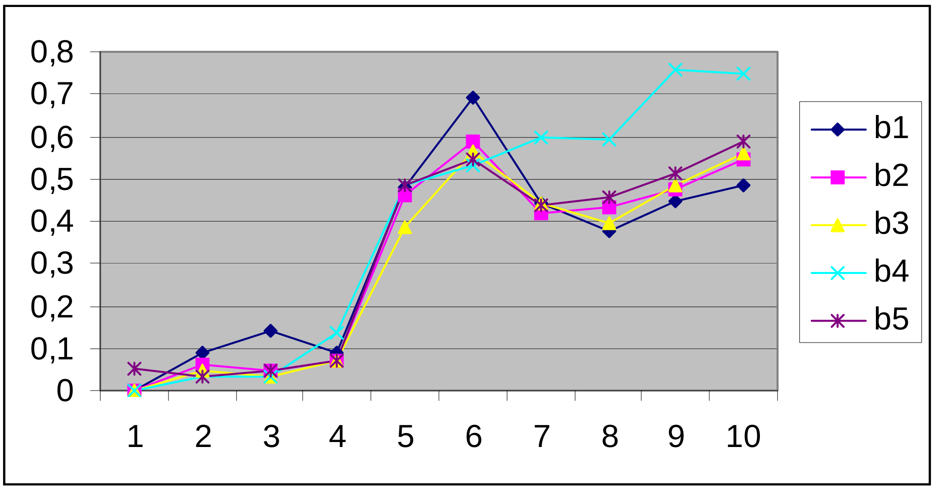

Figure 2 Variation of basis in the cognitive process

Analysis of the variation seen in Figure 2 allows one to judge the capability of group members in choosing correct solutions during the cognitive process. In particular, in the given example, as seen in Figure 2, all groups formed, with the exception of group № 4, exhibit a peak of coincident correct solutions during the test session, followed by a decay. This may indicate some unnecessary uncertainty among the members.

An **average estimate of basis** can be obtained as follows (Table 3, Figure 3):

$B_i = N_{bi}/N_{ai}$

where : N_{bi} is the total number of coincident correct solutions of all members of the i-th group during the solution of all problems for all testing times.

Table 3. Average estimate of basis

i	1	2	3	4	5
Bi	0,259	0,239	0,234	0,284	0,249

Figure 3 shows that the average estimates of basis allow the ranking of the groups. In the given example the reordering of the groups formed with respect to an average estimate of like-mindedness from best to worst yields the following order:

№ 4 , № 1 , № 5 , № 2 , № 3

The order obtained differs from the ranking obtained by the average estimate of different-mindedness in the fourth and fifth places. Therefore, an average estimate of basis can be used to equalize or specialize the operators of groups based on test results.

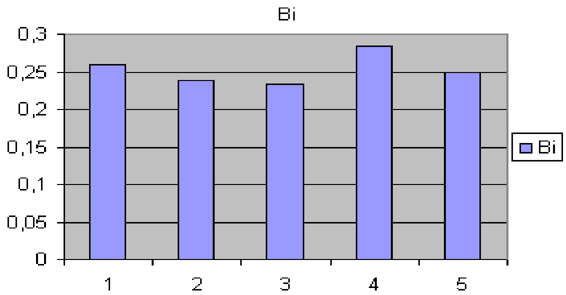

Figure 3. Average estimates of the basis of groups

Group stability is calculated as follows (Table 4 and Figure 4):

$s_i(K) = n_{si}(K)/n_{ai}(K)$

where : $n_{si}(K)$ is the number of problems solved correctly by more than half of all the members of the group during the solution of all problems by time $K(t - t_0)$.

Table 4. Group Stability

K	1	2	3	4	5	6	7	8	9	10
s1	0	0	0	0,017	0,195	0,586	0,302	0,375	0,447	0,576
s2	0	0	0,031	0,052	0,146	0,552	0,279	0,405	0,474	0,613
s3	0	0	0	0,034	0,184	0,567	0,279	0,395	0,486	0,592
s4	0	0	0	0,077	0,282	0,5	0,567	0,714	0,72	0,833
s5	0	0	0,016	0,036	0,205	0,548	0,293	0,429	0,514	0,69

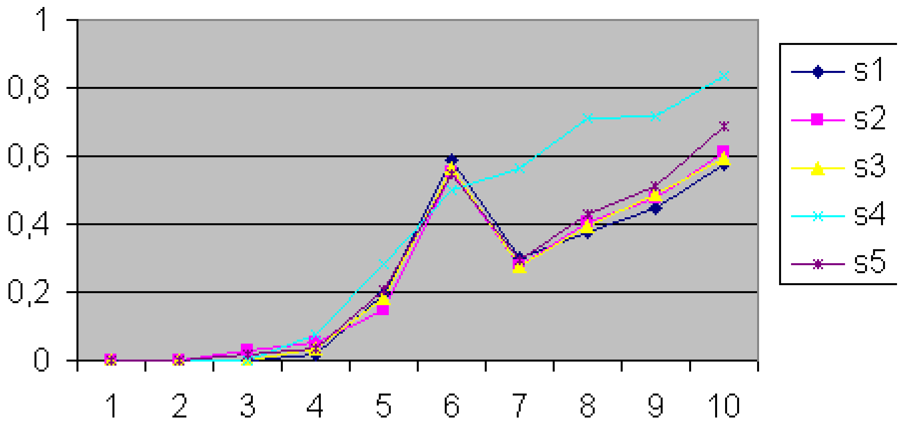

Figure 4. Stability variation in the cognitive process

Analysis of the variation seen in Figure 4 allows one to judge the suitability of groups for proper decision-making during the cognitive process. In particular, in the given example, as seen in Figure 4, only group №4 is not liable to hesitation in proper decision selection and during the cognitive process it systematically augments a number of proper decisions obtained by the majority of group members. All these facts demonstrate the psychological stability of this group of operators.

An **average estimate of stability** can be obtained as follows (Table 5 and Figure 5):

$S_i = N_{si}/N_{ai}$

where : N_{si} is the total number of problems which were properly solved by more than half of all the members of the i-th group during the solution of all problems for all testing times.

Table 5. Average estimate of stability

i	1	2	3	4	5
Si	0,183	0,188	0,187	0,252	0,197

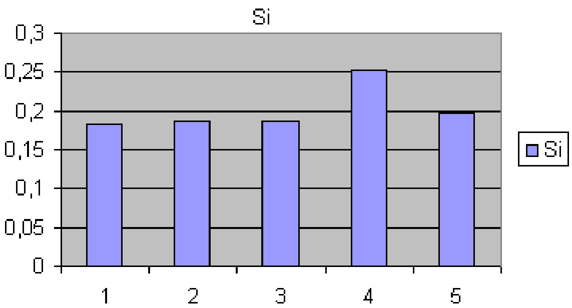

Figure 5 Average estimates of stability for groups

Figure 5 shows that the average estimates of stability allow ranking the groups. However, if the leading group is obviously superior, the remaining groups appear to be very similar. In other words, in practice we can mark out two categories of groups: the psychologically stable and the psychologically unstable. In the given example a reordering of the groups formed with respect to the average estimate of stability from best to worst we obtain the following order: №4 ; № 5 ; № 2 ; № 3; №1.

In this case, only group №4 can be considered to belong to the psychologically stable category. It is important to mention that this group appears to be the best in all other categories.

The ***group confidence*** is calculated as follows (Table 6 and Figure 6):

$f_i(K) = n_{fi}(K)/n_{ai}(K)$,

where: $n_{fi}(K)$ is the number of problems with only correct answers, which coincided among all the members of the i-th group during the solution of all problems by time $K(t - t_0)$.

Table 6. Group Confidence

K	**1**	**2**	**3**	**4**	**5**
f1	0	0	0	0	0,024
f2	0	0	0	0	0
f3	0	0	0	0	0,02
f4	0	0	0	0,019	0,026
f5	0	0	0	0	0
K	**6**	**7**	**8**	**9**	**10**
f1	0,379	0,023	0,15	0,184	0,273
f2	0,345	0,046	0,189	0,184	0,355
f3	0,333	0,046	0,158	0,216	0,312
f4	0,25	0,333	0,481	0,6	0,667
f5	0,258	0,049	0,171	0,257	0,31

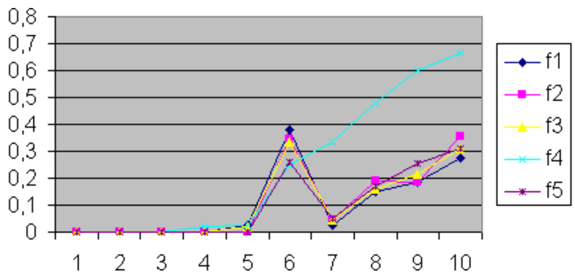

Figure 6 Confidence variation in the cognitive process

Analysis of the variation seen in Figure 6 allows one to judge the inevitability of a group in obtaining correct decisions during the cognitive process. In particular, in the given example, as seen in Figure 6 and in the estimate of the stability factor, only group №4 is not liable to hesitation in making correct decisions and during the cognitive process it systematically augments a number of correct decisions, obtained by all group members. These facts also demonstrate the psychological stability of this group of operators, which are assured in the correctness of their decisions. In this case we do not obtain any new additional information about the psychological features of groups, as in the previous case. However, from a computational perspective, it is easier to obtain this estimate.

An average estimate of confidence can be obtained as follows (Table 7 and Figure 7):

$F_i = N_{fi}/N_{ai}$

where: N_{fi} is the total number of problems with correct answers only, which coincided among all the members of the i-th group for all the testing times during the solution of all problems.

Table 7. Average estimate of confidence

i	1	2	3	4	5
F i	0,071	0,076	0,075	0,154	0,082

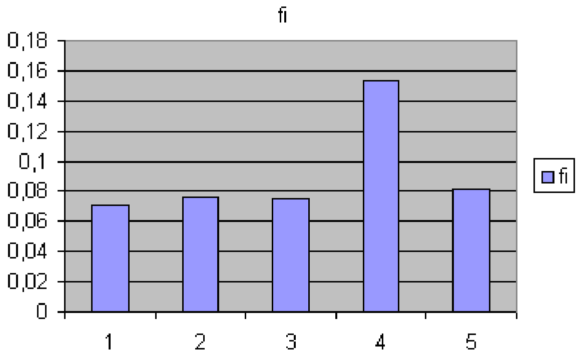

Figure 7. Average estimates of confidence of groups

Figure 7 shows that the average estimates of confidence allow ranking the groups. However, as in the previous case, if the leading group is obviously superior, the remaining groups appear to be very similar. In the given example, when reordering the groups formed with respect to an average estimate of stability from best to worst, we obtain an order that is the same as before. In this case, group №4 can be assigned to the psychologically stable category and the other groups should be assigned to the psychologically unstable category. Therefore, only one stability estimate and confidence estimate can be used. We use an average estimate of stability because it is easier to obtain.

The obtained average estimates of the psychological traits of groups can be calculated as the components of the vector estimate of psychological and professional competence of a group of MMS operators (Table 8 and Figure 8), or some average estimate of psychological and professional competence can be calculated based on the following components (Table 9 and Figure 9):

$P_i^{Gr} = k_C C_i - k_R R_i + k_B B_i + k_F F_i$

where: k_C, k_R, k_B and k_F are some weighting coefficients, which are chosen according to the type of problem. In the given example, with the aim of retaining the approximate equality of contributions from every component of the vector estimate to the average estimate, it was assumed that:

$k_C = k_R = k_B = 1$ and $k_F = 3$

Table 8. Vector estimate of components of psychological and professional competence

i	1	2	3	4	5
Ci	0,299	0,264	0,252	0,303	0,262
Ri	0,267	0,282	0,277	0,264	0,271
Bi	0,259	0,239	0,234	0,284	0,249
Fi	0,071	0,076	0,075	0,154	0,082

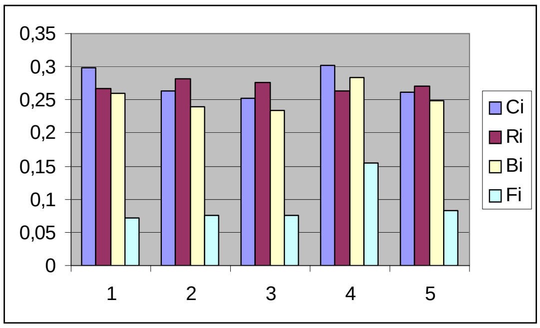

Figure 8. Vector estimate of components of psychological and professional competence

Analysis of Figure 8 allows us to take into account both the psychological features of the formed groups of operators and the preferences of competitive groups. In particular:

- If we allow only for estimates of group intelligence, we obtain an order of groups from best to worst: № 4 , № 5 , № 3 , № 1 , № 2
- If we allow only for estimates of trainability, we obtain the following order: №4 , № 5, № 1 , № 2 , № 3
- If we allow only for estimates of psychological competence, we obtain the following order: № 4 , № 1 , №5 , № 2 , № 3

In this case, based on the psychological competence estimates, all groups can be impartially divided into two classes: the psychologically stable (group №4) and the psychologically unstable (all the remaining groups).

Table 9. Average estimates of psychological and professional competence

i	1	2	3	4	5
Pi	0,504	0,449	0,434	0,785	0,485

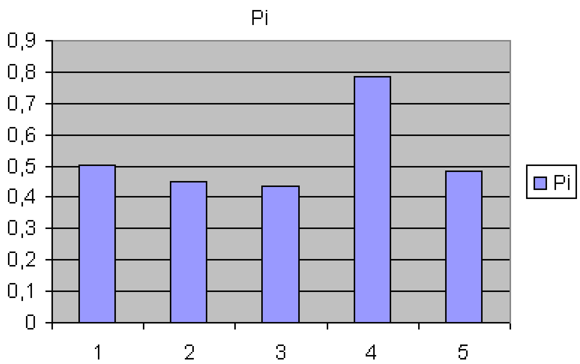

Figure 9. Average estimates of psychological and professional competence of groups

An analysis of the average estimates of psychological and professional competence of the groups formed of tested candidates (see Table 9 and Figure 8) confirms the conclusion that it is possible to mark out only two classes of groups based on their psychological stability. Let us form an average index of professional competence as follows:

$$Q_i = k_I I_i^{Gr} + k_P P_i^{Gr}$$

where : k_I and k_P are coefficients that allow for the preferences of a competitive group.

In the given example $k_I = k_P = 1$ was taken and the indexes given in Table 10 and illustrated in Figure 10 were obtained.

Table 10. Indexes of professional competence

i	1	2	3	4	5
Qi	0,917	0,842	0,846	1,401	0,924

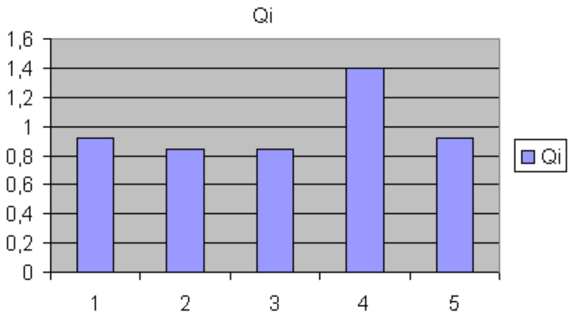

Figure 10. Indexes of professional competence

Figure 10 shows that average indexes of professional competence allow ranking the groups. However, as in the previous case, if the leading group is obviously superior, the remaining groups appear to be very similar. In the given example a reordering of the formed groups with respect to the average index of professional competence from best to worst yields the following order: (№ 4 , №5 , № 1 , № 3 , № 2). This order differs from all previous orders. In this case, the best group №4, as obtained earlier, belongs to the category of psychologically stable groups.

3. Conclusion

Introduced estimates of test results for candidates to work as a member of group MMS operator allow to take account of peculiarities of their thinking and psychology. Firstly, these estimates have static and dynamic components taking into account both, abilities for decision- making under uncertainty conditions and abilities for training in the process of work. Secondly they have components characterizing psychological stability of groups. In some cases vector estimates can be replaced by average estimates, which allow for easy ranking candidates from best to worst. However, in this process some part of information is being lost.

It seems, that more subtle study of a nature of variation in time of suggested group estimates by candidates' testing results will help to reveal a number of other group psychological peculiarities important for operation in MMS, such as indecision, nervousness, patience, thoroughness etc. In this case generation of the most self-descriptive test tasks for concrete MMS is the problem of no less importance.

It's also important to mention that the first two best groups are the same ones (№4 and №5) by ranking by professional convenience, be group intelligence and by trainability estimate of groups. However, the index of professional convenience estimates not only group ability to intellectual work and trainability, but their psychological stability, which in many cases can have a key meaning in proper decision-making under uncertainty conditions.

Acknowledgement

The paper presents results of research project performed in Germany . The project was supported and funded by German Research Association (DFG), Jordanian higher council for science and technology, Applied Science Konstanz and Al-Balqa' Applied University, Center for Security and Crisis Management, Hashemite University .

We would like to thank and acknowledge all these organizations for their support.

The authors would like to thank Mr. Andrew P. Smith at the University of Applied Science Konstanz for his English corrections.

References

[1] Gorodetsky A. E. Fuzzy Decision Making in Design on the Basis of the Hubituality.// Fuzzy System Design, L. Reznik, V. Dimitrov, J. Kasprzyk, Physica Verlag, 1998, ISBN 3-7908-1118-1.

[2] Gorodetskiy A. E. (editor) (2002) .Control under the condition of indetermination. St.Petersburg University, Russia, , 398 pages.

[3] Popchetelev, E.P. 1988. Training for studying group. Leningrad Technical University News, Leningrad. Pp. 65-67.

[4] Antonets V. A., N.M.Anishkina "Measurements and perceptionin man/machine systems" Preprint of IAP RAS, N 518,Nizhny Novgorod, 1999, 12p.

[5] Kitaura Wataru, Ujita Hiroshi "Man-machine system" United States Patent 5247433.

[6] Jung Hwa S., Jung Hyung-Shik. Establishment of overall workload assessment technique for various tasks and workplaces// International journal of industrial ergonomics (Int. j. ind. ergon.) ISSN 0169-8141 vol. 28, 2001, 341-353.

[7] Sinha, N.K. and Kutsza, B. Modelling and Identification of Multivariable Dynamic Systems. Van Nostrand, New York, 1983.

[8] Desai, R.C. and Lalwani, C.S. Identification Techniques , Tata McGraw Hill Inc., 1973.

[9] Anon, E. USAF stability and control DATCOM, Flight Control Division, AFFDL, Wright Patterson Airforce Base, Ohio, USA 1975.

[10] Maine, R.E. and Iliff, K.W. Application of parameter estimation to aircraft stability and control - the output error approach . NASA RP 1168, 1986.

[11] Jategaonkar, R.V. and Plaetschke, E. Maximum likelihood parameter estimation from flight test data. DFVLR-FB 83-14, IFM/ Germany, 1983

JJMIE

Volume 4, Number 2, March. 2010
ISSN 1995-6665
Pages 330 - 339

Jordan Journal of Mechanical and Industrial Engineering

Improvement in Adhesion Behavior of Aluminum Due to Surfaces Treatment with Arc Discharge

Nabil Anagreh*, Amin Al Robaidi

Al-Balq'a Applied University, Materials Eng. Dept., Al-Salt Jordan.

Abstract

Adhesive bonding of aluminum requires activating of part surfaces to improve the adhesion process. In the present study, The influence of arc discharge on the adhesion of epoxy, polyurethane and acrylic adhesives to aluminum is investigated whereby the influence of arc discharge parameters (amperage, frequency, work distance and treatment speed) on the improvement of adhesive strength are examined. Changes in surface topography and chemical composition of the surfaces are also identified, using Scanning Electron Microscopy (SEM) and Energy Disperse X-ray analysis (EDX).The results indicated that, two-components epoxy and polyurethane adhesives enable high adhesive strength, in comparison to thermosetting of single component epoxy. Similar behavior was determined for cold setting of two-component acrylic adhesive. Cohesive rupture was found in the two component epoxy and acrylic adhesives to be predominant. The rupture occurred in the layer nearby the aluminum surface whereby the rupture took place cohesively in the center of the adhesive layer in the polyurethane adhesive joint. The adhesion improvement achieved can be attributed to increasing roughness, complete removal of organic layers and reduction of inorganic magnesium oxide layers

Keywords: Arc Discharge, Adhesive Strength, Surface Pretreatment, Epoxy Adhesives (One-Component, Two-Components), Acrylic and Polyurethane Adhesives.

1. Introduction

In industrial applications, surface pretreatment of Al samples is a must to achieve strong and stable adhesion. Chemical and electro-chemical pretreatment of Al surfaces exhibit favorable adhesion. Disadvantages regarding those pretreatment methods are the disposal of chemicals involved, long pretreatment times and high operating costs. For said reasons, the application of mentioned or similar pretreatment methods is not recommended in many industries. On the other hand, mechanical pretreatments result often in unsatisfactory adhesion and long-term stability. The results of adhesion and long-term behavior of excimer- and CO_2-laser treatments show also some restrictions. The application of arc-discharge pretreatment methods could be considered as an alternative technique. Research related to arc-discharge pretreatment is limited right now. This art of pretreatment could be considered to fulfill both requirements, environmentally friendly preparation method, and could be developed to be fully automated in the industry.

2. Literature Review

For initial strength bonding, degreasing of Al surface is sufficient, whereas long-term-steady joints require a mechanical, chemical or electro-chemical pretreatment. Chemical and electro-chemical pretreatment produces reliable adhesion if suitable adhesive and primer were selected [1]. In summary, an oxide coating must develop as a result of the pretreatment, which stabilizes and enlarges the joint surface area and thus increases the interactions between adhesive and Al surface [1-27]. Surface anodizing with phosphoric, sulphuric, chromic acid or pickling agents provides excellent results because the adhesive, with the oxide coating, forms a composite structure [1, 9]. After Digby and Packham [6], the penetration of adhesive depends on the wetting behavior and viscosity of the adhesive and cavity dimensions. Disadvantages regarding the disposal of chemicals, high operating cost and long pretreatment times oppose application in automobile and vehicle industry.

Environmental-friendly pretreatment methods include: Excimer laser [12], CO_2-laser [20, 21], cryoblasting [13], dry ice blasting [19], organosilane [22-26], warm or boiling water [15, 27] and arc-discharge [14]. The application of excimer laser leads to removal of organic contamination, to an increase of the surface roughness and porosity, which results in an increase of adhesive surface and supplies satisfactory long-term stability [12]. CO_2-laser treatment causes a removal of organic contamination and an increase of the oxide coating thickness from 10 nm up to 85 nm, and a reduction of the Mg:Al ratio [9, 10]. Adhesive strength and long term behavior of CO_2-laser pretreated surfaces is satisfactory compared with cryoblasting and dry ice blasting treated samples [13,19]

* Corresponding author. anagreh1961@yahoo.com

whereas the long term stability of sandblasted Al surfaces is insufficient [11]. Adhesion and long-term endurance of Al surfaces treated with arc-discharge correspond to chemical pretreatments [14]. The use of organosilane pretreatment has shown to be effective in increasing the adhesive joint strength and the joint durability [22, 24]. Samples pretreated with warm or boiled water shows improvement in the adhesive performance due to the formation of hydroxyl layer. Those hydroxyl layers improve the molecular interactions with the adhesives. Furthermore, the layers show porous and highly rough surfaces that are responsible for mechanical interlocking with the applied adhesives, [15 and 27]. The chemical interactions resulting in a “micro/nano-composite” inter-phase leads to no appreciable loss in peeling resistance after aging in warm water or exposure to a corrosive environment [27].

3. Test Materials and Conditions

Throughout this project, Metallic partner's as used by automobile industry for body application was 1 mm thick aluminum sheet (AlMg4, 5Mn0, 4). Sheets were supplied by VAW Aluminum AG/Germany.

The adhesives were selected to fulfill industrial requirements as used by the automobile industry, like high strength, ductility, as well as high temperature and aging resistance. The two-component cold setting epoxy adhesives (Araldite 2011 (EP 1) and Permabond E 32 (EP 2)), the two-component cold setting polyurethane adhesive (Tivopur 1667+1600/07 (PU)) and the two-component cold setting acrylic adhesives (Permabond 6050 (AC 1) and Quickbond 5002 (AC 2)) were tested. In addition to the two components, single component thermosetting epoxy adhesives ESP 109 (EP 3) and ESP 104 (EP 4) were tested. Permabond/Germany provided us with the epoxy resin EP 2, 3, 4 and acrylic adhesives AC 1 and AC 2. Spezialitätenchemie GmbH/Germany provided the epoxy adhesive EP 1. PU was supplied by Tivioli Werke/Germany. The thermosetting epoxy adhesive ESP 104 is suitable because of its relativity to fast hardening at low temperature and its ability to glue plastics sensitive to high temperature. The adhesive EP 1 contains bisphenol A-epoxy resin with a molecular weight smaller than 700, 3-Dimethylaminopropyl and 1, 3-Propylenediamin. The adhesive EP 3 contains magnesium oxide filler. In the PU adhesive, the A-component consists of polyolen, fillers and 10-25% polyether modified bisphenol whereas the B-component contains a isocyanate hardener, Diphenylmethan, -4, 4`-diisocyanat (<75%) and Hexamethylen-1,6-Diisocyanat (0,1-1%). The acrylic adhesive AC 1 uses a multi-phase technology to reduce crack growth by embedding microscopically small rubber particles. **Table 1** indicates the adhesives selected that was investigated in this project.

Table 1. Used adhesives and processing conditions

Adhesive basis	***two-component epoxy***		single component epoxy	
Manufacturer	Ciba Spezialitätenchemie	Permabond	Permabond	Permabond
Trade name	Araldite 2011	Permabond E 32	ESP 109	ESP 104
Abbreviation	EP 1	EP 2	EP 3	EP 4
Resin A	Aradite 2011A	Resin A	ESP 109	ESP 104
Hardener B	2011B	Hardner B	-	-
Mixing proportion A:B	100:80 (wt. parts)	1:1 (vol.-parts)	single-component	single-component
Pot life	85 min at 30°C	120 min at RT	-	-
Processing	Manually	Manually	Manually	Manually
Hardening conditions	30 min bei 80°C	45 min at 60°C	90 min at 120°C	60 min at 100°C

Adhesive basis	***Polyurethane***	Acrylic	
Manufacturer	Tivoli	Permabond	Permabond
Trade name	Tivopur 1667	Permabond 6050	Quickbond 5002
Abbreviation	PU	AC 1	AC 2
Resin A	Tivopur 1667	-	Harz A
Hardener B	Tivopur 1600/07	-	Härter B
Mixing proportion A:B	100:30 (wt. Parts)	1:1 vol. parts	1:1 (vol. parts)
Pot life	14 min bei RT	5 min bei RT	3 min bei RT
Processing	Manually	Static mixer	Bead on bead
Hardening conditions	48 h at RT + 3 h at 100°C	24 h at RT	24 h at RT

The Al sheets as received were contaminated and were covered with a layer of oil. Therefore the surfaces were cleaned and degreased with ultrasonic activated ethanol for 5 min and dried with oil-free compressed air. To achieve optimal adhesion, the surfaces were afterwards treated by spark discharge under argon. A Navigtor 240 AC/DC V-box 1 was used. **Fig. 1a** shows the experimental setup for the pretreatment. Variable pretreatment parameters were selected; amperage (5, 10 and 20 A), frequencies (100, 200 and 300 Hz), and the treatment speed (25, 50, 75, 100 and 150 cm/min). The distances between electrode and Al surface (2 and 4 mm) were chosen. Tungsten electrodes with a diameter of 1.6 mm were used, considering that the Al surface was acting as a cathode, whereby the electrodes were used as anode.

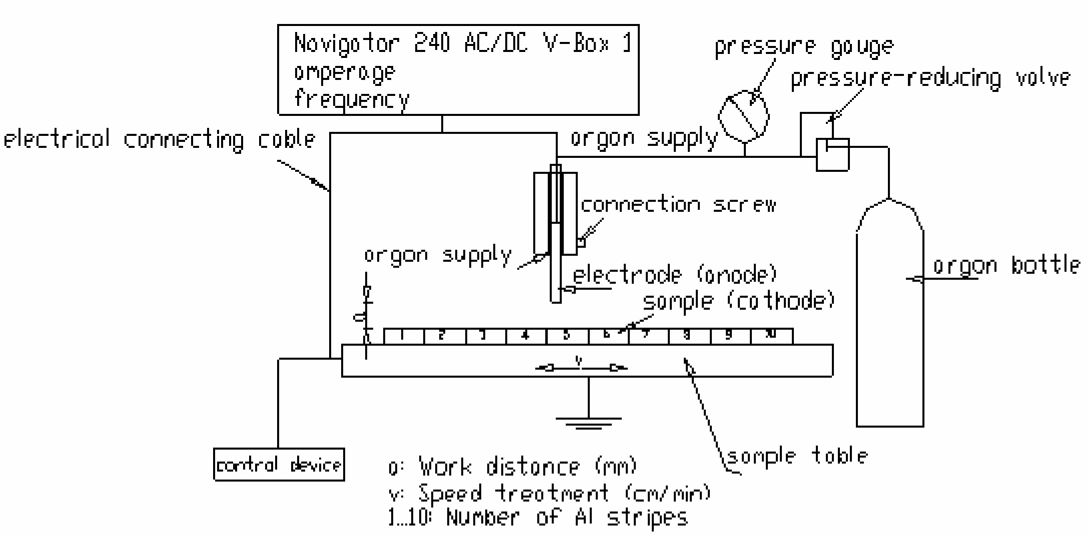

Fig. 1a. Experimental setup used throughout the investigations.

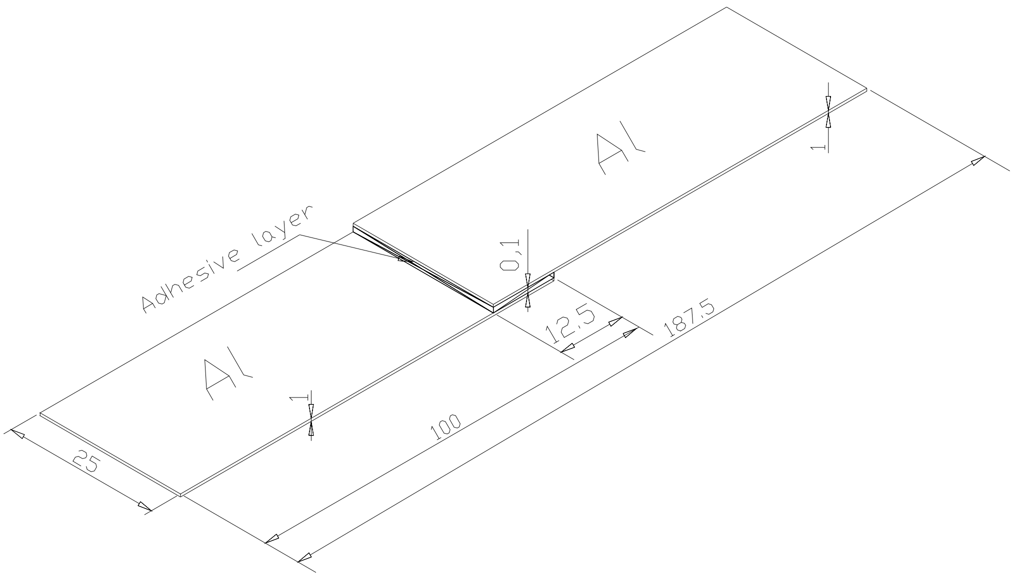

Fig. 1b: Sample dimensions and form

The two-component adhesives EP 1, EP 2, PU were mixed manually, degassed in vacuum for some minutes to avoid bubbles. The single component epoxy adhesives EP 3 and EP 4 were laminated by a cartouche pistol on the Al sheets. For keeping an even layer of 0.1 mm adhesive thickness, copper wires of 0.1 mm diameter were inserted. To keep a constant applied pressure, a device with constant weights was used. The adhesive joints were warm-hardened in a circulating air furnace, **Table 1**. Resin and hardener with the AC 1 were supplied in chamber cartouches with static mixer. The joining parts were fixed into appropriate device by means of pressure weights, so that they do not slide. The adhesive AC 2 was spread by double chamber cartouches in the "Bead on bead" procedure. The adhesive hardening by AC 1 and AC 2 took place at ambient temperature within 24 h, **Table 1**.

To determine adhesive strength, single overlapped tensile shear test specimens were used according to DIN EN 1465. **Fig. 1b** shows the specimen shape and dimensions. To measure the adhesion, strength mechanical test were conducted. The samples were pulled on an instron tensile testing machine with a test speed of 5 mm/min under normal climate. For each test series 5 samples were examined, from which the average strength was determined. To see the topographic structure of the differently pretreated Al surfaces as well as the fractured occurred on the fractured surfaces, Scanning Electron Microscopy (SEM) was used. EDX analyses were applied to determine the chemical composition of Al surfaces before and after treatment. Furthermore EDX was used to determine where fracture took place on the fractured samples

4. Test Results

The organic layers on Al surfaces represent residuals of the lubricating oil during the rolling process of Al sheets as well as contamination from the environment, which minimized the adhesion. Degreasing the samples with ethanol did not cause a complete removal of organic and hydrocarbon layers as well as inorganic MgO layers. After degreasing, the carbon concentration on sample surface (area integral) decreased up to 1%, and the oxygen decreased insignificantly, Table 2. Arc-discharge lead to the complete removal of organic hydrocarbon layers and reduced the inorganic MgO layers. Magnesium concentration was reduced independently of the treatment parameters approximately 3%. The reduction of oxygen concentration was influenced by the treatment parameters. The Al concentration increased in the outer surfaces after arc-discharge by 7% in relation to the delivered state. After arc-discharge the elements manganese and iron were found. This could be related to elements presents in the Al alloy. The concentration of these elements did not show significant dependence on amperage, treatment speed and work distance, **Table 2**.

SEM photographs show that arc-discharge causes a strong surface roughness in relation to the delivered and degreased surfaces, **Fig. 2, 3**. Arc-discharge changes the topographic structures. The topography changes were strongly influenced by treatment parameters, work distance, amperage, frequency and speed; however speed was not significant as the other parameter. At a 4 mm work distance, the surface shows cotton wool-topographic structures. Magnification (10000) shows this microstructure very clearly, **Fig. 2d, f.** At 20 A current, the surface roughness is more pronounced with a pretreatment speed of 100 cm/min rather than with 50 cm/min, **Fig. 2g, h**. **Fig. 3 a and b** show the surface topography at 100 Hz and 2 mm distance. The structure was a homogenous fine grain structure. Increasing the frequency to 200 Hz influenced the structure and generated a semi fine-rough structure, **Fig. 3c, d**. At 4 mm distance, the structure was homogenous and rougher at 200 Hz than 100 and 300 Hz, **Fig. 3e, f, g**.

Fig. 4, 6-8 indicates the Influence of the treatment parameters of arcs on the determined average adhesive strength of Al surfaces bonded with epoxy adhesive EP 1, EP 2, EP 3, and EP 4, and polyurethane adhesive (PU), and acrylic adhesive AC 1 and AC 2. The adhesive strength of Al - arc-discharge pretreated surfaces depends strongly on adhesive type. In this report, it is clearly

Table 2. Chemical composition (area integrals) of differently pre-treated aluminum surfaces

Pretreatment	Area integrals [COUNTS of the x-ray quanta in %]					
Elements	C	O	Mg	Al	Mn	Fe
None (Delivered state)	2.045	3.345	8.857	85.75		
Ethanol degreased	0.928	2.834	8.279	87.96		
5 A, 200 Hz, 50 cm /min, 2 mm		0.959	5.612	92.83	0.316	0.286
5 A, 200 Hz, 100 cm/min, 2 mm		1.067	5.812	92.58	0.301	0.240
5 A, 200 Hz, 50 cm/min, 4 mm		2.092	5.100	92.21	0.311	0.284
5 A, 200 Hz, 100 cm/min, 4 mm		1.651	5.428	92.21	0.333	0.378
10 A, 200 Hz, 50 cm/min, 2 mm		1.089	5.233	93.14	0.287	0.249
10 A, 200 Hz, 100 cm/min, 2 mm		1.002	5.581	92.82	0.315	0.283
10 A, 100 Hz, 100 cm/min, 2 mm		0.958	5.708	92.71	0.289	0.335
10 A, 300 Hz, 100 cm/min, 2 mm		1.245	5.426	92.71	0.298	0.322
10 A, 200 Hz, 50 cm/min, 4 mm		1.208	5.045	93.04	0.337	0.367
10 A, 200 Hz, 100 cm/min, 4 mm		1.243	5.302	92.78	0.314	0.362
10 A, 100 Hz, 50 cm/min, 4 mm		1.212	5.616	92.48	0.325	0.370
10 A, 300 Hz, 50 cm/min, 4 mm		0.999	5.269	93.13	0.331	0.270
20 A, 200 Hz, 50 cm/min, 2 mm		1.476	5.532	92.41	0.317	0.264
20 A, 200 Hz, 100 cm/min, 2 mm		0.938	5.354	93.03	0.353	0.323

indicated that treatment parameters have low impact on the adhesion.

The adhesion of the two-component epoxy cold setting was improved approximately by 9-29% when the surface was arc treated for EP 1 type and 40-77% for EP 2, respectively, **Fig. 4**. The Adhesion depended strongly on the amperage but slightly on work distance and treatment speed applying EP 1. The adhesion values for samples treated with 5 and 10 A are 2-2.5 MPa, higher than samples treated with 20 A. Degreasing the samples with ethanol, the adhesive strength decreases in relation to the delivered state approximately 40%. The same sample pretreated by arc-discharge, the adhesion increased to double as compared to degreased sample, **Fig. 4**. Visual inspections show that the samples glued with EP 1 and EP 2 failed independently of pretreatment parameters in the boundary layer between adhesive and Al surface. Fig. 5 a and b show the SEM photographs of fractured Al joint glued with EP 1 and EP 2. SEM photograph of fractured joint glued with EP 1 shows, when samples pretreated at 10 A, 2 mm and 50 cm/min, traces of cohesive rupture in the adhesive layer, **Fig. 5a**. EDX analysis of the fracture surface showed the elements carbon, oxygen, magnesium,

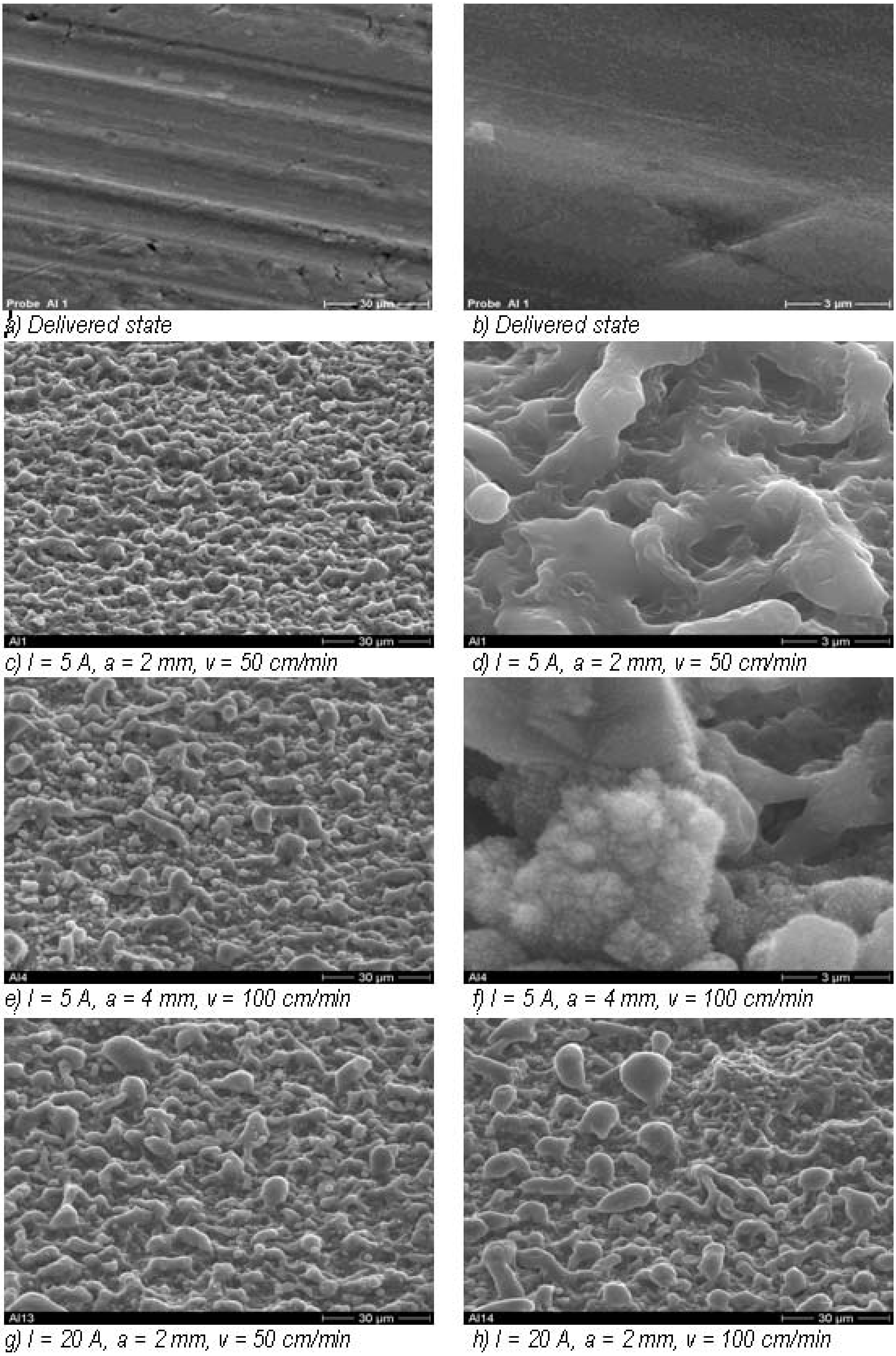

Fig. 2. Topographic structures of aluminum surfaces pre-treated with arc discharge. Frequency = 200 Hz. I: Amperage, a: Work distance, v: Treatment speed

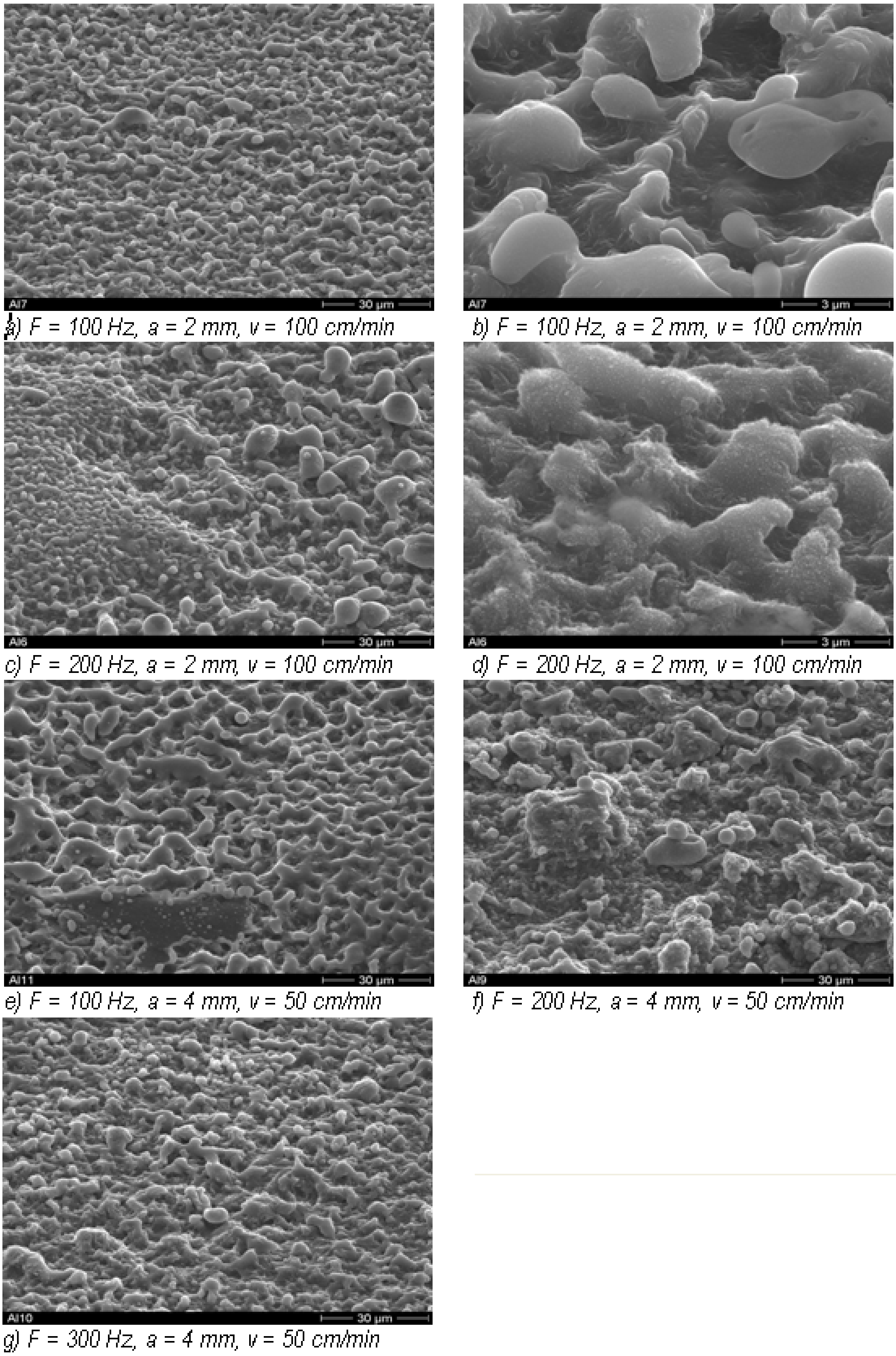

Fig. 3. Influence of the treatment parameters of arc discharge on the topographic structures of aluminum. Amperage = 10 A. F: Frequency, a: Work distance, v: Treatment speed

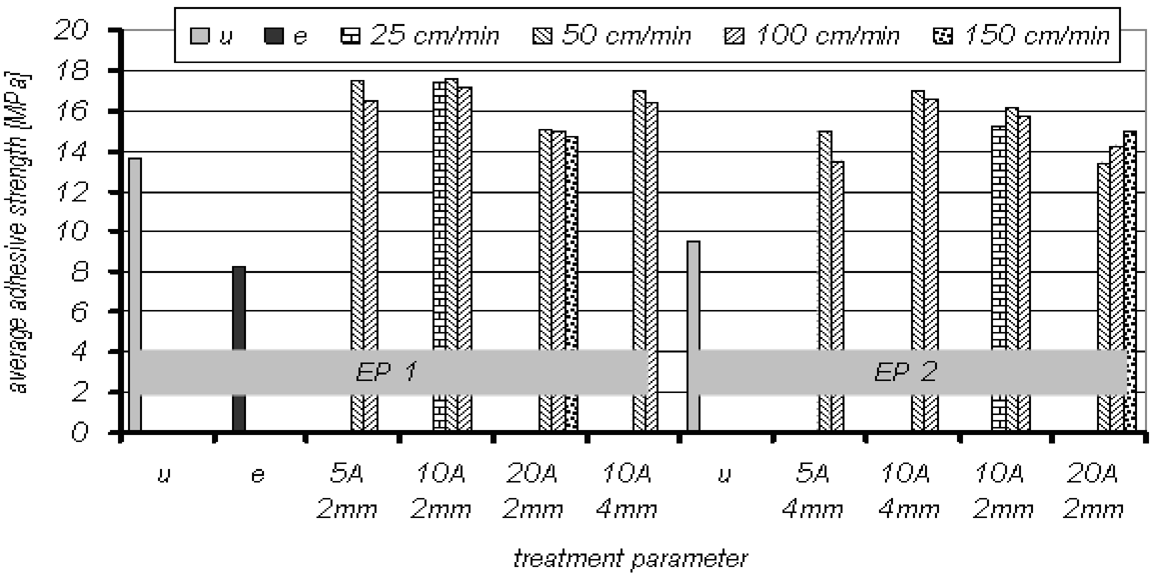

Fig. 4. Influence of the treatment parameters of arcs on the determined average adhesive strength of aluminum surfaces bonded with epoxy adhesive EP 1 and EP 2. u: untreated, e: ethanol degreased.

Al and silicon, **Table 3**. From SEM photographs and EDX analyses, it can be concluded that the rupture was cohesively in the adhesive layer and took place closely to the Al surface and in the oxide layer. SEM photographs of fractured Al joint glued with EP 2 indicate that oxide layers were pulled out partially from the aluminum surface, **Fig. 5b**. Further it could be concluded that the fracture was adhesively between oxide and adhesive layer. EDX analysis indicated that Al oxide on both fracture surfaces was available, that is to some extent responsible for the increase of adhesion **Table 3.** The rupture occurred cohesively in the adhesive layer since on both fracture surfaces carbon and calcium were present, **Table 3**.

Table 3. Chemical composition of the fracture surfaces with different adhesives after arc discharge pretreatment of aluminum surfaces

Pretreatment parameter / Adhesives		Area integrals [COUNTS of the x-ray quanta in %]							
		C	O	Mg	Al	Si	Ca	Cl	K
10 A, 200 Hz, 2 mm, 50 cm/min, EP 1	A	5.823	2.084	7.01	84.47	0.614			
	B	87.18	9.553		0.911	2.352			
10 A, 200 Hz, 4 mm, 50 cm/min, EP 2	A	27.51	6.650	6.558	53.87	4.917	0.492		
	B	66.98	13.17	3.078	3.021	9.713	3.442	0.593	
20 A, 200 Hz, 2 mm, 75 cm/min, EP 3	A	29.39	14.36	51.14	0.508	4.165	0.426		
	B	31.83	8.090	7.705	48.79	3.400	0.184		
10 A, 200 Hz, 4 mm, 50 cm/min, PU	A	53.70	18.24		1.077	5.098	21.41		0.475
	B	58.21	18.39		1.703	4.866	16.47		0.356
5 A, 200 Hz, 2 mm, 50 cm/min, AC 1	A	45.47	10.48	2.967	38.68	2.402			
	B	77.84	17.02		0.569	4.577			
5 A, 200 Hz, 2 mm, 50 cm/min, AC 2	A	31.47	8.669	4.370	54.84	0.653			
	B	80.34	17.59	0.246	1.285	0.529			

A and B are the opposite fracture surfaces for each sample

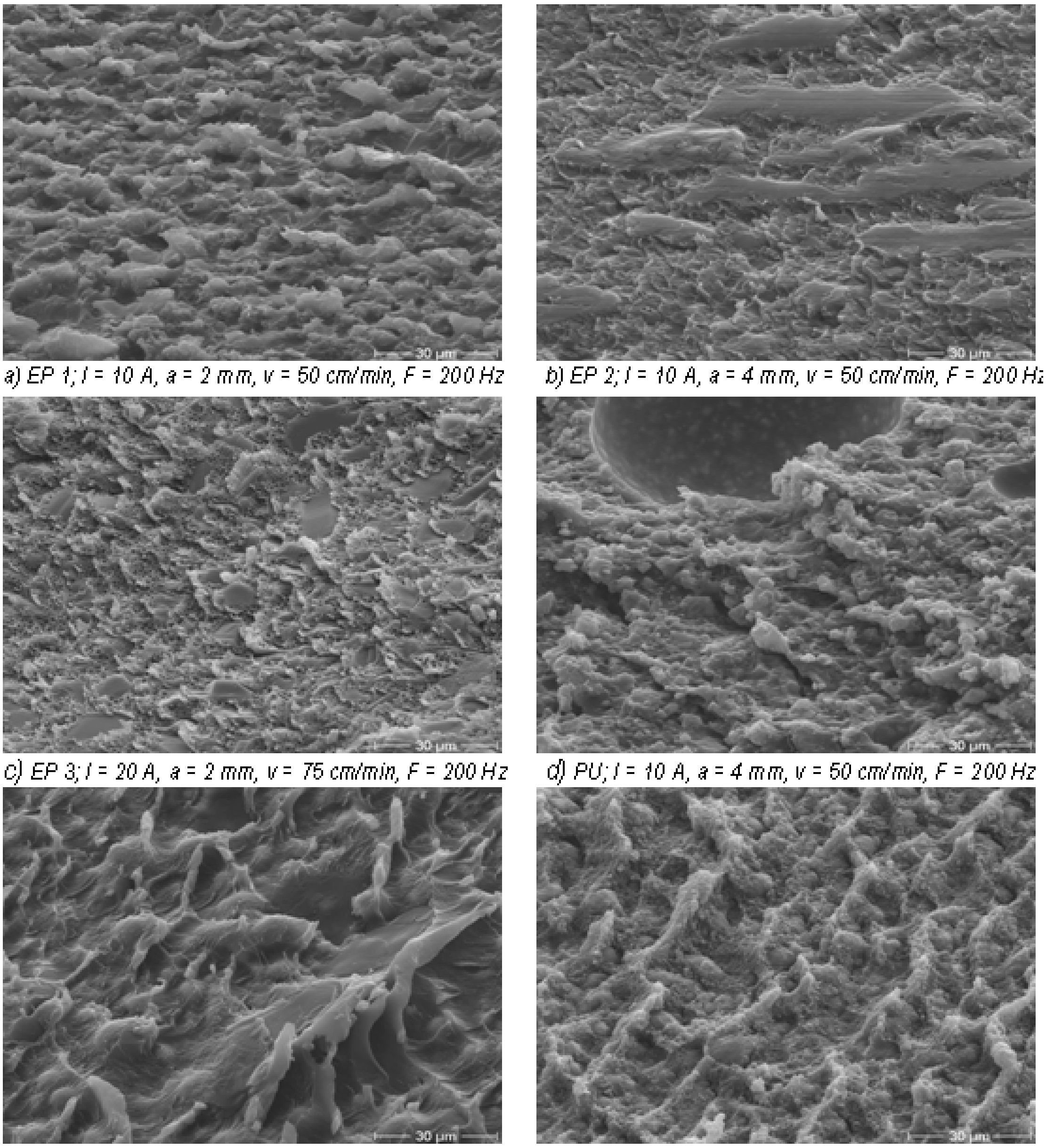

a) EP 1; I = 10 A, a = 2 mm, v = 50 cm/min, F = 200 Hz

b) EP 2; I = 10 A, a = 4 mm, v = 50 cm/min, F = 200 Hz

c) EP 3; I = 20 A, a = 2 mm, v = 75 cm/min, F = 200 Hz

d) PU; I = 10 A, a = 4 mm, v = 50 cm/min, F = 200 Hz

e) AC 1; I = 5 A, a = 2 mm, v = 50 cm/min, F = 200 Hz

f) AC 2; I = 5 A, a = 2 mm, v = 50 cm/min, F = 200 Hz

Fig. 5. Fracture surfaces of aluminum bonded with different adhesives. I : Amperage. F : Frequency, a : Work distance, v : Treatment speed.

For the single component epoxy adhesive EP 3, the adhesive strength is approximately 30% lower after sample treatments with arc-discharge in relation to the sample as delivered, **Fig. 6**. The adhesive strength is higher with 10 A compared to 20 A. Degreasing the Al sheets with different solvents before arc-discharge has small influence on adhesion. The rupture took place independently of the treatment parameters in the boundary layer between adhesive and Al surface. SEM fracture analysis exhibited fine porous surface texture, **Fig. 5c**. The presence of carbon on both fracture surfaces demonstrated that the rupture in the adhesive layer took place. EDX analysis of the fracture surface (**Table 3**) provided higher magnesium concentration as compared with the pretreated Al surface (**Table 2**), since MgO was added as filler in the formulation of the adhesive. After [16] heat curing of adhesives causes a drastic increase of magnesium concentration in the surface due to diffusion of Mg^{2+}-Ions from the adhesive mass. According [18] less adhesion rupture occurs with thermosetting adhesives because the deposit of magnesium in the boundary layer during hardening process reduces the adhesion, so that the fracture occurs partially in the magnesium-rich layer. Further, magnesium can favor the electro-chemical dissolution of Al [16].

The thermosetting single component epoxy adhesive EP 4 increases adhesion of arc-treated Al surfaces only slightly compared to untreated ones, **Fig. 6.** The samples failed predominantly adhesively.

PU adhesive causes an increase adhesion after arc-discharge of approximately 10-23%. The adhesion is only slightly dependent of the treatment parameters, **Fig. 7**. The rupture changed from the mixed fracture in the delivered state to coherence rupture after arc-discharge, **Fig. 5d**. Closed bubbles were seen, generated during the hardening process.

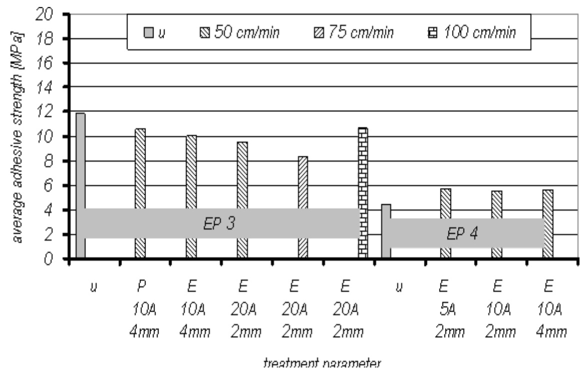

Fig. 6. Influence of the treatment parameters of arcs on the determined average adhesive strength of aluminum surfaces bonded with epoxy EP 3 and EP 4 adhesive. u: untreated, E: ethanol degreased, P: Permaclean degreased

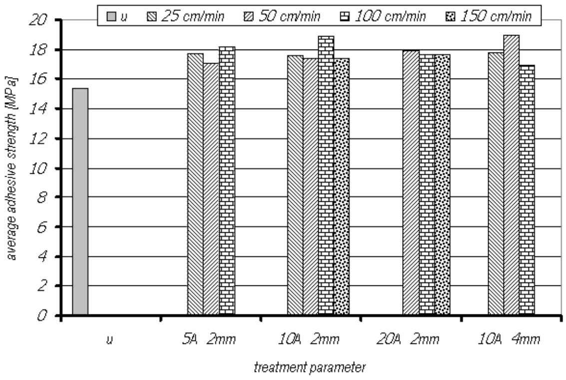

Fig. 7. Influence of the treatment parameters of arcs on the determined average adhesive strength of aluminum surfaces bonded with polyurethane PU adhesive. u: untreated

The adhesive strength for the two-component acrylic adhesives AC 1 and AC 2, increase after arc-discharge treatment up to 17% and 23%. The adhesive strength values differ slightly in relation to the different treatments parameters, **Fig. 8**. Samples with AC 1 adhesives failed in the delivered state adhesively in the boundary layer between the Al and adhesive. With increasing adhesive strength, the samples show both adhesive and cohesive rupture, **Fig. 5e**. Samples with AC 2 adhesives exhibit in delivered state and after arc-discharge adhesion rupture in the boundary layer between Al and adhesive, **Fig. 5f**. AC 1 shows higher adhesive strength than with AC 2.

Change the arc-discharge frequency from 100 to 200 and 300 Hz, the adhesive strength increases with EP 1, EP 2 and AC 1 slightly, whereby the adhesive strength increases with PU obvious more, **Fig. 9**.

Table 4 shows the differences between the measured maximum and minimum adhesive strength values for each adhesive as a function of the pretreatment parameters

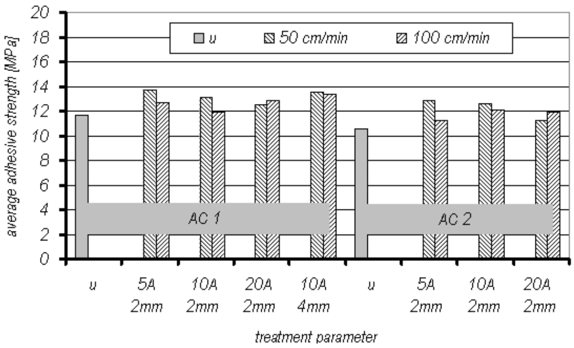

Fig. 8. Influence of the treatment parameters of arcs on the determined average adhesive strength of aluminum surfaces bonded with acrylate AC 1 and AC 2 adhesive. u: untreated

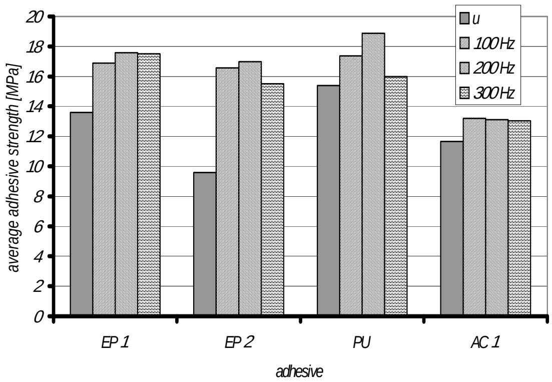

Fig. 9. Influence of the frequency on the determined average adhesive strength of aluminum surfaces bonded with different adhesives. u: untreated.

5. Conclusions

Arc-discharge of Al sheets causes a strong improvement of adhesion on Al surfaces, which exceeds the adhesive strength of sand-blasting. **This fact was investigated and reported by Anagreh, etc [18].** This was related to the strong roughening of the surface topography, and thus an increase of the surface area. The adhesive penetration in the porosity, the removal of organic contamination layers (lubricating oil and contamination) and the strong reduction of inorganic magnesium oxide layers contribute to the increase in adhesive strength. The cold setting two-component epoxy adhesives show strong adhesive strength compared to the thermosetting single component epoxy adhesives. Maximum adhesive strength was achieved using polyurethane adhesive. Two-component acrylic adhesives indicate lower adhesive strength than the two-component epoxy and polyurethane adhesives. SEM photographs and the EDX analyses of fracture surfaces point out that the rupture occurred with the epoxy and acrylic predominantly cohesively in the adhesive layer closely to the Al surface. Polyurethane adhesive shows different behavior, and the sample failed cohesively in the center of adhesive layer.

References

[1] G.W. Critchlow, D.M. Brewis, "Review of surface pretreatments for aluminum alloys". Int. J. Adhesion& Adhesives Vol. 16, 1996, 255-275.

[2] A. Higgins, "Adhesive bonding of aircraft structures". Int. J. Adhesion& Adhesives Vol. 20, 2000, 367-376.

[3] A. N. Rider, D. R. Arnott, "Boiling water and silane pre-treatment of aluminum alloys for durable adhesive bonding". Int. J. Adhesion& Adhesives Vol. 20, 2000, 209-220.

[4] A. F. Harris, A. Beevers, "The effect of grit-blasting on surface properties for adhesion". Int. J. Adhesion& Adhesives Vol. 19, 1999, 445-452.

[5] J. P. Sargent, "Adherend surface morphology and its influence on the peel strength of adhesive joints bonded with modified phenolic and epoxy structural adhesives". Int. J. Adhesion& Adhesives Vol. 14, 1994, 21-30.

[6] R. P. Digby, D. E. Packham, "Pretreatment of aluminum: topography, surface chemistry and adhesive bond durability". Int. J. Adhesion& Adhesives Vol. 15, 1995, 61-71.

[7] G.W. Critchlow, D.M. Brewis, "Influence of surface macro roughness on the durability of epoxide-aluminum joints". Int. J. Adhesion&Adhesives Vol. 15, 1995, 173-176.

[8] T. Neeb, S. Emrich, W. Brockmann, "Wie Wirksam sind mechanische Vor-behandlungen von Metallen. Adhäsion kleben&dichten Vol. 41, 1997, 18-23.

[9] A. Bjorgum, F. Lapique, J. Walmsley, K. Redford, "Anodising as pretreatment for structural bonding". Int. J. Adhesion& Adhesives Vol. 23, 2003, 401-412.

[10] B. B. Johnsen, F. Lapique, A. Bjorgum, J. Walmsley, B. S. Tanem, T. Luksepp, "The effect of pre-bond moisture on epoxy-bonded sulphuric acid anodised aluminium". Int. J. Adhesion& Adhesives Vol. 24, 2004, 183-191.

[11] A. J. Kinloch, "The service performance of structural adhesive joints”. Haftung als Basis für Stoffverbunde und Verbundwerkstoffe, Oberursel 1982.

[12] R. Broad, J. French, J. Sauer, "New, effective, ecological surface pretreatment for highly durable adhesively bonded metal joints". Int. J. Adhesion& Adhesives Vol. 19, 1999, 193-198.

[13] D.M. Brewis, G.W. Critchlow, C.A. Curtis, "Cryo blasting as a pretreatment to enhance adhesion to aluminium alloys: an initial study". Int. J. Adhesion& Adhesives Vol. 19, 1999, 253-256

[14] H. Kleinert, S. Groβer, B. Schultrich, P. Siemroth, "Activating adherend surfaces by applying arc-discharge treatment". Int. J. Adhesion& Adhesives Vol. 17, 1997, 203-206.

[15] P. R. Underhill, A.N. Rider, D.L. DuQuesnay, "Warm water treatment of aluminum for adhesive bonding". Int. J. Adhesion& Adhesives Vol. 23, 2003, 307-313.

[16] A.C. Moloney,"In Surface Analysis and Pre-treatment of Plastics and Metals” (Ed. D.M. Brewis). Applied Science Publishers. London.1982. Ch.8.

[17] A. V. Pocius, D. A. Wangsness, C. J. Almer, A. G. Mc Kown, "In Adhesive Chemistry” (Ed. L.H. Lee). Plenum Publishing Corp., New York, 1984.

[18] N. Anagreh, L. Dorn, "Oberflächenstruktren und Adhäsionseigenschaften unterschiedlich vorbehandelter Aluminium-Klebflächen". Aluminium Vol. 77, 2001, p. 81-87 and p. 178-184.

[19] F. Elbing, N. Anagreh, L. Dorn, E. Uhlmann, "Dry ice blasting as pretreat-ment of aluminum surfaces to improve the adhesive strength of aluminum bonding joints". Int. J. Adhesion&Adhesives Vol. 23, 2003, 69-79.

[20] G.W. Critchlow, D.M. Brewis, D.C. Emmony, C.A. Cottam, "Initial investigation into the effectiveness of CO_2-laser treatment of aluminium for adhesive bonding". Int.J. Adhesion& Adhesives Vol. 15, 1995, 233-236.

[21] G. W. Critchlow, C. A. Cottam, D. M. Brewis, D. C. Emmony, "Further studies into the effectiveness of CO_2-laser treatment of metals for adhesive bonding". Int. J. Adhesion& Adhesives Vol. 17, 1997, 143-150.

[22] M.-L. Abel, R.D. Allington, R.P. Digby, N. Porritt, S.J. Shaw, J.F. Watts, "Understanding the relationship between silane application conditions, bond durability and locus of failure". Int. J. Adhesion& Adhesives Vol. 26, 2006, 2-15.

[23] A.N. Rider, "Factors influencing the durability of epoxy adhesion to silane pretreated aluminium". Int. J. Adhesion& Adhesives Vol. 26, 2006, 67-78.

[24] M.-L. Abel, A.N.N. Adams, A.J. Kinloch, S.J. Shaw, J.F. Watts, "The effects of surface pretreatment on the cyclic-fatigue characteristics of bonded aluminium-alloy joints". Int. J. Adhesion& Adhesives Vol. 26, 2006, 50-51.

[25] P. R. Underhill, D. L. DuQuesnay, “The dependence of the fatigue life of adhesive joints on surface preparation". Int. J. Adhesion& Adhesives Vol. 26, 2006, 62-66.

[26] A. Rider, P. Chalkley, "Durability of an off-optimum cured aluminium joint". Int. J. Adhesion& Adhesives Vol. 24, 2004, 95-106.

[27] C. Spadaro, C. Dispenza, C. Sunseri, “The influence of the nature of the surface oxide on the adhesive fracture energy of aluminum-bonded joints as measured by T-peel tests". Int. J. Adhesion& Adhesives Vol. 28, 2008, 211-221.

المملكة الأردنية الهاشمية

الجامعة الهاشمية

المجلة الأردنية
للهندسة الميكانيكية والصناعية

JJMIE

مجلة علمية عالمية محكمة

http://jjmie.hu.edu.jo/

ISSN 1995-6665

المجلة الأردنية للهندسة الميكانيكية والصناعية
مجلة علمية عالمية محكمة

المجلة الأردنية للهندسة الميكانيكية والصناعية: مجلة علمية عالمية محكمة أسستها اللجنة العليا للبحث العلمي في وزارة التعليم العالي والبحث العلمي،الأردن، وتصدر عن عمادة البحث العلمي والدراسات العليا، الجامعة الهاشمية، الزرقاء، الأردن.

ترسل البحوث إلى العنوان التالي :

رئيس تحرير المجلة الأردنية للهندسة الميكانيكية والصناعية
عمادة البحث العلمي والدراسات العليا
الجامعة الهاشمية
الزرقاء - الأردن
هاتف : 3903333 5 00962 فرعي 4147
Email: jjmie@hu.edu.jo
Website: www.jjmie.hu.edu.jo